

**Sea-level variability at select coastal and island regions in the  
Indian Ocean**

Thesis submitted for the Degree of

**Doctor of Philosophy**

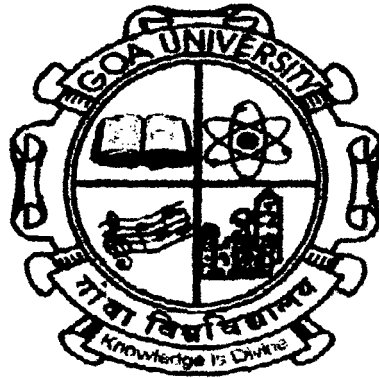
in

**Marine Sciences**

to the

**Goa University**

577.77  
MEH/Sea



by

T- 78781

**Prakash Mehra**

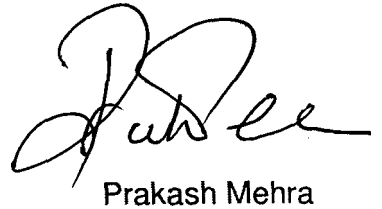
National Institute of Oceanography (CSIR)  
Dona Paula, Goa – 403 004, India  
July 2016

**Dedicated to...**  
**my "Parents"**

## Statement

As required under the University Ordinance 0.19.8 (vi), I state that the present thesis entitled "**Sea-level variability at select coastal and island regions in the Indian Ocean**" is my original research work carried out at the CSIR-National Institute of Oceanography, Goa and that no part thereof has been submitted for any other degree or diploma in any University or Institution.

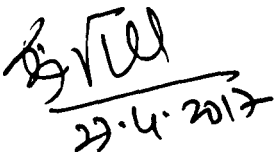
The literature related to the problem investigated has been cited. Due acknowledgements have been made wherever facilities and suggestions have been availed of.



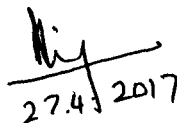
Prakash Mehra

CSIR-National Institute of Oceanography  
Dona Paula, Goa - 403 004  
April 2017

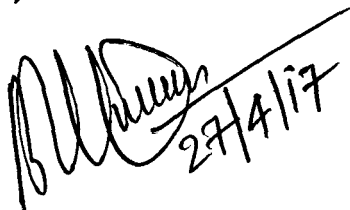
The corrections suggested by the Examiners  
have been incorporated.



23.4.2017



27.4.2017



27/4/17

---

## Certificate

This is to certify that the thesis entitled "**Sea-level variability at select coastal and island regions in the Indian Ocean**" submitted by **Prakash Mehra** for the award of the degree of Doctor of Philosophy in the Department of Marine Sciences is based on his *original studies* carried out by him under my supervision. The thesis or any part thereof has not been previously submitted for any degree or diploma in any University or Institution.



Dr. P. Vethamony

CSIR-National Institute of Oceanography

Dona Paula, Goa – 403 004

April 2017



---

## Acknowledgments

I joined CSIR- National Institute of Oceanography (NIO) on 13 August 1993 and was working towards the design and development of autonomous systems for marine applications with Shri. R. G. Prabhudesai. It was in 2002, that we used the in-house designed sea-level gauges in the Gulf of Kutch and had an opportunity to work under the leadership of Dr. P. Vethamony. Since then, I had in my mind to work under his guidance for my PhD work. In the mean time, I started working with Dr. Antony Joseph and got involved in sea-level studies. I am extremely thankful to my senior colleagues Shri. R.G. Prabhudesai and Dr. Antony Joseph for enabling me to harness the rich technological and scientific experience.

It was in November 2011, when I met Dr Vethmony on the staircase while he was proceeding towards his laboratory, I expressed my desire to work for my doctoral thesis under his guidance. Without thinking even once, with all the loads of other students and ongoing projects, he gave me the consent. He spent his valuable time with me for scientific discussions, improved my understanding of sea-level and meticulously corrected the thesis manuscript. It gives me immense pleasure to thank him on this occasion.

I am very grateful to the CSIR-NIO for providing all the facilities to conduct my work. I am grateful to Dr. E. Desa, former Director who helped me to learn the design and development of autonomous technologies. I would also like to thank Dr. S.R. Shetye, former Director for providing exposure to harmonic analysis techniques. I express my sincere gratitude to Dr. S.W.A. Naqvi, Director, NIO, Goa, for providing me necessary facilities to carry out my work at NIO.

I thank Prof. H.B. Menon, former Head, Department of Marine Sciences, Goa University for his valuable advice on several occasions, both scientific and administrative. Thanks to Dr. C. U. Rivonkar, Head, Marine Sciences, Goa University for his support. I am thankful to the VC's nominee, Dr. M.R. Ramesh Kumar, Chief Scientist, CSIR-NIO, Goa, for providing critical comments and reviews on progress reports.

---

Special thanks to my colleague and friend, Dr. Jayakumar Seelam, who helped me to use the "TASK" software and with whom I had a lot of discussion during the course of the work. I would thank all my colleagues Yogesh A., Anil Shirgaonkar, Vimala D., Nitin, D and Surekha, N for providing all the support in the Lab and during the field work. I extend my sincere gratitude to all my colleagues Sanjeev A, Antonio M, R Madhan, Gajanan N, Ilangovan D, Vijay kumar K, Pramod M, Bubu M T, Sudheesh K and former colleagues and friends Venugopal C and MVV Prasad for all support and encouragement received.

It would be a difficult task to list all my friends who supported directly or indirectly throughout my career. I extend my thanks to all those who helped me in various occasions. My special thanks and gratitude to all my project students. Thanks to Soumy M, Bharat H and Devika G who helped me a lot in data processing and documentation.

All the success in my life is due to everlasting support, love and prayers of my family members. It was the strong belief of my parents in education with their very limited resources, which supported myself, my brother and my sister in our endeavours. Last but not the least, I thank my wife Bindu who always pushed me towards higher studies and took the burden of all the responsibilities when I went for my M.Tech and also while doing my PhD work. My son Tanishq and daughter Preeti have always been a source of inspiration.

May "Krishna" bless all my colleagues, friends and family with good health, happiness and prosperity.

**Prakash Mehra**

CSIR-National Institute of Oceanography, Goa

April 2017

---

## Abstract

Sea-level variability is caused by various forcings such as tides, winds, currents and other oceanic and meteorological phenomenon. The sea-level energy has large bandwidth with periods varying from minutes to tens of years. Many studies have been carried out to understand the low frequency variability of sea-level to understand the seasonal, annual and decadal variations using monthly-mean tide gauge data. With improvement in computing and data storage technologies, it is possible now to obtain high frequency sea-level and surface meteorological data ( $\leq 5$  minutes) for long durations ( $\geq$  year). High frequency sea-level oscillations result from tides, direct forcing from atmosphere and different kinds of propagating and standing ocean waves, which can be amplify over shelves, in bays, harbours due to topographical features. This study examines sea-level variability at time scales ranging from minutes to annual at different coastal and island locations in the north Indian Ocean and the effect of local meteorological forcings and extreme atmospheric events on sea-level variability.

The data and methodology used in this work are described along with data quality checks, editing using the Matlab and C-programming and data processing using harmonic and spectra analyses. Multi-linear regression and numerical models were used to segregate and simulate the sea-level variations due to local surface meteorological forcing. Sea-level residuals (SLR) were estimated as the difference between the observed and predicted tides, representing the exchange of energy between the ocean and atmosphere, and used to study the low (periods  $>$  day) and high frequency (period minutes to few hours) oscillations at different locations.

The study describes the mechanism and characteristics of oscillation of water body in the Mandovi estuary (Verem) on the central west coast of India and at Kavaratti Island due to extreme events such as meteorological disturbances and geophysical tsunami. The episodic events are:

- Event 1 (E1): 23 - 25 June 2007; passage of cyclonic storm *Yemyin*.
- Event 2 (E2): 12 - 14 September 2007; occurrence of Sumatra tsunami.
- Event 3 (E3): 9 - 12 November 2009; passage of cyclonic storm *Phyan*

---

The sea-level response at Verem and Kavaratti has been manifested in terms of positive surges upto ~40 cm and 36 cm, respectively due to E1. The sea-level exhibited a positive surge upto ~47 cm due to E3 at Verem. Unlike a positive surge observed in the case of episodic meteorological conditions, the September 2007 Sumatra tsunami at Verem (E2) caused oscillations only upto  $\pm 15$  cm in sea-level residuals.

The spectral ratio between the event (geophysical tsunami or atmospheric disturbance) and the respective background spectrum provides information on the external source. This method has been used to separate out the source (events) and the topographic effects. The transfer function obtained for one event has been used to reproduce the sea-level spectra for the other event using the coastal atmospheric pressure spectra. The computed SLR spectrum has been found to be in good agreement with the measured spectrum for the event. The spectrum analysis showed that sea-level and surface meteorological measurements collected during storms exhibit strong synoptic disturbances leading to coherent oscillations in the estuary with significant energy bands centered at periods 24, 45 and 80 minutes. Kavaratti Island lagoon showed no prominent spectral peaks to indicate seiches (i.e. natural oscillations). Another prominent feature noticed is the pre-earthquake enhanced seawater temperature oscillations in this tropical estuary (Mandovi). The routine monitoring of seawater temperature with fine temporal resolution may provide early information about impending underwater earthquakes.

The response of sea-level variations at coastal and island locations of India during the normal and tropical cyclones in the north Indian Ocean has been studied by taking into account the contribution of local winds (crossshore, U and alongshore, V components) and atmospheric pressure ( $A_p$ ) to the sea-level variability. The study also strives to characterise the response of the sea-level to the following two episodic meteorological events:

- Event 4 (E4): 26 November to 1 December 2011, occurrence of deep depression in the Arabian Sea (AS).
- Event 5 (E5): 25-31 December 2011, passage of Thane cyclone in the Bay of Bengal (BOB).

---

The study describes and compares the characteristics of the two tropical cyclones using wind speed, sea-level pressure and storm forward translation speed data from IMD, JTWC and UNISYS. A 2D depth averaged hydrodynamic model has been setup for the AS and BOB to estimate the surges at the coast due to these events. The estimated peaks at the measurement locations in AS are only upto ~40% of the measured surges. In BOB, at Gangavaram, harbour oscillations are observed. At Kakinada, the estimated surge peaked upto 75% of the measured surge. Detailed investigations were carried out using multi-linear regression analysis with SLR as the dependent variable and wind stress components ( $T_U, T_V$ ) and atmospheric pressure ( $A_p$ ) as the independent variables. The regression model showed that the local surface meteorological data (daily-mean wind and atmospheric pressure) could be able to account for ~57% and ~69% of daily-mean sea-level variability along the east and west coasts of India.

Spectrum analysis showed that the events E4 (E5) generated sea-level oscillations at the measuring stations on the west and east coasts with significant energy bands centred at periods of 96, 43 and 23 minutes. It was also observed that SLR from tide gauge stations along the west coast of India and coast of Pakistan showed a surge peak of constant amplitude propagating northward with a speed of ~6.5 ms<sup>-1</sup> during E4. The propagating surges along the western coast have been identified as forced Kelvin waves with almost constant amplitude.

Most of the studies conducted in the north Indian Ocean were to understand the seasonal, annual and sea-level rise trends using monthly-mean sea-level anomalies. Probably, this may be the first attempt to study the high-frequency sea-level oscillations with periods ranging from several minutes to a day in the coastal regions of India. The present work could be further extended to understand the role of distant long waves in modulating the sea-level at coast, and also to estimate Eigen frequencies of harbours and estuaries exhibiting oscillations, using hydrodynamic models.

---

# Contents

<b>Statement</b>	<b>iii</b>
<b>Certificate</b>	<b>iv</b>
<b>Acknowledgements</b>	<b>v</b>
<b>Abstract</b>	<b>vii</b>
<b>List of Figures</b>	<b>xiv</b>
<b>List of Tables</b>	<b>xxi</b>
<b>1 Chapter 1 Introduction.....</b>	<b>1</b>
1.1 Nature of sea-level variations.....	1
1.1.2 Definitions and relations.....	2
1.2 Types of ocean surface waves.....	3
1.2.1 Surface gravity waves.....	3
1.2.2 Seiches.....	3
1.2.3 Tides.....	4
1.2.4 Storm Surges.....	4
1.2.5 Tsunamis.....	4
1.3 Mean sea-level and trends.....	5
1.3.1 Global Navigation Satellite System (GNSS) installation.....	7
1.4 Overview of the thesis.....	8
1.4.1 Significance of this study.....	8
1.4.2 Objectives.....	9
1.5 Study area.....	9
1.5.1 Sea-level measurements along the coast of India including islands....	11
1.6 Literature review.....	12
1.6.1 Sea-level estimation using tide gauges.....	12
1.6.2 Sea-level estimation using altimeter.....	14

1.6.3	Sea-level variability along the coast of India.....	16
1.5.4	High frequency sea-level variability.....	18
<b>2</b>	<b>Chapter 2 Data and Methodology.....</b>	<b>22</b>
2.1	Introduction.....	22
2.2	Sea-level measurements.....	23
2.2.1	Pressure gauge.....	24
2.2.2	Radar gauge.....	26
2.3	Integrated coastal Observation Network (ICON).....	29
2.3.1	Sea-level gauge.....	30
2.3.2	Surface Meteorological Measurements:.....	33
	Autonomous Weather Station (AWS)	
2.3.2.1	Wind velocity.....	34
2.3.2.2	Barometric pressure.....	35
2.3.2.3	Solar radiation.....	35
2.3.2.4	Air temperature.....	35
2.3.2.5	Relative humidity.....	35
2.3.2.6	Rain fall.....	36
2.4	Other data sets: sea-level and surface met.....	38
2.5	Processing of data.....	38
2.5.1	Data quality, checks and edition.....	38
2.5.2	Harmonic analysis.....	38
2.5.3	Spectral analysis.....	39
2.5.4	Regression model.....	39
2.5.5	Comparison method.....	40
2.6	Comparison of sea-level data.....	41
2.6.1	Sea-level variations in north Indian Ocean.....	41
2.6.2	Comparison of Sea-level measurements from.....	43
	radar and pressure gauge	
2.6.3	Harmonic constituents at west central Indian.....	45
	coast (Verem, Goa)	
2.6.4	Effect of atmospheric pressure.....	47
2.7	Conclusions.....	49

<b>3</b>	<b>Chapter 3 Sea-level variability in the north Indian Ocean.....</b>	<b>51</b>
3.1	Introduction.....	51
3.2	Data and methodology.....	51
3.3	Tidal properties in the north Indian Ocean.....	53
	3.3.1 Tidal ranges.....	53
	3.3.2 Tidal constituents.....	57
	3.3.3 Form number.....	58
3.4	Sea-level residuals (SLR).....	60
	3.4.1 Low frequency sea-level residuals.....	63
	3.4.2 High frequency sea-level residuals.....	69
3.5	Conclusions.....	73
<b>4</b>	<b>Chapter 4 Sea-level variability during extreme events.....</b>	<b>75</b>
4.1	Introduction.....	75
4.2	Data and methods.....	76
4.3	Extreme events.....	79
	4.3.1 Responses of sea-level to cyclone Yemyin.....	79
	4.3.2 Response of sea-level to cyclone Phyan.....	80
	4.3.3 Response of sea-level to Sumatra Tsunami (2007).....	81
4.4	Non-resonant character of Kavaratti Island lagoon.....	84
4.5	High frequency oscillations at Verem.....	86
	4.5.1 Sea-level spectrum during events E1, E2 and E3.....	86
	4.5.2 Sea-level background spectrum.....	86
4.6	Transfer function for atmospherically generated oscillations.....	91
	4.6.1 Topographic admittance.....	92
	4.6.2 Spectral ratio.....	93
	4.6.3 Estimation of spectrum using transfer function.....	95
	4.6.4 Amplification due to resonance.....	96
4.7	Observed pre- and post-earthquake enhanced seawater temperature.....	97
	oscillations at Verem	
	4.7.1. Pre-earthquake water temperature oscillations.....	98
	4.7.1.1 Earthquake precursors.....	98
	4.7.1.2 Short acoustic waves.....	98
4.8	Conclusions.....	101



<b>5</b>	<b>Chapter 5 Sea-level response to meteorological forcing.....</b>	<b>103</b>
5.1	Introduction.....	103
5.2	Data and methodology.....	104
	5.2.1 Sea-level and meteorological data.....	104
	5.2.2 Tropical cyclone track data.....	105
5.3	Observed coastal sea-level response to meteorological events.....	106
	5.3.1 Response of sea-level to depression in the Arabian Sea.....	107
	5.3.2 Response of sea-level to meteorological events in Bay of Bengal.....	111
	5.3.3 Sea-level changes by local winds.....	113
5.4	Estimation of surges.....	114
	5.4.1 Hydrodynamic model.....	114
	5.4.2 Regression model.....	117
	5.4.2.1 Surge estimation in Arabian Sea.....	118
	5.4.2.2 Surge estimation in Bay of Bengal.....	121
5.5	High frequency oscillations due to meteorological forcing.....	124
	5.5.1 SLR spectrum.....	124
	5.5.1.1 SLR Spectrum in the AS.....	125
	5.5.1.2 SLR Spectrum in the BOB.....	126
5.6	Storm surge propagation.....	129
5.7	Conclusions.....	133
	<b>Chapter 6 Summary and conclusions.....</b>	<b>135</b>
6.1	Summary.....	135
6.2	Conclusions.....	136
6.3	Future perspective.....	139
	<b>References.....</b>	<b>140</b>
<b>Annexure I:</b>	<b>Papers published from the thesis.....</b>	<b>151</b>
<b>Annexure II:</b>	<b>List of conference papers and presentations.....</b>	<b>152</b>
<b>Annexure III:</b>	<b>Supplementary figures and table.....</b>	<b>153</b>

---

## List of Figures

- 1.1. Spectrum of sea-level variations. The long period variations and mean sea-level changes are part of the enhanced energy at low frequencies (WMO-No. 1076, 2011). 2
- 1.2 Tsunami signal at Takoradi Harbour subsequent to the 26 December 2004 Sumatra earthquake. E = earthquake time; TAT = tsunami arrival time (Joseph et al., 2006). 5
- 1.3 Time-series of annual mean sea-level anomalies at the tide-gauge station in Mumbai (blue line); altimeter annual mean sea-level anomalies (red line) extracted at an offshore point close to Mumbai tide-gauge location (refer Fig.5 of Unnikrishnan et al., 2015). 6
- 1.4 GNSS antenna at Data and Information building in CSIR-NIO. 7
- 1.5 Map of Oceans of the world along with the geography of the Indian Ocean. The zonal extent of the Indian Ocean (light blue) is much less than that of the Pacific (dark blue). (<http://www.worldatlas.com>) 10
- 1.6 Integrated Coastal Observation Network (ICON) of sea-level gauges and autonomous weather stations (AWS) along the coast of India and islands (<http://inet.nio.org>). 12
- 1.7 Map of sea-level trend patterns from mean reconstructed sea-level grid during 1950–2009 with tide gauge sites superimposed as black circles. Co-located GPS and DORIS stations are represented in blue; black stars indicate tide gauge records used in the global reconstruction grid (Fig.4 from Palanisamy et al., 2014). 15
- 1.8 Monthly mean sea-level anomaly at [a] Verem, Goa, [b] Gangavaram, Andhra Pradesh and [c] Mandapam, Tamil Nadu. 17
- 1.9 Hourly time series of sea-level and surface meteorological data: (a) Sea-level residual after removing the astronomical tide, (b) Geostrophic currents 'GC' estimated from the average of the current obtained from the sea-level anomaly gradient from 13°N to 14° N along the Jason satellite track 181, (c) U Crossshore wind, (d) V Along-shore wind, (e) Atmospheric pressure anomaly and (f) Water density. SM refers to summer monsoon (refer Fig. 5 of Mehra et al. 2010). 21
- 2.1 Schematic diagram of subsurface pressure sensor based sea-level gauge. 25
- 2.2 Typical installation of a subsurface pressure gauge at Verem, Goa. 26
- 2.3 Schematic diagram of downward looking microwave radar sensor 27

	based sea-level gauge.	
2.4	Typical installations of downward-looking aerial microwave radar gauge at Ratnagiri, Maharashtra.	28
2.5	Network of near real-time reporting sea-level, sea state and surface meteorological stations (schematic).	30
2.6	Typical installation of downward-looking aerial microwave radar sensor based sea-level gauges incorporated in the NIO's ICON at [a] Karwar, [b] Port Blair and [c] Dona Paula.	31
2.7	Near real-time data from CSIR-NIO sea-level gauge accessible at <a href="http://inet.nio.org">http://inet.nio.org</a> .	32
2.8	A typical installation of AWS in NIO's ICON at [a] Ratnagiri, Maharashtra and [b] Gopalpur, Odisha.	33
2.9	Near real-time data from CSIR-NIO Autonomous Weather Station accessible at <a href="http://inet.nio.org">http://inet.nio.org</a> .	34
2.10	Sea-level measurements at Goa using [a] radar gauge (RG), [b] pressure gauge (PG) and respective residuals from [c] RG and [d] PG.	42
2.11	Monthly sea-level residual (SLR) variability at Verem, Goa.	43
2.12	Sea-level measurements at Tuticorin using [a] radar gauge (RG), [b] pressure gauge (PG), and [c] difference (PG-RG) and at Mandapam using [d] radar gauge (RG), [e] pressure gauge (PG) and [f] difference (PG-RG).	43
2.13	Comparison between sea-level measurements of radar gauge and pressure gauge; linear fit is shown as red line at [a] Verem, [b] Tuticorin and [c] Mandapam. The percentage occurrence of difference [PG-RG] along with respective RSMEs marked with dashed line at [d] Verem, [e] Tuticorin, and [f] Mandapam. N is the number of data points at respective stations.	44
2.14	Major tidal constituents at Verem, Goa obtained using radar and pressure gauges. [a] amplitude and [b] phase.	47
2.15	Time series of [a] atmospheric pressure (AP) anomaly (mb), [b] difference ( $d_0$ ) between sea-level estimated from pressure and radar gauge without measured atmospheric pressure correction and [c] difference ( $d_1$ ) between sea-level estimated using pressure and radar gauges with measured atmospheric pressure correction.	48
3.1	Predicted tides at different coastal and island locations of India in the Arabian Sea (AS) and the Bay of Bengal (BOB): [a] Ratnagiri, [b]	55

---

	Verem, [c] Karwar, [d] Malpe, [e] Kavaratti, [f] Kochi and [g] ] Colachel in AS. [h] Gopalpur, [i] Gangavaram, [j] Kakinada, [k] Yanam, [l] Port Blair, [m] Mandapam and [n] Tuticorin in BOB. Time is in Indian Standard Time (IST).	
3.2	Mean spring tide ranges at different coastal and island locations of India in the AS and the BOB. [a] Measurements locations in AS: 1- Ratnagiri, 2- Verem, 3- Karwar, 4- Malpe, 5- Kavaratti, 6- Kochi and 7- Colachel. [b] Measurement locations in BOB: 1- Gopalpur, 2- Gangavaram, 3 Kakinada, 4- Yanam, 5- Port Blair, 6- Mandapam and 7- Tuticorin.	56
3.3	A few major tidal constituents at different coastal and island locations in the AS and the BOB: [a] and [b] show the amplitude and phase of the tidal constituents in AS (west coast): 1- Ratnagiri, 2- Verem, 3- Karwar, 4- Malpe, 5- Kavaratti, 6- Kochi and 7- Colachel. [c] and [d] show the amplitude and phase of the tidal constituents at in BOB (east coast): 1- Gopalpur, 2- Gangavaram, 3 Kakinada, 4- Yanam, 5- Port Blair, 6- Mandapam and 7- Tuticorin.	57
3.4	Sea-level residual (SLR) at different coastal and island locations in the AS and the BOB: [a] Ratnagiri, [b] Verem, [c] Karwar, [d] Colachel and [e] Kavaratti in the AS; [f] Gangavaram, [g] Kakinada, [h] Mandapam, [i] Tuticorin and [j] Port Blair in the BOB.	61
3.5	Monthly sea-level residual (SLR) variance at different coastal and island locations of India. In AS for the year [a] 2010, [b] 2011, [c] 2012 and in BOB for the year [d] 2010, [e] 2011 and [f] 2012.	62
3.6	Daily-mean sea-level residual (SLR) at different coastal and island locations in the AS and the BOB: [a] Ratnagiri, [b] Verem, [c] Karwar, [d] Colachel and [e] Kavaratti in AS. [f] Gangavaram, [g] Kakinada, [h] Mandapam, [i] Tuticorin and [j] Port Blair in BOB.	64
3.7	Frequency spectrum of daily-mean sea-level residuals (SLR) at different locations of the coastal and island locations in AS and BOB: [a] Ratnagiri, [b] Verem, [c] Karwar, [d] Colachel and [e] Kavaratti in AS. [f] Gangavaram, [g] Kakinada, [h] Mandapam, [i] Tuticorin and [j] Port Blair in BOB.	66
3.8	Time series of frequency spectrum of daily-mean sea level residual (SLR) at different coastal and island locations in the Arabian Sea: [a] Ratnagiri, [b] Verem, [c] Karwar, [d] Colachel and [e] Kavaratti	67
3.9	Time series of frequency spectrum of daily-mean sea-level residual (SLR) at different coastal and island locations in BOB: [a] Gangavaram, [b] Kakinada, [c] Mandapam, [d] Tuticorin and [e] Port Blair.	68
3.10	High-pass filtered sea-level residual (hf-SLR) using a 5th order	70

---

Butterworth filter (time period  $\leq 2$ h) at different coastal and island locations in the AS and the BOB: [a] Ratnagiri, [b] Verem, [c] Karwar, [d] Colachel and [e] Kavaratti in AS. [f] Gangavaram, [g] Kakinada, [h] Mandapam, [i] Tuticorin and [j] Port Blair in BOB.

- 3.11 Frequency spectrum of sea-level residual (sampled every 5 minutes) at different coastal and island locations in the AS and the BOB: [a] Ratnagiri, [b] Verem, [c] Karwar, [d] Colachel and [e] Kavaratti in the AS. [f] Gangavaram, [g] Kakinada, [h] Mandapam, [i] Tuticorin and [j] Port Blair in BOB. 71
- 4.1 The study region in the Arabian Sea [a] cyclone tracks of Yemyin and Phyan ([www.imd.gov.in](http://www.imd.gov.in)) and Sumatra earthquake epicentre; [b] the locations of autonomous weather station (AWS) and pressure gauge stations in the Mandovi estuary region (Fig. 4.1b is adapted from Fig.1, Sundar & Shetye, 2005). 78
- 4.2 Sea-level and surface meteorological parameters at Verem and Kavaratti during the episodic events: [a.1-5] wind speed, wind direction, atmospheric pressure anomaly, sea surface temperature anomaly and sea-level residual during the atmospheric disturbance event E1 (cyclone Yemyin) in June 2007 at Verem. [b.1-5] Variables are same as in [a] at Kavaratti Island region during E1 and [c.1-5] Variables are same as in [a] during the atmospheric disturbance E3 (cyclone Phyan) in November 2009 at Verem. 82
- 4.3 Sea water parameters observed at Verem, in response to the episodic event E2 of 12th September 2007 due to Sumatra earthquake (M-w=8.4). [a] sea-level residual (cm), [b] measured SST anomaly ( $^{\circ}$ C), [c] high pass filtered SST ( $^{\circ}$ C), [d] low pass filtered SST anomaly ( $^{\circ}$ C), and [e] spectrum of measured SST anomaly before (28 August to 8 September [Julian days 240-251] 2007), during (9-25 September [Julian days 252-268] 2007) and after (26 September - 5 October [Julian days 269-278] 2007) the tsunami arrival time (TAT) at Verem. The TAT at Verem was 00:45 IST on 13th September 2007. The number associated with significant peaks is time period in hours. 83
- 4.4 Characteristics of sea-level residual (SLR) and atmospheric pressure at Kavaratti Island lagoon region during event E1: [a] time series of high pass filtered SLR (period  $< 2$  h), [b] spectrum of SLR over 7 days 18-25 June [Julian days 169-176; N=2016] 2007 along with background spectrum (black), and [c] spectrum of atmospheric pressure anomaly over 7 days 18-25 June [Julian days 169-176; N=2016] 2007 along with background spectrum (black). The numbers marked over the significant peaks are period in minutes. 85
- 4.5 Time-series of two-weeks long, high-pass filtered (period  $< 2$  h) SLR at Verem during different episodic events [a] E1, [b] E2, and [c] E3. The X-axis represents time of the respective year. 87

4.6	Sea-level residual (SLR) spectra at Verem during different events (red) along with the corresponding background spectra (black): [a] E1 over 3 days (Julian days 174-176, 2007; N=864), [b] E2 over 3 days (Julian days 255-258, 2007; N=864), and [c] E3 over 4 days (Julian days 313-317, 2009; N=1152). N represents the number of data samples used in estimating the spectra. The numbers marked over the significant peaks are period in minutes.	89
4.7	Atmospheric pressure anomaly spectra during different events (red) along with the corresponding background spectra (black) at Verem: [a] E1 over 3 days (Julian days 174-176, 2007; N=864) [b] E2 over 3 days (Julian days 255-258, 2007; N=864) and, [c] E3 over 4 days (Julian days 313-317, 2009; N=1152). N represents the number of data samples used in estimating the spectra. The numbers marked over the significant peaks are period in minutes.	90
4.8	Spectral ratio (i.e., ratio of spectrum during the event to that of the respective background spectrum) of [a] SLR at Verem (Goa) during the events E1, E2, and E3, [b] SLR at Kavaratti during event E1, [c] atmospheric pressure anomaly at Verem (Goa) during the events E1, E2 and E3. [d] Observed (black) and the computed (red) spectra of SLR at Verem for event E1. The computed SLR spectrum is obtained using atmospheric pressure during E3 based on equation-4.10. The numbers marked over the significant peaks are period in minutes.	94
4.9	Sea water parameters observed at Verem, Goa during event E2 of 12 <sup>th</sup> September 2007 due to Sumatra earthquake ( $M_w = 8.4$ ). [a] sea level (cm) and [b] measured water temperature anomaly ( $^{\circ}\text{C}$ ).	100
5.1	Study location showing the tracks of meteorological events during the year 2011.	104
5.2	Cyclone parameters during E4 and E5: (a) and (d) wind speed, (b) and (e) sea-level pressure, (c) and (f) storm forward translation speed.	105
5.3	Sea-level residual (SLR) at [a] Ratnagiri, [b] Verem, [c] Karwar, [d] Tuticorin, [e] Mandapam, [f] Gopalpur, [g] Gangavaram, [h] Kakinada and [i] Port Blair.	108
5.4	Sea-level residual and surface meteorological parameters during the episodic event E4. [a.1 to a.6] SLR, wind speed, wind direction, atmospheric pressure anomaly, air temperature and relative humidity at Ratnagiri. [b.1 to b.6] same as in [a] at Verem. [c.1 to c.6] same as in [a] at Karwar. The atmospheric pressure anomaly is estimated by subtracting the mean atmospheric pressure (1 September 2011 to 31 January 2012) from the measured atmospheric pressure for respective stations.	110

- 
- 5.5 Sea-level residual and surface meteorological parameters during the episodic event E5. [a.1 to a.6] SLR, wind speed, wind direction, atmospheric pressure anomaly, air temperature and relative humidity at Gopalpur, Odisha. [b.1 to b.6] same as in [a] at Gangavaram, Andhra Pradesh. [c.1 to c.6] same as in [a] at Kakinada, Andhra Pradesh. Atmospheric pressure anomaly is estimated by subtracting the mean atmospheric pressure (1 September 2011 - 31 January 2012) from the measured atmospheric pressure for respective stations. 112
- 5.6 Setup of the storm surge model (MIKE) domain for the events E4 and E5. The colour bar shows the depth (m). Model boundary coordinates during E4 are 65.06°E, 0.9°N; 59.62°E, 20.31°N; 77.46°E, 8.10°N; 72.7°E, 20.31°N. Model boundary coordinates during E5 are 85.43°E, 6.5°N; 79.94°E, 10.8°N; 88.43°E, 21.68°N; 93.60°E, 16.21°N. 115
- 5.7 Measured sea-level residual (black) and SLR estimated by storm surge model (red) at [a] Ratnagiri, [b] Verem, [c] Karwar, [d] Gangavaram and [e] Kakinada. 116
- 5.8 Daily-mean wind, wind-stress, measured sea-level residual and estimate sea-level residual from September 2011 to January 2012 at [a] Ratnagiri, [a.1] daily averaged cross-shore (black) and along-shore (red) winds-stress along with respective winds (dotted black or red), [a.2] daily-mean measured sea level residual (black) and estimated residual (red); [b] Verem, [b.1] and [b.2] same as in [a]; [c] Karwar, [c.1] and [c.2] same as in [a]. Daily-mean estimated SLR is obtained using the multi-linear regression method using daily-mean cross-shore ( $T_U$ ), along-shore ( $T_V$ ) components of wind-stress and atmospheric pressure ( $A_p$ ) as independent variables. 120
- 5.9 Daily-mean wind, wind-stress, measured sea-level residual and estimated sea level residual from September 2011 to January 2012 at [a] Gopalpur, [a.1] daily averaged cross-shore (black) and along-shore (red) winds-stress along with respective winds (dotted black or red), [a.2] daily-mean measured sea level residual (black) and estimated residual (red); [b] Gangavaram, [b.1] and [b.2] same as in [a]; [c] Kakinada, [c.1] and [c.2] same as in [a]; Daily-mean estimated SLR is obtained using the multi-linear regression method using daily-mean cross-shore ( $T_U$ ), along-shore ( $T_V$ ) components of winds-stress and atmospheric pressure ( $A_p$ ) as independent variables. 122
- 5.10 Daily-mean sea-level variability explained ( $Var_e$  %) by the multi-linear regression during different months from September 2011 to January 2012. [a]  $Var_e$  (%) at Ratnagiri (black), Verem (red) and Karwar (blue). [b]  $Var_e$  (%) at Gopalpur (black), Gangavaram (red) and Kakinada (blue). 123
-

---

5.11	High-pass filtered sea-level residual (hf-SLR) using a 5th order Butterworth filter (time period $\leq$ 2h) at [a] Ratnagiri, [b] Verem, [c] Karwar, [d] Tuticorin, [e] Mandapam, [f] Gopalpur, [g] Gangavaram, [h] Kakinada and [i] Port Blair.	125
5.12	Spectrum of sea-level residual (SLR) during E4 at [a] Ratnagiri, [b] Verem, [c] Karwar, [d] Tuticorin and [e] Mandapam. The data duration for estimating the spectrum of the SLR during E4 (background) is from 26 November - 1 December (1 September - 20 November) 2011. Vertical red (black) line shows the 95% confidence interval of the event (background) spectrum for the respective stations.	127
5.13	Spectrum of sea level residual (SLR) during E5 at [a] Gopalpur, [b] Gangavaram, [c] Kakinada and [d] Port Blair. The data duration for estimating the spectrum of the SLR during E5 (background) is 25-31 December (1 September - 10 December) 2011. Vertical red (black) line shows the 95% confidence interval of the event (background) spectrum for the respective stations.	128
5.14	Hourly sea-level residual at [a] Colombo, [b] Mandapam, [c] Tuticorin, [d] Kochi, r, [e] Karwar, [f] Verem, [g] , Ratnagiri, [h] Karachi, [i] Chabahar, [j] Jask and [k] Masirah.	132
5.15	Sea-level residual at [a] Minicoy and [b] Hanimaadhoo.	133
S1	Measured (black) and estimated (red) sea-level residual at 10 minute interval from September 2011 to January 2012 at [a] Verem and [b] Karwar.	153
S2	Measured (black) and estimated (red) sea-level residual at 60 minute interval from September 2011 to January 2012 at [a] Verem and [b] Karwar.	154
S3	Measured (black) and estimated (red) sea-level residual at 6 h interval from September 2011 to January 2012 at [a] Verem and [b] Karwar.	155
S4	Measured (black) and estimated (red) sea-level residual at 12 h interval from September 2011 to January 2012 at [a] Verem and [b] Karwar .	156
S5	Measured (black) and estimated (red) sea-level residual at 24 h interval from September 2011 to January 2012 at [a] Verem and [b] Karwar	157

---



---

## List of Tables

2.1	Major technical specifications of the sensors used in radar gauge and pressure gauge deployed at Verem, Goa and SBE26 deployed at Tuticorin and Mandapam, Tamil Nadu.	28
2.2	Specifications of in-house (NIO) developed autonomous weather station.	36
2.3	Summary of field observations (ICON) from different coastal and island locations of India considered in the present study.	37
2.4	Summary of observations (Refer Table 2.3 for position of the measurement stations).	41
2.5	Quantitative measures of comparison between radar gauge and pressure gauge at different coastal locations of India. The terms $N$ , $a$ , $b$ , $d$ , and $r$ are dimensionless, while the remaining terms have the units in cm.	45
2.6	Major tidal constituents obtained from radar gauge (RG) and pressure gauge (PG) deployed at Verem, Goa during January 2009 - May 2010. Refer Pugh, D.T. (1987) for the details of harmonic tidal constituents.	46
2.7	Statistical inferences from the difference between radar and pressure gauge measurements of sea-level.	49
3.1	Summary of sea-level observations obtained from different coastal and island locations of India using indigenously developed microwave radar based sea-level gauge. The sea-level data is sampled every 5 min except at Malpe (Kochi), where the sampling interval is 30 (60) min. Time is in Indian Standard Time (IST).	52
3.2	Form number estimated using the tidal constituents for different locations.	59
3.3	Sea-level residual variance estimated at different measurement locations.	62
3.4	Correlation coefficients at 95% confidence level for daily-mean sea-level residuals at different measurement locations.	65
4.1	Summary of observations.	77
4.2	Meteorological and sea-level observations at Verem and Kavaratti during the cyclones Yemyin and Phyan.	81

---

5.1	Meteorological and sea-level observations at Ratnagiri, Verem and Karwar during E4 from 26 November to 1 December 2011 (Time in IST).	109
5.2	Meteorological and sea-level observations at Gopalpur, Gangavaram and Kakinada during the event E5 from 26-31 December 2011.	113
5.3	Estimated storm surge peaks using hydrodynamic model during E4 and E5. % difference is obtained as $(\text{measured}-\text{estimated}) \times 100 / \text{measured}$ .	115
5.4	The daily-mean sea-level variability explained ( $\text{Var}_\theta$ ) by linear ( $T_U, T_V, A_p$ individually) and multi-linear ( $[T_U, T_V, A_p]$ together) regression during different months from September 2011 to January 2012.	119
5.5	The peak response of the daily-mean sea level residual (SLR) along with the estimated daily-mean SLR during E4 & E5.	119
5.6	Parameter estimates of the events E4 and E5.	131
5.7	Surge propagation parameters during E4 along the coast of Arabian Sea.	131
S1	Sea level residual variance explained by the regression at different averaged intervals	157

# Chapter 1

## Introduction

### 1.1 Nature of sea-level variations

Sea-level variability is caused by various forcings such as tides, winds, currents and other oceanic and meteorological phenomenon. The sea-level energy defined in the frequency domain has large bandwidth with periods from minutes to tens of years. However, it is mainly concentrated between diurnal and semidiurnal periods. The astronomical components (tides) are predictable from previously observed sea-level variations even for locations where only a short data record of a few months are available (Pugh, 1987). The non-astronomical component of sea-level known as residual is considered as sea-level variability in the proposed study.

Energy is transferred from atmosphere to ocean in the frequency band corresponding to time scales of seconds for small wind waves to hours to days for longer waves and wind setup. The atmospheric pressure causes sea-level changes generally following the inverse barometric effect for a fully developed stationary pressure system in the open sea (Proudman, 1953) and may be much higher in the coastal waters (Pugh, 1987). However, an atmospheric system with a pressure anomaly of tens of hPa may setup a significant horizontal pressure gradient in the open ocean and may generate meteo-tsunami at harbours, bays, fjords, estuaries, etc. due to resonant amplification (Rabinovich, 2009).

Spatial gradient of salinity and temperature influenced by river run-off, ice melting at smaller scale to a larger scale due to changes in the evaporation and precipitation patterns and advection of water masses also gives rise to sea-level variability. The seasonal solar heat input causes density changes with minimum density (maximum sea-level) in autumn and maximum density (minimum sea-level) in spring known as steric effect (Gill and Niiler, 1973). Seasonal changes in the coastal currents give rise to sea-level variability due to Coriolis deflection. The coastal currents may undergo seasonal, annual or inter-annual variability due to climate related factors such as variability in evaporation and precipitation.

### 1.1.2 Definitions and relations

The general representation of the observed sea-level  $X(t)$  which varies with time may be written as:

$$X(T) = Z_0(t) + T(t) + S(t) \quad (1.1)$$

where  $Z_0(t)$  is the mean sea-level which changes slowly with time,  $T(t)$  is the tidal part of the variation and  $S(t)$  is the meteorological surge component as shown in Fig. 1.1. Variations in sea-level contain contributions from different physical sources that are usually distinguished by their period. IOC manual and guides (WMO/TD No. 1339, 2006) have listed various components ranging from surface gravity waves with periods of 1 to 20 s; seiches and tsunamis with periods of minutes to over an hour; tides centred around 1/2 and 1 day; meteorological effects of several days to 1 year; interannual and decadal variability; and long term trends in the mean level caused by geological and climatological effects. The magnitudes of these components vary enormously. Surface gravity waves during extreme weather events can reach heights upto 30 m. Tsunami tend to be less than 1 m in the deep ocean, but may be several metres near the coast. Tides are relatively small in the ocean but may reach as high as 12 m near the coast. Storm surges are of the order of a few metres.

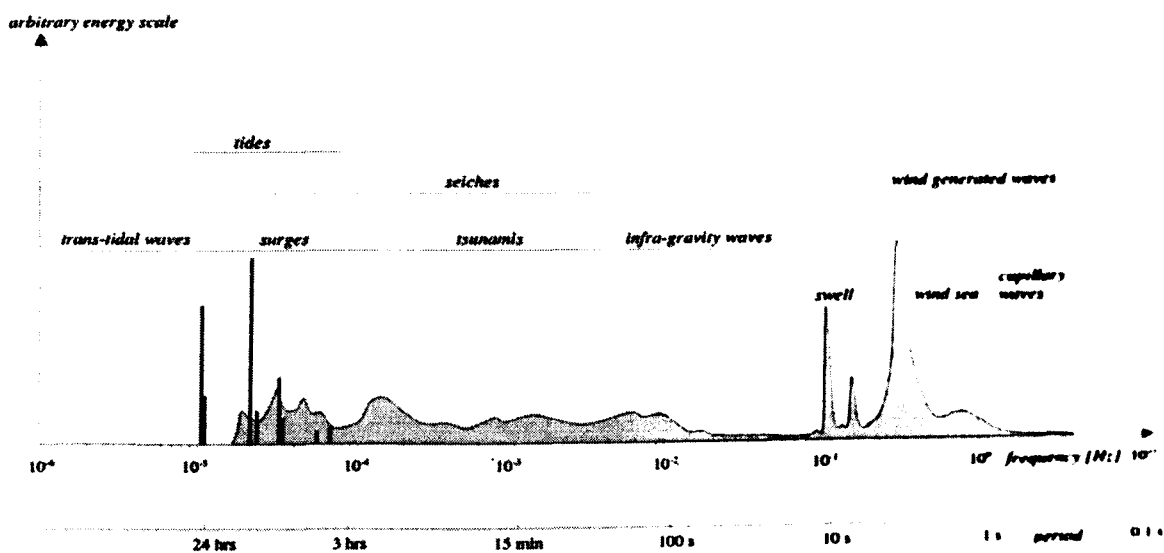


**Figure 1.1.** Spectrum of sea-level variations. The long period variations and mean sea-level changes are part of the enhanced energy at low frequencies (WMO-No. 1076, 2011).

## **1.2. Types of ocean surface waves**

The different types of ocean surface waves that could be classified based on the frequency (or period) are given below.

### **1.2.1. Surface gravity waves**

Surface waves are probably the most noticeable variation of the sea surface to a casual observer. These waves are characterized as wind-waves or gravity waves. Wind waves are generated by the effect of wind on the sea surface and have relatively a broad spectrum with a time period from 1 to 25 s. Swell is produced when the waves propagate out of a storm area. They occupy a narrower part of the spectrum with periods from  $\approx 7$  s to 25 s. Waves are subject to amplification, dispersion, refraction and focusing. In general, significant wave heights of the order of 10 m are common during a storm, but individual waves upto 30 m have been measured.

Wave activity with a period of a few minutes can be caused by non-linear effects; e.g. when the waves encounter a current or a change in bottom topography. Wind waves reacts in a non-linear way with the shallow near-shore water producing changes in mean sea level and oscillations with periods of minutes, known as wave set-up and surf beat. The degree of 'set-up' depends on many factors, of which the shape of the beach is the most critical. Set-up can be of the order of a few tens of centimetres during a severe storm (Pugh, 1987; WMO-No. 1076, 2011).

### **1.2.2. Seiches**

Any body of water has a set of natural periods of oscillations at which it is easy to set up motions, and this could be caused by disturbances such as a strong wind, current, a sudden atmospheric pressure jump or even a tsunami. The period of seiches depends on the horizontal dimensions and the depth of the water body and their lifetime is determined by the frictional effects. Typical periods are in the range of a few minutes to a few hours (between wind waves and tides), and typical amplitudes are centimeter to decimeter. They can be observed in tide gauge records from almost all regions. Seiches have largely been ignored, owing primarily to their local origin, but knowledge of them is important for coastal and harbour engineering, where

small-amplitude seiches may be associated with strong currents at the entrance of the harbour. Moreover, seiches can have major effect on sea-level data analysis. For example, if their amplitude is large enough, and if the sampling rate of the tide gauge is not sufficient, then their energy can be aliased into tidal and other sea level signals (Pugh, 1987; Rabinovich, 2009; WMO-No. 1076, 2011).

### **1.2.3. Tides**

The oceans respond to the gravitational attraction of the moon, sun and other celestial bodies to produce tides, which are normally the predominant signals in sea-level records. Tides are easy to distinguish from other components of sea-level variation as they have regular and predictable pattern with well defined periods depending on astronomical cycles (Pugh, 1987 and references therein).

### **1.2.4. Storm surges**

The exchange of energy between the atmosphere and the ocean is one of the most important topics in geophysics. Storm surges are generated in coastal waters due to tangential wind stress and atmospheric pressure gradients mainly associated with the meteorological forcing field of travelling synoptic scale weather systems such as tropical cyclones (TCs) and extra-tropical cyclones. In the open sea, these currents decay by the action of dissipative forces. Where the current is impeded by the presence of a continental shelf or other discontinuity in depth, or by a coastline, more of the kinetic energy of the sea tends to be converted into potential energy. Abnormal elevations of sea-level may then occur with disastrous results if the coast is low-lying (Pugh, 1987; Murty, 1999; WMO-No. 1076, 2011).

### **1.2.5. Tsunamis**

A tsunami is a wave train generated by a vertical displacement of the water column. Virtually all tsunamis are generated by submarine earthquakes, but landslides, volcanic eruptions, explosions and even the impact of cosmic bodies such as meteorites can generate tsunamis. Not all submarine earthquakes produce tsunami; however, the important aspect appears to be the vertical crustal movement displacing the sea-bed. Tsunamis which propagate across deep water typically have periods of the order of 10 minutes to over an hour depending on the generation mechanism. Tsunamis have longer wavelengths (>100km) compared to water depth.

Therefore, a tsunami behaves like a shallow-water wave and propagates at a speed  $= \sqrt{gd}$ , where,  $g$  = acceleration due to gravity  $= 9.8 \text{ ms}^{-2}$  and  $d$  is water depth (m). For a wave of period of 10 minute and a typical ocean depth of 4,000 m, a tsunami travels at a speed of about  $\sim 700 \text{ kmh}^{-1}$  with a wavelength of 120 km. Tsunamis not only propagate at high speeds, they can also travel great distances as reported by Joseph et al. [2006]. Analysis of sea-level data obtained from the Atlantic Global Sea Level Observing System (GLOSS) sea-level station at Takoradi, Ghana, clearly revealed a tsunami signal associated with Sumatra earthquake ( $M_w = 9.3$ ) of 26 December 2004 in the Indian Ocean (Fig. 1.2).

Amplitudes of the Tsunami in deep water are small ( $\sim 1 \text{ m}$ ) and can pass by ships unnoticed. However, where they impact the coast, amplitudes are significantly higher and can be as large as 10 m (30 m in extreme cases). Wave refraction, caused by segments of the wave moving at different speeds as the water depth varies, can cause extreme amplification in localized areas. Where they impact a coastline, they can cause severe property damage and loss of life.

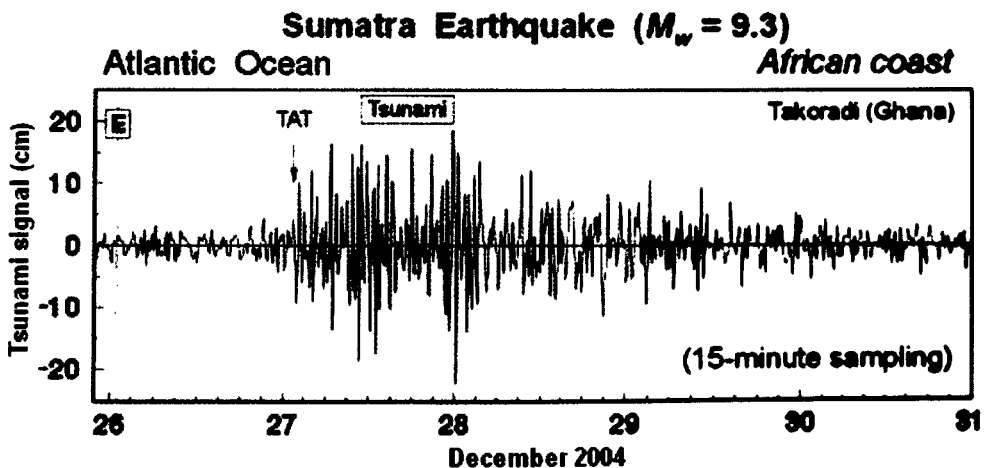


**Figure 1.2.** Tsunami signal at Takoradi Harbour subsequent to the 26 December 2004 Sumatra earthquake. E = earthquake time; TAT = tsunami arrival time (Joseph et al., 2006).

### 1.3. Mean sea-level and trends

Sea-level at any instance is the sum of mean sea-level (MSL), tidal and surge components (equation 1.1). MSL is a time dependent function as changes in MSL are evident from the long time-series measurements now available. Whereas

accuracy of an instrument which determine the properties of tides or storm surges needs to be about 1 cm, the long-term trend in sea-level has a magnitude of around 1 mm per year. However, the geological records show that over a period of millions of years, enormous vertical movements of land relative to sea have occurred. In the recent 2 million years of geological records, there are evidences for erosion platform, gravel terraces and shallow submarine deposits, with relative sea level being 100 m lower than the present.

The change in mean sea-level relative to a fixed point on land is a measure of the difference between the vertical movements of the sea surface and of the land itself. Long-term changes of measured mean sea-level are termed as 'secular' changes. Global changes in the mean sea-level are called 'eustatic' changes. Vertical land movements of regional extent are called eperiogenic movements. Unnikrishnan et al. [2015] reported sea-level-rise trend off the coast of India derived from satellite altimeter and tide gauge data. Fig. 1.3 shows the trends in relative mean sea-level-rise ( $\sim 0.77 \text{ mm yr}^{-1}$ ) from 1878-1993 in Mumbai location. One of the major problems of mean sea-level interpretation is the identification of separate eustatic and eperiogenic changes when only secular changes are directly measurable at a particular location (Pugh, 1987; WMO-No. 1076, 2011).

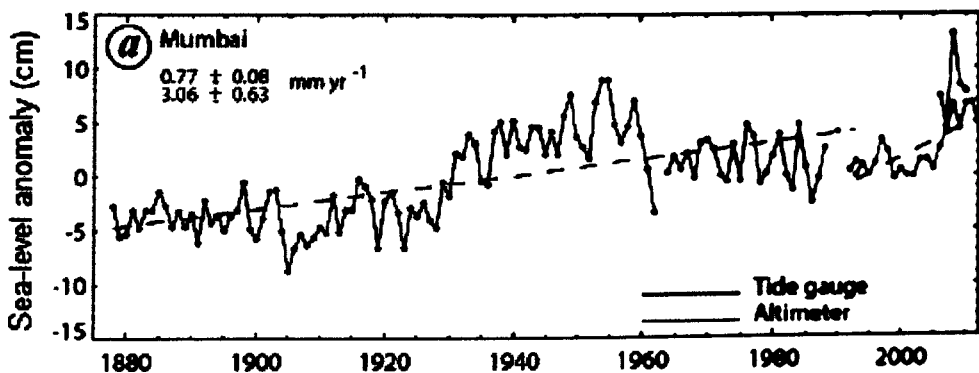


**Figure 1.3.** Time-series of annual mean sea-level anomalies at the tide-gauge station in Mumbai (blue line); altimeter annual mean sea-level anomalies (red line) extracted at an offshore point close to Mumbai tide-gauge location (refer Fig. 5 of Unnikrishnan et al., 2015).



### 1.3.1. Global Navigation Satellite System (GNSS) installation

Tide-gauges are used to estimate mean sea-level by averaging observations of the vertical variations of sea-level with respect to physical markers located at solid ground. The time-series observations should be long enough (though may contain a few data gaps) to remove variations associated with tides and other periodical effects. The observed time-series also permit us to estimate possible variations in the mean sea-level by fitting polynomials through the observations. However, there is an ambiguity associated with any observed variation of the mean sea-level with respect to the ground reference. For example, when a positive vertical variation is observed, the question is whether it is due to rise in sea-level or ground subsidence (vice-versa, in the case of a negative vertical variation). Such ambiguity can be efficiently removed by installing Global Navigation Satellite System (GNSS) stations as close to the tide-gauges as possible. Since the vertical positions directly derived from the GNSS observations are completely independent of the sea-level variations (they are referred to the ellipsoid), they allow us to remove the above-mentioned ambiguity, and consequently, to estimate the absolute variations of sea-level.



**Figure 1.4.** GNSS antenna at Data and Information building in CSIR-NIO.

In order to improve sea-level measurements, the GNSS antenna was installed on the Data & Information building of NIO, Goa in collaboration with University of Beira Interior, Portugal in October 2012 to complement the existing radar based tide-gauge at Dona Paula jetty (Fig. 1.4). Observations together with sea-level gauge will allow one to monitor crustal motions at the sea-level gauge location in order to derive absolute or climate related signals in mean sea level from the tide records.

#### **1.4. Overview of the Thesis**

Many studies have tried to identify the climatic factors that drive sea-level variability. Generally, fluctuations in the sea-level at the coast are caused by astronomic tides, atmospheric forces and “steric oscillations” (Patullo et al., 1955). Steric oscillations are due to changes in specific volume forced by surface fluxes and horizontal and vertical advection of heat and salt. Steric sea-level is low (high), when the water is cold (warm), or has high (low) salinity. Coastal upwelling and downwelling also influences the steric sea-level even in the absence of horizontal advection and fluxes across the boundaries of the ocean. Similarly, the meteorological forces drive regional sea-level changes through the effects of wind and atmospheric pressure. While wind pushes sea-level towards or away from the coastline, atmospheric pressure influences the sea-level through the inverse barometric effect, i.e. hydrostatic de-/compression. In some areas, river runoff or climatic effects are other prominent forcing factors of sea-level variability (Tsimplis and Woodworth 1994). Therefore, there are four causes of changes in monthly sea-level at a coast: astronomic tides, atmospheric pressure, wind-forced coastal currents and thermohaline effects. Of these, the astronomic tides contribute around 1 cm, which is an order of magnitude less than the meteorological effects (Patullo et al., 1955) and hence, tide contribution is ignored.

##### **1.4.1. Significance of this study**

Several studies have been conducted in the north Indian Ocean with a view to understand the sea-level rise trends (Unnikrishnan et al., 2015 and related references therein) using monthly-mean sea-level anomalies. However, high-frequency sea-level oscillations with periods ranging from several minutes to a day in coastal regions of India have not been adequately addressed. This may be due to the non-availability of high frequency sampled sea-level data.

With the availability of high frequency sampled sea-level data, it has become feasible to analyse sea-level oscillations from a few minutes to a day and characterise their behaviour during different seasons. High frequency oscillations result from a variety of processes: tides, direct forcing from the atmosphere and different kinds of propagating and standing ocean waves, all of which can be amplified over shelves, in bays, harbours and over other topographical features (LeBlond and Mysak, 1978).

Out of the above sea-level components, tides are forecasted precisely and storm surges are forecasted satisfactorily. Then there are some events which occur suddenly and cannot be predicted. For example, tsunamis which can lead to severe coastal floods; atmospherically generated ocean gravity waves and coastal edge waves can also cause severe flooding, especially in harbours characterised by a large amplification factor (Rabinovich, 2009).

### **1.4.2. Objectives**

The primary objective of this work is to carry out detailed analyses of sea-level signals collected along the coast of India and islands to study the sea-level variability of long period waves, and the effect of local meteorological forcings and extreme atmospheric events on sea-level variability. The specific objectives are given below:

- to understand sea-level variability at time scales from minutes to annual at different coastal and Island locations in the Indian Ocean.
- to study the influence of local surface meteorological forcings on sea-level variability.
- to study the sea-level variability during extreme atmospheric events.
- to model the sea-level variability using the dominant forces such as winds and atmospheric pressure during meteorological events.

### **1.5. Study area**

Select locations along the coast of India and islands have been considered in the present study to understand sea-level variations and interaction between local

surface meteorological forcing. The Asian continent confines the Indian Ocean, which is essentially a tropical basin at  $\sim 25^\circ\text{N}$  in the north and its southern boundary is arbitrary, but could be distinguished from the Antarctic or Southern Ocean (Fig. 1.5). The north Indian Ocean basin is relatively small; at equator, it measures 6500 km as compared to the Pacific Ocean, which is 17000 km (Shetye, 1998). The west and east coasts of India differ in their topographic and bathymetric features and prevailing weather conditions. The east coast of India is characterized by narrow continental shelf width compared to the west coast. The sudden decrease in water depth causes the waves to surge further during extreme events, creating severe coastal hazards.

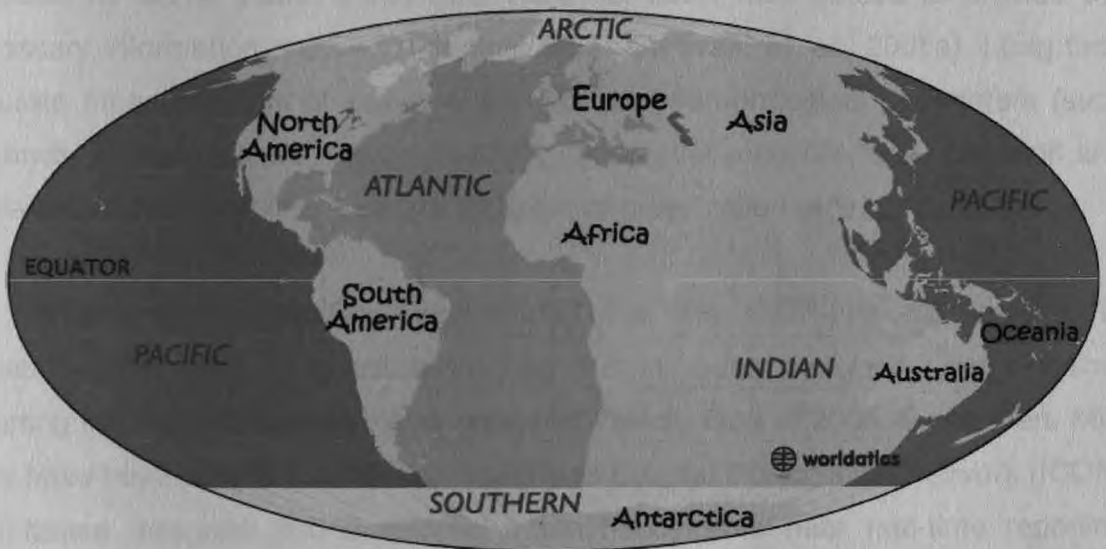


**Figure 1.5.** Map of Oceans of the world along with the geography of the Indian Ocean. The zonal extent of the Indian Ocean (light blue) is much less than that of the Pacific (dark blue). (<http://www.worldatlas.com>).

The land-ocean contrast forces the seasonally reversing monsoon winds over the north Indian Ocean, unlike in the north Atlantic or the north Pacific. The north Indian Ocean responds to this forcing, resulting in significant seasonal cycle of sea-level as seen in the tide-gauge records along the coast of India. The Bay of Bengal experiences three different weather conditions—fair weather, southwest (SW) monsoon and northeast (NE) monsoon. The most influencing wind system in the Arabian Sea is SW monsoon, which has considerable impact along the west coast. During pre-monsoon and NE monsoon seasons, the global winds are generally weak, and the local winds play the major role of controlling the dynamics along the west coast of India. Extreme weather events are common during NE monsoon

(October–December) season and rare during SW monsoon (June–September) season.

### **1.5.1. Sea-level measurements along the coast of India including Islands**

In order to make a quantitative assessment of sea-level variability at finer temporal as well as spatial scales, a well developed network of automated sea-level gauges and surface meteorological stations is required. However, presently there is a scarcity in the fine resolution (both temporal and spatial) sea-level and surface meteorological data along the coast of India and islands. Even where data have been collected for some years, these data have not been fully utilised to provide the necessary information required (Shankar, 2000; Srinivas, et. al., 2005a). Long term accurate measurements of sea-level and surface meteorological parameters (such as winds, air temperature, relative humidity, barometric pressure, solar radiation and rainfall) at higher sampling rates are therefore of great importance.

Marine Instrumentation Division (MID) of the CSIR-National Institute of Oceanography (NIO), Goa established its first in-house designed near real-time reporting internet enabled sea level gauge at Verem, Goa in 2005. Since then, MID team have been able to establish an Integrated Coastal Observation Network (ICON) of in-house designed and developed Internet-accessible near real-time reporting cellular based sea-level, sea-state and surface meteorological (Met) stations at several locations on the coasts and islands of India (Prabhudesai, et. al., 2006). These measurements constitute some of the densely sampled set of sea-level and surface meteorological recordings in the north Indian Ocean (Fig. 1.6). The ICON is also linked with International data banks for sea-level information at the Permanent Service for Mean Sea Level (PSMSL) located at the Proudman Oceanographic Laboratory (POL), UK. These in-situ sea-level observations are also valuable for validation and error estimations of satellite altimeter data. Based on satellite altimeter observations, global tidal models have been improved in such a way that the root-mean-square errors to the in-situ data have reduced to a few cm in the main tidal constituents (Andersen et. al., 1995; Shum et. al., 1997).

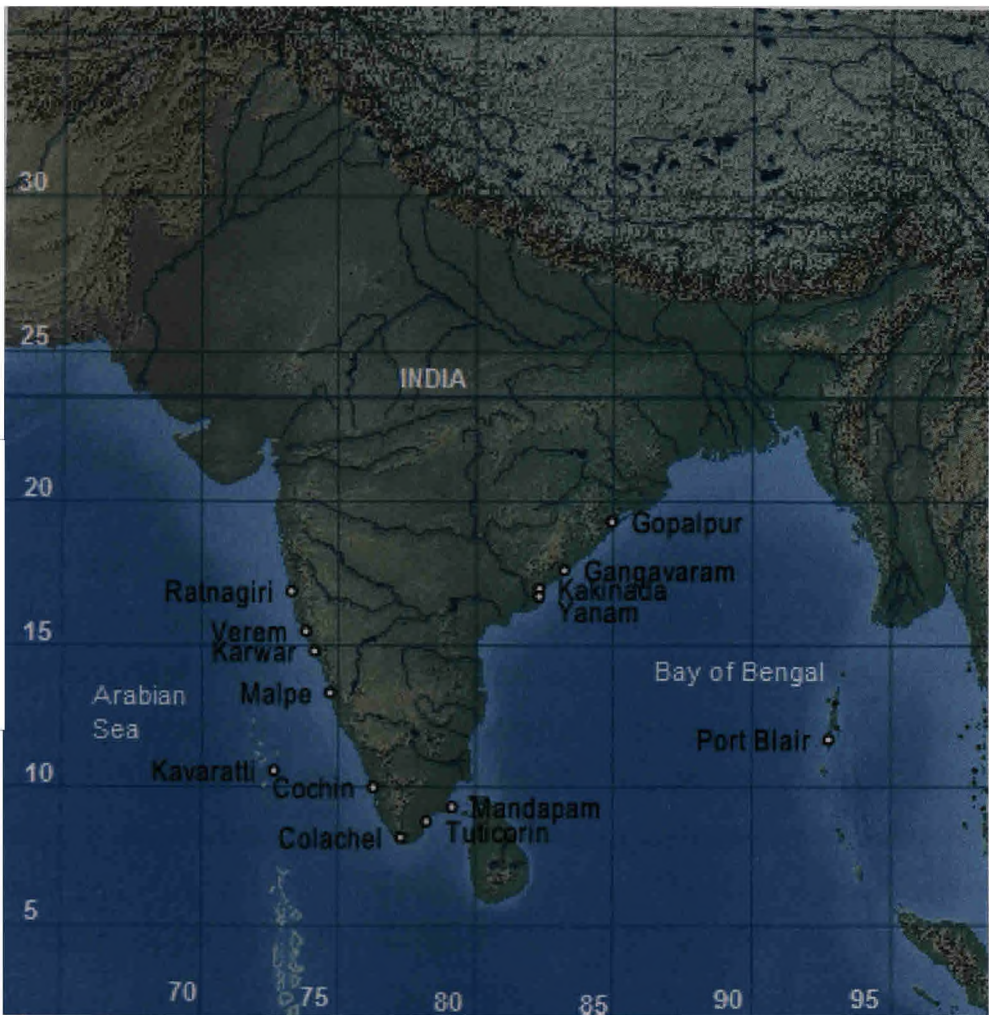


**Figure 1.6.** Integrated Coastal Observation Network (ICON) of sea-level gauges and autonomous weather stations (AWS) along the coast of India and islands (<http://inet.nio.org>).

## 1.6. Literature review

### 1.6.1. Sea-level estimation using tide gauges

The earlier sea-level studies conducted along the coast of India examined the seasonal cycle using tide gauge data (Patullo et al., 1955). Varadarajulu et al. [1982] and Prasad and Reddy [1985] have studied sea-level variability using tide-gauge data of 10 years at Paradip (1966–1975) and Chennai (1970–1979), respectively. Both these studies related sea-level changes to heating and cooling during summer and winter, influence of rainfall and seasonality of reversing monsoons. The survey of

India, then headed by Colonel S.G. Burrad carried out the great trigonometrical survey during 1858-1909 to map the surface topography of the Indian subcontinent. The levelling operations gave rise to a suspicion that mean sea-level in the Bay of Bengal is slightly higher than that in the Arabian Sea. The suspicion of Colonel Burrad was confirmed by Ghildyala and Kumar, [1984] when they carried out the "Adjustment of the First Level Net of India". A difference of ~30 cm was noticed between the mean sea-level in the Bay of Bengal and the Arabian Sea. Their observations show that the mean sea-level at Visakhapatnam (Chennai) is 32 (17) cm higher than that at Mumbai (Mangalore).

Emery and Aubrey [1989] while computing sea-level long-term trends, observed that only five tide gauge station data are usable from different stations along the Indian coast. Three on the west coast (Mumbai, Kochi, Mangalore) and two on the east coast (Chennai and Visakhapatnam) from 1979-1982, and reported a trend of  $+1.3 \text{ mm yr}^{-1}$  and  $-2.1 \text{ mm yr}^{-1}$ , respectively. The change of land level relative to sea-level with an average of  $-0.7 \text{ mm yr}^{-1}$ , indicates either marginal subsidence of land or slow rise in sea-level. Their study expected, increased submergence in coming decades owing to higher temperatures (greenhouse effect of worldwide burning of fossil fuels) that can expand the volume of ocean water as well as augment the return of glacial melting water. In an another study Das and Radhakrishnan [1991] analysed the tide gauge records of Bombay, Madras, Cochin and Visakhapatnam. They observed a rising trend at Bombay (1940-1986) to be  $0.8 \text{ mm yr}^{-1}$ . In Madras (1910-1933) the sea-level trend was estimated to be  $\sim 0.4 \text{ mm yr}^{-1}$ . Tsimplis and Woodworth [1994] used data from 1043 tide gauges around the world to map the global distribution of seasonal cycle of mean sea level. Clarke and Liu [1994] used monthly sea-level along the Indian coast to study inter-annual variability. They found a significant correlation between the sea-levels at Visakhapatnam and Chennai, Kochi and Mumbai. However, the maximum correlation was observed at non-zero lags, hinting at the possibility of wave propagation along the coast. Shankar and Shetye [1999] used the Mumbai tide gauge data which is the only century-long record data in the Indian Ocean to show that the interdecadal changes in sea-level mimic those in rainfall over the Indian subcontinent. It was proposed that the link between sea-level and rainfall arises from the changes in salinity in the coastal waters due to rivers fed by southwest monsoon (June-September) rainfall.



Unnikrishnan et al. (2006) estimated sea-level rise along the coast of India by analysing the past tide gauge data from Mumbai, Visakhapatnam, Kochi and Chennai. The first three gauges showed a sea-level rise of slightly less than  $1 \text{ mm yr}^{-1}$ ; however, the analysis for Chennai showed a rate of decrease ( $-0.65 \text{ mm yr}^{-1}$ ). They claimed that the present estimates are consistent with the global mean sea level rise estimates (Church et al., 2001), although lower in magnitudes. However, in order to get net sea-level rise, these estimates are required to be corrected for vertical land movements which are not available at present. As, the tide gauges are mostly located along the coastline of continents and islands, tide data are geographically sparse and distributed unevenly. These issues can now be tackled owing to the availability of sea-level data since 1992 from the satellite altimeter measurements.

### **1.6.2. Sea-level estimation using altimeter**

A few decades ago, the estimation of global sea-level was only a concept. In recent years, the good spatial and temporal coverage of altimeter data has led to an increasing number of studies using these data in conjunction with coastal tide-gauge records to discuss observed sea-level variability. Perigaud and Delecluse [1993] used Geosat satellite altimeter data for the period April 1985 - September 1989, and studied the sea-level variations of the Indian Ocean north of  $20^{\circ}\text{S}$ . The basin averaged observed and simulated sea-level correlated significantly and the sea-level rise was found to be  $\sim 1 \text{ cm}$  for the period 1985-1989. However, the uncertainty (due to orbit errors) also reaches  $\sim 1 \text{ cm}$  and therefore their study suggested that the Geosat may not be accurate enough to provide global budgets. There were several attempts to use TOPEX/Poseidon (T/P) satellite to estimate global mean sea-level since late 1992 with orbital rates of 10 days and 300 km spacing at the equator. Studies carried out by Nerem et al. [1997, 1999] and Minster et al. [1995, 1999] established the precision of global mean sea-level estimates at  $\sim 4 \text{ mm}$ . Sakova et al. [2006] used TOPEX/Poseidon data to show the existence of large sea-level signals in five frequency bands (semi-annual, annual, 18–20 months, 3 years, and 4–6 years. Thompson et al. [2008] reported that the modelled temperature and sea-level anomaly over the north Indian Ocean (NIO) show an increasing trend in the study period. The model thermocline heat content per unit area shows a linear increasing trend of  $0.0018 \times 10^{11} \text{ J/m}^2$  per year and sea-level anomaly (thermosteric



component) also shows a linear increasing trend of  $0.31 \text{ mm yr}^{-1}$  for NIO during 1958–2000. Vinogradov and Ponte [2011] compared tide gauge records to altimeter data in their vicinity for the period 1993–2008 to assess interannual variability.

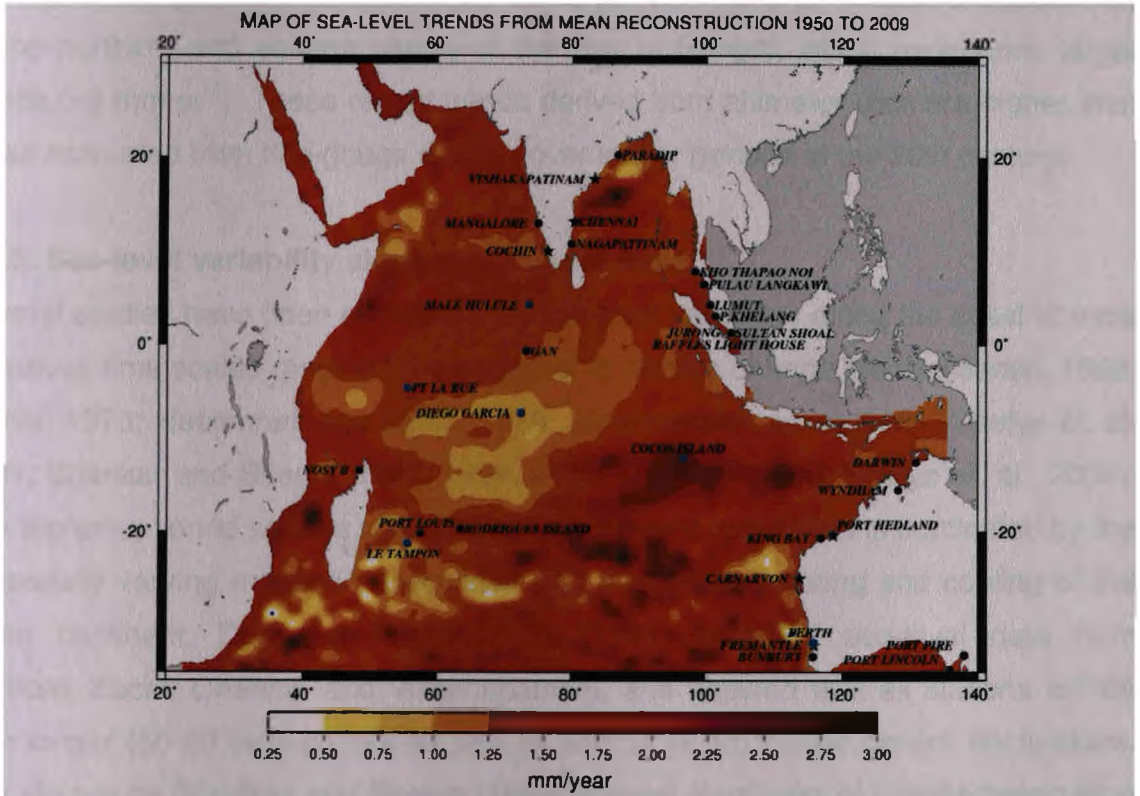


**Figure 1.7.** Map of sea-level trend patterns from mean reconstructed sea-level grid during 1950–2009 with tide gauge sites superimposed as black circles. Co-located GPS and DORIS stations are represented in blue; black stars indicate tide gauge records used in the global reconstruction grid (Fig.4 from Palanisamy et al., 2014).

The recent Fifth IPCC report provided a global mean sea-level-rise trend of  $\approx 1.7 \text{ mm yr}^{-1}$  for the period 1901–2010 (Church et al., 2013). Palanisamy et al. [2014] estimated sea-level rise and regional sea-level variability in the Indian Ocean ( $20^\circ\text{E}$ – $140^\circ\text{E}$ ,  $30^\circ\text{N}$ – $35^\circ\text{S}$ ) over a period of 60 years (1950–2009). They inferred that the changes in the Indian Ocean sea-level are of steric origin and are also driven by short-term Indian Ocean Dipole events. The trend in this region over 60 years amounts to  $1.5 \text{ mm yr}^{-1}$ . There is also an east–west increase in sea-level trend pattern below  $15^\circ\text{S}$  latitude which is more amplified since the two recent decades (Fig. 1.7). Unnikrishnan et al. [2015] reported the recent trends in sea-level rise in the

NIO, particularly off the Indian coasts, based on estimates derived from satellite altimeter and tide gauge data. Altimeter data analysis over the period 1993–2012 reveals that the rate of sea-level rise is spatially homogeneous over most part of NIO. The average trend in the NIO (entire basin) is close to the global mean sea-level-rise trend ( $3.2 \text{ mm yr}^{-1}$ ) estimated over the same period. The only notable exception lies in the northern and eastern coasts of the Bay of Bengal, which experience larger trends ( $>5 \text{ mm yr}^{-1}$ ). These recent trends derived from altimeter data are higher than those estimated from tide-gauge records over longer periods in the 20th century.

### **1.6.3. Sea-level variability along the coast of India**

Several studies have been carried out on sea-level variability along the coast of India in various time scales ranging from seasonal to climate change issues (Banse, 1968; Wyrski, 1973; Hastenrath and Lamb, 1979; Johannessen, et. al. 1981; Shetye et. al. 1991; Shankar and Shetye, 1997, 1999, 2001; Shankar, 2000; Shetye et. al., 2008). The aforementioned studies suggest that atmospheric circulation is dominated by the seasonally varying monsoon associated with the annual heating and cooling of the Asian continent. Das and Radhakrishna [1991] analysed sea-level data from Mumbai, Kochi, Chennai and Visakhapatnam, and showed that all stations exhibit both longer (50-60 year period) as well as shorter (4.5-5.7 year period) fluctuations. The studies by Shankar and Shetye [1997] showed formation of Lakshadweep high (low) during northeast (southwest) monsoon. The Lakshadweep high (low) propagate westward across the Arabian Sea a few months after its genesis. They concluded that, this phenomenon is a consequence of westward propagating Rossby waves radiated by the Kelvin waves propagating poleward along the western margin of the Indian subcontinent. Shankar et. al. [2002] also reported that the seasonal cycle of sea-level along the Indian coast matches with that of the observed along-shore coastal current computed from ship drifts. For example, the west India coastal current (WICC) is southward off Goa during summer monsoon (May-September) and northward during winter monsoon (November-February). The monthly mean sea-level anomaly during summer (winter) monsoon is trough (crest) due to the influence of the WICC as shown in Fig. 1.8 at Verem, Goa. It is interesting to note the sharp change in sea level from October to November, when the WICC reverses from southward to northward. Similarly, the east India coastal current (EICC) is northward (southward) during the summer (winter) monsoon off Gangavaram and Andhra

Pradesh. The monthly mean sea-level anomaly is also trough (crest) at Gangavaram (Fig. 1.8b). However, Mandapam coastal region (Fig. 1.8c) appears to be a topographically complex region because of the presence of channel between southeast India and Sri Lanka. This complexity is also reflected in the monthly mean sea-level variability at Mandapam. In any case, the sea-level variability along the Indian coast is determined partly by local forcing and partly by remote forcing (Lighthill, 1969).

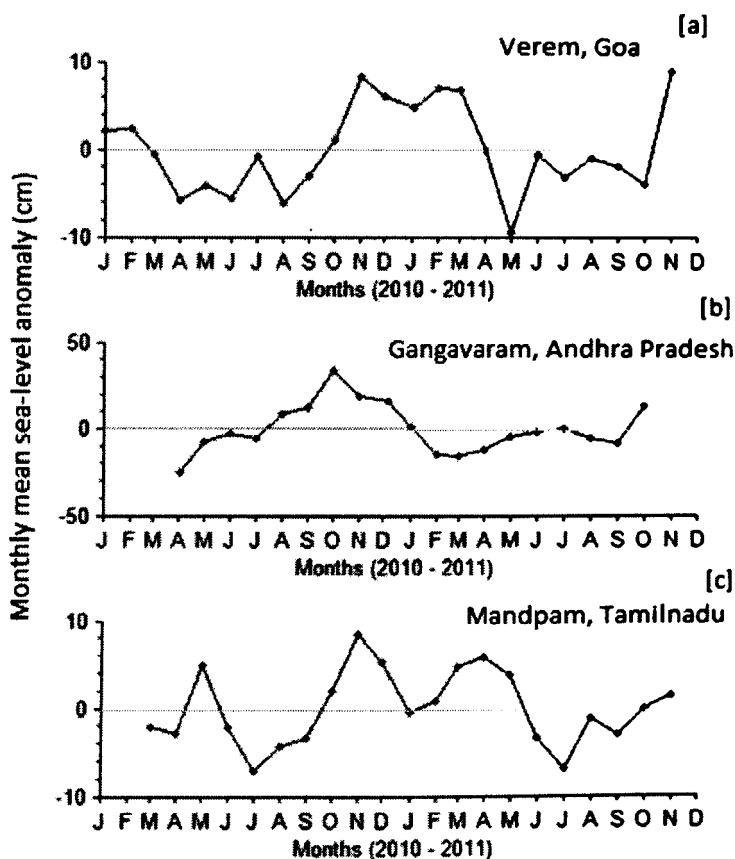


**Figure 1.8.** Monthly mean sea-level anomaly at [a] Verem, Goa, [b] Gangavaram, Andhra Pradesh and [c] Mandapam, Tamil Nadu.

Srinivas [2002] estimated that 40% variance in inter-annual sea-level is attributable to the along-shore wind stress at Kochi. Joesph et al. [2005] examined the seasonal variability of non-tidal contributions of the sea-level oscillations off Tikkavanipalem coast in Andhra Pradesh, which is located on the western boundary of the Bay of Bengal. They showed that local wind pattern, coastal current and air

pressure variations influence the residual sea-level elevation in this region. The observed response of the sea-level elevation to the barometric pressure anomalies represents an amplified/delayed inverted barometer effect. Srinivas and Dinesh Kumar [2006] studied seasonal cycle of meteorological forcing over sea-level using long-term time series data at Kochi. They showed that the equatorward alongshore wind stress and currents are the important factors for sea-level drop during the southwest monsoon. During post-monsoon, alongshore wind stress does not play any major role and the high sea-level is due to the poleward volume transport by coastal alongshore currents. Suresh et al. [2013] showed that a linear, continuously stratified ocean model reproduces observed wind-driven intraseasonal sea-level variability in the coastal waveguide of NIO. The sensitivity experiments conducted by them show that a large part of the basin-scale sea-level variations are driven by zonal wind fluctuations along the equator. During the southwest monsoon, intraseasonal wind variations become stronger over the NIO, resulting in a larger contribution of local wind forcing to sea-level variability along the west (up to 60%) and east (up to 40%) coasts of India.

#### **1.6.4. High frequency sea-level variability**

Sea-level varies at various time and space scales. It comprises of a mean level, tidal elevation and a residual elevation. Knowledge of what causes maximum water levels is often key in coastal management. Hilmi et al. [2002] listed few of the processes contributing to sea-level variation which include: glacio-eustasy, shelf subsidence due to oceanic lithosphere cooling and sediment/water loading, glacio-isostatic changes, shelf sediment accumulation (locally near large river deltas), neotectonic uplift/subsidence, geostrophic currents, low-frequency atmospheric forcing ENSO events, tides, storm surges, tsunamis, continental shelf and edge waves, and finally anthropogenic activities. The last includes water impoundment in dams and reservoirs, ground water mining, river run-off changes and subsidence due to ground water, oil and gas withdrawal locally. High-frequency sea-level oscillations with periods ranging from several minutes to a day in coastal regions are not studied sufficiently until recently due to the non-availability of fast sampling system and restrictions in technology (for e.g. storage memory, sensors, near real real-time communication, etc). Following the 2004 Sumatra devastating tsunami, most of the

countries upgraded sea-level network which is able to record the high-frequency sea-level oscillations.

Very few studies have been devoted to sea-level residuals and their long term variations. Pugh and Vassie [1976] used one year simultaneous current and water level measurements in Dowsing Region of the North Sea to study the tidal, shallow-water tidal components and the non-tidal water movements. They observed that the low-frequency residuals have very high coherence between the coastal and offshore measurements. Long-period oscillations of water level were spread across the low frequency spectrum with peaks at periods of 40 and 70 hours. Tsimplis [1995] studied the interaction between sea-level and atmospheric forcing in the Mediterranean Sea using monthly and daily mean values from days to decades. They inferred that response of sea-level to changing atmospheric pressure is frequency dependent and is almost never the theoretically predicted isostatic response of -1 cm/mb. The contribution of the wind components is found to be very small for most frequencies. Nevertheless, wind is found to be the dominant parameter characterizing the annual cycle in the north coasts of the Mediterranean.

Hilmi et al. [2000] used Hourly sea-level records from three stations in the eastern Canada (Qu'ebec-Lauzon, Harrington-Harbour and Halifax), and analyzed the data both in frequency domain from 1970 to 1979 and time domain during 1973. Their deterministic model could explain 90 to 96% of the total variability of sea-level contributed mainly by semidiurnal and diurnal tides. Residuals were observed to be less than 10% of the initial variations of sea-level, containing irregular values including extreme values of seiches and storm surges. Hilmi et al. [2002] again reviewed the sea-level data from the above stations (Qu'ebec-Lauzon, Harrington Harbour, and Halifax) and investigated the seasonal, long-term and short-term changes which occurred since the beginning of the 20th century. Their study showed that the water discharge from the St. Lawrence River contributes 29% to the monthly residual sea-level at Qu'ebec-Lauzon. The atmospheric pressure and winds contribute 8.1% and 8.9%, respectively at this station; contribute 52.1% and 7.7% at Harrington Harbour; 41.8% and 14.3% at Halifax.

In a similar attempt, Mehra et al. [2010] investigated the contribution of atmospheric pressure and local winds to sea-level variability off Goa for the period 2007–2008. The sea-level variability has been compared and statistically modelled by the use of various forcing parameters (Fig. 1.9). Wind and surface geostrophic alongshore currents were found to be coherent with the observed sea level variations. The analysis performed indicates that cross-shore wind component ( $U$ ) remains landward ( $U > 0$ ), except during winter monsoon ( $U < 0$ ) when the currents along the coast of west India returns to northward (Fig 1.9 b&c). However, during the period November–January, the local wind components are small in magnitude. The alongshore wind component  $V$  remains generally southward ( $V < 0$ ) during the period of observations (Fig. 1.9d). During the summer monsoon,  $V$  started changing direction (in May) and flowed northward with maximum energy  $\sim 1.3 \text{ m}^2\text{s}^{-2}$  during June ( $V > 0$ ). The intensity of  $V$  reduced by  $\sim 0.3 \text{ m}^2\text{s}^{-2}$  in August for the years 2007–2008, and it flowed southward during winter monsoon.

The seasonal variations in pressure are caused by the differential heat capacity resulting in thermal contrast during summer and winter between the land and the ocean. An inverse relation of winds and atmospheric pressure is evident (Fig. 1.9c, e), with a significant correlation of approx.  $-0.7$ . They observed that during summer monsoon season (May–September), the sea level variability attributable to wind is upto 47% and 75% for 2007 and 2008, respectively; however, it reduced to  $< 20\%$  during winter monsoon (November–February) season. A significant part of the variability observed in the sea level remains unaccounted for, and can be attributed to remote forcing.

Using observations in the Dee Estuary, northwest England, Brown et al. [2012] investigated components of the residual elevation within a macrotidal estuary. They stressed upon the importance of different methods to obtain residual through harmonic analysis, filtering and modelling techniques. Pasquet et al. [2013] made a systematic survey of high-frequency sea-level oscillations ( $< 6 \text{ h}$ ) measured between 2006 and 2011 along the US East Coast using 1-min resolution sea-level data. They identified, the nine most intense events, with maximum recorded wave heights ranging from 40 to 100 cm. Their study recognized two different generation mechanisms: (i) topographically-trapped edge waves which are found to be a

significant contributor to the strongest observed oscillations, and (ii) standing waves, which occur over enclosed shallow waters and may result in significant wave heights upto 100 cm.

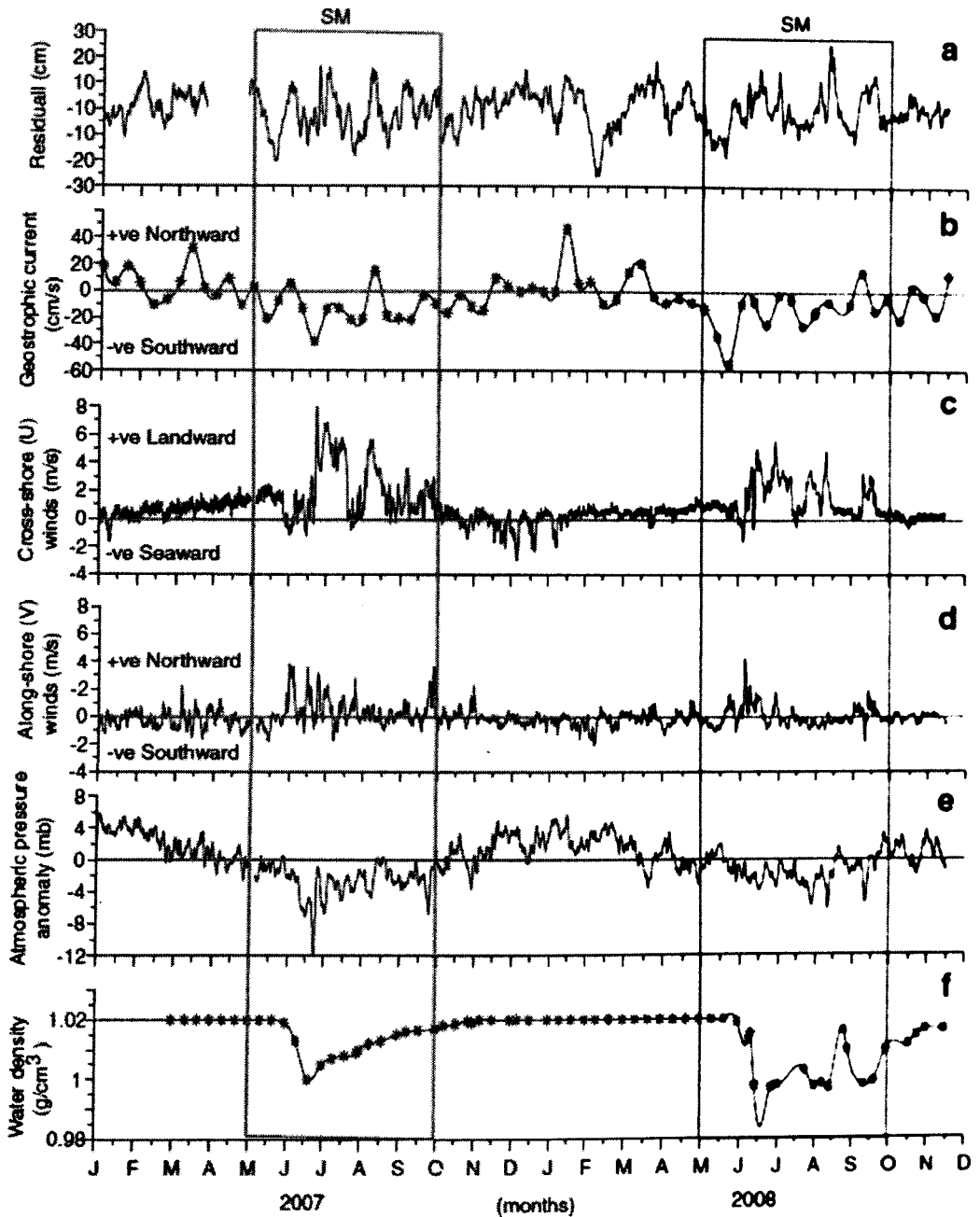


**Figure 1.9.** Hourly time series of sea-level and surface meteorological data: (a) Sea-level residual after removing the astronomical tide, (b) Geostrophic currents 'GC' estimated from the average of the current obtained from the sea-level anomaly gradient from  $13^{\circ}\text{N}$  to  $14^{\circ}\text{N}$  along the Jason satellite track 181, (c) U Crossshore wind, (d) V Along-shore wind, (e) Atmospheric pressure anomaly and (f) Water density. SM refers to summer monsoon (refer Fig. 5 of Mehra et al. 2010).

## Chapter 2

### Data and Methodology

#### 2.1 Introduction

Information on sea-level and its variability along coastal locations is essential for operational applications as well as scientific studies. Apart from safer navigational and coastal management activities at local level, sea-level data are also needed for measuring and predicting storm surges, understating the current sea-level variability and its implications to the coastal population (e.g. Church, et. al., 2001; Cazenave and Nerem, 2004), validating circulation models and calibrating satellite radar altimeters (e.g. Griffies and Greatbatch, 2012; Chang-Kou and Carl, 2011; Richard and Byrne, 2010). On a global scale, sea-level studies are crucial to understand changes in the earth's climate and its multi-decadal fluctuations (e.g. Chamber et al., 2012; Woodworth et al., 2009; Feng et al., 2004). The average global sea-level rise which is consistent with warming is estimated at an average rate of 1.8 [1.3-2.3] mm per year over the period 1963 to 2003 (Bernstien et al., 2007). However, the impact of the powerful December 2004 global tsunami (Titov *et al.*, 2005; Joseph *et al.*, 2006), the historically known vulnerability of the Indian coasts to storm surges (Joseph and Prabhudesai, 2005) and the disastrous consequence of Japan Tsunami (11 March, 2011), emphasize the need for near real-time reporting of sea-level, sea-state and surface meteorological information for multi-hazard monitoring and warning purpose. Although a single system at a given location may not be of much practical use for warning, a network of spatially distributed near real-time reporting gauges in the coastal and island locations will be greatly beneficial to disaster managers and local administrators because a signal of any natural event takes time to travel from the source region to a distant location. In such a situation, a network of near real-time reporting gauges will allow monitoring the progress of the event, helping the decision-makers to take necessary precautions.

The December 2004 Indian Ocean tsunami episode prompted all the countries with ocean boundaries to prepare for a possible disaster due to tsunamis and storm surges. Since then, many countries have developed and deployed deep-ocean tsunami monitoring systems and networks of near real-time monitoring coastal sea-



level gauges. It is prudent for countries with coastlines vulnerable to tsunamis and storm surges to have prior knowledge of technologies that are suitable for their specific needs. As many of the countries that are threatened by tsunamis are resource-limited, choosing the wrong or inappropriate technology may lead to heavy casualties during the next episode. A comprehensive description that offers an unbiased comparative evaluation and assessment of the optimum technology suitable for specific situations is given by Joseph [2011]. Martin et al. [2005, 2008], Kranz et al. [2001] and Woodworth and Smith [2003] reported the test results of radar tide gauges manufactured by different firms and comparison between other types of gauges. Thus, relative performance of different systems and evaluation of technologies serve as a reference to the personnel responsible for protecting the coastal population.

In this chapter, an Integrated Coastal Observation Network (ICON), established by the CSIR-National Institute of Oceanography, Goa which is internet-accessible, providing cellular based near real-time sea-level, sea-state and surface meteorological observations at several locations on the Indian coast and islands are described (Fig. 1.6; <http://inet.nio.org>) along with other data sources. The sea-level and meteorological data collected by ICON have been used in this research work to study sea-level variations at different locations and its response to meteorological events in the north Indian Ocean. In this chapter, the sea-level measurements using microwave-radar and pressure sensor based sea-level gauges (SLG), autonomous weather station (AWS) and ICON are briefly described. The sea level measurements at Verem, Goa and Tuticorin and Mandapam, Tamil Nadu obtained from the downward-looking aerial microwave radar and pressure gauge have also been utilised. The importance of atmospheric pressure variability in estimating the sea-level using sub-surface absolute pressure gauges is also evaluated.

## **2.2. Sea-level measurements**

The most common sea-level measuring technologies are stilling-well and float, pressure system, acoustic system and radar system (IOC, 2006). ICON uses pressure and microwave based radar sensors to measure the sea level. The principle of operation of pressure and radar gauge systems are briefly described below.

### 2.2.1. Pressure Gauge

This system measures the subsurface pressure (Fig. 2.1) according to the following relation:

$$h = \frac{(p - p_a)}{\rho \times g} \quad (2.1)$$

where,  $h$  is the height of the instantaneous sea surface above the pressure port,  $p$  is the measured subsurface pressure,  $p_a$  is the atmospheric pressure,  $\rho$  is the water density and  $g$  is earth's gravitational acceleration. Therefore, this system requires knowledge of local atmospheric pressure, water density and local gravity. The density ' $\rho$ ' is important in estuarine waters, as it undergoes seasonal variability due to changes in fresh water influx as well as semi-diurnal variability of tidal cyclicality. In such cases, density corrections need to be incorporated during post processing. However, in locations where the water is well mixed, density can be considered constant. The pressure sensors can be directly mounted along the jetty to monitor subsurface pressure as shown in Fig. 2.1. The sensor is connected by a cable carrying signal and power to the electronics unit placed onshore. The acquired data then can be transmitted using communication link (VHF, GPRS or satellite link) to remote monitoring unit. The sensor is usually placed in a copper or titanium housing to limit the marine growth. In the case of non-availability of stable platforms or data acquisition for short duration (couple of months) the self-recording type pressure gauge may be placed securely on the sea bed, however this method may require a diving team for maintenance. Fixing datum is a major problem for single pressure sensor measurements. A method frequently adopted is to make visual measurements against a tide staff over a period of one day and repeat this at regular intervals. Individual measurements should be accurate to 2–3 cm and on average should fix the datum to approximately centimeter accuracy (IOC, 2006).

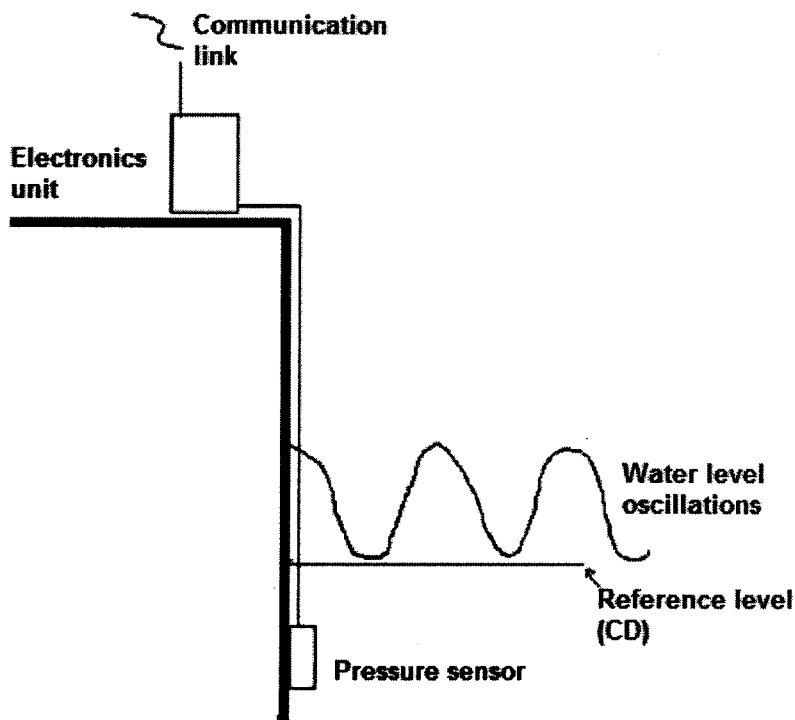


**Figure 2.1.** Schematic diagram of subsurface pressure sensor based sea-level gauge.

The pressure gauge at the Verem jetty uses pressure sensor from Honeywell Inc. (Table 2.1) and is deployed ~1 m below the chart datum. The electronics, power supply and solar panel are mounted at the top of the mounting structure fixed to the jetty as shown in Fig. 2.2. The self recording type pressure gauges from Sea-Bird electronics Inc. with metallic housing were deployed near the radar gauges, resting on the sea-bed (depth ~2 m) at Tuticorin and Mandapam. The metallic housing of the pressure gauge also acts as dead weights (~50 kg) to minimize the drift of the gauges; it was anchored with chains to the nearby jetty. The self recording type tide gauges are self-contained instruments powered by batteries. They are extensively used for short term measurements of coastal sea-level for comparative studies, coastal engineering applications and obtaining initial tidal knowledge of an area.

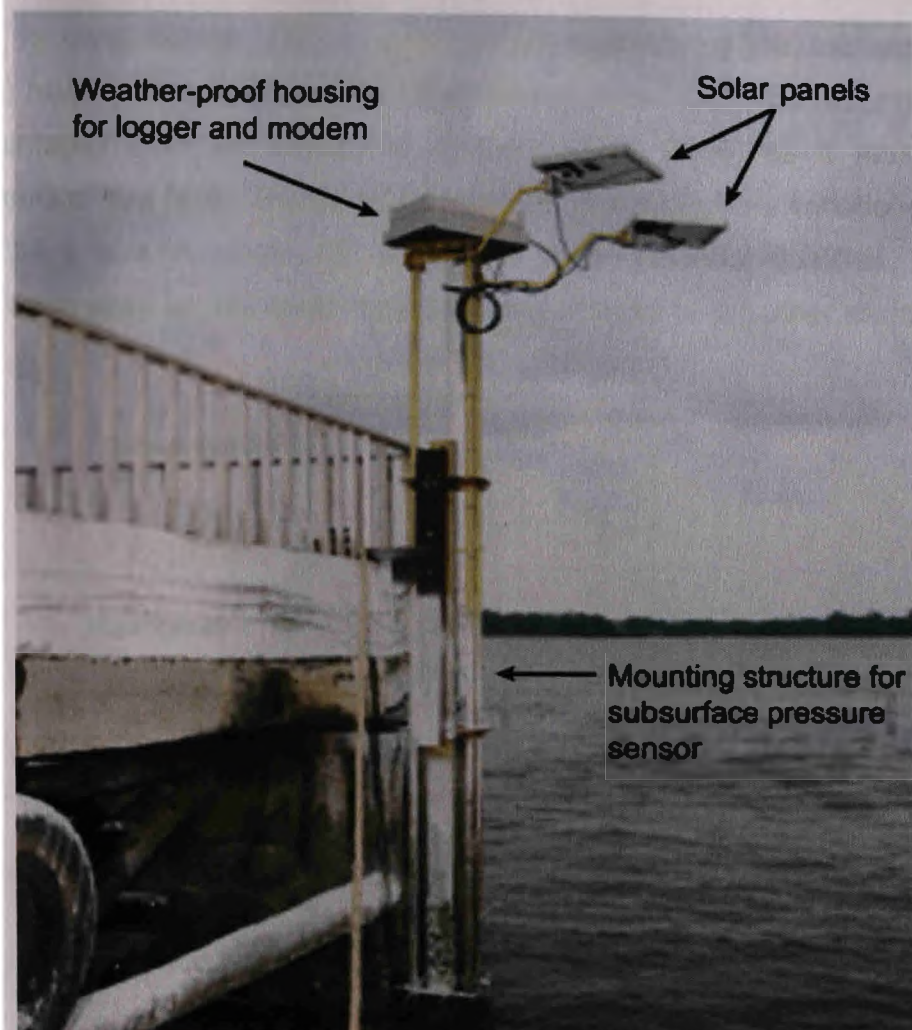


**Figure 2.2.** Typical installation of a subsurface pressure gauge at Verem, Goa.

### 2.2.2. Radar Gauge

Radar level sensor is a non-contact device that is capable of remote measurement of sea-level elevation from the air. The radar sensor is positioned well above the highest expected sea-level (also the highest expected wave to avoid damages to the unit) and measures the aerial distance from the sensor to the water surface (Fig. 2.3). The transmission frequency of the radar sensor is  $\sim 24$  GHz and the beam width is  $\sim \pm 5^\circ$ . The basic principle involved in the operation of the radar sensor is transmission of microwave pulses towards the sea surface and reception of the reflected/backscattered energy. The reflected microwaves are analyzed to estimate the aerial distance travelled by a given pulse. When averaged over 30 s, it filters out short-period variability due to wind-waves and swells. Sea-level elevation ( $H$ ),

referenced to chart datum (CD) is obtained by subtracting the measured aerial distance ( $L$ ) from the height ( $K$ ), of the radar sensor above CD. The radar gauge has many advantages over the traditional systems (IOC, 2006) as it makes direct measurements of sea-level. The effect of density and temperature variations, even in the atmosphere is unimportant. On account of these superior qualities, the radar gauge has been used for sea-level measurements at most of the other locations.

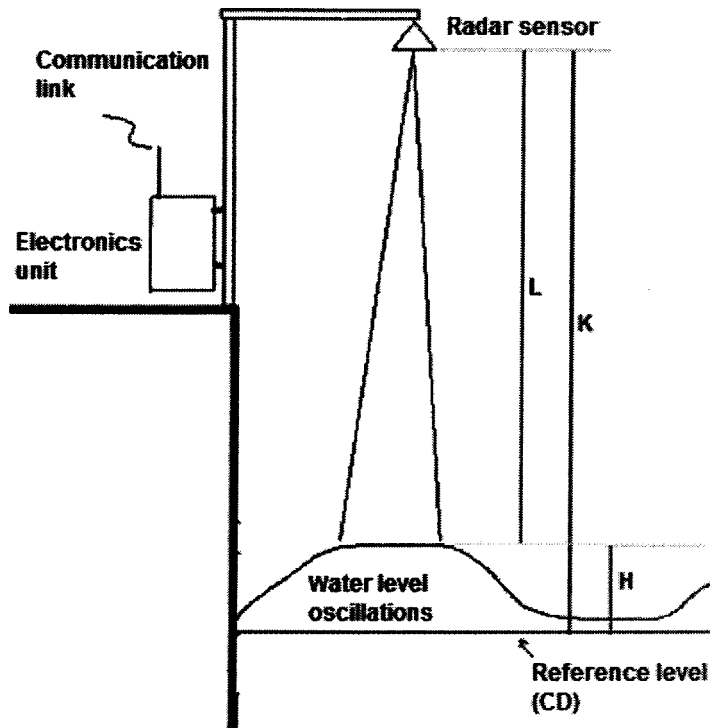


**Figure 2.3.** Schematic diagram of downward looking microwave radar sensor based sea-level gauge.

Typical radar based sea-level gauge installed at Ratnagiri, Maharashtra is shown in Fig. 2.4. The radar level sensor from OTT Hydromet GmbH (OTT-RLS) is used in the radar gauges of ICON in order to meet the national and international needs of sea-level monitoring and compatibility to the Global Sea Level Observation (GLOSS) program. Specifications of the sensors are listed in Table 2.1.

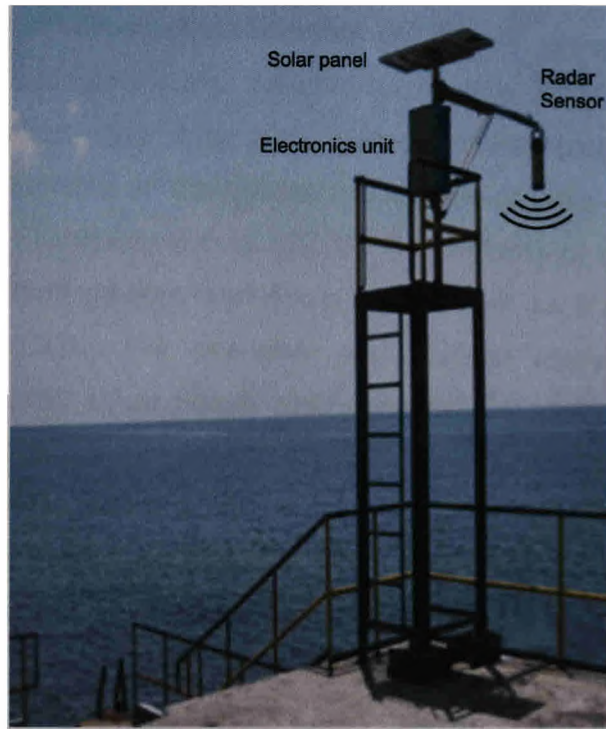


**Figure 2.4.** Typical installation of downward-looking aerial microwave radar gauge at Ratnagiri, Maharashtra.

**Table 2.1.** Major technical specifications of the sensors used in radar gauge and pressure gauge deployed at Verem, Goa and SBE26 deployed at Tuticorin and Mandapam, Tamil Nadu.

S. No.	Specifications	Radar gauge sensor		Pressure gauge Sensor
1	Make	OTT Hydromet GmbH.	Honeywell Inc. Precision Pressure Transducer-Ruggedized (PPTR)	Seagauge SBE26plus Sea-Bird Electronics
2	Range (m)	2-30	0-18	0-20
3	Accuracy (mm)	± 3	±18	±3
4	Resolution (mm)	1	0.2	0.01
5	Integration time (min)	5	5	1

### **2.3. Integrated Coastal Observation Network (ICON)**

In-house designed and developed Internet-accessible near real-time reporting cellular based sea-level, sea-state and surface meteorological (Met) stations deployed at several locations on the coasts and islands of India (Fig. 1.6) have been described in detail by Prabhudesai et al. [2010]. The network of autonomous weather stations (AWS), sea-level gauges and wave rider buoys as shown in Fig. 2.5 are incorporated in the ICON. The sea-level and surface meteorological data are acquired using dedicated Linux based data loggers and uploaded to an Internet server at 5 and 10-min intervals, respectively with the use of GPRS cellular modems. The sensors and data loggers are powered from sealed lead acid batteries, which are charged through solar panels (Figs. 2.2, 2.4 & 2.5). The ICON provides graphical presentation of sea-level information (observed sea-level, predicted tide and sea-level residual, Fig. 2.7) and surface meteorological information such as vector-averaged wind speed & direction, barometric pressure, atmospheric temperature, relative humidity, solar radiation and rainfall (Fig. 2.9). The network maintains accurate time-stamp of the dataset through Internet-time synchronization using network time protocol (NTP). The ICON provides several benefits such as remote monitoring of individual stations, remote health monitoring to aid timely maintenance and periodic arrival of data stream from all stations at a single central server. The ICON data could be assimilated to real-time running of numerical models for operational forecast. The network allows internet based near real-time tracking and monitoring of sea-level, sea-state and meteorological conditions along the Indian coasts and islands and from almost anywhere having a considerable practical significance during natural disasters such as storms, storm-surges and tsunamis.



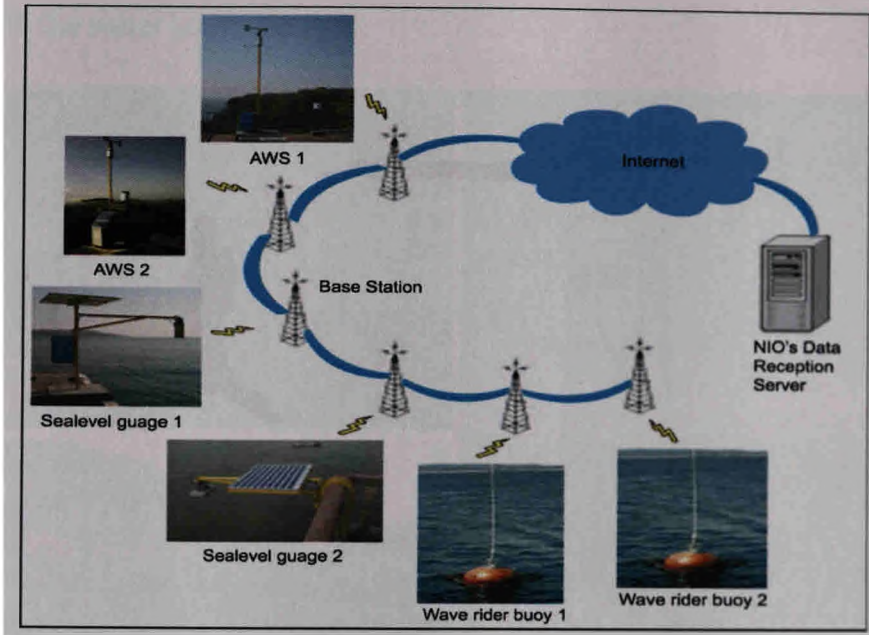


**Figure 2.5.** Network of near real-time reporting sea-level, sea state and surface meteorological stations (schematic).

### 2.3.1. Sea-level gauge

The sea-level gauge developed using downward-looking aerial microwave radar sensors is incorporated in the sea-level station network of NIO (refer section 2.2.2). The accuracy of sea-level measurements using the microwave radar principle is within  $\pm 1$  cm. The mounting mechanism of sea-level gauge depends upon the site available. Different types of sea-level gauge installation made under ICON are shown in Fig. 2.6. The sea-level gauge presents measured sea-level, tide and sea-level residual in graphical format as shown in Fig. 2.7. The main advantages of the downward-looking aerial microwave radar based sea-level measurements are the following:

- Sea-level measurements are insensitive to variations in air temperature, humidity and rainfall.
- Installation does not require conventionally used 'tide gauge cabin' and stilling-well.
- Can be installed at coastal jetties, bridges, harbour piers or offshore platforms with relatively lesser logistic problems.



- Trouble-free installation and maintenance due to absence of physical contact with the water body.



**Figure 2.6.** Typical installation of downward-looking aerial microwave radar sensor based sea-level gauges incorporated in the NIO's ICON at [a] Karwar, [b] Port Blair and [c] Dona Paula.

An advantage with the non-contact measuring principle used in the microwave radar gauge is that problems such as disruption of measuring operation caused by high water, silt accumulation, debris, plant growth and time-consuming maintenance are reduced considerably. Because of its compact design, the gauge can be installed easily and inconspicuously without the use of cumbersome stilling-well/protective-well. Further, the device is particularly suitable for areas where conventional measuring systems cannot be used or where a station needs to be set up quickly and inexpensively. Because the gauge does not come in direct physical contact with water, it is particularly useful for measurements from locations where the water contains a large amount of suspended matter.

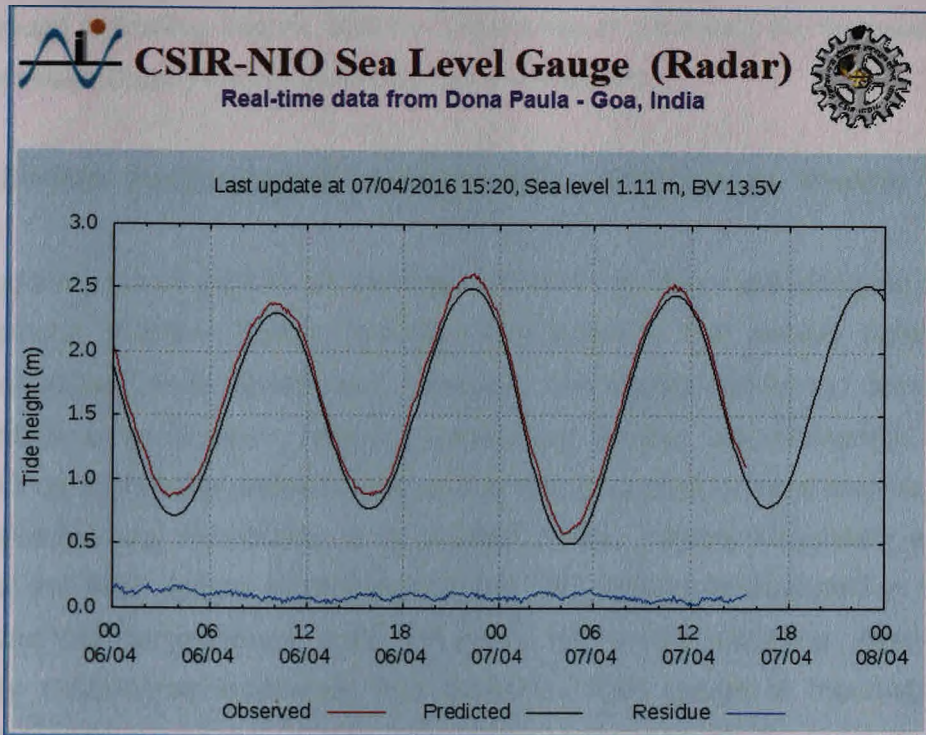


**Figure 2.7.** Near real-time data from CSIR-NIO sea-level gauge accessible at <http://inet.nio.org>.

A relatively meritorious feature that can be attributed to radar sensor based sea-level gauge is its suitability of measurement of large sea-level oscillations such as those occur during tsunamis. However, this feature can be achieved only if the gauge is suitably installed, taking this requirement into consideration. For example, the measurement range of radar sensor used in the present network is 1.5 to 30 m. However, the footprint of the beam increases as the distance of the radar sensor from the sea surface increases. Thus, more the distance between the radar sensor and the sea surface, more the safety distance between the vertically oriented central axis of the radar beam and the wall of the jetty where the gauge is erected. The recommended safety distance for the radar used in the NIO network (radiation angle =  $\pm 5^\circ$ ) to achieve the full range of 30 m is 3m.

An observed limitation with the radar based sea-level gauge is contamination of sea-level measurements by man-made lapses such as anchoring of floating objects below the radar sensor. This indicates the sensitivity of aerial microwave



radar gauge to floating objects, and the importance of protecting the footprint area of the microwave radar from contamination by such objects.

### 2.3.2. Surface meteorological measurements: Autonomous Weather Station (AWS)

The surface meteorological parameters acquired by the meteorological stations (Autonomous Weather Station [AWS]) incorporated in the present network are vector-averaged wind speed and direction, barometric pressure, atmospheric temperature, solar radiation, relative humidity and rainfall. The mechanical parts of the AWS consist of Stevenson's cage with a mounting stud for wind monitor and an electronics-housing mountable on a suitable flange. Typical installation schemes used for the AWS system incorporated in the NIO network is illustrated in Fig. 2.8. Hinge-and-lock arrangement used for fixing the sensor-mounting tower allows relatively trouble-free installation and servicing. Rain gauge is mounted as an independent device. However, like other sensors, it is electrically connected to the logger.



**Figure 2.8.** A typical installation of AWS in NIO's ICON at [a] Ratnagiri, Maharashtra and [b] Gopalpur, Odisha.

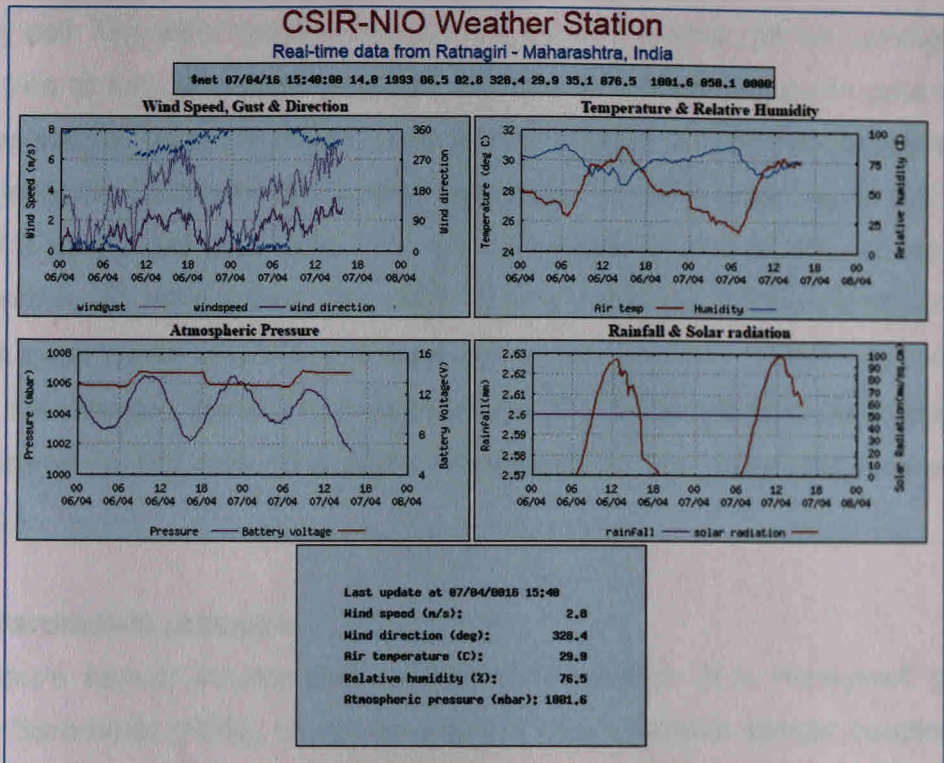


**Figure 2.9.** Near real-time data from CSIR-NIO Autonomous Weather Station accessible at <http://inet.nio.org>.

In the AWS, each parameter is sampled at an interval of 10 s. Surface meteorological measurements are recorded at 10-minutes interval, and each measurement is an average over 10 minutes (*i.e.*, average of 60 samples). Wind is vector-averaged. Gust (maximum wind speed within every 10-minute sampling) is also recorded. Thus, the 'gust' value recorded is the largest wind speed amongst an ensemble of 60 samples that are detected during the 10-minute sampling span. The acquired data in graphical form is also uploaded over internet for various stakeholders as shown in Fig. 2.9. Brief descriptions of the sensing methodologies are provided below and specifications are listed in Table 2.2.

### 2.3.2.1. Wind velocity

An anemometer (RM Young Model 5103), consisting of a propeller and a vane integrated into a single unit, measures the horizontal wind speed and direction. The sensor features near neutral torque. The speed sensor is an 18-cm diameter 4-bladed helicoid polypropylene propeller, which is coupled to a centrally mounted

stationary coil. The wind direction sensor is a balanced vane (38 cm turning radius), which is free to turn on sealed bearings, coupled to a linear precision potentiometer (10 k $\Omega$  resistance, 0.25% linearity). During wind-driven rotation of the propeller, a six-pole magnetic disc mounted on its shaft induces an AC sine wave signal in the coil at a rate of 3 cycles per revolution. The output frequency and amplitude are directly proportional to the wind speed. The AWS circuits mask the amplitude-signal through a back-to-back diode limiter-circuit and clamp the signal to  $\pm 0.6$  V. A comparator converts the clamped signal into a square wave at a threshold level corresponding to a wind speed of 0.5 m/s. The built-in hysteresis in the comparator avoids false triggering.

#### **2.3.2.2. Barometric pressure**

The pressure sensor incorporated in the AWS consists of a Honeywell precision Pressure Barometer (HPB), based on a silicon piezoresistive sensor coupled with a microprocessor. With pressure- and temperature-sensitive elements, the microprocessor corrects the sensor's non-linearity using a built-in calibration facility.

#### **2.3.2.3. Solar radiation**

A photodiode sensor (LICOR-LI200) which generates a DC current proportional to the incoming solar radiation (90  $\mu$ A per 1000 W/m<sup>2</sup>) in a broad spectrum of wave length is used for the measurement of solar radiation.

#### **2.3.2.4. Air temperature**

A linearized thermistor [YSI 44202] based temperature probe is used. This probe is mounted within a sun-shield similar to Stevenson's grid to inhibit direct solar heating.

#### **2.3.2.5. Relative humidity**

Rotronic MP-100 a capacitive type sensor, exclusively designed for outdoor applications, is used. Its dielectric properties vary in response to changes in the amount of water content in air and the ambient temperature. The active part of the sensor is a condenser, made of polymer foil sandwiched between two flat electrodes. A porous Teflon foil protects the sensor. The humidity probe mounted inside a

Stevenson's cage protects it from direct solar heating and allows free circulation of air.

### 2.3.2.6. Rainfall

An electrical version of the conventional tipping bucket rain gauge (RM Young Model 052202), whose catchment area is 200 cm<sup>2</sup> and measurement resolution 0.1 mm, is used for the measurement of rainfall.

**Table 2.2.** Specifications of in-house (NIO) developed autonomous weather station.

Specifications		
Sensor/Make	Range	Accuracy
Wind speed and wind direction (RM Young)	0-60 m/s 0-360 <sup>o</sup>	0.2 m/s 3 <sup>o</sup>
Air temperature (YSI)	0 - 45 <sup>o</sup> C	± 0.15 <sup>o</sup> C
Barometric pressure (Honeywell)	800 - 1060 mbar	0.4 mbar
Humidity (Rotronic)	0 - 100% RH	3 %
Solar radiation (Licor)	0-300 mW/cm <sup>2</sup>	5%
Rainfall (RM Young)	-	3% upto 50 mm/h
Data logger (NIO)	Based on 80c51f121 with RTC & 512 Mb MMC card and Embedded Linux TS7260 SBC	
Power supply	12V Battery and solar panel	
Intranet /Internet connectivity	Ethernet / Cellular GPRS	

Sea-level gauge which measures sea-level is described in detail by Prabhudesai et al. [2006 and 2008]. The sea-level data is sampled over 30 s window at every 1-minute and the average over 5-minutes duration is recorded every 5 minutes. The surface meteorological parameters are collected by autonomous weather station (NIO-AWS). AWS samples data every 10 s over a window of 10 minutes, averaged and then recorded at every 10 minute interval. Measurement locations of data used in the present study are provided in Table 2.3. Data duration and events considered for different studies are mentioned in the respective chapters.

**Table 2.3.** Summary of field observations (ICON) from different coastal and island locations of India considered in the present study.

1. Sea-level data from Kochi harbour is not a part of ICON.

S. No	Measurement Station	Position		Location type	System	Distance between AWS & RG (m)
		Lat (°N)	Lon (°E)			
1	Gopalpur, Odisha	19.3081	84.9613	Harbour	AWS	255
		19.3069	84.9634		RG	
2	Gangavaram, Andhra Pradesh	17.6174	83.2322	Harbour	AWS	726
		17.6235	83.2295		RG	
3	Kakinada, Andhra Pradesh	16.9764	82.2832	Harbour	AWS	2
		16.9764	82.2832		RG	
4	Yanam, Andhra Pradesh	16.7082	82.2734	Godavari River	RG	
5	Port Blair, Andaman & Nicobar Islands	11.7099	92.7386	Open Ocean	AWS	2984
		11.6884	92.7222		RG	
6	Mandapam, Tamil Nadu	9.2763	79.1295	Boundary of Palk Strait & Gulf of Mannar	AWS	615
		9.2713	79.1321		RG	
7	Tuticorin, Tamil Nadu	8.7500	78.2021	Gulf of Mannar	AWS RG	20
8	Colachel, Tamil Nadu	8.1714	77.2549	Open Ocean	RG	-
9	Kochi	9.7455	76.2842	Harbour	Float gauge	-
10	Kavaratti, Lakshadweep island	10.57172	72.6354	Open Ocean	AWS	2
					RG	
11	Malpe, Karnataka	13.5886	74.9208	Estuary	RG	-
12	Karwar, Karnataka	14.8464	74.1317	Open Ocean	AWS	5154
		14.8030	74.1144		RG	
13	Verem, Goa	15.4554	73.8022	Mandovi estuary	AWS	5265
		15.5019	73.8120		RG	
14	Ratnagiri, Maharashtra	16.8926	73.2758	Cove	AWS	525
		16.8890	73.2853		RG	



## **2.4. Other data sets: sea-level and surface met**

Apart from sea-level data under ICON, data (hourly sea-level) from a few more locations (Minicoy, Hanimaadhoo, Colombo, Kochi, Karachi, Chabahar, Jask and Masirah), from the Indian Ocean, have also been used ([www.gloss-sealevel.org](http://www.gloss-sealevel.org)).

The tropical cyclone track data from India Meteorological Department (IMD, [www.imd.gov.in](http://www.imd.gov.in)), Joint Typhoon Warning Center (JTWC, [www.usno.navy.mil/JTWC/](http://www.usno.navy.mil/JTWC/)) and UNISYS-Unisys Weather (<http://weather.unisys.com/hurricane/>) have been used to study the coastal sea level response during the tropical cyclones.

## **2.5. Processing of data**

ICON comprising of sea-level gauge (SLG) and autonomous weather station (AWS) provides data from the field locations to the server installed in CSIR-NIO, Goa. To process the raw data, various routines developed in C programming language and MatLab have been used. AWS provides surface meteorological data in respective engineering units and used directly for further analysis. However, the raw data file from the microwave radar based SLG provides distance between the sensor and the air-sea interface (Fig. 2.3). A suite of routines/algorithms are developed to convert the raw data into the usable engineering units and identifying/filling data gaps.

### **2.5.1. Data quality, checks and editing**

A C-program was written to check and edit the raw data files from AWS and SLG. Each record in the input raw data file was checked for consistency in each column, parameters, and must fit within a specified range in order to detect any missing fields. Consistency in time was verified by counting records between successive date/time labels in the file. Time jumps or gaps in records were automatically filled with NaNs and single gap in the record were compensated by interpolating the missing value.

### **2.5.2. Harmonic analysis**

Sea-level data was de-tided using TASK tidal analysis and prediction program (Bell et al., 2000) to obtain sea-level residual (SLR). In order to isolate the non-tidal higher frequency component in the data (i.e. SLR), the predicted tides were subtracted from the original records and further analysis was then performed on the residual series. This method is not suitable for data series that are not long enough to permit a



reliable calculation of the tidal constituents, and therefore records having at least one month of sea-level data were taken-up for harmonic analysis.

### 2.5.3. Spectral analysis

The sea-level and meteorological data were also used to calculate energy distributions and power spectra. 50% overlapping segments were taken in each case. Trend and mean were removed and Hamming window was applied to each segment. Each segment was then subject to Fast Fourier Transform (FFT) analysis to calculate spectra using the Welch method. Welch's method is implemented in the Signal Processing Toolbox function as  $pxx = pwelch(x)$  which returns the power spectral density estimate of the input signal  $x$ . The method consists of dividing the time series data into (possibly overlapping) segments, computing a modified periodogram of each segment, and then averaging the PSD estimates. The result is Welch's PSD estimate. By default, the data is divided into eight segments with 50% overlap between them. The spectra obtained over a long series suppress the influence of transient effects and the results thus determine the general phenomenology in the region of the measuring station.

Rabinovich [1997] proposed an approach to separate the influence of source and topography in observed tsunami/meteorological sea-level spectra. The method assumed a linear tide gauge response to external forcing and is based on comparative analysis of tsunami/meteorological and background spectra. This method has been used to understand the resonant influence of local topography and spectral characteristics of SLR during an event at a particular location.

### 2.5.4. Regression Model

A multi-linear regression model linking sea-level and atmospheric parameters has been established and used. The model can be described in general as:

$$\eta = B_0 + B_1\tau_U + B_2\tau_V + B_3A_p + \epsilon \quad (2.2)$$

In the above equation, sea-level residual ( $\eta$ ) is the dependent variable and the independent variables are cross-shore (along-shore) wind stress  $T_U$  ( $T_V$ ) and

atmospheric pressure ( $A_P$ ).  $B_0$ ,  $B_1$ ,  $B_2$  and  $B_3$  are regression coefficients and  $\epsilon$  is the difference between the measured and estimated SLR from multi-linear regression. How well, the model describes the sea-level residual is assessed by looking at the percentage of sea-level variance explained ( $Var_e$ ) by the model.

$$Var_e = \left(1 - \frac{\text{variance}(\epsilon)}{\text{variance}(\text{measured SLR})}\right) \times 100 \quad (2.3)$$

### 2.5.5. Comparison method

In general, to evaluate the accuracy or compare different measurement systems, the difference or error, especially the root-mean-square-error (RMSE) is used. As discussed by Willmott [1981] and Willmott et al. [1985], correlation coefficient ( $r$ ) and its square, the coefficient of determination ( $r^2$ ) may not be consistently related to the accuracy of predictions. Therefore, in this study, measures such as mean, standard deviation, the intercept and slope of the least square regression with PG on y-axis and RG on x-axis were computed. The different measures were derived from the fundamental quantity ( $P_i - O_i$ ), where  $P$  is predicted/ measurements under test and  $O$  is the reference standard. In the present study, the measurements from RG (PG) refer to  $O(P)$ . The different measures calculated are briefly defined below (for detailed explanation, please refer to Willmott [1982]):

$$MAE = N^{-1} \sum_{i=1}^N |P_i - O_i| \quad (2.4)$$

$$RMSE = [N^{-1} \sum_{i=1}^N (P_i - O_i)^2]^{0.5} \quad (2.5)$$

The systematic part of the error is:

$$RMSE_s = [N^{-1} \sum_{i=1}^N (\hat{P}_i - O_i)^2]^{0.5} \quad (2.6)$$

The unsystematic part is:

$$RMSE_u = [N^{-1} \sum_{i=1}^N (P_i - \hat{P}_i)^2]^{0.5} \quad (2.7)$$

The index of agreement ( $d$ ) is of the form

$$d = 1 - [\sum_{i=1}^N (P_i - O_i)^2 / \sum_{i=1}^N (|P_i'| + |O_i'|)^2], \quad 0 \leq d \leq 1 \quad (2.8)$$

where,  $N$  is the number of data points,  $\hat{P}_i = a + bO_i$  is the least square regression

with the intercept ( $a$ ) and slope ( $b$ ),  $P'_i = P_i - \bar{O}$  and  $O'_i = O_i - \bar{O}$ .

## 2.6. Comparison of sea-level data

Sea-level data were collected off Goa (Fig. 1.6) from January 2009 to May 2010 using near real-time reporting pressure and radar gauges at Verem, located near the mouth of the Mandovi estuary. The pressure gauge data were sampled at 2 Hz frequency for five minutes duration (600 samples), averaged, and subsequently recorded in the data-logger at every five minutes. The radar gauge samples were acquired over 30-second window at 1-minute interval and averaged over 5-minutes interval. Atmospheric pressure measurements collected from an AWS installed ~5 km away from the sea-level station were used for retrieving sea-level measurements from the absolute pressure (i.e. water pressure + atmospheric pressure) measurements acquired by the subsurface pressure gauge. For comparison, we have used time-series data at 10-minutes interval. The recording type pressure gauges deployed at Tuticorin and Mandapam acquired data at an interval of 10 minutes with integration duration of 1 minute. The AWS was installed at Mandapam near the radar gauge (~500 m distance), and ~115 km from the Tuticorin. The barometric pressure from this AWS was used for atmospheric pressure correction for both the pressure gauges at Tuticorin and Mandapam as the atmospheric perturbations have spatial characteristics of a few hundred kilometers (Table 2.4).

**Table 2.4.** Summary of observations (Refer Table 2.3 for position of the measurement stations).

Station	Distance between RG & PG	Measurement duration
Verem	50 m	January 2009 to 31 May 2010
Tuticorin	500 m	June 2010 to 14 March 2011
Mandapam	10 m	June 2010 to 12 March 2011

### 2.6.1. Sea-level variations in the north Indian Ocean

Sea-level measurements reported by radar and pressure gauges during January 2009 to May 2010 from Verem, Goa, located on the central west coast of India are shown in Fig. 2.10. Both the systems reported a tidal range upto 250 cm with fortnight variation in spring and neap tides (Fig. 2.10 a&b). The tides off Verem have

a 'form number' of 0.64, implying that the tides are mixed, mainly of semi-diurnal nature (Murty and Henry, 1983). When the tidal signal was removed from the sea-level records using the TASK (Bell et al., 2000) tidal analysis and prediction algorithm, both the systems produced similar sea-level residuals (SLR) as shown in Fig. 2.10 c&d.

The monthly SLR variance presented in Fig. 2.11 shows negligible difference. The high SLR variance ( $\sim 163 \text{ cm}^2$ ) found in November 2009 is the response of the sea-level to the tropical cyclonic storm 'Phyan', which developed in winter in the southeastern Arabian Sea and swept northward along the eastern Arabian Sea during 9–12 November 2009 (Joseph et al., 2010). Tidal range at Tuticorin (Mandapam) during the measurement period is  $\sim 125$  (126) cm (Fig. 2.12 a,b,d&e). The mean difference at Tuticorin (Mandpam) is  $\sim 2.1$ (1.1) cm as shown in Fig. 2.12 c&f (Table 2.5).

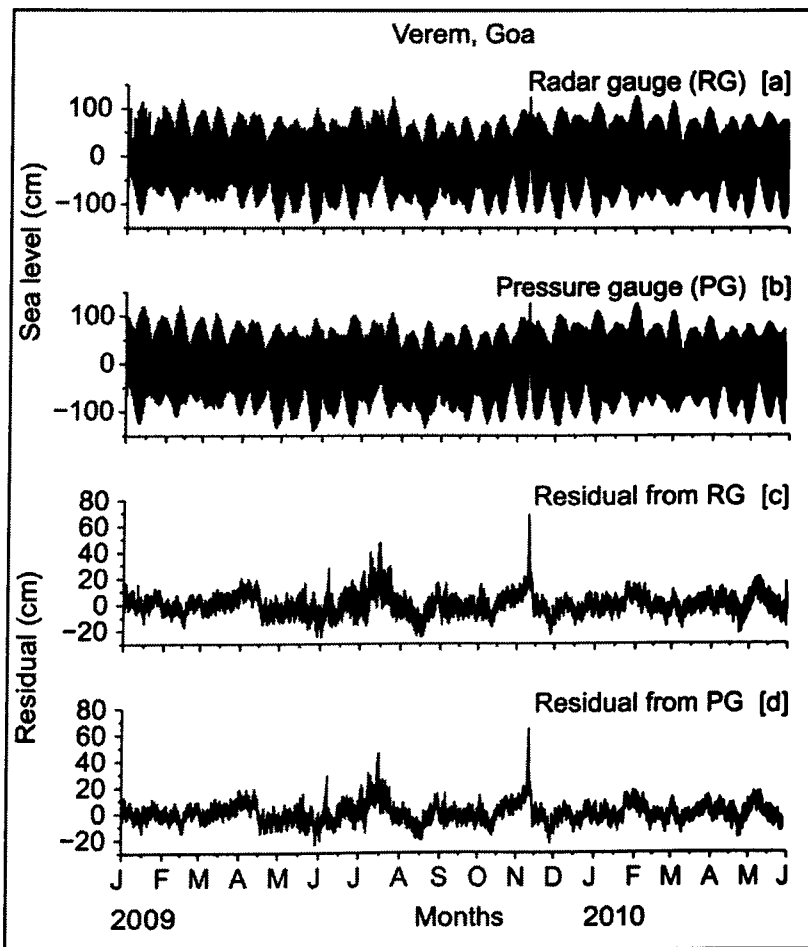


**Figure 2.10.** Sea-level measurements at Goa using [a] radar gauge (RG), [b] pressure gauge (PG) and respective residuals from [c] RG and [d] PG.

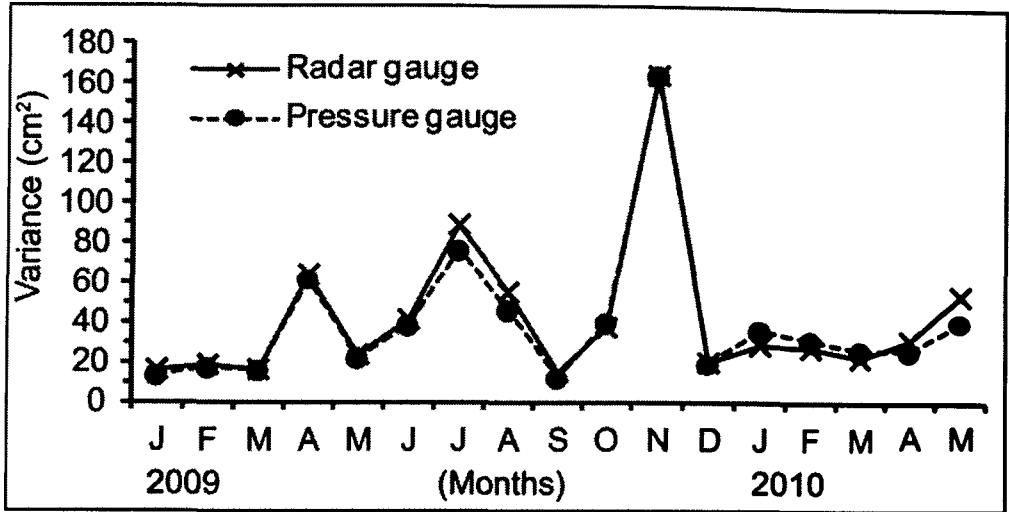


Figure 2.11. Monthly sea-level residual (SLR) variability at Verem, Goa.

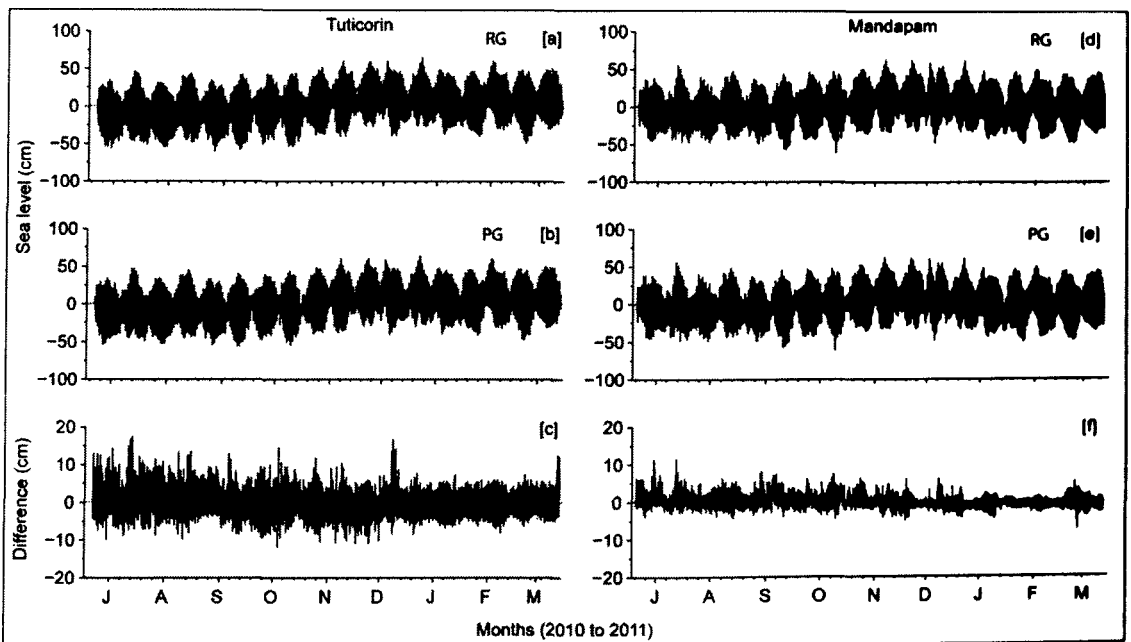
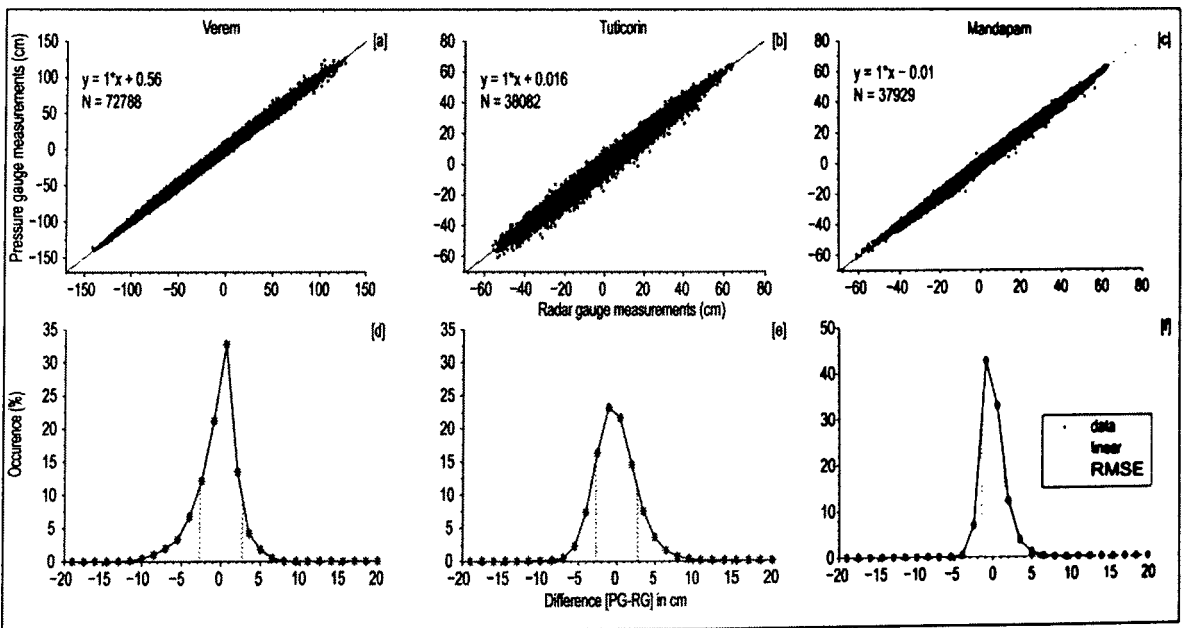


Figure 2.12. Sea-level measurements at Tuticorin using [a] radar gauge (RG), [b] pressure gauge (PG), and [c] difference (PG-RG) and at Mandapam using [d] radar gauge (RG), [e] pressure gauge (PG) and [f] difference (PG-RG).

### 2.6.2. Comparison of sea-level measurements from radar and pressure gauges

To evaluate and compare the results of RGs and PGs, the anomaly, i.e. mean value of the time series has been removed. Scatter plots along with quantitative indices are shown in Fig. 2.13 (also refer Table 2.5). From Fig. 2.13 a,b&c, it is clear that for all

the three sites, the slope ( $a$ ) is 1 and bias ( $b$ ) is less than 0.6 cm. Also, it appears that the variance of sea-level is higher at Tuticorin than Mandapam with an energy of  $\sim 7.48 \text{ cm}^2$  and  $2.15 \text{ cm}^2$  respectively (Table 2.7), which may be due to focussing effect of waves near the southern tip of India. Fig. 2.13 (d,e&f) shows the percentage occurrence of differences at the three sites, respectively. Examination of the summary position and scale parameters (Table 2.5) of RGs, i.e., mean of RG (i.e.,  $\overline{RG}$ ) and standard deviation ( $S_{rg}$ ) compares well with the corresponding PGs (i.e.,  $\overline{PG}$ ,  $S_{pg}$ ). The regression parameters ( $a$  &  $b$ ) show similar linear observations. MAE at Verem and Tuticorin is  $\sim 2 \text{ cm}$ , however at Mandapam, it is less,  $\sim 1.1 \text{ cm}$ . RSME which results from the square of  $(P_i - O_i)$  tends to inflate when the extreme values are present. RSME, therefore, can generally be regarded as a high estimate of MAE. RMSE at Verem and Tuticorin is  $\sim 2.7 \text{ cm}$  and at Mandapam it is  $\sim 1.5 \text{ cm}$ .



**Figure 2.13.** Comparison between sea-level measurements of radar gauge and pressure gauge; linear fit is shown as red line at [a] Verem, [b] Tuticorin and [c] Mandapam. The percentage occurrence of difference [PG-RG] along with respective RSMEs marked with dashed line at [d] Verem, [e] Tuticorin, and [f] Mandapam. N is the number of data points at respective stations.

$RMSE_s$  is a systematic linear function of difference, and it is  $\sim 0.6 \text{ cm}$  at Verem and  $\sim 0.01 \text{ cm}$  at Tuticorin and Mandapam, respectively. With the appropriate parameterization of the model,  $RMSE_s$  can be substantially reduced and therefore,

RMSE<sub>u</sub> can be interpreted as a potential measure of accuracy (Willmott, 1982). The index of agreement (*d*) and the coefficient of correlation (*r*) at significance level (95%) is same (0.99) at all the locations. The indices discussed above are listed in Table 2.5, and they provide a brief evaluation and comparison of PGs and RGs at Verem, Tuticorin and Mandapam.

**Table 2.5.** Quantitative measures of comparison between radar gauge and pressure gauge at different coastal locations of India. The terms *N*, *a*, *b*, *d*, and *r* are dimensionless, while the remaining terms have the units in cm.

Location	$\overline{RC}$	$\overline{PG}$	$s_{rg}$	$s_{pg}$	<i>N</i>	<i>a</i>	<i>b</i>	MAE	RMSE	RMSE <sub>s</sub>	RMSE <sub>u</sub>	<i>d</i>	<i>r</i>
Verem	0.00	0.00	48.72	48.53	72788	1	+0.56	1.91	2.69	0.56	2.86	0.99	0.99
Tuticorin	0.00	0.00	20.92	20.58	38082	1	+0.01	2.11	2.73	0.01	2.73	0.99	0.99
Mandapam	0.00	0.00	20.14	19.99	37929	1	-0.01	1.11	1.46	0.01	1.47	0.99	0.99

### 2.6.3. Harmonic constituents at central west coast of India: Verem, Goa

Tidal constituents from the RG and PG data at Verem, were estimated using harmonic analysis. The basis of harmonic analysis is the assumption that the tidal variations can be represented by a finite number "n", harmonic terms of the form (Pugh, 1987):

$$H_n \cos(\sigma_n t - g_n) \quad (2.9)$$

Where,  $H_n$  is an amplitude (cm),  $g_n$  is phase lag (degrees) on the Equilibrium Tide at Greenwich (local position in the present study),  $\sigma_n$  is an angular speed (degrees per mean solar hour). Table 2.6 shows the main tidal constituents along with their description, time period (days), amplitudes (cm) and phase (degrees) determined from the radar and pressure gauges during the study duration (see Fig. 2.14). The main diurnal and semi-diurnal tidal constituents are within  $\pm 2$  mm in magnitude and within  $1.5^\circ$  in phase. However, exception is the annual (Sa) and semi-annual (Ssa) for which the amplitude (phase) differ by 10.7 mm ( $-3.2^\circ$ ) and 2.2 mm ( $11.8^\circ$ ), respectively. This could reflect, to some extent, the seasonal changes in the density of the water in the Mandovi estuary, from which measurements were collected, and also due to the limited data series of  $\sim 1$  year duration.

**Table 2.6.** Major tidal constituents obtained from radar gauge (RG) and pressure gauge (PG) deployed at Verem, Goa during January 2009 - May 2010. Refer Pugh, D.T. (1987) for the details of harmonic tidal constituents.

Tidal constituents	Time period (days)	Description of tidal constituents	Magnitude (cm)		Difference (mm)	Phase (°)		Difference (°)
			RG	PG		RG	PG	
S <sub>a</sub>	365.2	Solar annual	6.65	7.72	-10.7	312.96	316.15	-3.2
S <sub>sa</sub>	182.6	Solar semi-annual	3.71	3.49	2.2	216.37	204.60	11.8
M <sub>m</sub>	27.55	Lunar monthly	2.06	1.68	3.8	347.24	345.86	1.4
M <sub>sf</sub>	14.77	Variational fortnightly	1.33	1.15	1.8	38.08	31.38	6.7
M <sub>f</sub>	13.66	Lunar Fortnightly	1.27	1.31	-0.4	53.11	51.64	1.5
Q <sub>1</sub>	1.12	Larger elliptical lunar	3.02	2.98	0.4	52.77	53.02	-0.2
O <sub>1</sub>	1.076	Principal lunar	14.82	14.75	0.7	55.52	55.56	0.0
P <sub>1</sub>	1.003	Principal solar	8.40	8.49	-0.9	56.48	56.14	0.3
K <sub>1</sub>	0.997	Luni-solar declinational diurnal	30.00	30.09	-0.9	58.72	58.94	-0.2
J <sub>1</sub>	0.962	Elliptical lunar	1.71	1.71	0.0	71.07	71.78	-0.7
N <sub>2</sub>	0.527	Larger elliptical lunar	12.14	12.20	-0.6	297.73	298.17	-0.4
v <sub>2</sub>	0.526	Larger evectional	2.41	2.34	0.6	301.75	302.80	-1.0
M <sub>2</sub>	0.518	Principal lunar	51.94	51.77	1.7	320.08	320.43	-0.3
L <sub>2</sub>	0.508	Smaller elliptical lunar	1.48	1.40	0.8	343.55	343.42	0.1
S <sub>2</sub>	0.5	Principal solar	18.37	18.22	1.4	358.25	358.86	-0.6
K <sub>2</sub>	0.499	Luni-solar declinational	4.74	4.74	0.0	352.60	353.67	-1.1



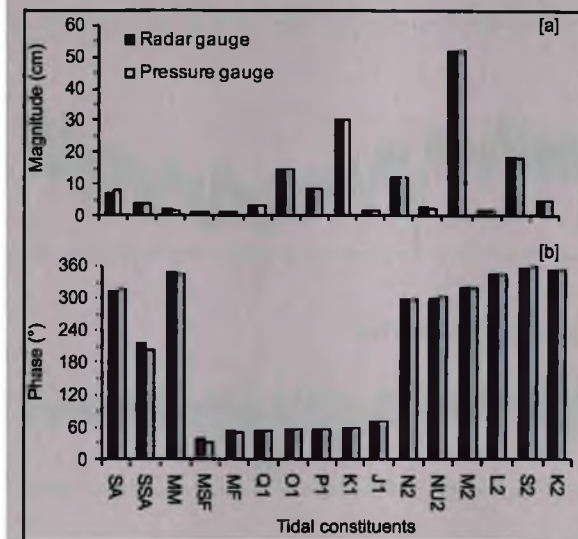


**Figure 2.14.** Major tidal constituents at Verem, Goa obtained using radar and pressure gauges. [a] amplitude and [b] phase.

#### 2.6.4. Effect of atmospheric pressure

Atmospheric pressure variations measured by the AWS at Dona Paula, Goa, are presented in Fig. 2.15a. The atmospheric pressure anomaly shows annual cycle, where the atmospheric pressure is low (high) during June-July (January). The atmospheric pressure variations are within  $\pm 10$  mb. The sea-level measurements obtained from the subsurface pressure gauge may lead to over (under) estimates, if atmospheric corrections are not applied (inverse barometric effect  $\sim -1$  cm/mbar). The sea-level was first estimated from the pressure gauge without using measured atmospheric pressure and, instead, standard values such as  $p_a = 1004.5$  mb,  $\rho = 1.020$  g cm $^{-3}$  and  $g = 980.665$  cm s $^{-2}$  were used (eqn. 2.1). Thus  $d_0$  is the difference between the sea-level measurements obtained from PG and RG, where a constant value of barometric pressure was used in estimating the sea-level from PG (Fig. 2.15b). This situation arises when the sea-level measurements are made using pressure sensors at remote/offshore locations, where atmospheric pressure measurements are not available. With reference to Fig. 2.15c,  $d_1$  is the difference between the sea-level measurements obtained from PG and RG, wherein the measured barometric pressure was used in estimating the sea level from PG. The availability of atmospheric pressure data provides an excellent opportunity to estimate its effect on sea level measurements obtained using pressure gauges.

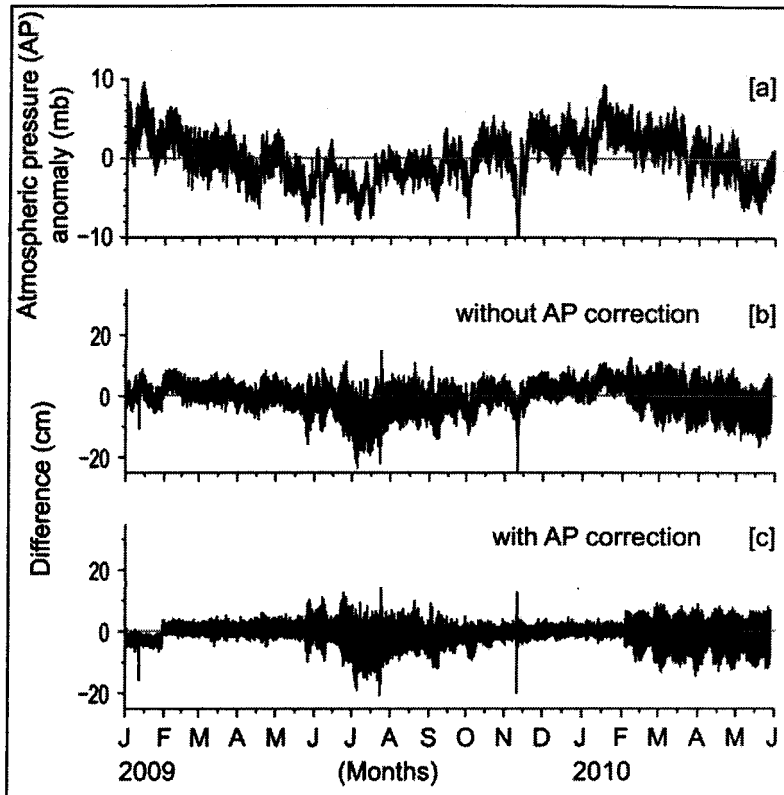


**Figure 2.15.** Time series of [a] atmospheric pressure (AP) anomaly (mb), [b] difference ( $d_0$ ) between sea-level estimated from pressure and radar gauge without measured atmospheric pressure correction and [c] difference ( $d_1$ ) between sea-level estimated using pressure and radar gauges with measured atmospheric pressure correction.

Table 2.7 presents the improvement in RMSEs at three study sites, when pressure gauge measurements were included with simultaneous barometric corrections. The difference ( $d_0$ ) at Verem is shown in Fig. 2.15b, with a variance of  $\sim 16.1 \text{ cm}^2$ . The difference ( $d_1$ ) between pressure and radar gauge with measured atmospheric pressure correction (eqn. 2.1) is shown in Fig. 2.15c. The variance in the difference reduces to  $\sim 7.0 \text{ cm}^2$ . The root-mean-square error (RMSE) for the difference with ( $d_1$ ) and without ( $d_0$ ) atmospheric pressure corrections is estimated to be 2.6 cm and 4.0 cm, respectively as listed in Table. 2.7. Similarly, the variations in  $d_0$  at Tuticorin (Mandapam) is  $10.46 (6.42) \text{ cm}^2$ , which reduced to  $7.48 (2.15) \text{ cm}^2$  for  $d_1$ .

**Table 2.7.** Statistical inferences from the difference between radar and pressure gauge measurements of sea-level.

Station	Verem		Tuticorin		Mandapam	
	$d_0$	$d_1$	$d_0$	$d_1$	$d_0$	$d_1$
Variance ( $\text{cm}^2$ )	16.11	6.95	10.46	7.48	6.42	2.15
RMSE (cm)	4.02	2.69	3.24	2.73	2.55	1.46

## 2.7. Conclusions

The “perfect” sea-level gauge does not exist, and various technologies/options need to be evaluated for different applications. For example, pressure gauge is more suitable for deployment in offshore locations, where height of the radar gauge tower is a limitation and jetties with high fishing activities.

This chapter described various data sources and methodologies used for processing the same. The results, thus obtained, suggest that both the systems (RG and PG) function very well and produce similar tidal constituents. The sea-level measurements from subsurface pressure gauge with measured barometric pressure correction applied at Verem, Tuticorin and Mandapam indicate an improvement in RMSE by 33%, 15% and 42%, respectively in the present study. However, during rainy season, the pressure gauge may underestimate the sea-level measurements due to water density variations resulting from fresh water influx from the river. For e.g. in a similar study at Verem from September 2007 to March 2009, Mehra et al. (2009) reported the variance of difference between the radar and absolute pressure gauge as  $15.9 \text{ cm}^2$ , which reduced to  $5.7 \text{ cm}^2$  and  $4.0 \text{ cm}^2$ , respectively, when atmospheric pressure alone and atmospheric pressure together with water density variations were introduced for obtaining sea level from an absolute pressure gauge. Also, Joseph et al. [2002] reported at Mormugao Port, Goa that the surface water density varied between  $1.020$  and  $0.996 \text{ gcm}^{-3}$  during June 1995 to July 1998. During June-July (2008), at Verem which is located in the Mandovi estuary, the water density remained low  $\sim 1.000 \pm 0.005 \text{ gcm}^{-3}$  and by September it increased to  $\sim 1.020 \text{ gcm}^{-3}$ , remained at this level till May and then it sharply declined to  $1.000 \pm 0.005 \text{ gcm}^{-3}$ .

<sup>3</sup> by June (Mehra et al., 2009). The water density measurement site is ~2.4 km upstream from the pressure gauge location in the Mandovi estuary. The effective density used at Verem is  $1.020 \text{ gcm}^{-3}$  ( $g=980.665 \text{ cms}^{-2}$ ; atmospheric pressure is obtained from AWS). However, variations in the effective density  $\nabla\rho = (1.020-0.995) = 0.025 \text{ gcm}^{-3}$  could lead to an underestimation of 2.45% in sea-level by the pressure gauge. The long-term measurement of water density is practically difficult but the importance of concurrent measurements of atmospheric pressure along with the pressure gauge measurements is duly emphasized in the present study.

It is worth mentioning that the sea-level station deployed for the present study measures the sea-level in a completely different way than the traditional float or bubbler gauges. The ICON is developed with simple supporting structure to mount the sensors, powered by solar energy, and communicating data (using cellular modems) automatically to a base server located at CSIR-NIO, Goa. The sea-level gauges at Verem and Kavaratti Island enabled real-time monitoring of the tsunami at Goa and Kavaratti Island during the  $M_w$  8.4 earthquake off Sumatra on 12 September 2007 (Prabhudesai et al., 2008). Also, sea-level gauges, surface meteorological instruments and wave-rider buoys in the network enabled near real-time monitoring of the response of west India coastal waters and Kavaratti lagoon to the November 2009 tropical cyclone *Phyan* (Joseph et al., 2010). The relatively inexpensive and simple network system described in this chapter will be affordable to economically moderate institutions/countries in their natural hazard mitigation efforts.

## Chapter 3

### Sea-level variability in the north Indian Ocean

#### 3.1. Introduction

Several studies have been carried out on sea-level variability along the coast of India in various time scales, ranging from seasonal to climate change as discussed in section-1.6.3. However, they lack fine temporal resolution data. The development of technologies having high sampling and large data storage capabilities have enabled us to acquire time synchronized multi-parameters of sea-level and surface meteorology from spatially distributed locations. The overall objective of this work is to carry out detailed analysis of sea-level signals collected along the coast and islands of India to study sea-level variability at time scales ranging from minutes to annual in the north Indian Ocean (NIO).

#### 3.2. Data and Methodology

In the present study, sea-level measurements obtained from various coastal and island locations of India have been used (Fig. 1.6). Summary of observations are given in Table 3.1 and also refer to Table 2.3 for positions of the locations.

Sea-level data is de-tided using harmonic analysis (section-2.5.2) to obtain sea-level residual (SLR). SLR data is high-pass filtered using 5th order Butterworth filter to remove oscillations with periods greater than 2 h in order to distinguish the high frequency sea-level oscillations. The spectrum of SLR data is obtained using “pwelch” function from Matlab with Hamming window of 1/4 data length with 25% overlap and 512 FFT points (section-2.5.3).



T- 781 781

**Table 3.1.** Summary of sea-level observations obtained from different coastal and island locations of India using indigenously developed microwave radar based sea-level gauge. The sea-level data is sampled every 5 min except at Malpe (Kochi), where the sampling interval is 30 (60) min. Time is in Indian Standard Time (IST).

Sr No	Measurement Station	Data duration
1	Gopalpur, Odisha	1 September 2011 to 14 July 2012
2	Gangavaram, Andhra Pradesh	1 May 2010 to 31 December 2012
3	Kakinada, Andhra Pradesh	12 July 2011 to 31 December 2012
4	Yanam Andhra Pradesh	1 January to 31 March 2011 and 1 February 2012 to 31 December 2012
5	Port Blair, Andaman & Nicobar Islands	27 February 2011 to 31 December 2012
6	Mandapam, Tamil Nadu	1 March 2010 to 2 August 2012
7	Tuticorin, Tamil Nadu	10 February 2010 to 31 December 2012
8	Colachel, Tamil Nadu	7 January 2012 to 31 December 2012
9	Kochi, Kerala	1-30 September 2007
10	Kavaratti, Lakshadweep island	1 January 2010 to 30 July 2011 and 1 August to 31 December 2012
11	Malpe, Karnataka	1 January 2008 to 31 May 2010
12	Karwar, Karnataka	1 January 2010 to 7 November 2012
13	Verem, Goa	1 January 2010 to 31 December 2012
14	Ratnagiri, Maharashtra	29 September 2010 to 31 December 2012

### 3.3. Tidal properties in the north Indian Ocean

Before analysing the sea-level variability at select locations in the Indian Ocean region, it is prudent to understand the tidal properties along the coastal and island locations of India. Predicted tides, at 7 locations in the Arabian Sea (AS), covering west coast and Kavaratti Island and the Bay of Bengal (BOB), covering the east coast and Port Blair, Andaman and Nicobar Islands, are shown in Fig. 3.1 for May 2012.

#### 3.3.1. Tidal ranges

The two main tidal features of any sea-level record are the range, measured as the height difference between successive highs and lows, and period, the time between one high (low) and the subsequent high (low) level. Srinivas and Dinesh Kumar [2002] documented that the harmonic tidal constituents enable us to recognise the characteristic features of tides at different locations. The four types of tides, which may be of importance in the study region are (Srinivas and Dinesh Kumar, 2002):

1. Diurnal tide - only one high water occurs daily. At neap tide, when the moon has crossed the equatorial plane, two high tides may occur. The mean range of spring tide is  $2(K_1+O_1)$ .
2. Mixed, predominantly diurnal tide - at times only one high water level occurs per day after the extremes of the moon's declination. When the moon has passed over the equator, the high waters per day show large inequalities in range and time. The mean range of spring tide is  $2(K_1+O_1)$ .
3. Mixed, predominantly semidiurnal tide - two high and low water levels occur daily with large inequalities in range and time. The maximum in inequality occurs when the moon's declination has passed its maximum value. The mean range of the spring tide is given by  $2(M_2+S_2)$ .
4. Semi-diurnal tide - two tidal cycles occur daily (12 h 25 minutes) corresponding to each transit of the moon at a particular location. The mean range of the spring tide is given by  $2(M_2+S_2)$ .

From Table 3.2, it is observed that the tides in the present study are mainly semi-diurnal, the spring tidal range could be estimated using  $2(M_2+S_2)$  as shown in Fig. 3.2. It is observed that the tidal range increases from south to north along the west coast of India (Fig 3.1g-3.1a). The mean spring tidal range at southernmost location (Colachel) is ~57 cm, which increases to ~185 cm at Ratnagiri (Fig. 3.2a). The tidal range at Gulf of Khambhat is the largest along the Indian coastline, with spring tidal range of ~9 m and thereby resulting in strong currents (Sanil Kumar and Ashok Kumar, 2010). Unnikrishnan et al. [1999] successfully developed a barotropic numerical model of the Gulf of Khambhat and surrounding areas to simulate tidal amplification. Nayak and Shetye [2003] found that the semi-diurnal tides in the Gulf of Khambhat amplify about threefold from mouth to head, whereas the amplification of diurnal tides is much smaller. Vethamony and Babu [2010] reported that the mean spring tidal range increases from mouth to head in Gulf of Kachchh: 3.06 m at Okha, 4.67 m at Sikka, 5.82 m at Kandla and 6.43 m at Navlakhi. The reasons for amplification of tides are season, bathymetry, funnel shape of the Gulf, coastal configuration and orientation of the coast.

Along the east coast of India, the tidal amplitude at Yanam (Fig. 3.1k) to Gopalpur (Fig. 3.1h) appears to be constant. The two southern measurement locations, Mandapam and Tuticorin, along the east coast of India report low tidal amplitudes (Fig. 3.1m & 3.1n). The mean spring tide range estimated in BOB is shown in Fig. 3.2b. The mean spring tide range along the east coast depicts different features and is lower in amplitude as compared to that along the west coast. The range along the east coast varies from ~65 cm at Tuticorin and Mandapam to ~151 cm at Gopalpur (Fig. 3.2b). The mean spring tide range is high at Port Blair (~182 cm). The mean spring tide range is almost constant from Yanam to Gangavaram ~133 cm.



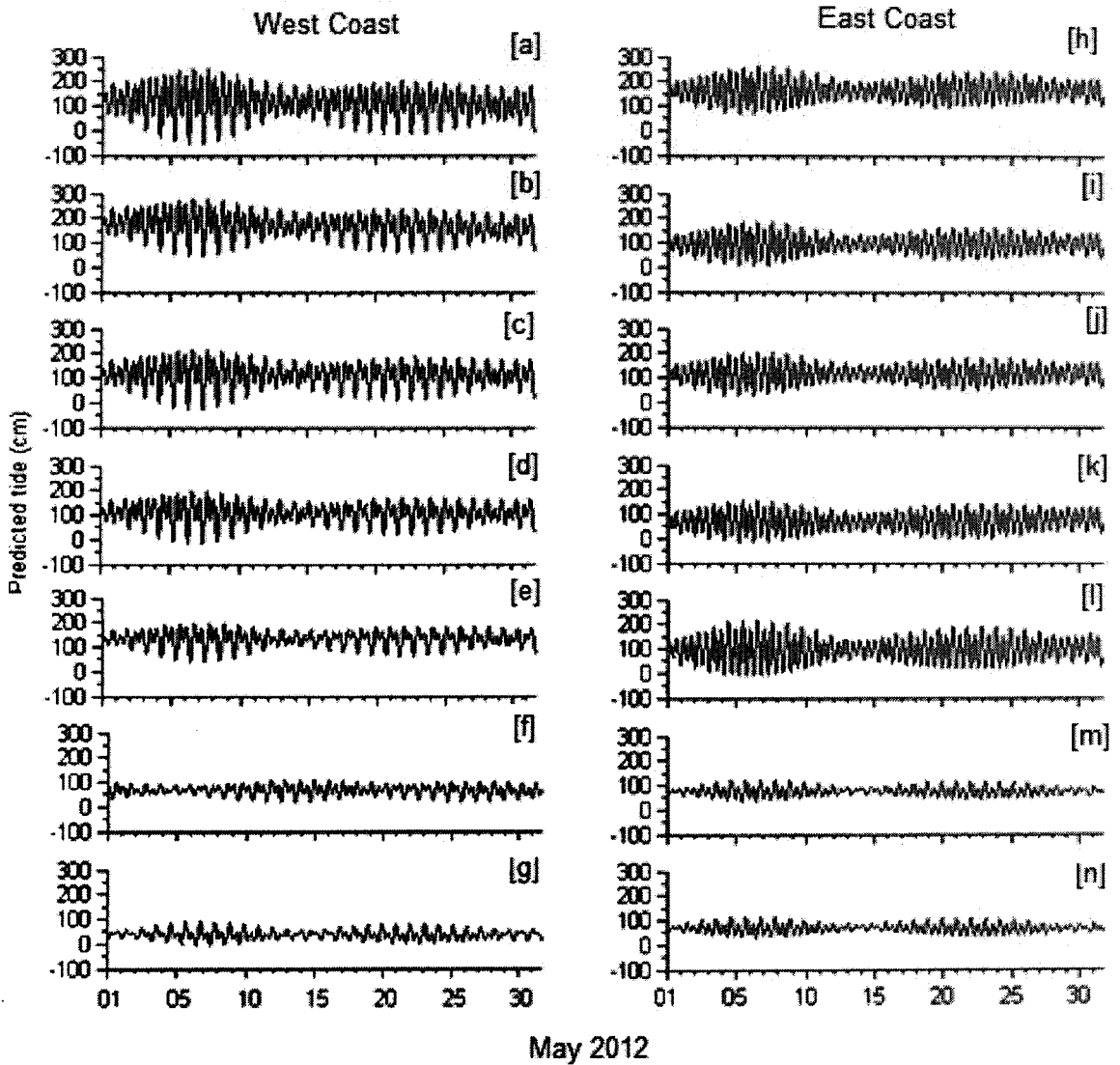


**Figure 3.1.** Predicted tides at different coastal and island locations of India in the Arabian Sea (AS) and the Bay of Bengal (BOB): [a] Ratnagiri, [b] Verem, [c] Karwar, [d] Malpe, [e] Kavaratti, [f] Kochi and [g] Colachel in AS. [h] Gopalpur, [i] Gangavaram, [j] Kakinada, [k] Yanam, [l] Port Blair, [m] Mandapam and [n] Tuticorin in BOB. Time is in Indian Standard Time (IST).

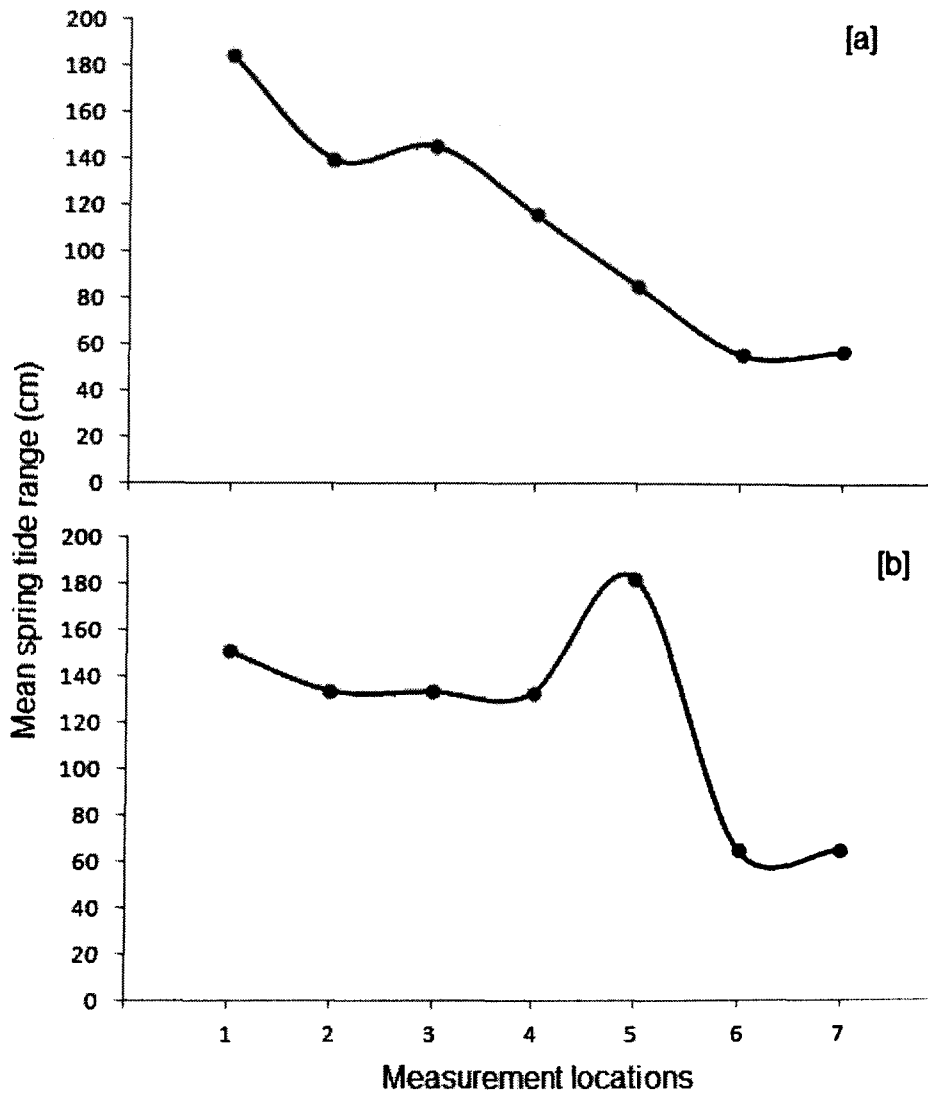


**Figure 3.2.** Mean spring tide ranges at different coastal and island locations of India in the AS and the BOB. [a] Measurements locations in AS: 1- Ratnagiri, 2- Verem, 3- Karwar, 4- Malpe, 5- Kavaratti, 6- Kochi and 7- Colachel. [b] Measurement locations in BOB: 1- Gopalpur, 2- Gangavaram, 3 Kakinada, 4- Yanam, 5- Port Blair, 6- Mandapam and 7- Tuticorin.

### 3.3.2. Tidal constituents

A few of the major harmonic tidal constituents ( $M_2$ ,  $S_2$ ,  $N_2$ ,  $K_1$ ,  $O_1$  and  $P_1$ ) which enable the recognition of tidal characteristics of a particular location are shown in Fig. 3.3. The harmonic tidal constituents as shown in Fig. 3.3a show a linear variation from the southern location Colachel to Ratnagiri as we move northwards. Tidal constituent  $M_2$  (time period=12.4206 h) in AS varies from ~10 cm at Colachel to ~67 cm at Ratnagiri.  $K_1$  (time period=23.9345 h) and  $S_2$  (time period=12.000 h) increase from ~ 10 cm to 32 cm from Colachel to Ratnagiri. The other tidal constituents  $N_2$  (time period=12.6584 h),  $O_1$  (time period=25.8193 h) and  $P_1$  (time period=24.0659 h) have low amplitudes varying from 2 cm at Colachel to 15 cm at Ratnagiri (Fig. 3.3a). Fig. 3.3b shows the phase of the tidal constituents in the AS. Phase of the  $M_2$ ,  $S_2$  and  $N_2$  constituents from Ratnagiri to Kochi lies in fourth quadrants, and at Colachel it lies in the first quadrants; however, the phase of the  $K_1$ ,  $O_1$  and  $P_1$  is in the first quadrant (~ 53°) only.

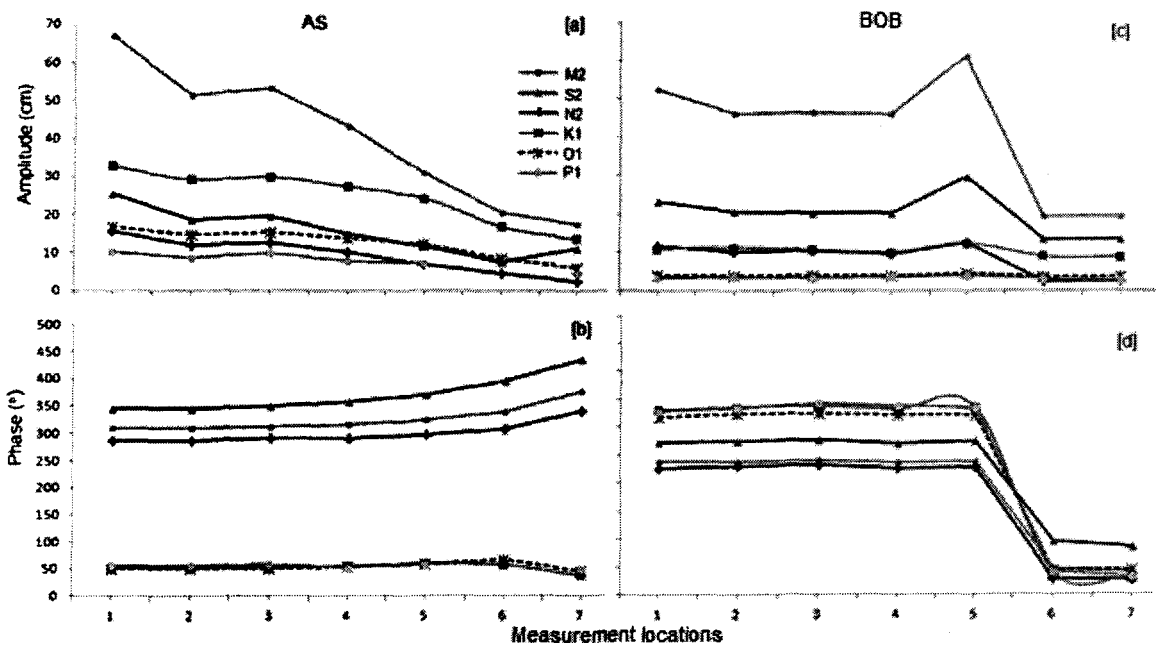


**Figure 3.3.** A few major tidal constituents at different coastal and island locations in the AS and the BOB: [a] and [b] show the amplitude and phase of the tidal constituents in AS (west coast): 1- Ratnagiri, 2- Verem, 3- Karwar, 4- Malpe, 5- Kavaratti, 6- Kochi and 7- Colachel. [c] and [d] show the amplitude and phase of the tidal constituents at in BOB (east coast): 1- Gopalpur, 2- Gangavaram, 3 Kakinada, 4- Yanam, 5- Port Blair, 6- Mandapam and 7- Tuticorin.

The values of tidal constituents in the BOB are less as compared to those in the AS (Fig. 3.3c). The amplitude of the semi-diurnal tidal constituents  $M_2$ ,  $S_2$  and  $N_2$ , remains almost constant from Yanam to Gopalpur with values of 47, 21 and 10 cm, respectively. At Port Blair, the amplitude of these components is observed to be high, and comparable to those at Ratnagiri in AS. The reason could be that the measurement locations (Fig. 1.6) are in the closed basins. At Mandapam and Tuticorin, the amplitude of the semi-diurnal constituents  $M_2$ ,  $S_2$  and  $N_2$  reduces to ~ 19, 13 and 2 cm, respectively. Amplitude of diurnal constituents  $K_1$ ,  $O_1$ , and  $P_1$  remains almost constant from Tuticorin to Gopalpur with 10.7, 4.0 and 3.5 cm, respectively. The phase of the constituents  $M_2$ ,  $S_2$ ,  $N_2$ ,  $K_1$ ,  $O_1$  and  $P_1$  from Port Blair to Gopalpur is observed to be constant at 238.2°, 273.8°, 228.4°, 322.0° and 33.8°, respectively. The phase of  $S_2$  at Mandapam and Tuticorin is ~ 90° and the phase of all other constituents is ~36° (Fig. 3.4d). Clarke and Batisti [1981] derived and used a continental margin theory to discuss several aspects of the effect of "smooth" continental shelves on tides. They showed that semi-diurnal tides should be amplified on wide shelves in mid and low latitudes, but diurnal tides should not be amplified. They showed that the tidal resonance occurs on the shelf when

$$\frac{g \alpha}{\omega^2 - f^2} = a$$

where,  $g$  is gravity,  $\alpha$  is the slope of the shelf bottom,  $\omega$  is the frequency of the tidal constituent,  $f$  is the Coriolis parameter, and  $a$  is the shelf width. Murty and Henry [1983] calculated the above parameter for nine locations for  $M_2$  and  $K_1$  constituents and reported that the highest amplitudes for  $M_2$  occur near Sandwip Island, Bangladesh.

### 3.3.3. Form number

The importance of diurnal and semi-diurnal tidal constituents is expressed in terms of the Form number ( $F$ ) as:

$$F = \frac{K_1 + O_1}{M_2 + S_2}$$

where, the amplitudes of the tidal constituents are used to compute the form number

which describes the form of the curve during a day. The tides at a particular location may be classified as (Defant, 1961):

F = 0.00 - 0.25	Semi-diurnal tide
F = 0.25 - 1.50	Mixed, mainly semi-diurnal tide
F = 1.5 - 3.00	Mixed mainly diurnal tide
F > 3.00	Diurnal

Form number for the present study locations are listed in Table 3.2. Form number of the measurement locations in the AS varies within 0.25-1.5, and the tides in these locations could be classified as mixed, mainly semi-diurnal tides. However, in BOB, the Form number is less than 0.25 from Port Blair to Gopalpur, indicating semi-diurnal tides. At Mandapam and Tuticorin the tides are mixed, mainly semidiurnal type. Tides in BOB have been reported as semi-diurnal almost everywhere, except the southwest sector, where they are mixed and predominantly semidiurnal (Murty and Henry, 1983). Srinivas and Dinesh Kumar [2002] reported sea-level variations at Kochi (11°10'N, 75°48'E) and Beypore (~ 200 km northward alongshore distance from Kochi) for 1997, and they classified the tides at both locations as mixed, mainly semi-diurnal, having the Form number of 0.92 (0.80) at Kochi (Beypore).

**Table 3.2.** Form number estimated using the tidal constituents for different locations.

Locations in the Arabian Sea		Location in the Bay of Bengal	
Location	Form factor	Location	Form factor
Ratnagiri	0.53	Gopalpur	0.20
Karwar	0.62	Gangavaram	0.22
Verem	0.63	Kakinada	0.22
Malpe	0.49	Yanam	0.22
Kavaratti	0.85	Port Blair	0.18
Kochi	0.89	Mandapam	0.38
Colachel	0.68	Tuticorin	0.38

### 3.4. Sea-level residuals (SLR)

Sea-level residual (SLR) is estimated as the difference between the observed and predicted tides, which represents the exchange of energy between the ocean and atmosphere. The general representation of the observed level  $X(t)$  which varies with time may be written as (Pugh, D.T., 1987):

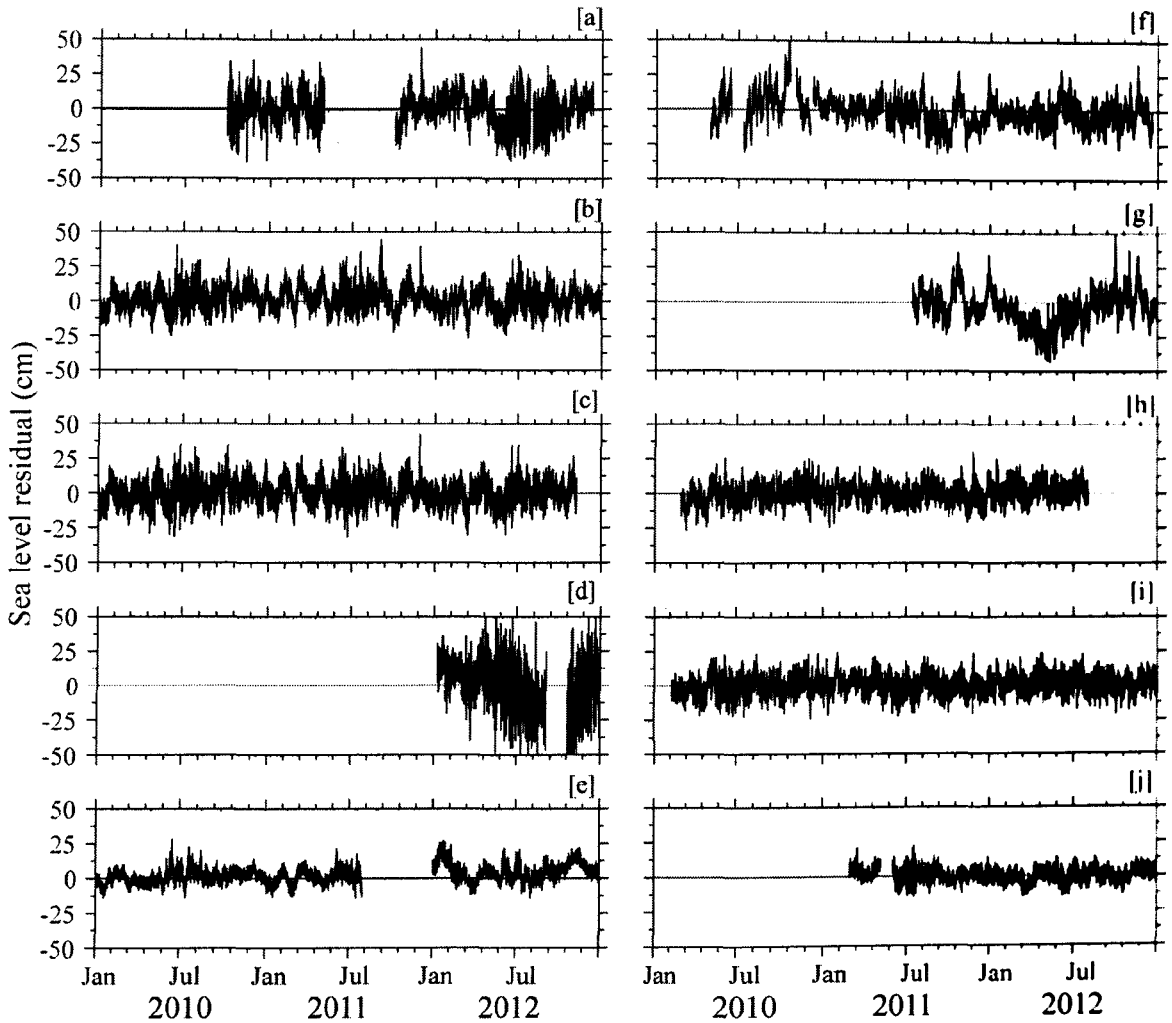
$$X(T) = Z_0(t) + T(t) + S(t) \quad (3.1)$$

where,  $Z_0(t)$  is the mean sea-level which changes slowly with time,  $T(t)$  is the tidal part of the variation and  $S(t)$  is the meteorological surge component.

Fig. 3.4 shows the SLR at different locations in the AS and BOB. It is observed that the variability exists at all the locations throughout the measurement period (or throughout the year). The SLR varies within  $\pm 25$  cm at most of the locations, except at Colachel (Fig. 3.4d), where the variations are upto  $\pm 50$  cm. However, at the island locations of Kavaratti (Port Blair) in AS (BOB), the variations are within  $\pm 15$  cm. Annual SLR energy at different measurement locations are given in Table 3.3. Monthly variance of SLR is shown in Fig. 3.5. The SLR energy during the period as shown in Fig. 3.4a,b&c at Ratnagiri, Verem, and Karwar is estimated to be  $\sim 74$ ,  $55$  and  $52 \text{ cm}^2$  respectively. The SLR energy is high at Colachel  $\sim 150 \text{ cm}^2$  in 2012 (Fig. 3.4d). It is observed that the SLR variability at Kakinada is high compared to other locations in the BOB. The SLR fall of approx.  $-40$  cm during February to May is also noticed in 2013. This fall is not due to meteorological or tsunami events which normally last for a few days. Therefore, it appears to be a local phenomenon, and needs detailed investigation with numerical models and related local meteorological and oceanic information like winds, currents, salinity, water temperature, etc. The monthly mean variance peaks during May-August at almost all the locations (Fig. 5a & 5c).

Sea-level along the coasts is also influenced by floods that are caused by episodes of excess water from ocean (storm surges), tsunamis or from rivers (precipitation). Murty et al. [1986] compiled the cyclonic storm surges in the BOB and showed that the water height (surge plus tide plus waves) reach its maxima during May and October. Emery and Aubrey [1989] reported that the monsoon brings more than 75 percent of the annual rainfall to most of India and Bangladesh. Discharges of

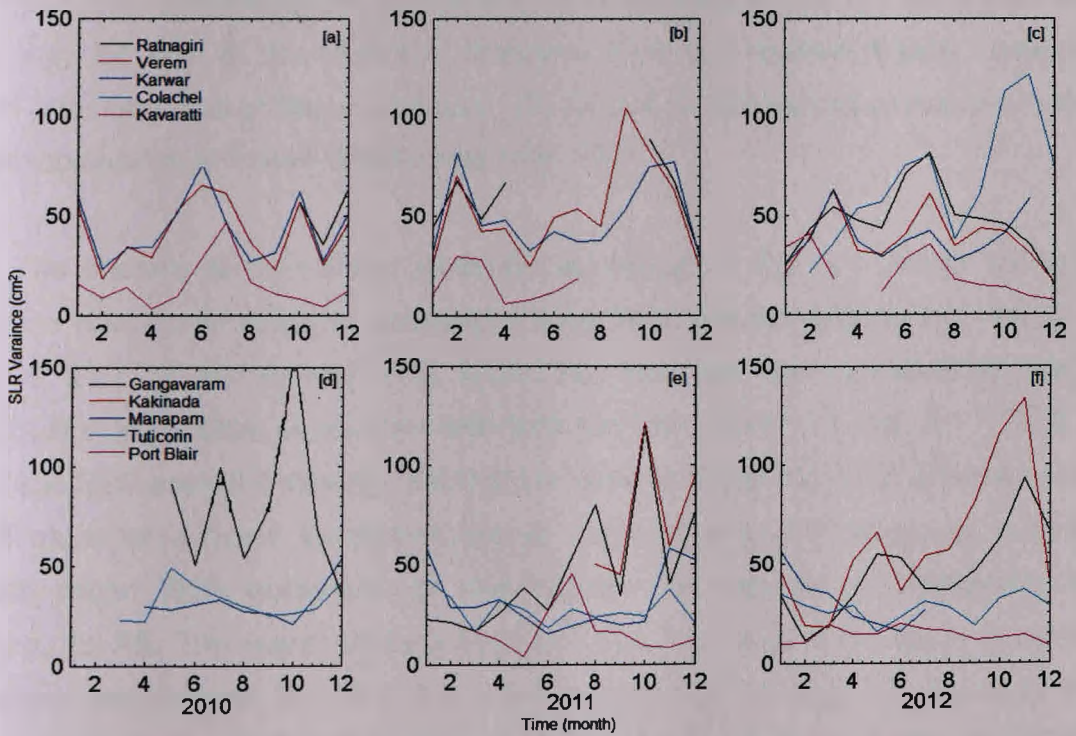
the rivers reach their maxima about a month after peak rainfall, in August and September.



**Figure 3.4.** Sea-level residual (SLR) at different coastal and island locations in the AS and the BOB: [a] Ratnagiri, [b] Verem, [c] Karwar, [d] Colachel and [e] Kavaratti in the AS; [f] Gangavaram, [g] Kakinada, [h] Mandapam, [i] Tuticorin and [j] Port Blair in the BOB.

**Table 3.3.** Sea-level residual variance estimated at different measurement locations.

Location	Sea-level variance (cm <sup>2</sup> )		
	2010	2011	2012
Ratnagiri	59.1	71.4	86.9
Verem	51.2	62.7	50.2
Karwar	51.5	54.9	49.4
Colachel			150.8
Kavaratti	22.1	23.5	41.5
Gangavaram	124.4	74.9	62.6
Kakinada		104.3	145.5
Mandapam	43.2	36.4	33.2
Tuticorin	38.5	33.5	31.5
Port Blair		21.3	19.7

**Figure 3.5.** Monthly sea-level residual (SLR) variance at different coastal and island locations of India. In AS for the year [a] 2010, [b] 2011, [c] 2012 and in BOB for the year [d] 2010, [e] 2011 and [f] 2012.



### 3.4.1. Low frequency sea-level residuals

In this section, low frequency SLR (lf-SLR) components having periods above 1 day and their variability in the north Indian Ocean are discussed. Daily-average SLRs are shown in Fig. 3.6. One of the remarkable features observed is that at Verem (Fig. 3.6b) and Karwar (Fig. 3.6c), ~200 km apart, the daily-mean SLR variations are almost similar. This may imply existence of non-tidal forcing over a large area in the region. Table 3.4 is listed with the correlation coefficients at 95% significant level between different measurement locations. Along the west coast of India, Ratnagiri is significantly correlated (~0.64) to Verem and Karwar. However, the daily-mean SLR at Verem and Karwar with similar variation for three years (2010-2012) has significant correlation coefficient of 0.93. Similarly, the daily-mean SLR at Tuticorin and Mandapam, ~115 km apart are also observed to be similar with significant correlation of ~ 0.85. The variance of daily-mean SLR at Mandapam (Tuticorin) in BOB is ~ 30.2 (25.1) cm<sup>2</sup>, which is lower than at Verem (Karwar) in AS ~ 46.6 (38.9) cm<sup>2</sup>. However, daily-mean SLR at Mandapam (Tuticorin) is more oscillatory than at Verem (Karwar) which may be due to the nonlinear influence from the shallow depths, irregular coastal geometry and bottom topography of the Gulf of Mannar as compared to the coastal topography of Verem and Karwar (Fig. 1.6).

The spectra of daily-mean residuals are shown in Fig. 3.7. Along the west coast, the daily-mean residual oscillations have time periods around 2.6, 3.8, 5.4, 7.7, 11.6, 20.1, 36 and 64 days (Fig. 3.7a-3.7e). However, the spectra of the daily-mean SLR in BOB show oscillations with time periods around 2.4, 3.9, 5.1, 7.4, 9.7, 12.3, 18.9, 36.0 and 64.0 minutes. Most of the stations along the coast of India in the present study have shown the periodicities at ~ 36 days (Fig. 3.7). However, in BOB, the daily-mean SLR comprises of less number of frequency components as compared to AS. The island stations Kavaratti and Port Blair show some common oscillations with periods 12.6, 8.5, 5.2 and 3.7 days. Fig 3.8 (Fig. 3.9) presents the time series of daily-mean SLR spectra of measurement locations in the AS (BOB), showing the existence of monthly and bimonthly periods at all the measurement locations. Hilmi et al. [2002] studied long-term and short term variations of sea level in eastern Canada. They reported that in the residual signals, variations between 2 and 30 days can be attributed to meteorological forcing (atmospheric pressure and

winds), 2–10 h to longitudinal seiches, 12–24 h to atmospheric tides and 16–18 h to inertial oscillations.

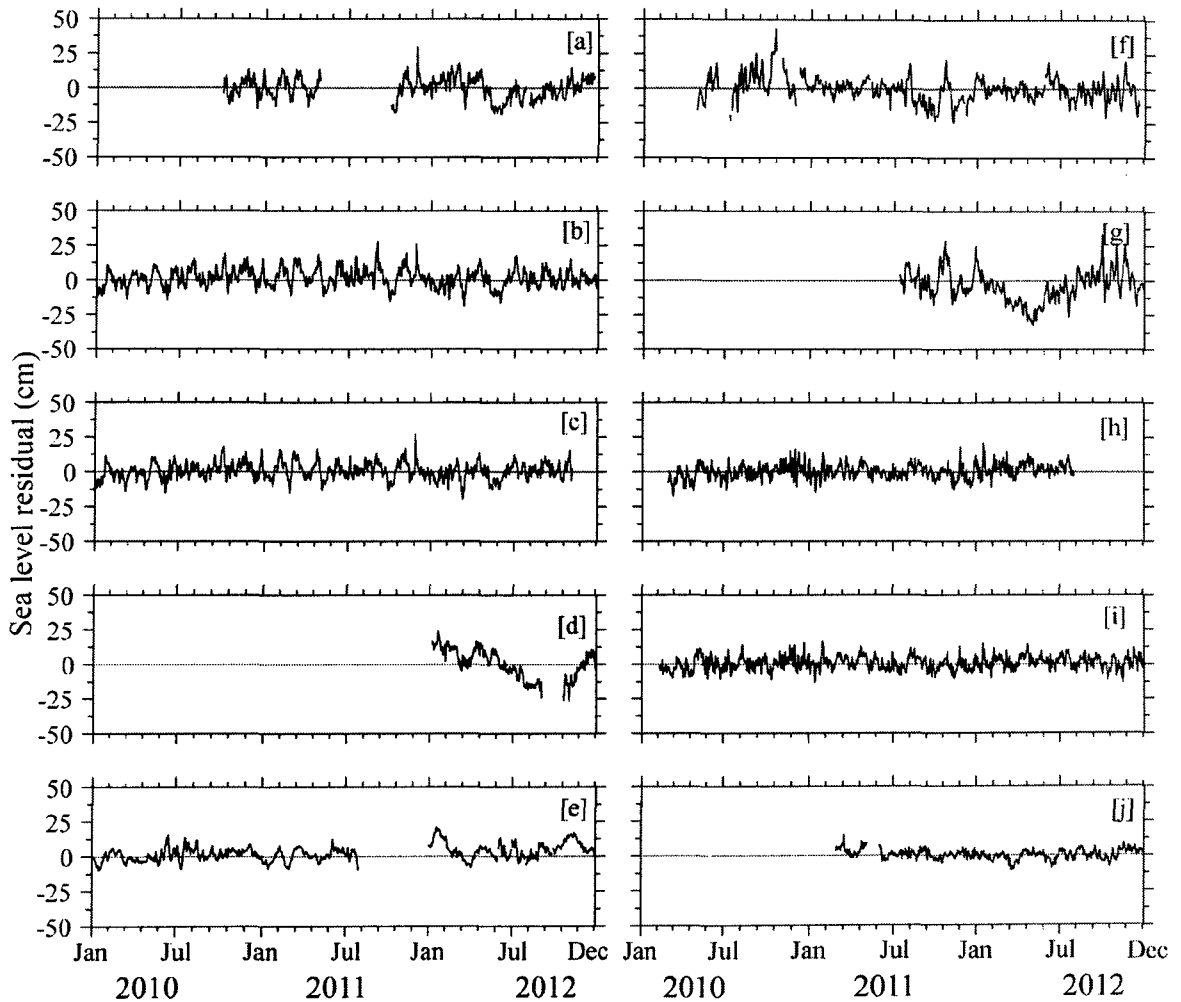


**Figure 3.6.** Daily-mean sea-level residual (SLR) at different coastal and island locations in the AS and the BOB: [a] Ratnagiri, [b] Verem, [c] Karwar, [d] Colachel and [e] Kavaratti in AS. [f] Gangavaram, [g] Kakinada, [h] Mandapam, [i] Tuticorin and [j] Port Blair in BOB.

**Table 3.4.** Correlation coefficients at 95% confidence level for daily-mean sea-level residuals at different measurement locations.

Measurement stations	West coast of India			
	Ratnagiri	Verem	Karwar	Colachel
Ratnagiri	1.00			
Verem	0.60			
Karwar	0.68	0.93		
Colachel	0.28	-0.14	-0.17	
Kavaratti	0.20	0.15	0.13	0.11
Measurement stations	East coast of India			
	Gangavaram	Kakinada	Mandapam	Tuticorin
Gangavaram	1.00			
Kakinada	0.47			
Mandapam	0.02	-0.14		
Tuticorin	-0.07	-0.12	0.85	
Port Blair	0.04	0.11	0.22	0.29

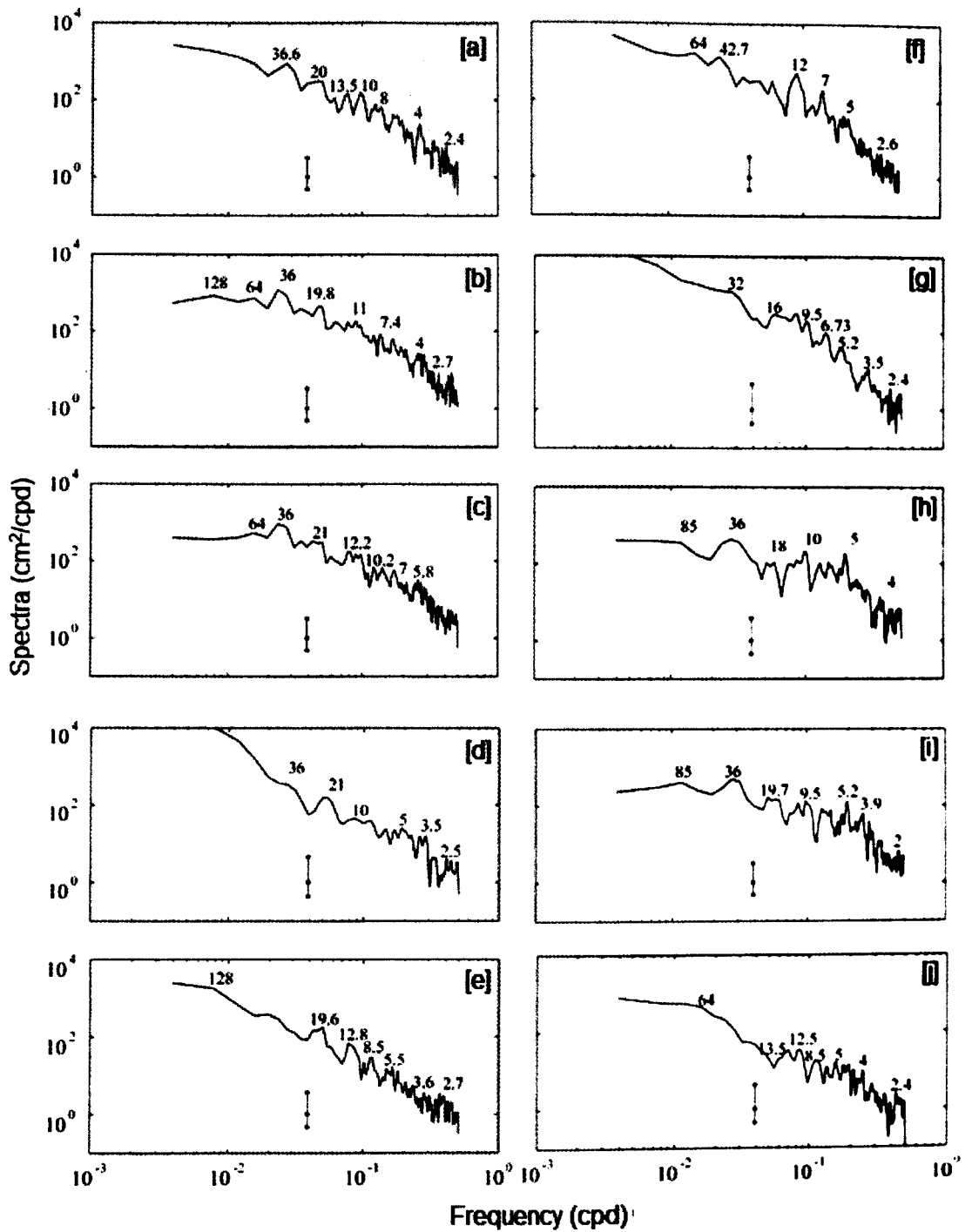


**Figure 3.7.** Frequency spectrum of daily-mean sea-level residuals (SLR) at different locations of the coastal and island locations in AS and BOB: [a] Ratnagiri, [b] Verem, [c] Karwar, [d] Colachel and [e] Kavaratti in AS. [f] Gangavaram, [g] Kakinada, [h] Mandapam, [i] Tuticorin and [j] Port Blair in BOB.

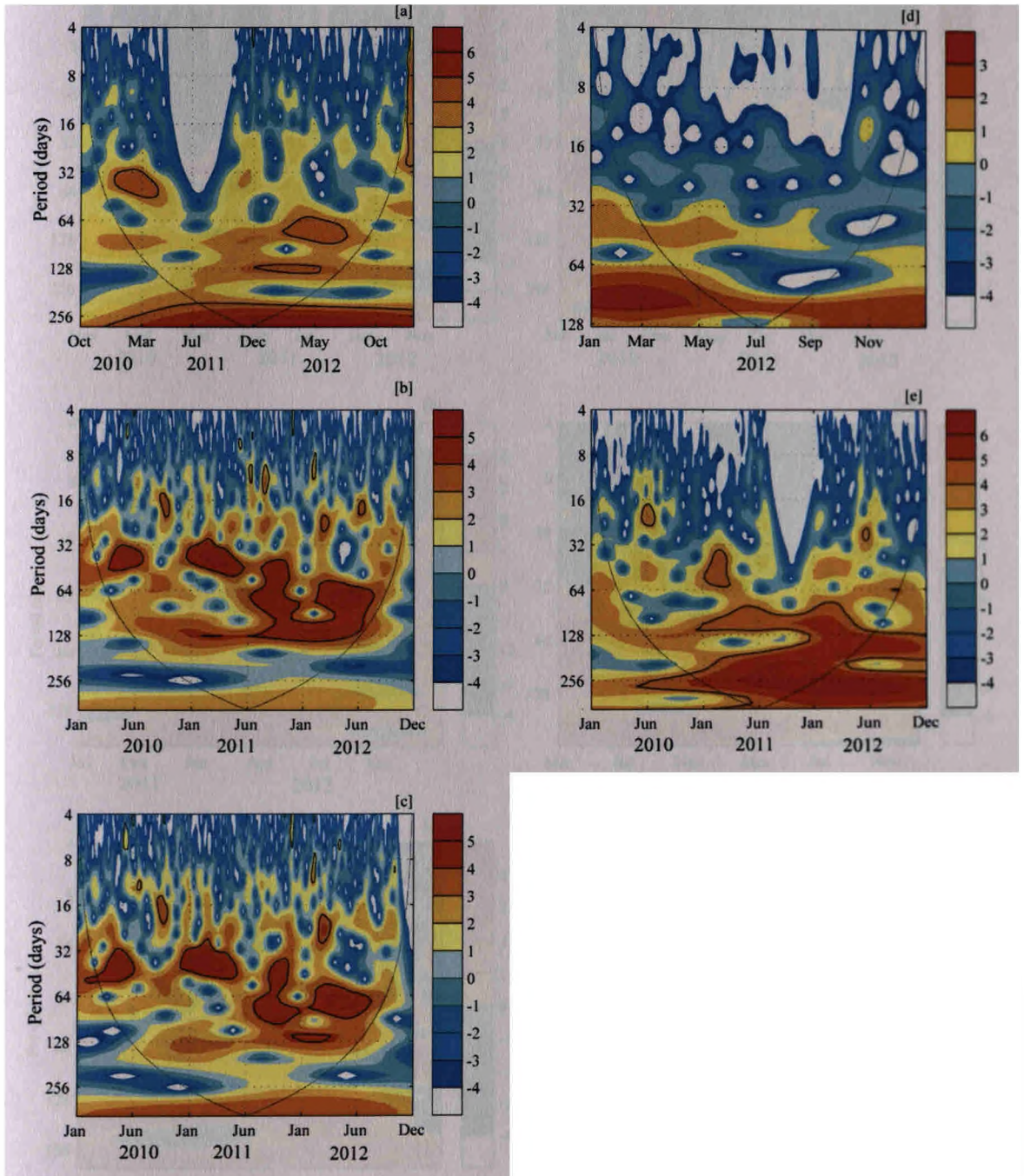


**Figure 3.8.** Time series of frequency spectrum of daily-mean sea level residual (SLR) at different coastal and island locations in the Arabian Sea: [a] Ratnagiri, [b] Verem, [c] Karwar, [d] Colachel and [e] Kavaratti



## Sea-level variability in the north Indian Ocean

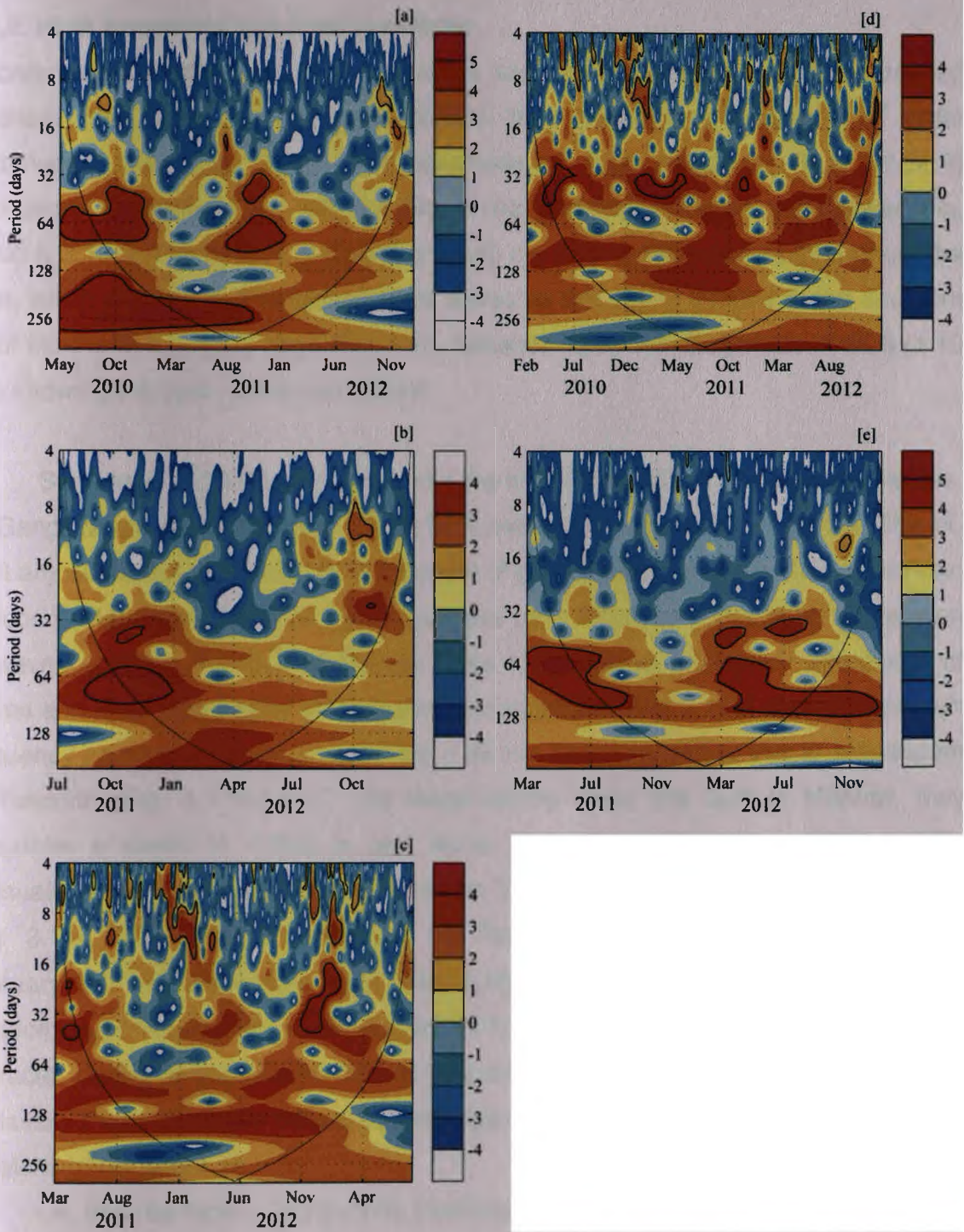


**Figure 3.9.** Time series of frequency spectrum of daily-mean sea-level residual (SLR) at different coastal and island locations in BOB: [a] Gangavaram, [b] Kakinada, [c] Mandapam, [d] Tuticorin and [e] Port Blair.

### 3.4.2. High frequency sea level residuals

In order to understand the high frequency sea-level residuals (hf-SLR) at various locations, the SLRs are high-pass filtered (time period  $\leq 2h$ ) using a 5<sup>th</sup> order Butterworth filter (Fig. 3.10). The amplitude of high frequency SLR (hf-SLR) oscillations at Ratnagiri is  $\sim \pm 25$  cm (Fig. 3.10a) and less at Verem and Karwar (Fig. 3.10b & 3.10c). The hf-SLR at Colachel  $\sim \pm 40$  cm (Fig. 3.10d) occurs throughout the year, which may be due to focussing of waves as the site is located at the southern tip of India with a bulging edge (Fig. 1.6). Kavaratti has a low magnitude hf-SLR ( $\pm 10$  cm) showing the open ocean conditions.

Stations in BOB (Fig.3.10:f-j) show the hf-SLR variations of lesser amplitudes. At Gangavaram and Kakinada, the hf-SLR oscillations are within  $\pm 20$  cm. The hf-SLR amplitude from Colachel to Mandapam (Fig. 1.6) reduces in the Gulf of Mannar. Tuticorin (Mandapam) hf-SLR oscillations are upto 10 (5) cm, indicating attenuation of waves entering the Gulf of Mannar. Due to focussing, non-linear interaction of waves and local topography off Colachel, the spectrum (Fig. 3.11d) shows more high frequency components with time period  $< 30$  min as compared to that at Mandapam or Tuticorin (Fig. 3.11h-3.11i). As these waves enter the Gulf of Mannar, they encounter a depth of  $\sim 1000$  m and some of the high frequency waves will be attenuated during their propagation towards Tuticorin as seen in the SLR spectrum (Fig. 3.11i). The hf-SLR oscillations off Port Blair are almost negligible during February 2011 to December 2012 (Fig. 3.10j). The hf-SLR variations have larger duration (June-November) in BOB than in AS. A visual analysis of the oscillation character during strong events was carried out by Rabinovich and Monserrat [1996] to classify these events in different types, apparently related to different mechanisms of seiche generation:

- A. Impulse type - strong initial oscillation(s) and then fast or slow decay of seiches heights;
- B. Resonance type - a gradual amplification of consecutive oscillations till the maximum is achieved, then (sometimes) a period of stability, and a gradual reduction;
- C. Complex type - a few consecutive abrupt and gradual amplification and reduction of seiche oscillations.

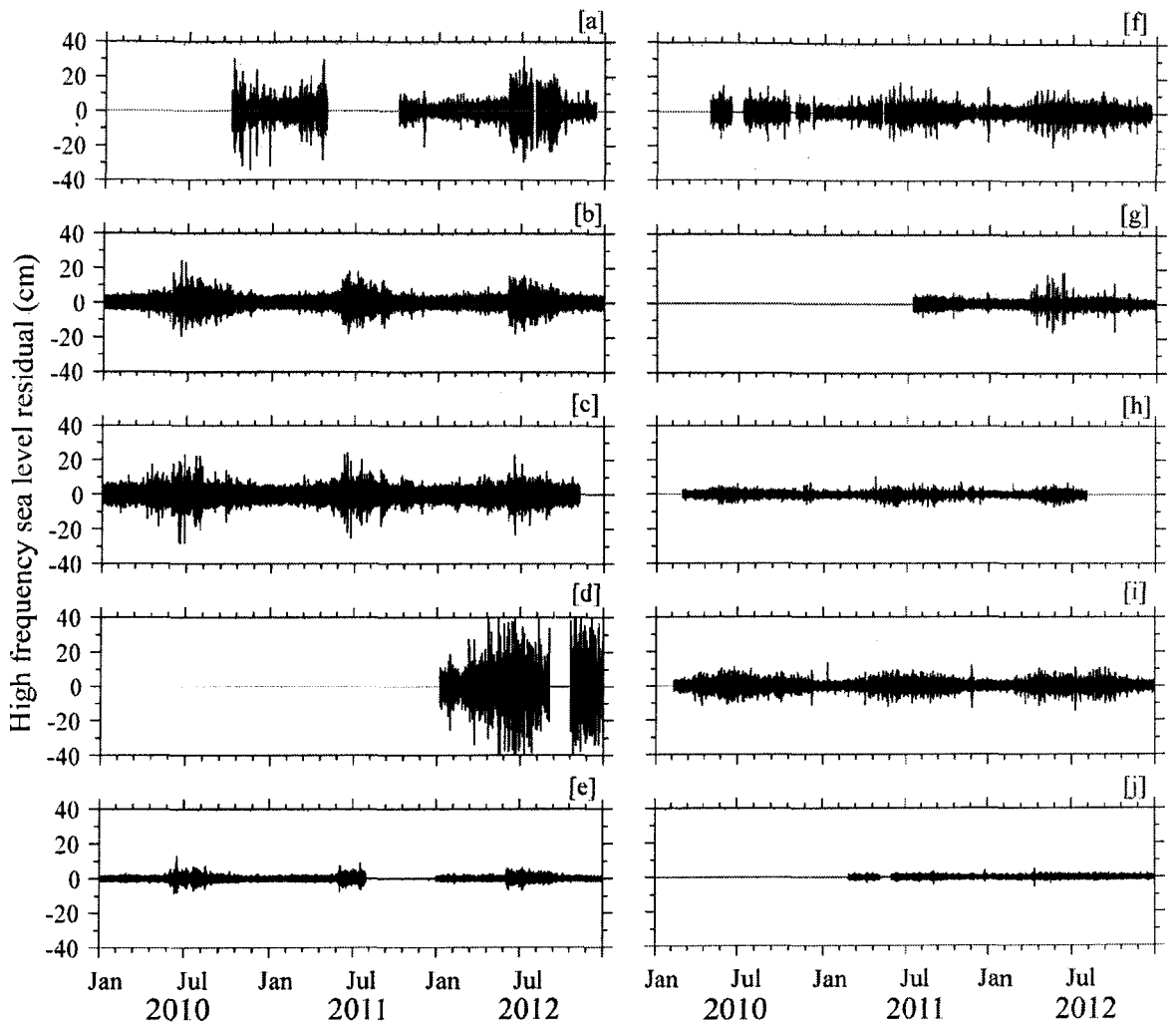


**Figure 3.10.** High-pass filtered sea-level residual (hf-SLR) using a 5th order Butterworth filter (time period  $\leq 2$ h) at different coastal and island locations in the AS and the BOB: [a] Ratnagiri, [b] Verem, [c] Karwar, [d] Colachel and [e] Kavaratti in AS. [f] Gangavaram, [g] Kakinada, [h] Mandapam, [i] Tuticorin and [j] Port Blair in BOB.

If a similar classifications could be used for the background residual signals, then the hf-SLR oscillations observed are of type-A at Ratnagiri, Verem and Port Blair (Fig. 3.10a, 3.10b and 3.10e). However, at Karwar it is observed to be of type-C (Fig. 3.10c) during the summer monsoon. In BOB, the hf-SLR oscillations are of the type-B at Gangavaram, Mandapam and Tuticorin (Fig. 3.10f, 3.10h and 3.10i), except at Kakinada, which is of type-B.



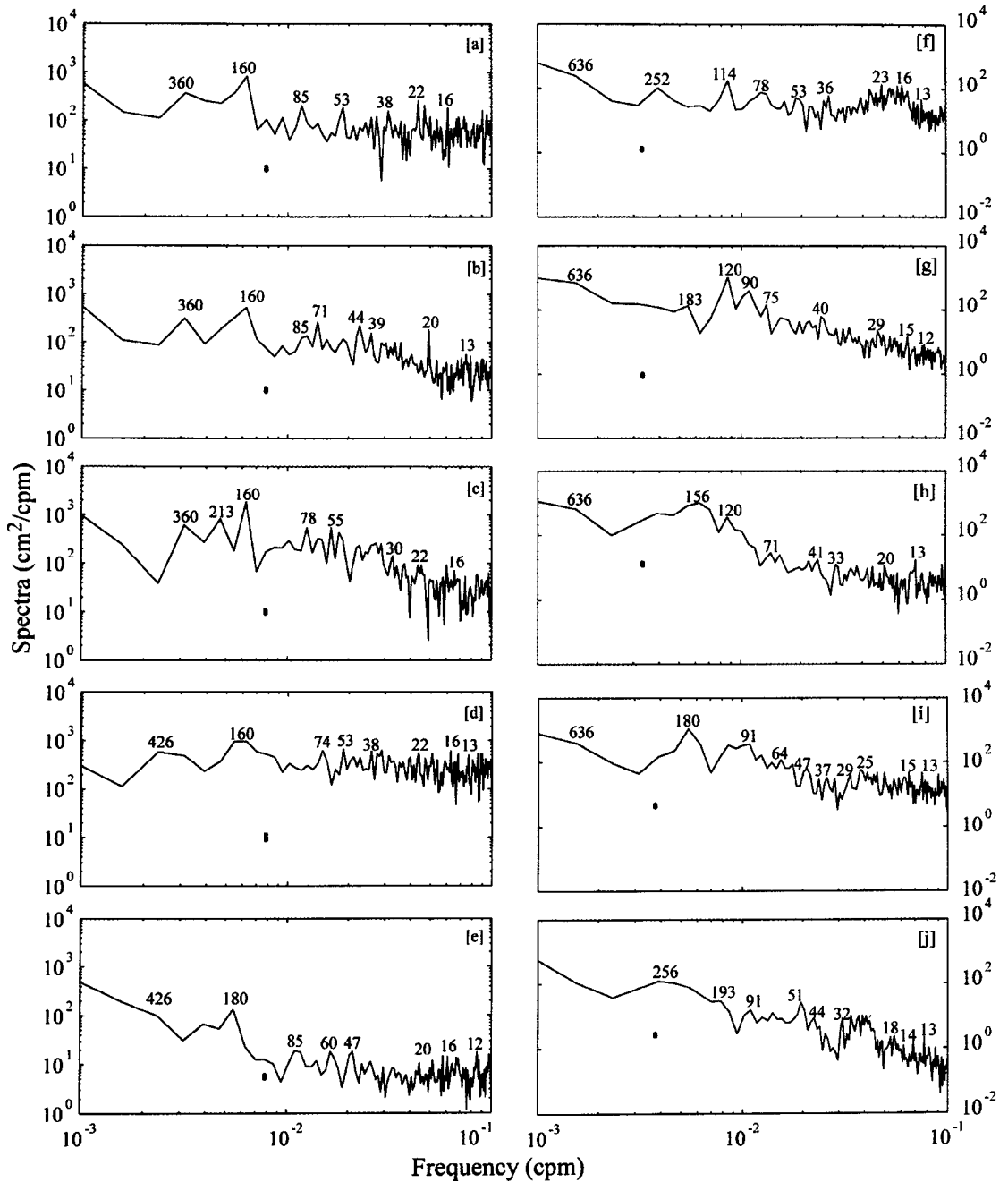


**Figure 3.11.** Frequency spectrum of sea-level residual (sampled every 5 minutes) at different coastal and island locations in the AS and the BOB: [a] Ratnagiri, [b] Verem, [c] Karwar, [d] Colachel and [e] Kavaratti in the AS. [f] Gangavaram, [g] Kakinada, [h] Mandapam, [i] Tuticorin and [j] Port Blair in BOB.

The spectral analysis of long series of SLR (Fig. 3.11) makes it possible to determine the principal features of the region related mainly to the local topography. The spectrum of SLR data are obtained using 'pwelch' function from Matlab with Hamming window of 256 data points and 50% overlap. Comparison between the spectra of different stations may be less accurate as the data duration is not the same for all the stations, and the spectrum is obtained using the data as shown in Fig. 3.4. However, along the west coast, the spectra at Ratnagiri, Verem and Karwar are observed to have major peaks at 360, 160, 75, 85, 49 and 21 min (Fig. 3.11a-3.11c). At Colachel, hf-SLR spectra are energetic at all the frequencies with a few major peaks at 160, 74, 53 and 38 minutes (Fig. 3.11d). Kavaratti, the Island location in the AS<sub>2</sub> shows spectral peaks at 180, 85, 60, 47, 20 and 16 min (Fig. 3.11e). Spectral energy at locations in BOB (Fig. 3.11f-3.11j) is lower compared to those in AS (Fig. 3.11a-3.11e). The typical spectral peaks are observed at time periods of ~118, 90, 75, 43, 32, 20 and 14 min. Apparently, the low frequency maxima may be related to the eigen frequencies of the respective shelf and the basin in AS and BOB. The high frequency extrema are probably related to the eigen frequencies of harbour (or the local topography). Rabinovich and Monseratt [1996] reported spectra from the region of Balearic Islands, Western Mediterranean (Palma de Mallorca and Sol de Mallorca) with spectral peaks at 222, 75, 33, 27, 24, 13.2, 11.6, 9.6-10.0 and 5.9 min. They attributed the low-frequency maxima to the eigen frequencies of Palma Bay and southwestern Mallorca shelf, and some of the high-frequency extrema were inferred to be related to eigen oscillations of Palma harbour.

These hf-SLR oscillations also consist of the so called harbour oscillations or coastal seiches, a specific type of seiche motion that occurs in partially enclosed basins (bays, fjords, inlets and harbours) which are connected through one or more openings to the sea. They are mainly generated by long waves entering through the open boundary (harbour entrance) from the open sea. If the tsunamis and internal waves are ignored, then the main source of background long waves in the ocean is the atmospheric process. Rabinovich [2009] mentioned three different mechanisms to transfer the energy of atmospheric process into long waves in the ocean as:

1. Direct generation of long waves by atmospheric forcing (pressure and wind) on the sea surface.

2. Generation of low-frequency motions (for example, storm surges), and subsequent transfer of energy in higher frequency due to non-linearity, topographic scattering and non-stationarity of the resulting motions.
3. Generation of high-frequency gravity waves (wind and swell) and subsequent transfer of energy into larger scale, lower frequency motions due to non-linearity.

### 3.5. Conclusions

An attempt has been made to investigate the variation in sea-level residuals along the coastal and island locations of India with time periods ranging from a few minutes to an year. Usually, most of the studies neglect the residual (non-tidal) variations of sea-level which are responsible for higher amplitudes of seiches and storm surges. Sea surges (positive or negative), which are short-period events (several hours to few days), are the most extreme oceanic phenomena resulting from weather systems. These variations are stochastic in nature. Extreme low pressures, in addition to wind effects and tides, contribute to destructive storm surges affecting coastal areas (Tsimplis, 1995). Also, abnormal low water levels can affect safety of navigation in rivers and harbours. The present study examined the measured sea-level variations at different coastal and island locations in the Arabian Sea (AS) and the Bay of Bengal (BOB) during 2010 to 2012, and the observations are as follows:

- the tidal amplitude increases linearly from south towards north till the central west coast of India. However, along the east coast of India, the tidal amplitude at Yanam to Gopalpur appears to be constant.
- the measurements at two southern locations (Mandapam and Tuticorin) along the east coast of India in the Gulf of Mannar reports low tidal amplitudes.
- the tides measured in the AS locations could be classified as mixed, mainly semi-diurnal tides with Form number varying within the range of 0.25-1.5. However, in BOB, the Form number is less than 0.25 from Port Blair to Gopalpur indicating semi-diurnal tides. At Mandapam and Tuticorin, the tides are mixed, mainly semi-diurnal type.
- the sea level residual variability exists at all the locations throughout the measurement period (or throughout the year). The SLR varies within  $\pm 25$  cm at most of the locations, except at the southern tip of India (Colachel), where

the variations are up to  $\pm 50$  cm due to focussing of waves because of local topography.

- the low frequency spectra of the sea level residuals have time periods around 2.5, 3.8, 5.3, 7.6, 19.5, 36 and 64 days. However, the spectra of the daily-mean SLR in BOB show oscillations with time periods around 2.4, 3.9, 5.1, 7.4, 9.7, 12.3, 18.9, 36.0 and 64.0 days.
- the high frequency oscillations of the sea level residual in the AS have major peaks at 360, 160, 85, 75, 49 and 21 min. However, the spectral energy peaks observed at time periods of ~118, 90, 75, 43, 32, 20 and 14 min at locations in the BOB are lower compared to that at the measurement locations in the AS.

## Chapter 4

### Sea-level variability during extreme events

#### 4.1. Introduction

The open ocean long waves generated in response to major forcing such as under-sea seismic activity and atmospheric disturbances, while approaching the coast occasionally generate large amplitude seiches in certain regions. Although these waves may have different sources and therefore different characteristics, the local topography may modify them in similar ways, thereby producing similar oscillations and sometimes even destructive consequences. The meteotsunamis are mainly associated with atmospheric gravity waves, pressure jumps, frontal passages, squalls and other types of atmospheric disturbances, which normally generate barotropic ocean waves in the open ocean and amplify them near the coast through specific resonance mechanisms (Proudman, Greenspan, shelf, harbour). Therefore, the observed sea-level oscillations near the coast are a combined effect of one or more external forcing and topographic influence. The periods of such sea-level oscillations may range from minute to hour.

The synoptic atmospheric perturbations, such as atmospheric pressure or wind patterns, generally have characteristic spatial scales of a few hundred kilometres and may have time periods larger than a few hours. The spatial and temporal scales normally associated with the large-scale synoptic perturbations are of the order of ~500 km and >1 day period, respectively. However, the sea-level variability observed is of high-frequency in spatial and temporal scales of the order of 50 km and few minutes. Therefore, synoptic atmospheric systems are not likely to excite directly high-frequency sea-level oscillations even if realistically they are considered to be quite broadband (both in frequency and wave number), as they usually do not contain much energy at the scales and periods required for the excitation of seiches (Candela et. al., 1999). However, synoptic atmospheric systems are known to develop instabilities that radiate energy in the form of high frequency gravity waves (Fujita, 1955; Monserrat and Thorpe, 1992). Excitation of short-period (minutes) sea-level oscillations near a coast by the passage of atmospheric pressure gravity waves has been observed in other places such as Nagasaki Bay in Japan,

where the phenomenon is known as “Abiki” (Hibiya and Kajiuira, 1982). Similar short-period (minute) oscillations of meteorological origin are observed to occur at times at some bays and estuaries and have local names such as “Rissaga” in Belearic Island, “Marubbio” in Sicily, “Milghuba” in Malta, and “Seebär” in Baltic Sea. However, several authors suggested the term “meteotsunami” or “meteorological tsunami” to describe these oscillations, signifying their similarity to tsunami waves. Rabinovich and Monserrat [1996] and Monserrat et al. [2006] provide a comprehensive account on observations and nomenclature of such phenomena.

In this chapter, the mechanism and characteristics of oscillation of the water body in the Mandovi estuary in the central west coast of India due to the following two different extreme events are described: (i) the passage of cyclones *Yemyin* (June 2007) and *Phyan* (November 2009) and (ii) geophysical tsunami (September 2007). The characteristics of these oscillations were investigated by analyzing the sea-level data from a subsurface pressure-based sea-level gauge deployed at Verem in the Mandovi estuary along with surface meteorological measurements from the region.

### 4.2. Data and methods

In the present study, time-series data from two locations have been used: Verem (Goa) and Kavaratti Island (Lakshadweep Archipelago) as shown in Fig. 4.1a. These stations are part of ICON. At Dona Paula, Goa, an autonomous weather station (AWS) is installed on the terrace of the National Institute of Oceanography (NIO) at a height of ~48 m above MSL, and at Kavaratti the AWS is installed on the top of the sea-level station building at a height of ~10 m above MSL. Evaluation of AWS sensors has been described by Mehra et al. [2005]. Sea-levels were measured (see Fig. 4.1 and Table 4.1) using near real-time reporting subsurface pressure-based sea-level gauges deployed at Verem and Kavaratti. The pressure transducer (Honeywell Inc.) incorporating silicon piezoresistive technology used in the pressure tide gauge has been evaluated by Vijaykumar et al. [2005] and Mehra et al. [2008] for oceanographic and limnological measurements. The horizontal distance between the sea-level gauge and the weather station locations at Goa is ~5 km. The observed parameters (Table. 4.1) and the observation periods covered under different events are as follows:

- Event 1 (E1): 23 - 25 June 2007; passage of cyclonic storm *Yemyin*.
- Event 2 (E2): 12 - 14 September 2007; occurrence of Sumatra tsunami.
- Event 3 (E3): 9 - 12 November 2009; passage of cyclonic storm *Phyan*.

**Table 4.1.** Summary of observations.

# For the pressure gauge and AWS, the depth and height are given relative to chart datum and mean sea level, respectively.

Measurement station	Measured variable	Event	System	Depth/ Height (m) <sup>#</sup>
Verem, Goa	Sea level, water temperature	E1, E2 and E3	Subsurface pressure gauge and temperature sensor	-1.0
Dona Paula, Goa	Wind and air pressure	E1 and E3	AWS	48.0
Kavaratti, Lakshdweep archipelago	Sea level, water temperature	E1	Subsurface pressure gauge	-1.0
	Wind and air	E1	AWS	10.0

## Sea-level variability during extreme events

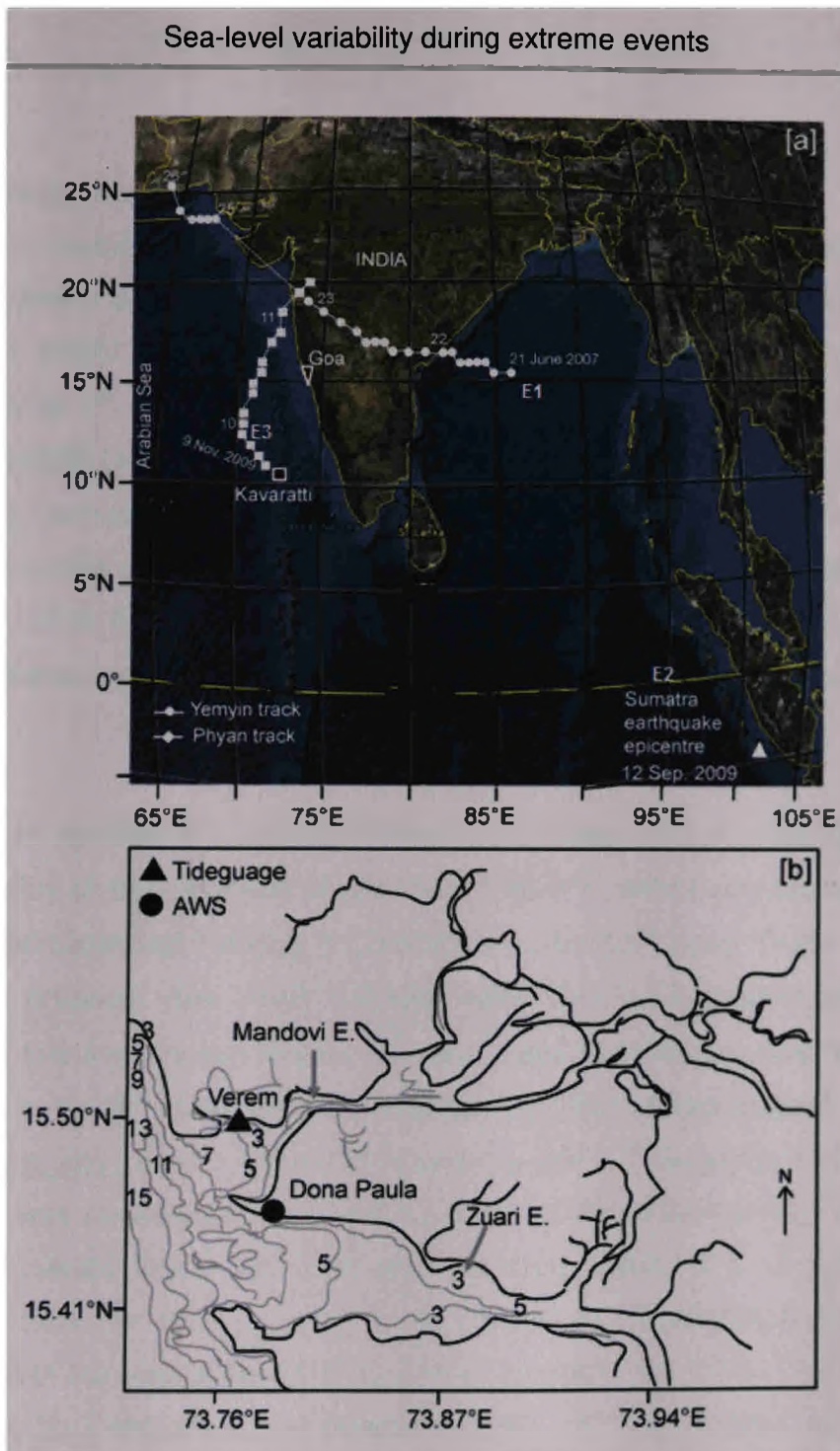


**Figure 4.1.** The study region in the Arabian Sea [a] cyclone tracks of Yemyin and Phyan ([www.imd.gov.in](http://www.imd.gov.in)) and Sumatra earthquake epicentre; [b] the locations of autonomous weather station (AWS) and pressure gauge stations in the Mandovi estuary region (Fig. 4.1b is adapted from Fig.1, Sundar & Shetye, 2005).



### 4.3. Extreme events

In 2007, the Arabian Sea (AS) experienced three atmospheric disturbances and arrival of Sumatra tsunami waves. In particular, two meteorological events occurred during June 2007. The first, named "Gonu", originated at 15.0°N, 68.0°E in the Arabian Sea on 1<sup>st</sup> June 2007 and crossed the northeast Oman coast near Muscat during 0200-0300 UTC on 6<sup>th</sup> June and moved further north to 25.5°N, 58.5°E on 7<sup>th</sup> June. During the course of cyclone movement, the estimated central pressure (ECP) dipped to 920 hPa and the corresponding sustainable surface winds peaked to 127 knots about 20°N, 64°E on 4<sup>th</sup> June during 1500-1800 UTC. However, Gonu was not able to generate any noticeable influence over the sea-level along the west coast of India.

Another cyclone (E1) named "Yemyin" originated on 21<sup>st</sup> June 2007 at 0300 UTC in the Bay of Bengal (BoB) about 15.5°N, 86.0°E, which crossed north Andhra Pradesh (Machilipatanam) during 0100-0300 UTC on 22<sup>nd</sup> June. There was a well-marked low pressure over north Konkan region and its neighborhood (~19.0°N, 74.0°E) and this then moved toward the west coast of Pakistan (near 64.0°E) as a cyclonic storm by 26<sup>th</sup> June 2007 as recorded by India Meteorological Department (IMD, [www.imd.gov.in](http://www.imd.gov.in)). A tsunami (E2), caused by the 12<sup>th</sup> September 2007 Sumatra earthquake, was observed at Goa and Kavaratti Island lagoon in AS. The tsunami arrived at Kavaratti Island and Goa after travelling nearly 5 h 15 min and 8 h, respectively from the source region in Sunda trench (Prabhudesai et al., 2008). Manifestation of the September-2007 Sumatra tsunami in the Indian Ocean has been reported also by Pattiaratchi and Wijeratne [2009]. Another tropical cyclonic storm (E3) "Phyan", which developed in the southeastern AS moved northward along the eastern AS during 9-12 November 2009, and made landfall at the northwest coast of India. Phyan was also examined to study the response of the coastal waters at Verem (Fig. 4.1).

#### 4.3.1 Response of sea-level to cyclone Yemyin

The response of sea-level to cyclone "Yemyin" was manifested as storm surges at the study sites as indicated in Fig. 4.2 and Table 4.2. Event E1 occurred during the

40-day period, in which wind, atmospheric pressure, water temperature and sea-level data were collected at Verem and Kavaratti (Fig. 4.2). The large scale extent of E1 is evident in wind and atmospheric pressure measurements at Verem and Kavaratti Island; the latter being ~550 km away down south of the former (Fig. 4.1). Almost, similar meteorological conditions existed at Verem and Kavaratti (Fig. 4.2 & Table 4.2). During E1 (22-25 [Julian days 173-176] 2007) as shown in Figs. 4.2a.1 & 4.2b.1, the wind energy is ~ 9.4 (11.2)  $\text{m}^2\text{s}^{-2}$  with speeds peaking upto 16.6 (16.8)  $\text{ms}^{-1}$  at Verem (Kavaratti). The wind direction at Verem and Kavaratti stations remained stabilized at ~249° and 239° (Table 4.2) as shown in Figs. 4.2a.2 & 4.2b.2, respectively with respect to north during and after Yemyin (23 June - 17 July [Julian days 174-198], 2007). The atmospheric pressure (Figs. 4.2a.3 & 4.2b.3) showed a variance of ~18.0 (10.8)  $\text{mb}^2$  and fall of ~10.8 (6.9) mb during E1 (21-29 [Julian days 172-180, 2007] at Verem (Kavaratti). During this event, sea surface temperature (SST) at Verem dropped by ~4.5°C, but, no noticeable drop at Kavaratti. The observed selective water temperature drop at Verem is due to the influx of rain-induced fresh water (rainfall of ~555 mm in the study region during 19-29 June (Julian days 170-180) 2007, discharged into this region from the Mandovi and Zuari estuaries. Kavaratti being an open ocean station, such cold water discharge was absent. The sea-level responses at Verem and Kavaratti were manifested in terms of positive surges upto ~40 cm and 36 cm, respectively.

#### **4.3.2 Response of sea-level to cyclone Phyan**

Meteorological conditions at Verem during Phyan (E3) are shown in Fig. 4.2c. Wind speed during 10-12 (Julian days 314-316) November 2009 peaked upto 12.6  $\text{ms}^{-1}$  and wind direction shifted from 54° to 192° with respect to north. The atmospheric pressure dipped by ~12.9 mb and SST dropped by ~1°C. The sea-level exhibited a positive surge upto ~47 cm (Table 4.2). A detailed study on the response of the coastal regions of eastern Arabian Sea (AS) and Kavaratti Island lagoon to this tropical cyclonic storm 'Phyan' during 9–12 November 2009 (till it made the landfall at the northwest coast of India) has been reported by Joseph et. al.[2010]. The present study is mainly concerned with sea-level residual oscillations generated in Kavaratti lagoon and Verem estuary due to E3. Also to understand the changes in the frequency spectrum at these locations due different events than during the calm period (background spectrum).

**Table 4.2.** Meteorological and sea-level observations at Verem and Kavaratti during the cyclones Yemyin and Phyan.

S. No	Variables	E1, Verem	E1, Kavaratti	E3, Verem
1	Maximum wind speed (m/s)	16.6	16.8	12.5
2	Wind direction (°N)	249 <sup>#</sup>	239 <sup>#</sup>	185
3	Atmospheric pressure drop (mb)	10.8	6.9	13.5
4	SST drop (°C)	4.5	-	1
5	Sea-level residual (cm)	40	36	47
6	Atmospheric pressure fall time from maximum to minimum (h)	79.2	88.8	64.8
7	Atmospheric pressure rise time from minimum to maximum (h)	76.8	64.8	55.2
8	Surge rise time from minimum to maximum (h)	45.6	144.0	43.2
9	Surge fall time from maximum to minimum (h)	81.6	168.0	84.0

# wind direction stabilized during and after cyclone *Yemyin* (E1) at Verem and Kavaratti stations.

#### 4.3.3. Response of sea-level to Sumatra Tsunami (2007)

Response of the sea (sea-level and SST) at Verem station to the September 2007 Sumatra tsunami (E2) is shown in Fig. 4.3. Unlike a positive surge observed in the case of episodic meteorological conditions, the September 2007 Sumatra tsunami at Verem caused oscillations upto  $\pm 15$  cm in sea-level residuals (Fig. 4.3a). The response of the sea at Verem station to the tsunami waves was also clearly manifested in SST, which showed oscillations during 7-13 September (Julian days 250-258) with relatively larger variance of  $\sim 17.9^{\circ}\text{C}^2$  in contrast to a lesser variance of  $\sim 12.0^{\circ}\text{C}^2$  during normal days just before the event 3-5 September 2007 (Julian days

246-248). Some aspects related to the observed SST anomaly during pre- and post-earthquake are presented in Section 4.7.

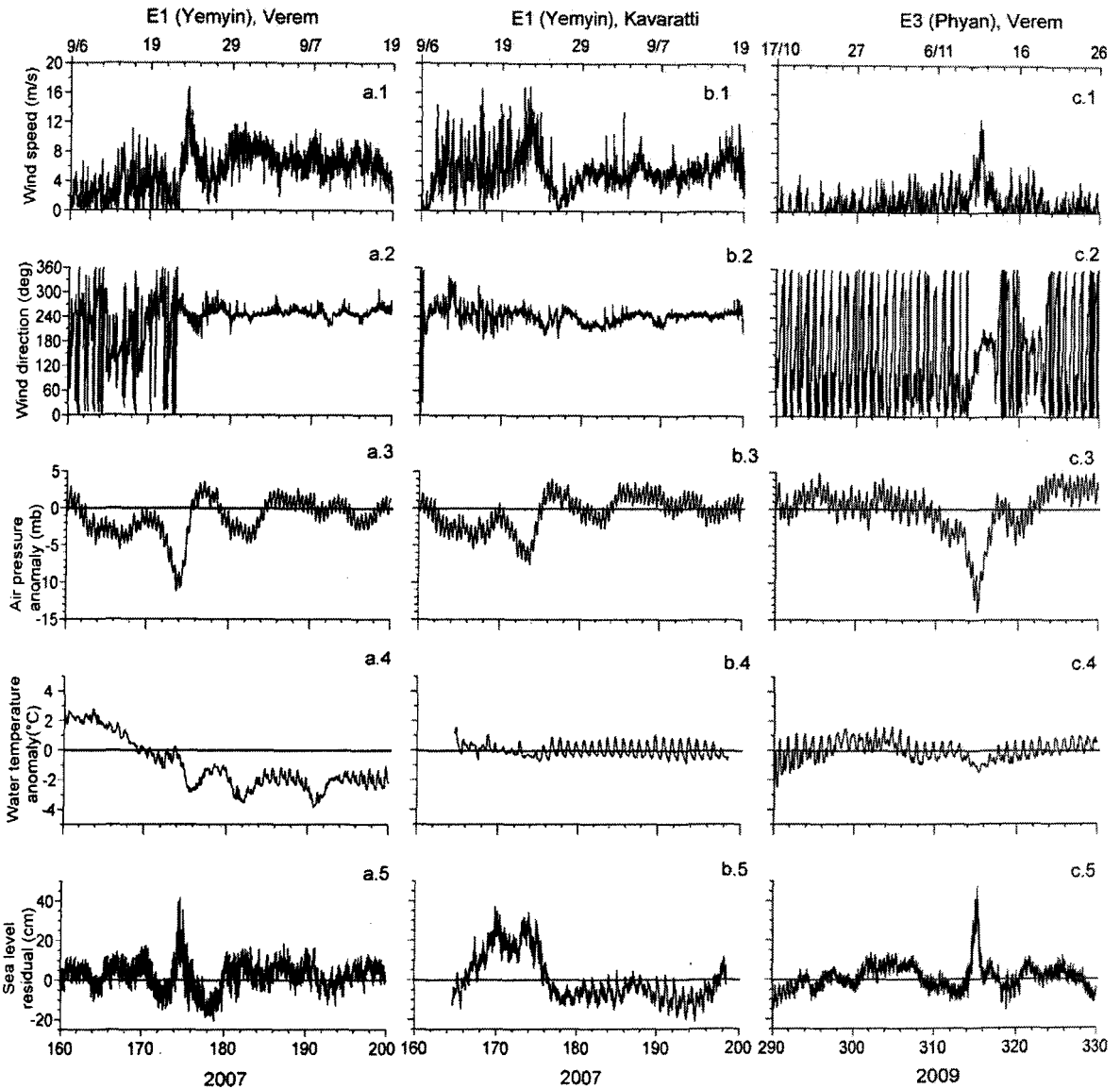


**Figure 4.2.** Sea-level and surface meteorological parameters at Verem and Kavaratti during the episodic events: [a.1-5] wind speed, wind direction, atmospheric pressure anomaly, sea surface temperature anomaly and sea-level residual during the atmospheric disturbance event E1 (cyclone Yemyin) in June 2007 at Verem. [b.1-5] Variables are same as in [a] at Kavaratti Island region during E1 and [c.1-5] Variables are same as in [a] during the atmospheric disturbance E3 (cyclone Phyan) in November 2009 at Verem.

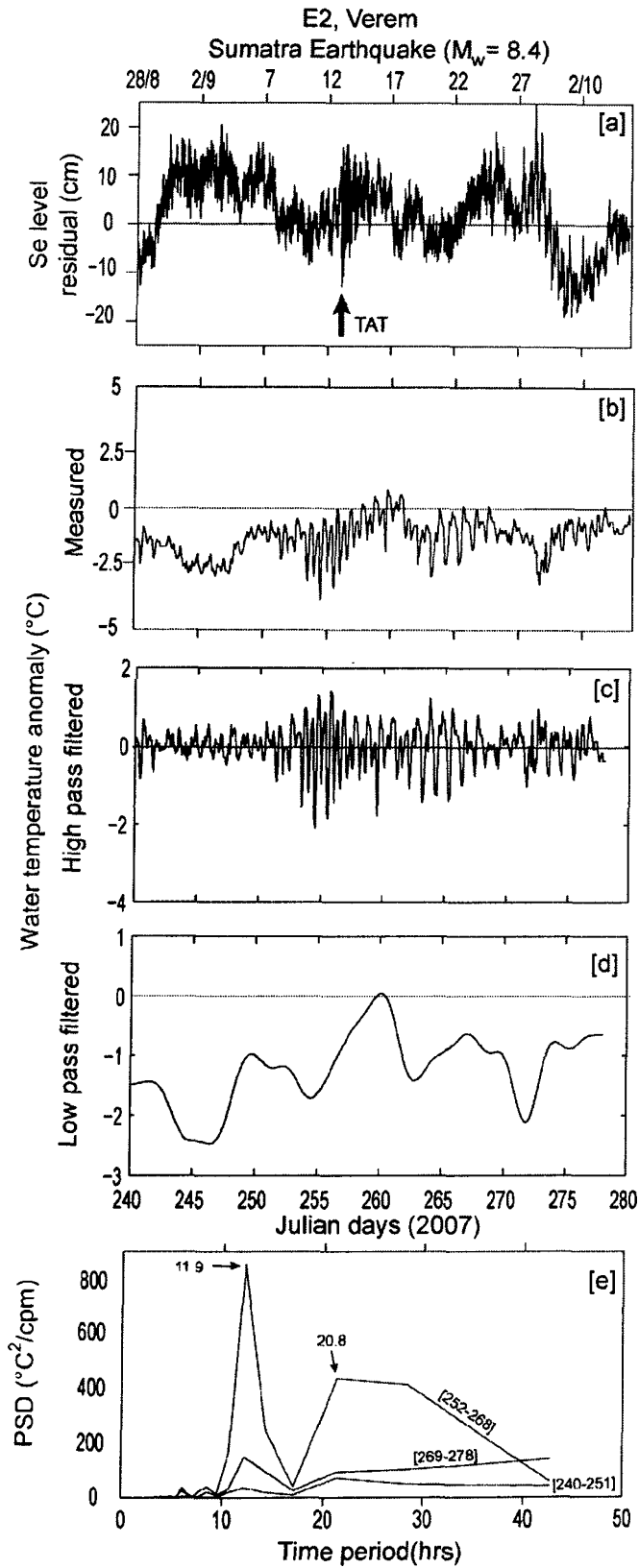


**Figure. 4.3.** Sea water parameters observed at Verem, in response to the episodic event E2 of 12<sup>th</sup> September 2007 due to Sumatra earthquake ( $M_w=8.4$ ). [a] sea-level residual (cm), [b] measured SST anomaly ( $^{\circ}\text{C}$ ), [c] high pass filtered SST ( $^{\circ}\text{C}$ ), [d] low pass filtered SST anomaly ( $^{\circ}\text{C}$ ), and [e] spectrum of measured SST anomaly before (28 August to 8 September [Julian days 240-251] 2007), during (9-25 September [Julian days 252-268] 2007) and after (26 September - 5 October [Julian days 269-278] 2007) the tsunami arrival time (TAT) at Verem. The TAT at Verem was 00:45 IST on 13<sup>th</sup> September 2007. The number associated with significant peaks is time period in hours.

#### 4.4. Non-resonant character of Kavaratti Island lagoon

Kavaratti Island's lagoon is an open sea station. Sea-level residuals (SLR) were passed through a 5<sup>th</sup> order Butterworth high-pass filter (with period < 2h) to obtain high frequency oscillations as shown in Fig. 4.4a. The amplitude of high-frequency oscillation at Kavaratti lagoon in response to the cyclonic storm "Yemyin" was found to be  $\sim \pm 10$  cm during E1 (Fig. 4.4a). The event spectrum during E1 at Kavaratti and the corresponding background spectrum for SLR and atmospheric pressure are shown in Figs. 4.4b & 4.4c, respectively. The spectrum was obtained using the 'pwelch' function from Matlab with the following parameters: sampling frequency was 0.2 (0.1) cpm for SLR (atmospheric pressure); Hamming window of 256 data points with 50% overlap; length of the FFT with the integer  $nfft = 256$ . The background spectrum of SLR for Kavaratti station is over the duration 1<sup>st</sup> September - 9<sup>th</sup> October 2007. The background spectrum of atmospheric pressure in respect of this station is over the duration 29<sup>th</sup> June - 28<sup>th</sup> July 2007. The background spectra provide a good estimate of the topographic response of a site, where the natural oscillations are not subdued by the energetic characteristics of the forcing.

It is clearly seen from Fig. 4.4b that at Kavaratti lagoon, both in background and event spectra, energy is present at higher frequencies. This could probably be associated with high-frequency infragravity (IG) waves generated by nonlinear interaction of wind waves and swells at this site. These waves have typical periods of 30 s to 300-600 s and length scales from 100m to 10 km (Rabinovich, 2009). There are no prominent spectral peaks and hence no natural oscillations. The oscillations found in Fig. 4.4a could be characteristics of storm-generated broad-frequency signal. In any case, there was no visible seiches at this site (i.e. natural oscillations), as there are no prominent spectral peaks. The non-resonant character of Kavaratti Island lagoon was also noticed during cyclonic storm "Phyan", despite intense wind forcing; the surge at this lagoon was insignificantly weak due to the combined effect of absence of non-resonant amplification and lack of river water discharge into the lagoon (Joseph et. al., 2010) .

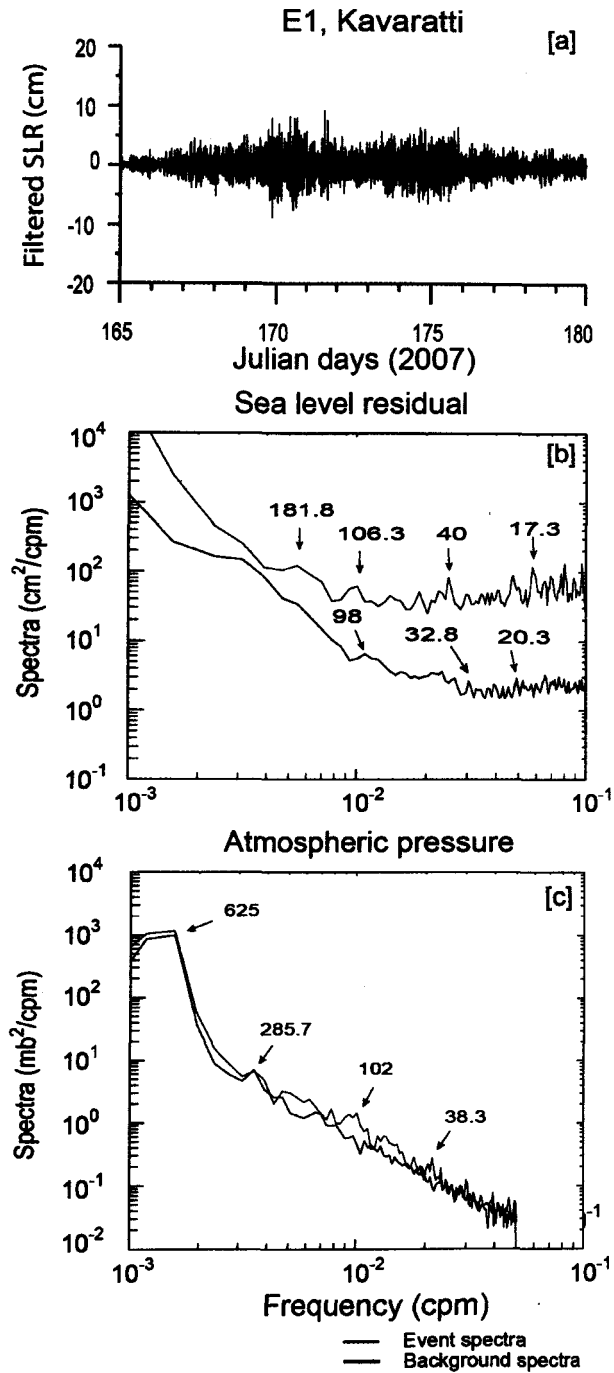


**Figure 4.4.** Characteristics of sea-level residual (SLR) and atmospheric pressure at Kavaratti Island lagoon region during event E1: [a] time series of high pass filtered SLR (period < 2 h), [b] spectrum of SLR over 7 days 18-25 June [Julian days 169-176; N=2016] 2007 along with background spectrum (black), and [c] spectrum of atmospheric pressure anomaly over 7 days 18-25 June [Julian days 169-176; N=2016] 2007 along with background spectrum (black). The numbers marked over the significant peaks are period in minutes.

#### **4.5. High frequency oscillations at Verem**

The high-pass filtered SLR (hf-SLR) oscillations (5<sup>th</sup> order Butterworth filter as mentioned in Section 4.4) observed at Verem station during E1, E2 and E3 are shown in Fig. 4.5. The hf-SLR oscillations are  $\sim \pm 15$  cm during E1 (Fig. 4.5a) and E2 (Fig. 4.5b). The hf-SLR due to E2 shows a step response and decays exponentially (Fig. 4.5b). However, the hf-SLR during E1 and E3 (due to meteorological disturbances) shows a gradual rise and fall (Fig. 4.5a & 4.5c). During E3, hf-SLR oscillations remained  $\sim \pm 10$  cm at Verem (Fig. 4.5c). Kavaratti data is excluded in the present study (i.e., harbour resonance) because it is an open sea station, not having the resonance features of a harbour.

##### **4.5.1. Sea-level spectrum during the events E1, E2 and E3**

The event spectra estimated (method explained in section 4.4) for Verem station during E1 (Yemyin), E2 (September 2007 Sumatra tsunami) and E3 (Phyan) and the corresponding background spectra for SLR and atmospheric pressure anomaly are presented in Figs. 4.6 and 4.7, respectively. The background spectrum of SLR in respect of Verem station is the average of spectra over 10-30 October, 10-30 November and 8-31 December of 2007. The background spectrum of atmospheric pressure in respect of this station is over the duration 1<sup>st</sup> January - 31<sup>st</sup> March 2007.

##### **4.5.2 Sea-level background spectrum**

The background spectra may differ if the response of the estuary is sensitive to the characteristics of forcing conditions such as angle of incidence of ocean waves, and may oscillate differently under varying conditions. To determine the spectral properties of longwave oscillations at a particular location, analysis of spectrum over a long period (more than 2 months) called background spectra is carried out. The background spectra at Verem are event independent, and remains same during the different periods as the local geometry remains same (Fig. 4.6). Although the 'event' (atmospheric disturbance or geophysical tsunami) spectra are more energetic and different (Fig. 4.6), the background spectra at different sites have significant differences at high frequencies as seen at Kavaratti (Fig. 4.4b), indicating the influence of local topography.



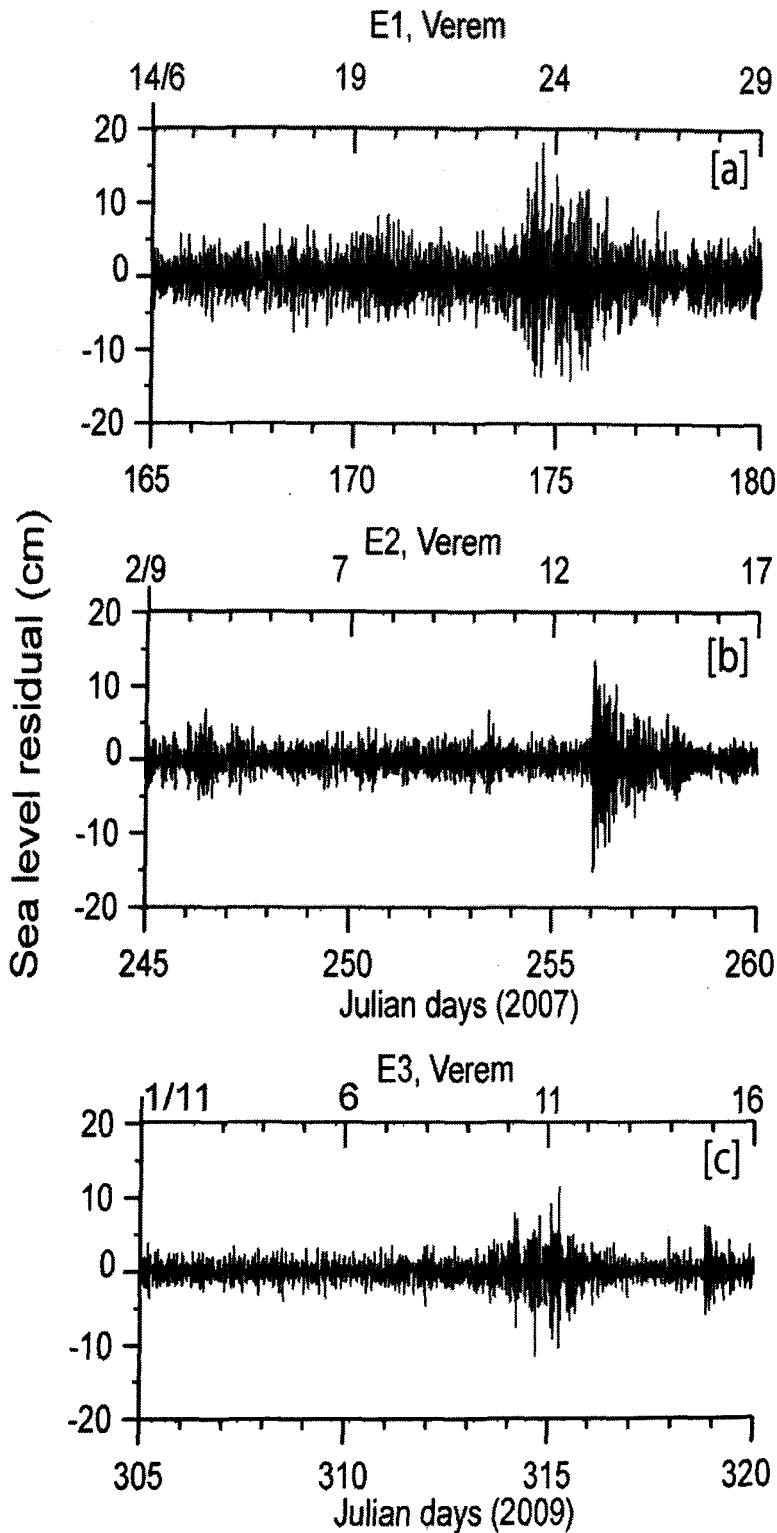


**Figure 4.5.** Time-series of two-weeks long, high-pass filtered (period < 2 h) SLR at Verem during different episodic events [a] E1, [b] E2, and [c] E3. The X-axis represents time of the respective year.

The Mandovi estuary, where the pressure gauge at Verem station is located, is ~4 km wide at the mouth (also known as Aguada Bay), and ~4 km long stretch of the bay is marginally deeper than the rest of the estuarine channel (average depth of the bay is about 5 m). Then the channel narrows considerably from the bay for another ~6 km stretch (750 m wide & 5 m deep; Shetye et al., 2007). Thus, in the case of partially enclosed basins such as gulfs, bays, fjords, inlets, ports and harbours, a specific type of seiche motion occurs which are known as harbour oscillation (coastal seiche), mainly generated by the long waves entering through the open boundary from the open sea. In a simple case of a narrow rectangular bay with uniform depth, the lowest mode known as Helmholtz's mode of oscillations normally dominate (Rabinovich, 2009), and it is estimated as:

$$T_n = \frac{4L}{(2n+1)\sqrt{gH}}, \text{ for mode } n = 0, 1, 2, 3, \dots \quad (4.1)$$

Thus a rough estimate of the fundamental (Helmholtz) mode could be obtained assuming the above dimensions of the Aguada bay. The fundamental period ( $T_0$ ) of oscillation ( $T_0 = \frac{4L}{\sqrt{gH}}$ ) is ~38 minutes, where  $L$  ( $m$ ) is the length of the bay,  $H$  ( $m$ ) is the mean water depth and  $g$  ( $ms^{-2}$ ) is acceleration due to gravity.

The spectrum during E1 (Fig. 4.6a) shows major peaks at 80, 45.6, 40, 35.6 and 21.3 min. During E3, the major peaks are found at 41.3, 32.7 and 20.6 min (Fig. 4.6c). During the September 2007 Sumatra tsunami (E2) the major spectral peaks are at 91.7, 42.7, 35.5 and 21.6 min (Fig. 4.6b). The fundamental time period estimated using equation-4.1 is valid for a simple, narrow and long rectangular basin with constant depth, while the Aguada bay (as shown in Fig.4.1b) is much more complex. It is probable that the specific period of ~41.3 minutes (average of 40.0, 41.3 and 42.7 min) as evident in Fig. 6 (a, b & c) is associated with the fundamental bay period (Helmholtz mode), which is in broad agreement with the theoretically estimated value of 38 minutes.

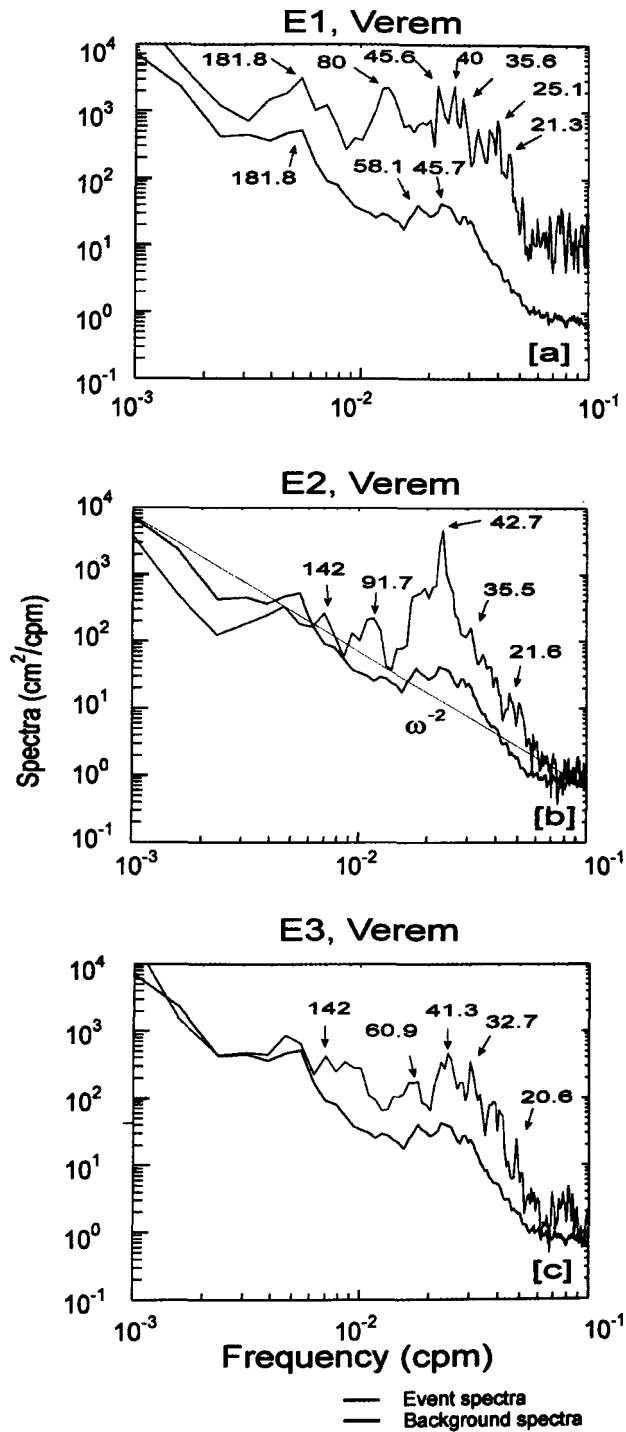


**Figure 4.6.** Sea-level residual (SLR) spectra at Verem during different events (red) along with the corresponding background spectra (black): [a] E1 over 3 days (Julian days 174-176, 2007;  $N=864$ ), [b] E2 over 3 days (Julian days 255-258, 2007;  $N=864$ ), and [c] E3 over 4 days (Julian days 313-317, 2009;  $N=1152$ ).  $N$  represents the number of data samples used in estimating the spectra. The numbers marked over the significant peaks are period in minutes.

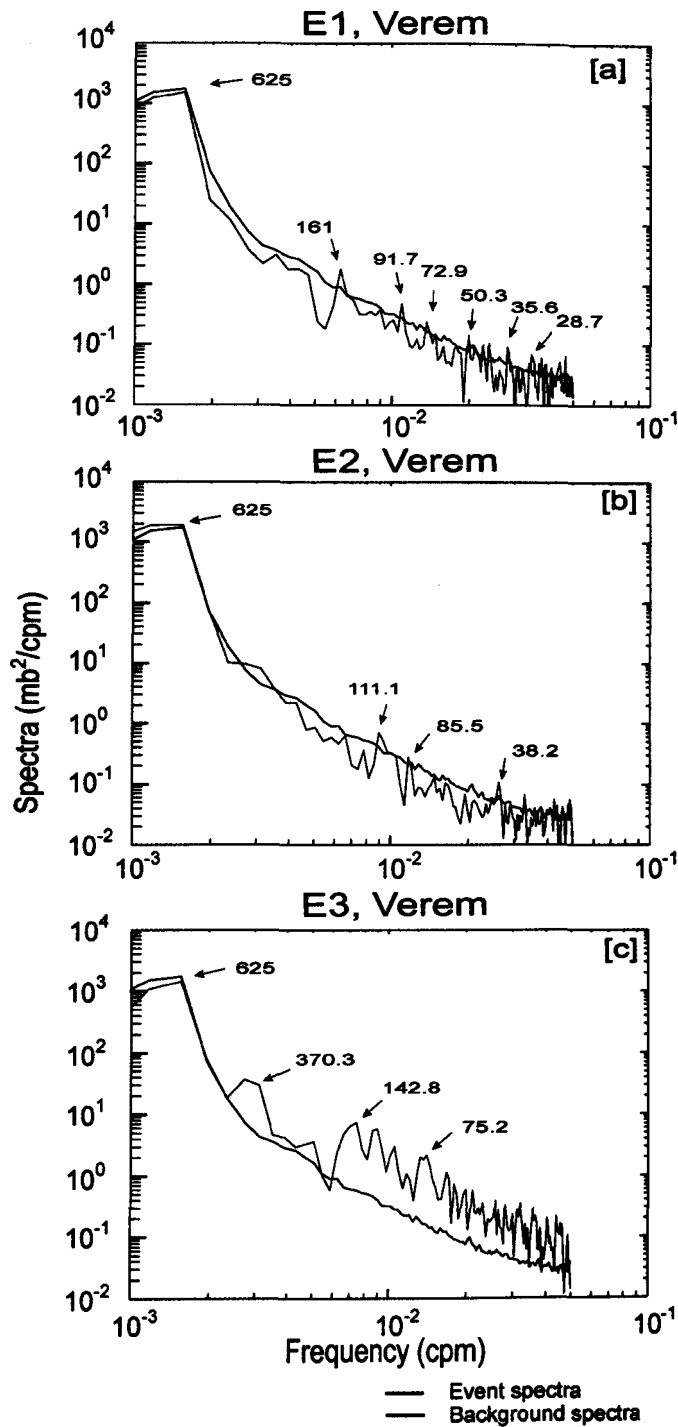


**Figure 4.7.** Atmospheric pressure anomaly spectra during different events (red) along with the corresponding background spectra (black) at Verem; [a] E1 over 3 days (Julian days 174-176, 2007; N=864) [b] E2 over 3 days (Julian days 255-258, 2007; N=864) and, [c] E3 over 4 days (Julian days 313-317, 2009; N=1152). N represents the number of data samples used in estimating the spectra. The numbers marked over the significant peaks are period in minutes.

#### 4.6. Transfer function for atmospherically generated oscillations

The spectral ratio between the event (geophysical tsunami or atmospheric disturbance) and the respective background spectrum provides information on the external source. The method to separate out the tsunami source and the topographic effects as explained by Rabinovich (1997) and also revised and applied to atmospherically generated seiches by Monserrat et. al. (1998) is briefly outlined below:

Assuming the instrumental noise is negligible, the observed spectrum  $S_{OBS}(\omega)$  may be considered as the sum of the energy associated with the event  $S_E(\omega)$  (tsunami or atmospheric disturbance) and the energy of the background oscillation  $S_B(\omega)$  as:

$$S_{OBS}(\omega) = S_E(\omega) + S_B(\omega) \quad (4.2)$$

If we assume that topographic response  $W(\omega)$  remains unchanged for both the event and background spectra (this may not be true and should be confirmed posteriori) then:

$$S_E(\omega) = W(\omega)E_E(\omega), \quad (4.3)$$

$$S_B(\omega) = W(\omega)E_B(\omega), \quad (4.4)$$

Where,  $E_E(\omega)$  and  $E_B(\omega)$  represent the external forcing during the event and the background conditions, respectively. The spectral ratio during the event and the background signals is then:

$$R(\omega) = \frac{S_{OBS}(\omega)}{S_B(\omega)} = \frac{E_E(\omega)}{E_B(\omega)} + 1 \quad (4.5)$$

Assuming that the initial sea-level variations in the open sea are forced by the atmospheric pressure, we may express  $E_E(\omega)$  as:

$$E_E(\omega) = T(\omega)P_o(\omega) \quad (4.6)$$

Where,  $P_o(\omega)$  is the open ocean atmospheric pressure spectrum and  $T(\omega)$  is the

transfer function between the atmosphere and the ocean. The transfer function depends on the direction and phase speed of the atmospheric waves, bathymetry of the generation region, etc. In most of the cases, the open ocean spectrum may not be available and if the atmospheric wave is coherent over a large area, then the coastal atmosphere pressure  $P_c(\omega)$  may be used in equation-4.6. Rearranging equation 4.3, 4.4, and 4.5 we get:

$$T(\omega) = (R(\omega) - 1) \frac{E_B(\omega)}{P_o(\omega)}, \quad (4.7)$$

The long term bottom pressure measurements in the Pacific indicate that the background open-ocean spectrum  $E_B(\omega)$  is virtually universal (Kulikov et. al., 1983) and can be defined as:

$$E_B(\omega) = C\omega^{-2} \quad (4.8)$$

Where,  $C$  is a constant at a given depth, but increases with decreasing water depth; it also depends on atmospheric activity. The background spectrum at Verem station was used to estimate the value of  $C$  (equation 4.8). The best fit gave  $C = \sim 7 \times 10^{-3} \text{ cm}^2 \cdot \text{cpm}$  (straight line in Fig. 4.6b), which is in comparison with the values of  $C = 10^{-3} - 10^{-4} \text{ cm}^2 \cdot \text{cpm}$  found by Rabinovich (1997) for the open ocean.

#### 4.6.1. Topographic admittance

The constant 'C' is useful to estimate topographic response directly from sea-level spectra without complicated numerical computations. The topographical response function for a particular location is  $W(\omega) = H^2(\omega)$ , where,  $H(\omega)$  is the admittance of function describing the linear topographic transformation of long waves approaching the coast. Following equation-4.4, function  $H_j(\omega)$  for  $j^{\text{th}}$  station may be expressed as (refer Rabinovich and Stephenson, 2004)

$$H_j(\omega) = \left[ \frac{S_B^j(\omega)}{E_B(\omega)} \right]^{\frac{1}{2}} = \omega \left[ \frac{S_B^j(\omega)}{C} \right]^{\frac{1}{2}} \quad (4.9)$$

Using equation-4.9, Rabinovich and Stephenson [2004] computed  $H_j(\omega)$  for twelve stations on the British Columbia coast. They used the observed background spectra and assumed,  $C = 10^{-3} \text{ cm}^2 \cdot \text{cpm}$ . They were able to demonstrate individual resonant properties of the various sites. In fact, function  $H_j(\omega)$  describes integral effect of topography on arriving waves. However, to separate the effect of different topographic features and explain the exact nature of the resonant peaks in  $H_j(\omega)$ , specific numerical experiments have to be conducted.

#### 4.6.2. Spectral ratio

The spectral ratio defined as ratio of spectrum during the event to that of the respective background spectrum provides an estimate of the energy of the external incoming waves during an event. The spectral ratio of SLR for the three events at Verem station during atmospheric disturbances (E1 & E3) and September 2007 Sumatra tsunami (E2) are shown in Fig. 4.8a. The spectral ratio of SLR at Verem during E1 (Yemyin, red line) is more energetic than during E3 (Phyan, green line) with similar peaks at time periods 22 and 13 minutes, respectively. Few peaks in spectral ratio at Kavaratti (Fig. 4.8b) due to E1 are observed at frequencies 17, 21 and 40 minutes, but with less gain due to the open ocean conditions.

Spectral ratio peaks around time period  $\sim 42.7$  min, and it is present in all the three events at Verem, which appears to be associated with its Helmholtz period along with other spectral ratio peaks at 142, 25 and 13 minutes. Another prominent spectral ratio peak for Verem during E1 is at time period  $\sim 80$  min, but conspicuously absent during other events. The spectral ratio of event to background for atmospheric pressure is shown in Fig. 4.8c. The spectral ratio is high for E3 at Verem (Phyan, green) compared to other two events for periods  $\sim 370, 116$  and 73 min.

## Sea-level variability during extreme events

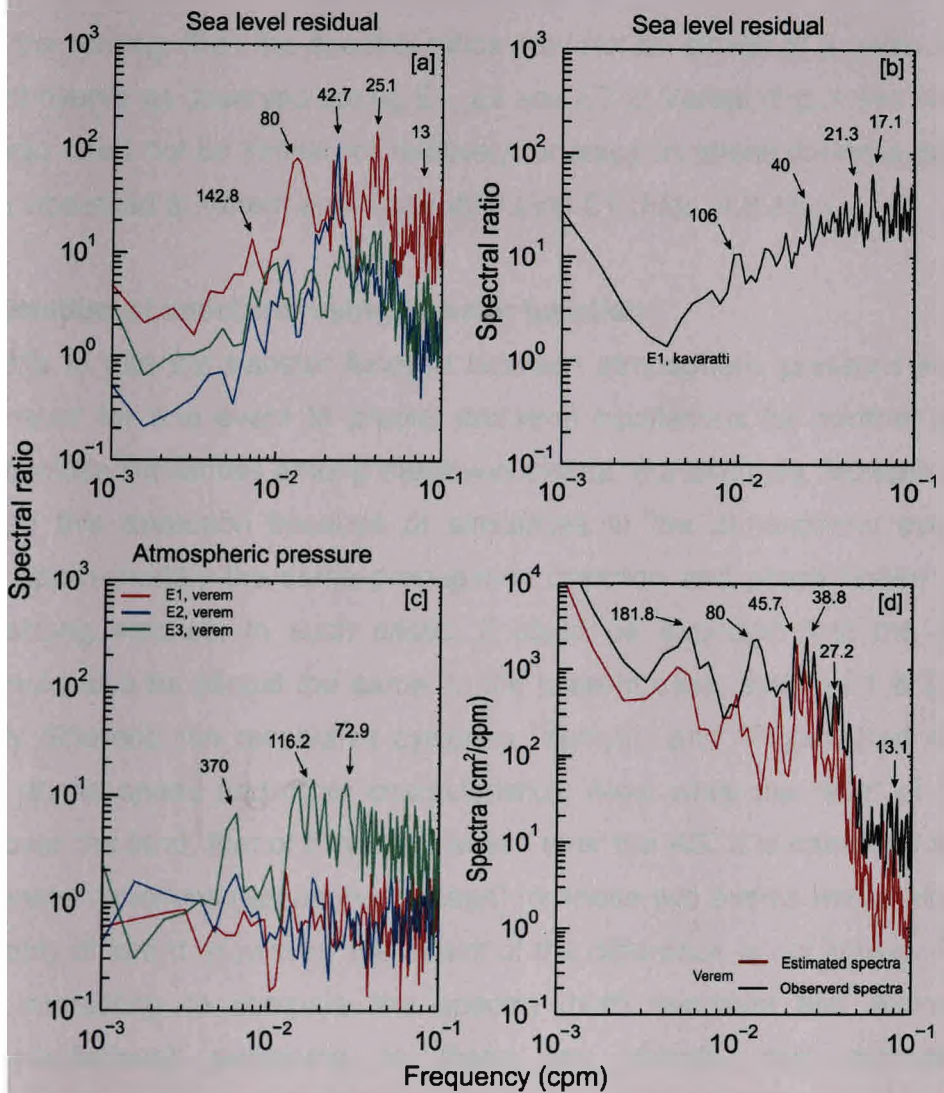


**Figure 4.8.** Spectral ratio (i.e., ratio of spectrum during the event to that of the respective background spectrum) of [a] SLR at Verem (Goa) during the events E1, E2, and E3, [b] SLR at Kavaratti during event E1, [c] atmospheric pressure anomaly at Verem (Goa) during the events E1, E2 and E3. [d] Observed (black) and the computed (red) spectra of SLR at Verem for event E1. The computed SLR spectrum is obtained using atmospheric pressure during E3 based on equation-4.10. The numbers marked over the significant peaks are period in minutes.

Rabinovich and Stephenson [2004] suggested that relatively high-frequency peaks with periods 2–15 min are related to eigen oscillations in local bays and harbours, while low-frequency peaks (20–130 min) are associated with the standing oscillations in larger bays, inlets and straits, as well as with the shelf resonance. If the spectral ratios are independent of measurement location (topography) and entirely



related to the forcing, then the spectral ratios may not be similar at a given location for different events as observed during E1, E2 and E3 at Verem (Fig. 4.8a). Also, the spectral ratio need not be similar for relatively far away locations during a particular event as is observed at Verem and Kavaratti during E1 (Figs. 4.8 a&b).

#### 4.6.3. Estimation of spectrum using transfer function

It is possible to use the transfer function between atmospheric pressure and sea-level estimated for one event to predict sea-level oscillations for another event if there exists close similarities among these two events. For example, Monserrat et al. [1998] used this approach because of similarities in the atmospheric events (in particular, approximately the same propagation direction and phase speed), which generate strong seiches. In such cases, it could be expected that the transfer function would also be almost the same. In the present case, events E1 & E3 were significantly different: the respective cyclones “Yemyin” and “Phyan” had different directions, phase speed and other characteristics. Also, while the “eye” of Yemyin traversed over the land, that of Phyan traversed over the AS. It is natural to assume that the transfer functions (atmosphere/ocean) for these two events would also have been probably different. However, the extent of the difference is not known. Thus, it would be interesting to compare the spectra (both sea-level and atmospheric pressure oscillations) pertaining to these two events, and estimate the event/background ratio for each event.

Following Monserrat et al. [1998] in the use of the transfer function obtained for one event to reproduce the sea-level spectra for the other events based on the coastal atmospheric pressure spectra, it can be inferred that:

$$S_{est}^Y(\omega) = S_B^Y(\omega) + T^P(\omega) \times W^Y(\omega) \times P_C^Y \quad (4.10)$$

Where, the superscripts *Y* and *P* denote the events at Verem during events E1 and E3, respectively, and  $W^Y(\omega) = \frac{S_B^Y(\omega)}{E_B(\omega)}$ . Using equation 4.10, we computed the sea

level spectra for E1 using the atmospheric pressure spectra and the transfer function of E3. The agreement between the estimated (red) and observed (black) spectra (Fig. 4.8d) is quite promising for periods upto 45 min. The major spectral peaks at

periods ~45.7, 38.8, 27.2 and 13.1 min (even though lower energy) are well represented, because they are mainly due to the influence of local topography. Except for a narrow band near the period of 80 min, otherwise, the computed SLR spectra for event E1 is found to be in good agreement with the measured spectrum for this event.

#### **4.6.4. Amplification due to resonance**

The power spectra of atmospheric pressure anomaly at Verem during E1 (Fig. 4.7a) provides no enhancement in energies for frequencies higher than 0.0125 cpm (period < 80 min). However, during E3 at Verem, a few spectral peaks are observed at time periods 142.8 and 75.2 minutes (Fig. 4.7c). The high-pass filtered air pressure (cut-off period < 120 min) does not exceed 0.4 mb. However, during 'E1,' high frequency sea-level oscillations with peak amplitude ~18 cm (Fig. 4.5a) is observed, when the lowest pressure monitored by IMD, India was on Julian days 173.5 and 174 (22 and 23 June) 2007 and the cyclone track was closest to the measurement site on 23 June 2007 (Fig. 4.1a). The estimated ratio of sea-level to atmospheric pressure is ~45 cm/mb, which is very high and therefore the atmospheric pressure alone may not be the cause for these oscillations. Even during extreme events, the observed dynamical multiplication of the static barometer ("inverted barometer = 1 cm/mb") response is usually less than 5.0 (Hibiya and Kajiura, 1982, Vilibic et al., 2004) due to controlling effects of friction, diffusivity and Coriolis forces. However, in the case of certain coastal topography (eg. funnel shaped basins), bays with large amplification factor along with suitable energy content and direction of disturbance may produce high waves of several meters; ~6m in Adriatic Sea (Orlić, 1980) and ~4 m at Balearic Island and Nagasaki bay (Hibiya and Kajiura, 1982; Rabinovich and Monserrat, 1998).

Such anomalous gain may be due to harbour resonance. The most common factors that initiate such oscillations are atmospheric processes and nonlinear interaction of wind waves and swell. It involves generation of long waves in the open ocean and amplification of these waves over the shelf and near the coast. Due to "harbour resonance", the arriving waves further amplify in the bay, thereby generating intense seiches, and sometimes even destructive meteorological tsunamis. During resonance, the atmospheric disturbance propagating over the

ocean surface is able to generate significant long ocean waves by continuously pumping energy into these waves with different possibilities (Rabinovich et. al., 2009 and related references therein).

In the case of E1 during Yemyin, the "eye" of the disturbance in the near vicinity of the study region moved over land at a speed of  $\sim 38$  km/h and oriented  $\sim 290^\circ$  ([www.imd.gov.in](http://www.imd.gov.in)) with respect to north. It is possible that the observed oscillations during E1 could be related to forced resonant oscillations triggered by air pressure variations and wind stress, which then propagated inward into the estuary. Also, as reported in a study by Candela et al. [1999], sea-level measurements in the open sea and inside the port indicated high coherence for the bands between 25 and 40 cpd (i.e., 36-57.6 minutes). In contrast, at periods shorter than 35 min the coherence between the two records dropped significantly, indicating that these oscillations are due to local topography. The SLR oscillations at Verem during E1 are  $\sim 18$  cm, whereas the SLR oscillations observed at Verem (Kavaratti) during E3 (E1) are within  $\sim 10$  cm. This difference could be reasoned that (Rabinovich and Monserrat, 1996) just as not every large underwater earthquake excites a tsunami, so even strong typhoons or atmospheric pressure jumps do not always generate destructive long waves. Both geophysical tsunamis and meteorological tsunamis are relatively infrequent events. Some specific resonance conditions are apparently necessary to generate noticeable meteorological tsunamis.

#### **4. 7. Observed pre- and post-earthquake enhanced seawater temperature oscillations at Verem**

An interesting observation pertaining to the event E2 at Verem station near the mouth of the Mandovi estuary is that approximately 3 days prior to the 12 September 2007 Sumatra earthquake, water temperature at this station started exhibiting a distinctly stronger semi-diurnal oscillation and these well-defined oscillations continued for a week after the earthquake also. Whereas the water temperature swing during the preceding normal days was weak ( $\sim 1.5^\circ\text{C}$ ), a much larger temperature swing ( $\sim 3.5^\circ\text{C}$ ) is clearly seen in the period beginning  $\sim 3$  days prior to the 12 September 2007 Sumatra earthquake (Fig. 4.3c). We also notice a relatively larger variance ( $\sim 17.9^\circ\text{C}^2$ ) during the period of enhanced temperature swing in

contrast to a lesser variance ( $\sim 12^{\circ}\text{C}^2$ ) during the preceding normal days of lesser temperature swing.

#### **4.7.1. Pre-earthquake water temperature oscillations**

##### **4.7.1.1. Earthquake precursors**

Based on available information, an attempt is made to provide explanation for the pre-earthquake water temperature oscillations observed at the Verem station. Earthquakes (i.e., ruptures within the earth caused by stress) are associated with the release of strained energy that has been building over many years. It is an accepted fact that a few days before a major earthquake occurs, when the plates begin to crack, a variety of signals (known as earthquake precursors) representing land, ocean, atmosphere, and ionospheric anomalies begin to emanate from the preparation zone of the earthquake (Joseph, 2011). The occurrence of a strong submarine earthquake entails intense ocean-floor oscillations in a rather large area during a prolonged period of time. Based on field measurements obtained from the JAMSTEC deep-sea ( $\sim 7500$  m depth) underwater observatory (Hirata et al., 2002) during the 2003 Tokachi-Oki tsunamigenic earthquake as well as a 3-D numerical model developed in the framework of linear potential theory of ideal "compressible" fluid, Nosov and Kolesov (2007) reported clear indications of the generation of depth-dependent low-frequency elastic oscillations of the seawater column and a complicated fast oscillating wave structure on the water surface in response to the elastic oscillations of the water layer. Nosov and Kolesov (2007) found that the bottom trembling associated with the cracking provides a resonant pumping of energy to the elastic oscillations of water column, in which the bottom topography plays a leading role in the formation of elastic oscillations spectrum.

##### **4.7.1.2. Short acoustic waves**

In another mechanism, seafloor motions generate short acoustic waves in the water medium, in which intense pressure jump behind the acoustic wave-front results in the propagation of these waves from the seafloor toward the sea surface. The nonlinear effects accompanying the wave-front motion result in the transport of liquid particles from the seafloor to the sea surface — a process known as "acoustic wind" (Ostrovskii and Papilova, 1974). The just mentioned vertical oscillations of the seawater column

extending from the seafloor upto the sea surface transports cold water from the ocean bottom to the subsurface and surface layers of the ocean. Such seismically-induced water-mass transport in the upward direction (like upwelling process) results in the appearance of water-temperature anomalies in the zones of submarine earthquakes. The cold water mass can then get transported to distant locations by several oceanographic and meteorological forcings. The vertical transport of nutrient-rich water, induced by this upwelling process, has been found to give rise to a significant increase of chlorophyll concentrations in the upper layers of the sea surface “prior” to the earthquake events (Singh et al., 2006), and its spatial and temporal variability occur due to large-scale disturbances in the oceanic circulation patterns, arising from sudden changes of thermal structure (Chaturvedi and Narain, 2003).

Sea surface temperature drop observed in the coastal and open sea water bodies prior to submarine earthquakes has been measured using satellite-borne sensors. In such cases, although measurements are obtained over a considerably large area, the temporal resolution is rather poor. Therefore, a clear description of evolution and fine-scale temporal variability of sea surface temperature is often not available. However, these measurements yield the average feature of the temperature variability. For example, during the 1996 earthquake event off Japan’s coast, the ocean surface water temperature deviation over a zone of horizontal dimension of ~500 km was minus 4-5°C, and the lifetime of anomaly exceeded two days (Levin et al., 2006). Such seismically induced sea surface water temperature drops were recorded also in the Sea of Okhotsk and in the Black Sea (Nosov, 1998; Zaichenko et al., 2002).

In the present study, time-series of water temperature measurements (sampled at a frequency of 2 Hz and averaged over 5 minutes) were obtained from Verem station from a depth of ~1 m below chart datum. It is evident from Fig. 4.3b that a distinct temperature oscillation at Verem started ~3 days before the Sumatra earthquake (12<sup>th</sup> September, 2007). The water temperature anomaly (over a 40-day period covering the event) is negative (Fig. 4.3d), indicating an effective drop in temperature during this period. The power spectral density (PSD, Fig. 4.3e) of water temperature oscillations during a fortnight covering the event 9-25 September (Julian days 252-268) 2007 indicate the highest PSD for the semidiurnal constituent (~12 h) and considerably smaller PSD (~50%) for the diurnal constituent (~24 h). The

corresponding PSDs for water temperature oscillations during approximately 10-days temporal segments, preceding (28 August to 8 September [Julian days 240-251] 2007) and succeeding (9-25 September [Julian days 269-278] 2007) the event segment were negligibly small (Fig. 4.3e). This indicates the selective enhancement of water temperature oscillations during the event segment. From Fig. 4.9 it is evident that the water temperature oscillation during the event segment is clearly semidiurnal, with its negative swing occurring during flood tide and positive swing during ebb tide.

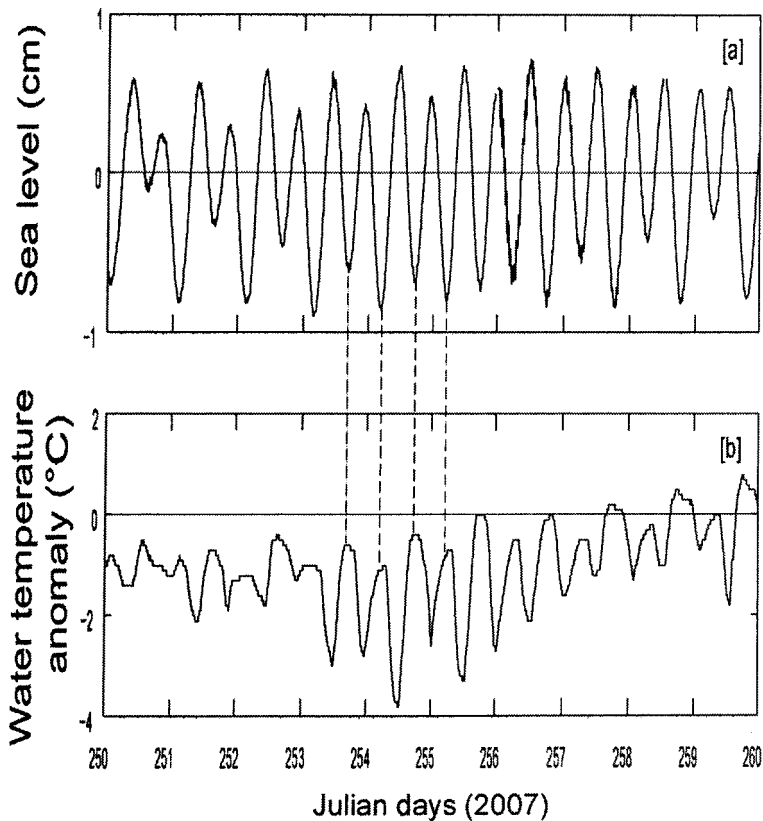


**Figure 4.9.** Sea water parameters observed at Verem, Goa during event E2 of 12<sup>th</sup> September 2007 due to Sumatra earthquake ( $M_w = 8.4$ ). [a] sea level (cm) and [b] measured water temperature anomaly ( $^{\circ}\text{C}$ ).

At the measurement site, which is located in a tropical estuary, during flood tide phase, the seismically cooled offshore sea surface water is progressively transported into the estuary. This causes the observed enhanced negative swing of the water temperature oscillation during flood in the event-segment. During ebb tide

phase, the seismically unaffected (and therefore relatively warmer) water mass in the upper regions of the estuary is progressively discharged into the mouth of the estuary. This is responsible for the observed enhanced positive swing of the water temperature oscillation during ebb phase in the event-segment. The observed insignificant swing of the water temperature oscillations preceding and succeeding the seismic event period arises from the absence of sea surface water cooling. This discussion hints that the observed enhanced negative and positive water temperature swings occurring during flood and ebb tide phases, respectively, could be a tropical estuarine phenomenon, and this may be absent in open sea. The observed enhanced water temperature oscillations may be absent also at inherently cold estuaries.

### 4.8. Conclusions

This chapter described the meteorologically and seismically induced water level and water temperature oscillations at a station (Verem) located in the tropical estuary (Mandovi) on the west coast of India. In particular, the response of sea-level to the passage of the "eye" of the cyclonic storm "Yemyin" has been studied using empirical as well as theoretical approaches. The observed oscillations are found to be related to large atmospheric disturbance associated with wind stress. These sea-level oscillations are similar in frequency content as reported in the case of the September 2007 Sumatra tsunami signals observed at this station (Prabhudesai et. al. 2008). The water level oscillations found at Verem during Yemyin appear to be the result of harbor resonance. Except for a narrow band near the period of 80 min, the computed SLR spectra for event E1 was found to be in good agreement with the measured spectrum for this event. This suggests that the structure of sea level spectra near the coast, although related to the local topography is also significantly affected by the external forcing. The disastrous geophysical tsunamis are normally generated by earthquakes, which are relatively infrequent. However, strong atmospheric disturbances of various types (passing fronts, squalls, and trains of atmospheric waves) are common and needs attention in this region in future studies using higher sampling frequencies (1 minute interval). The observations from this study show that:

- The study examined the observed storm-generated sea-level oscillations (Yemyin, June 2007 and Phyan, November 2009) along with the Sumatra

geophysical tsunami (September 2007), and found similarities in the sea level response in the Mandovi estuary.

- Sea-level and surface meteorological measurements collected during storms exhibit strong synoptic disturbances leading to the coherent oscillations in the estuary with significant energy bands centered at periods of 24, 45, and 80 minutes.
- The computed SLR spectra for event E1 was found to be in good agreement with the measured spectrum for this event, suggesting that structure of sea level spectra near the coast, although related to the local topography, can also be significantly affected by the external forcing.
- Kavaratti Island lagoon showed no prominent spectral peaks to indicate seiches (i.e. natural oscillations). The non-resonant character of Kavaratti Island lagoon remained despite intense wind forcing. The surge at this lagoon was insignificantly weak due to the combined effect of the absence of resonant amplification and lack of river water discharge into the lagoon.
- The pre-earthquake enhanced seawater temperature oscillations observed at this tropical estuary indicate that routine monitoring of seawater temperature with fine temporal resolution may provide early information about impending coastal earthquakes.



## Chapter 5

### Sea-level response to meteorological forcing

#### 5.1. Introduction

Understanding and modelling sea-level variability on the basis of its forcing is crucial for coastal planning and protection as well as forecasting the impacts of climate change that may have on particular locations. Sea level variability primarily results from oceanographic, meteorological and hydrological forcing (Tsimplis and Woodworth, 1994). The north Indian Ocean being purely tropical, is dominated by seasonally varying monsoon associated with the annual heating and cooling of the Asian continent. Sea-level variability is not only determined by local forcing factors (winds and coastal currents), but also affected by sea-level variations generated elsewhere (Lighthill, 1969).

Tropical cyclones (TCs) are the most destructive weather systems on the earth, producing intense winds, causing high surges, meteotsunamis, torrential rains, severe floods and damage to property and life. Intense winds associated with TCs, blowing over a large water surface, cause the sea surface to pile-up on the coast and lead to sudden inundation and flooding. Also, the heavy rainfall combined with tides and surges causes flooding of river deltas. A number of general reviews and description of individual cyclones and associated surges in BOB and AS have been published by several investigators (Murty et al. 1986; Dube et al. 1997; Sundar et al. 1999; Fritz et al. 2010; Charls and Unnikrishnan, 2013; Shaji et al., 2014). Developments in storm surge prediction in the Bay of Bengal and the Arabian Sea have been highlighted by Rao et al. [2013], Panigrahi et al. [2012], Dube et al. (2009) and references therein (e.g., Das, 1994, Chittibabu et al., 2000 & 2002, Dube et al., 2006, Jain et al., 2007 and Rao et al., 2008).

In this chapter, observed sea-level variability at select coastal and island locations of India, in particular, the contribution of atmospheric pressure and wind to the observed sea-level variations has been investigated during normal and cyclonic periods.

## 5.2. Data and methodology

The sea-level and surface meteorological data from September 2011 to January 2012 collected by the ICON is used in the present study. The study also strives to bring out the response of the sea-level to the two episodic meteorological events: (i) the deep depression in November 2011 in AS and (ii) the tropical cyclone "Thane" in BOB in December 2011 as shown in Fig. 5.1.

### 5.2.1. Sea-level and meteorological data

Sea-level and surface meteorological data collected from the radar gauges (RG) and autonomous weather station (NIO-AWS) are used in this study and the data acquisition details are given in Chapter 2. Summary of observations from different coastal and Island locations of India are provided in Table 2.3; periods covered for different events are as follows:

- Event 4 (E4): 26 November to 1 December 2011, occurrence of deep depression in the AS.
- Event 5 (E5): 25-31 December 2011, passage of Thane cyclone in the BOB.

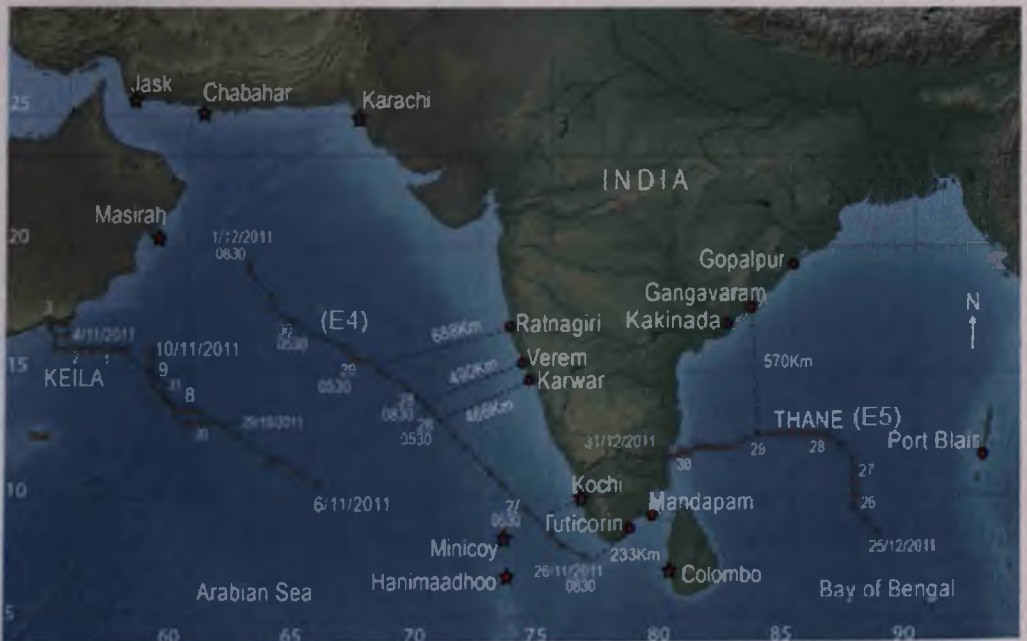


**Figure 5.1.** Study location showing the tracks of meteorological events during the year 2011.

Note: Sea-level data for Colombo, Kochi, Karachi, Chabahar, Jask, Masirah, Minicoy and Hanimaadhoo, which are downloaded from [www.gloss-sealevel.org](http://www.gloss-sealevel.org) are shown in red stars [Time in IST].

### 5.2.2. Tropical cyclone track data

The tropical cyclone track data from India Meteorological Department (IMD, [www.imd.gov.in](http://www.imd.gov.in)), Joint Typhoon Warning Center (JTWC, [www.usno.navy.mil/JTWC/](http://www.usno.navy.mil/JTWC/)) and UNISYS-Unisys Weather (<http://weather.unisys.com/hurricane/>) are shown in Fig. 5.2. The storm translational speed is calculated using the distance travelled between two consecutive positions and time interval. The average differences in wind speeds as shown in Fig. 5.2a & 5.2d between IMD and JTWC, and IMD and Unisys are 1.1 (4.2) and 3.7 (2.8)  $\text{ms}^{-1}$  during E4 (E5). The sea-level pressure reported by IMD and JTWC is nearly the same during E4 (Fig. 5.2b); however, during E5, the minimum sea level pressure differed by  $\sim 11$  mb with a time lag of  $\sim 3$  h (Fig. 5.2e).

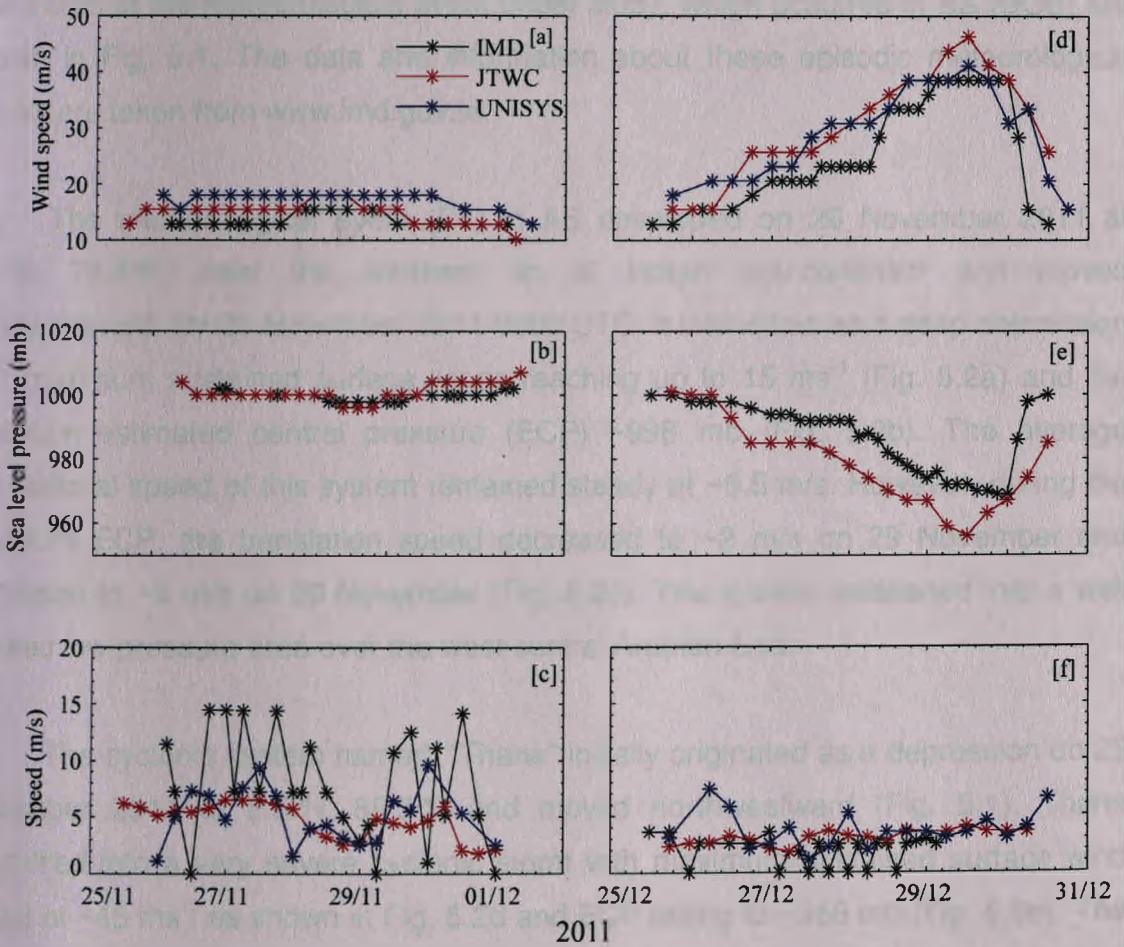


**Figure 5.2.** Cyclone parameters during E4 and E5: (a) and (d) wind speed, (b) and (e) sea-level pressure, (c) and (f) storm forward translation speed.

The cyclone translation speed estimated using JTWC and Unysis data during E4 varied between 2.5 and 6.4  $\text{ms}^{-1}$ , except for two spikes of  $\sim 9 \text{ ms}^{-1}$  observed in Unysis data (Fig. 5.2c). Similarly, the cyclone translation speed estimated using JTWC and Unysis data during E5 varied between 1.0 and 4.5  $\text{ms}^{-1}$ , except for a few spikes of  $\sim 5\text{-}7 \text{ ms}^{-1}$  (Fig. 5.2f). Cyclone translation speed using IMD data is observed to be fluctuating as the data is available at every 3 h interval (Fig. 5.2c), whereas the data of other two sites is every 6 h. However, the mean cyclone speed during E4 (E5) from IMD data is 7.8 (2)  $\text{ms}^{-1}$  (Fig. 5.2 c&f).

### 5.3. Observed coastal sea-level response to meteorological events

The tracks of the meteorological event under study, which occurred in AS (BOB) are shown in Fig. 5.1. The data and information about these episodic meteorological events are taken from [www.imd.gov.in](http://www.imd.gov.in).

The meteorological event (E4) in AS developed on 26 November 2011 at 7.5°N, 76.5°E, near the southern tip of Indian sub-continent and moved northwestward. By 28 November 2011 0000 UTC, it intensified as a deep depression with maximum sustained surface winds reaching up to 15  $\text{ms}^{-1}$  (Fig. 5.2a) and the minimum estimated central pressure (ECP)  $\sim 998 \text{ mb}$  (Fig. 5.2b). The average translational speed of this system remained steady at  $\sim 6.5 \text{ m/s}$ . However, during the minimum ECP, the translation speed decreased to  $\sim 2 \text{ m/s}$  on 29 November and increased to  $\sim 6 \text{ m/s}$  on 30 November (Fig. 6.2c). The system weakened into a well marked low pressure area over the west central Arabian Sea.

The cyclonic system named, "Thane" initially originated as a depression on 25 December 2011 at 8.5°N, 88.5°E and moved northwestward (Fig. 5.1). Thane intensified into a very severe cyclonic storm with maximum sustained surface wind speed of  $\sim 45 \text{ ms}^{-1}$  as shown in Fig. 5.2d and ECP falling to  $\sim 956 \text{ mb}$  (Fig. 5.2e). The cyclone track turned to westward on 29<sup>th</sup>, with an average translational speed of  $\sim 4 \text{ m/s}$  and then became steady at  $\sim 3.5 \text{ m/s}$  as shown in Fig. 5.2f. Thane crossed the Tamil Nadu coast just south of Cuddalore between 0100 and 0200 UTC of 30 December 2011 and weakened into a well marked low pressure area over north Kerala and its neighbourhood.



### 5.3.1. Response of sea-level to depression in the Arabian Sea

The sea-level residuals (SLR) at Ratnagiri, Verem and Karwar are shown in Fig. 5.3. The visual observation of SLR indicates that it is normally within  $\pm 25$  cm at all the three locations. Keila and the subsequent depression from 29 October to 10 November are not able to generate noticeable sea-level variations, probably due to large distance of the measurement sites from the cyclone tracks. For example, the distance of Verem to the trajectory of Keila's ECP is  $\sim 1554$  km. The variance of SLR observed during 29 October to 10 November at Ratnagiri, Verem and Karwar is  $\sim 26.1$ ,  $21.6$  and  $25.8$   $\text{cm}^2$ , respectively (Fig. 5.3). However, the deep depression which originated on 26th November 2011 (E4) was in the near proximity to the measurement sites. For example, the distance of Verem from the depression centre on 28 November 2011 was  $\sim 490$  km (Fig. 5.1). E4 was able to inflict surges at Ratnagiri, Verem and Karwar which peaked upto  $\sim 43$  cm with SLR variance of  $\sim 119.4$ ,  $95.4$  and  $108.2$   $\text{cm}^2$ , respectively during E4 (Fig. 5.3a-c). The storm surge has a well defined peak with a half-width (Fandry et al., 1984) of  $\sim 25$  h (Table 5.2). The local surface meteorological conditions along with SLR are shown in Fig. 5.4. During E4 (26 November to 1 December 2011), the wind variance was  $\sim 1.7$ ,  $4.8$  and  $0.8$   $\text{m}^2\text{s}^{-2}$  with wind speeds peaking up to  $\sim 8.5$   $\text{ms}^{-1}$  at Ratnagiri and Verem (Fig. 5.4 a.2-b.2). At Karwar, the wind energy is less compared to the other two sites, still the SLR peaks are of same magnitude (Fig. 5.4 c.1-c.2), indicating the effect of long waves generated by the forcing due to E4 in the open ocean. The wind direction (Fig. 5.4 a.3-c.3) stabilised with respect to North (Table. 5.2) at Ratnagiri, Verem and Karwar, respectively. The atmospheric pressure anomaly (Fig. 5.4 a.4-c.4) shows a variance of  $\sim 3.6$   $\text{mb}^2$  and a falloff  $\sim 6.0$  mb during E4 at the three stations. However, anomalous temperature variations due to E4 were not observed (Fig. 5.4 a.5-c.5), but the range narrowed, which is also the case with relative humidity at the three stations (Fig. 5.4 a.6-c.6).

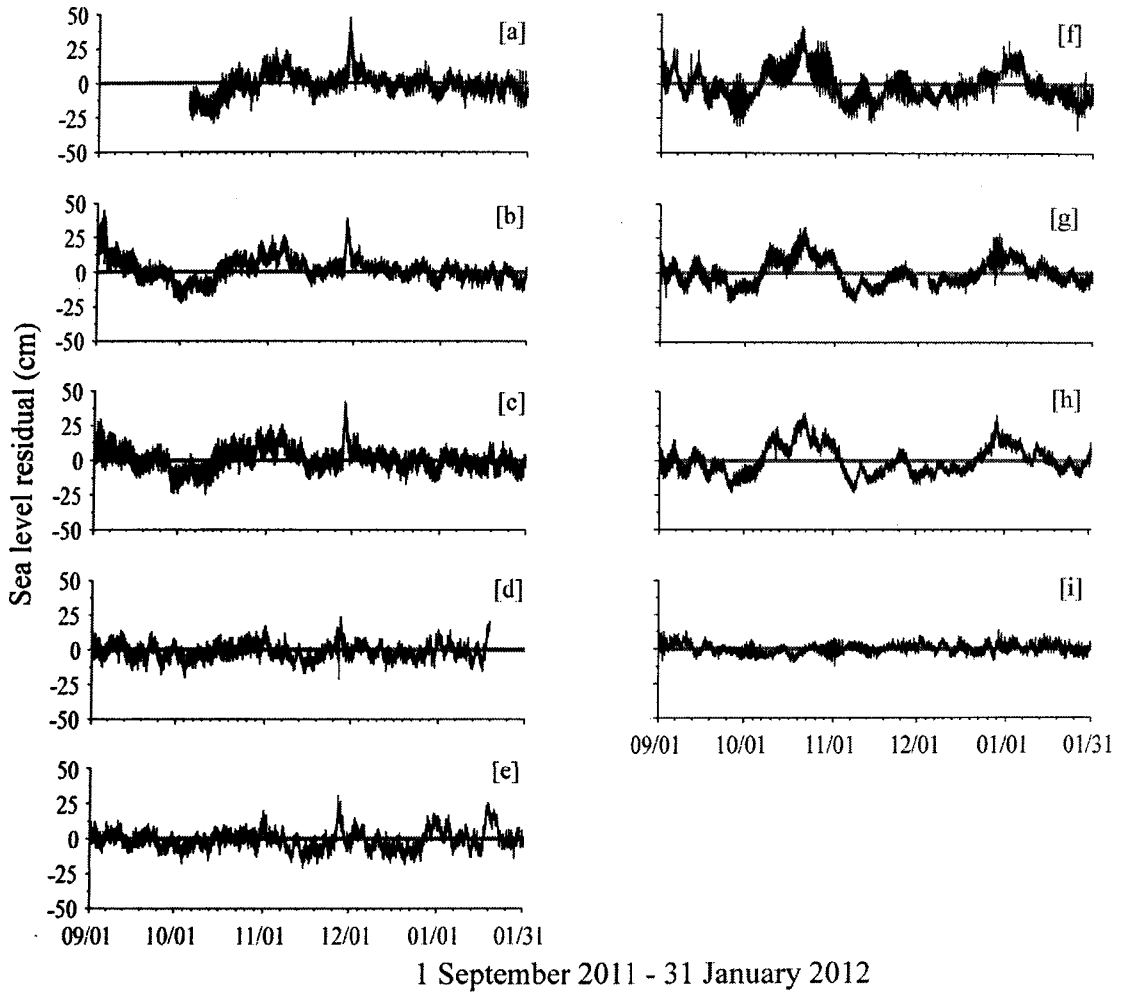


**Figure 5.3.** Sea-level residual (SLR) at [a] Ratnagiri, [b] Verem, [c] Karwar, [d] Tuticorin, [e] Mandapam, [f] Gopalpur, [g] Gangavaram, [h] Kakinada and [i] Port Blair.

**Table 5.1.** Meteorological and sea-level observations at Ratnagiri, Verem and Karwar during E4 from 26 November to 1 December 2011 (Time in IST).

S. No	Variables	Ratnagiri	Verem	Karwar
1	Sea-level residual (SLR in cm)	47	39	42
2	SLR rise time from zero-maxima (h)	44.16	39.33	32.58
3	SLR fall time from maxima-zero (h)	48.5	45.25	42.25
4	SLR peak time (h)	29-11-2011 03:15	28-11-2011 18:00	28-11-2011 12:25
5	Maximum wind speed (m/s)	7.4	9.6	4.3
6	Half amplitude surge width duration (h)	20	28	26
7	Wind direction (degrees)	253	112	246
8	Air temperature, reduction in range (°C)	8.3 - 3.0	13.3 - 6.8	15.5 - 8.3
9	Atmospheric pressure fall (mb)	5.8	6.3	5.9
10	Relative humidity range fall (%)	62.0 - 40.4	65.4 - 41.3	64.8 - 33.8

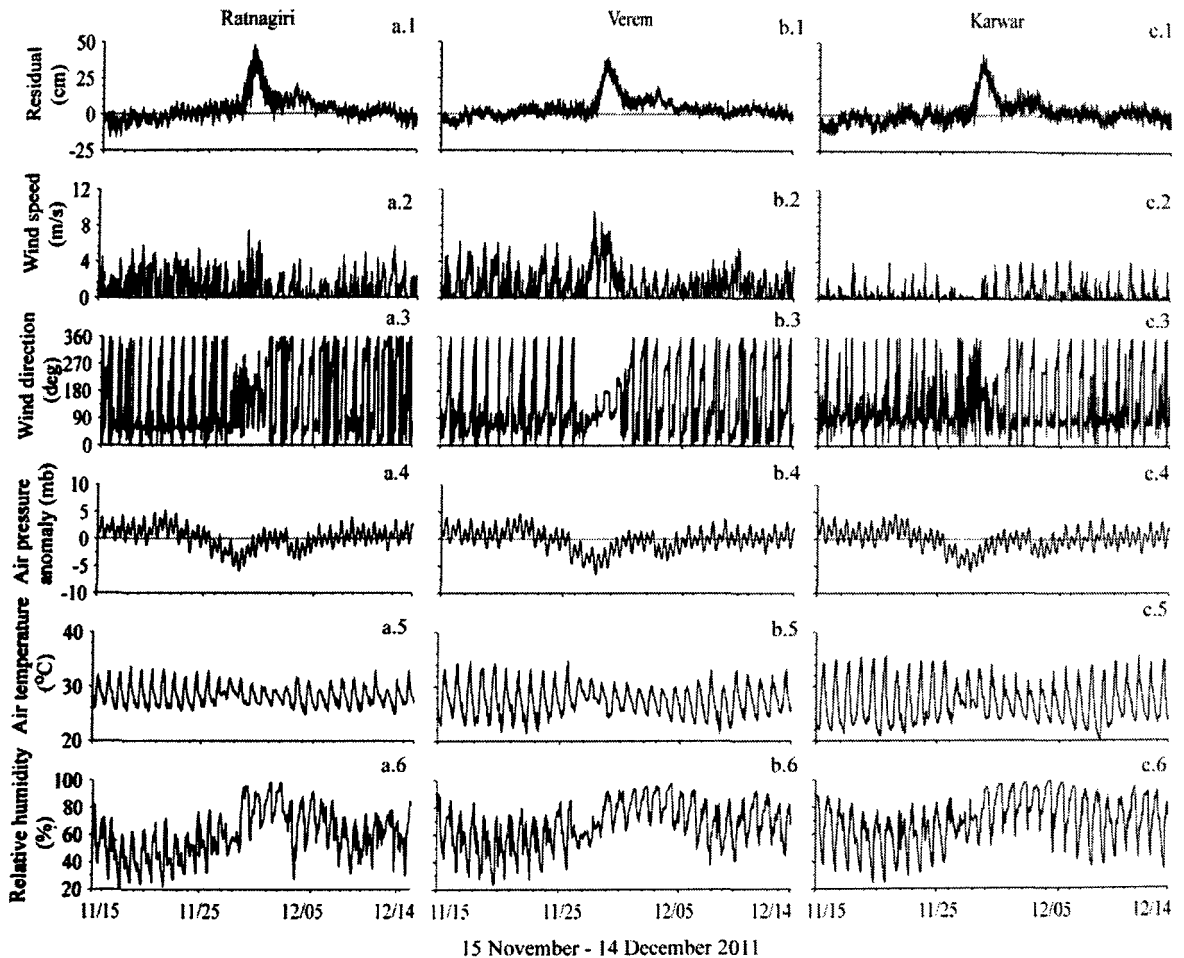


**Figure 5.4.** Sea-level residual and surface meteorological parameters during the episodic event E4. [a.1 to a.6] SLR, wind speed, wind direction, atmospheric pressure anomaly, air temperature and relative humidity at Ratnagiri. [b.1 to b.6] same as in [a] at Verem. [c.1 to c.6] same as in [a] at Karwar. The atmospheric pressure anomaly is estimated by subtracting the mean atmospheric pressure (1 September 2011 to 31 January 2012) from the measured atmospheric pressure for respective stations.



### 5.3.2. Response of sea-level to meteorological events in Bay of Bengal

Response of sea-level as storm surges at different sites, to the tropical cyclone Thane, E5, which occurred in BOB are shown in Fig. 5.3 (Table 5.2). SLR exhibits maximum oscillations (variance) of  $\sim 27$  cm ( $47.8$  cm<sup>2</sup> and  $11.7$  cm<sup>2</sup>) at Gopalpur (Fig. 5.5a.1) and Gangavaram (Fig. 5.5b.1), respectively. At Kakinada, the SLR peaked up to 33 cm, with a variance of  $23.3$  cm<sup>2</sup> during E5. Minor dip in SLR  $\sim 14.1$ ,  $10.3$  and  $15.0$  cm was also observed at the coastal sites located in the AS (Ratnagiri, Verem and Karwar) due to E5 (Fig. 5.3a-c). However, at the Island station, Port Blair, the SLR variations are within  $\pm 10$  cm, and less than at sites north of Thane (Fig. 5.3i). The SLR variability at Mandapam and Tuticorin was less compared to other sites north of Thane track (Fig. 5.3d and 5.3e), probably due to the following two reasons: (i) the geometrical amplification of the open ocean waves as they propagated northwards and (ii) wind speeds are less near the central depression point and increase towards the periphery. SLR rise was also seen at Mandapam (Tuticorin) by  $\sim 24.3$  ( $23.1$ ) cm even during E4. The local surface meteorological conditions along with SLR are shown in Fig. 5.5. The large scale extent of E5 is evident in wind and atmospheric pressure measurements at all the three locations and very similar meteorological conditions existed at Gangavaram and Kakinada. At Gopalpur, the winds were weak as compared to other two southern locations with maximum wind speed reaching upto  $\sim 6$  ms<sup>-1</sup>; the direction also fluctuated during E5 and remained southerly after 5 January 2012 and maintained this direction till 10 January 2012 (Fig. 5.5a.2 and a.3, Table 5.2). During E5, the wind speed remained high from 26 December 2011 till 4 January 2012. The wind speed peaked up to  $\sim 14.0$  ms<sup>-1</sup> with corresponding wind speed variance of  $\sim 13.7$  and  $10.3$  m<sup>2</sup>s<sup>-2</sup> at Gangavaram and Kakinada, respectively (Fig. 5.5b.2 and 5.5c.2). The wind direction stabilised and remained northeasterly (Fig. 5.5b.3 and 5.5c.3, Table 5.2) during E5 at Gangavaram and Kakinada. The atmospheric pressure (Fig. 5.5 a.4-c.4) shows a variance of  $\sim 2.7$  mb<sup>2</sup> and is devoid of any noticeable fall during E5 at Gopalpur, Gangavaram and Kakinada. Similarly, the anomalous variations in temperature due to E5 are not observed, however, the range is narrowed down from  $\sim 9.0^\circ\text{C}$  to  $2.7^\circ\text{C}$  at the three stations (Fig. 5.5 a.5-c.5). Similarly, a reduction in relative humidity range is also observed at the three stations in BOB (Fig. 5.5 a.6-c.6, Table 5.2).

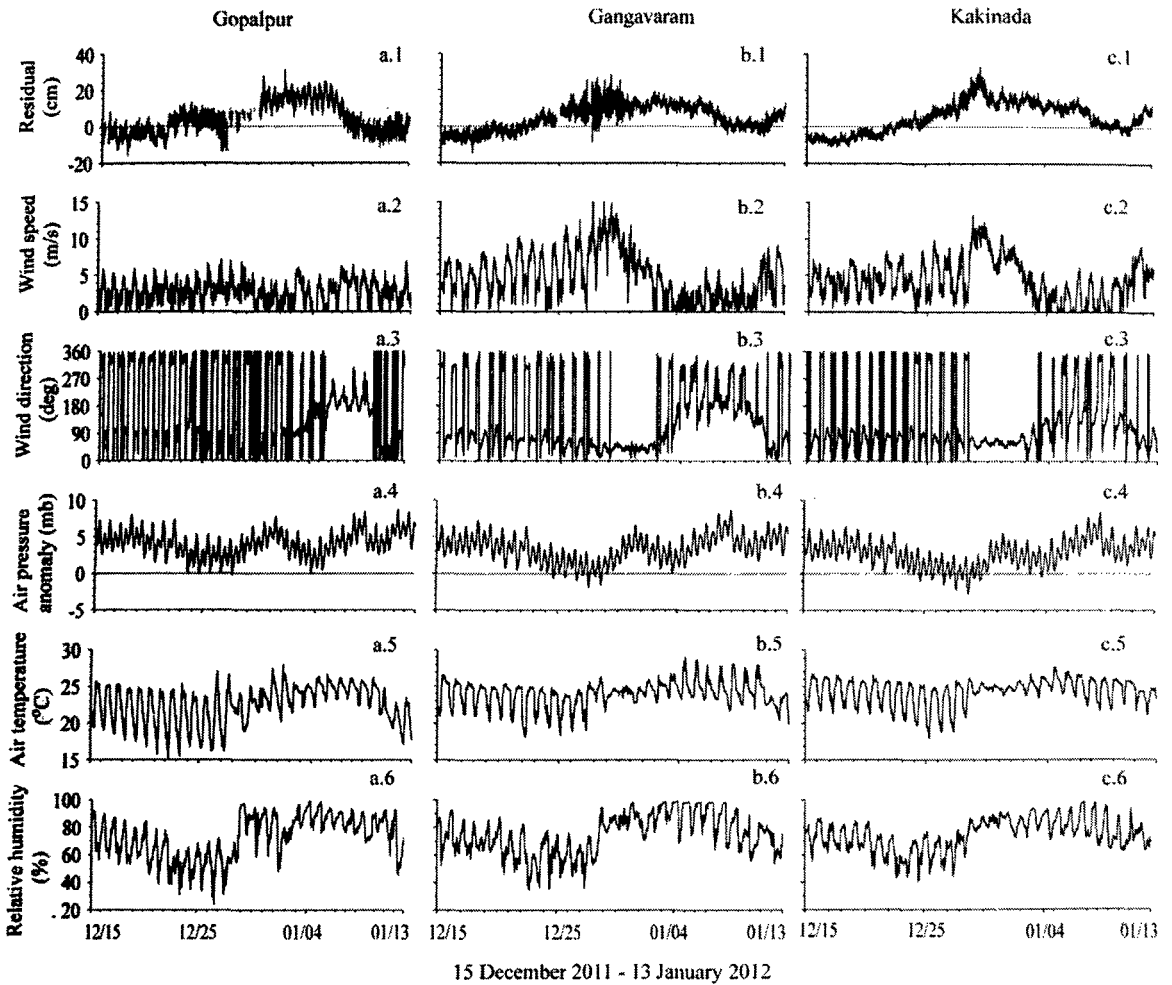


**Figure 5.5.** Sea-level residual and surface meteorological parameters during the episodic event E5. [a.1 to a.6] SLR, wind speed, wind direction, atmospheric pressure anomaly, air temperature and relative humidity at Gopalpur, Odisha. [b.1 to b.6] same as in [a] at Gangavaram, Andhra Pradesh. [c.1 to c.6] same as in [a] at Kakinada, Andhra Pradesh. Atmospheric pressure anomaly is estimated by subtracting the mean atmospheric pressure (1 September 2011 - 31 January 2012) from the measured atmospheric pressure for respective stations.

**Table 5.2.** Meteorological and sea-level observations at Gopalpur, Gangavaram and Kakinada during the event E5 from 26-31 December 2011.

S. No	Variables	Gopalpur	Gangavaram	Kakinada
1	Sea-level residual (cm)	27.4 <sup>a</sup>	26.5 <sup>a</sup>	32.9
2	SLR rise time from zero-maxima (h)	-	-	123.8
3	SLR fall time from maxima-zero (h)	-	-	233.25
4	Maximum wind speed (m/s)	6.1	15.0	13.3
5	Wind direction (deg)	184 <sup>b</sup>	41.9	60.9
6	Range of air temperature reduction (°C)	10.1- 2.6	8.4 - 3.1	8.5 - 2.6
7	Range of relative humidity reduction (%)	65.7 - 27.0	57.8 - 23.8	46 - 13.6

<sup>a</sup> Maximum SLR oscillation at Gopalpur and Gangavaram.

<sup>b</sup> Wind direction fluctuated during E5 and stabilised at ~184° with respect to North after 5 January 2012 and maintained this direction till 10 January 2012.

### 5.3.3. Sea-level changes by local winds

The contribution of atmospheric pressure and wind to sea level variability at Goa (west coast of India) for the period 2007-2008 was extensively investigated by Mehra et al. [2010]. Multilinear regression analysis was used to resolve the dependence of sea-level on various forcing parameters. The multilinear regression analysis was performed over two month duration for the year 2007-2008. During the summer monsoon season (May-September), the sea-level variability attributable to wind was upto 47% (75%) for 2007 (2008); however it reduced to less than 20% during the winter monsoon (November-February) season. A significant part of the variability observed in sea level remains unaccounted for and is attributed to remote forcing.

The analysis performed indicates that cross-shore wind component (U) remained land-ward (U>0), except during winter monsoon (U<0). The local wind components were small in magnitude during the period November-January. The alongshore wind component V remained generally southward (V<0) during the period of observations. During the summer monsoon (May), V started changing direction and has flown northward with maximum energy of ~1.3 m<sup>2</sup>s<sup>-2</sup> in June (V>0). The intensity of V reduced by August (~0.3 m<sup>2</sup>s<sup>-2</sup>) and has flown southward during winter monsoon.

### 5.4. Estimation of surges

North Indian Ocean is witnessing an increasing trend in cyclogenesis activities with an average of 5 to 6 cyclones occurring every year (Singh et al., 2001). The inundation caused by flooding due to extreme wind waves and rise in sea-level would be higher, if the cyclone crosses the coast during high tide. Therefore, it is important to know the maximum water elevation that could occur at a coastal location due to the combined effect of surge, tide and wind waves. In this section numerical (hydrodynamic model) and regression methods are used to estimate sea-level rise during events E4 and E5.

#### 5.4.1 Hydrodynamic model

Sea-level changes at coastal locations during events E4 and E5 in AS and BOB are estimated using a 2D depth averaged hydrodynamic model developed by DHI, Denmark (DHI, 2011). The model domain in AS (BOB) during E4 (E5) is shown in Fig. 5.6. The mesh size varied from ~ 1 km in the deep ocean to ~ 200 m in the coastal regions. The model was supplied with input parameters such as bathymetry, tide and cyclone wind speed and direction (IMD, [www.imd.gov.in](http://www.imd.gov.in)).

The impact of the TCs on the coastal locations during their propagation is estimated after removing the tides from the total water elevation. The estimated sea-level residual (SLR) obtained from the model, and the measured SLR are shown in Fig. 5.7 (Table 5.3). The estimated peaks at the measurement locations in AS are only upto ~40% of the measured surges (Fig. 5.7a-5.7c). At Gangavaram, the model output shows a water level rise of ~4 cm as harbour oscillations are observed at this location and not the storm surges (Fig. 5.7d). At Kakinada, the estimated surge peaked upto 75% of the measured surge. The measured water level at Kakinada starts rising on 24 December 2011; however, the model surge lags by ~3 days and starts rising only on 27 December 2011 (Fig. 5.7e). One of the important inputs to the hydrodynamical model for storm surges is cyclonic parameters (winds and atmospheric pressure). The cyclone track during E4 is almost parallel to the coastline with coast on the right side of the track. At all the three locations in the AS (Fig. 5.7 a-c), the percentage difference in estimated surge peaks is ~60%. The reason for this difference could be that the surges generated along the west coast are due to local

winds combined with coastally trapped waves propagating northwards. Whereas, along the east of coast of India (Kakinada), the surge is primarily due to cyclonic winds as the difference is only ~24%. Also the deep depression in AS has maximum sustained surface winds reaching upto 15 ms<sup>-1</sup> (Fig. 5.2a) and the minimum estimated central pressure (ECP) ~998 mb (Fig. 5.2b). The cyclone Thane was a severe cyclone with maximum sustained surface wind speed of ~45 ms<sup>-1</sup> (Fig. 5.2d) and ECP falling to ~956 mb (Fig. 5.2e).

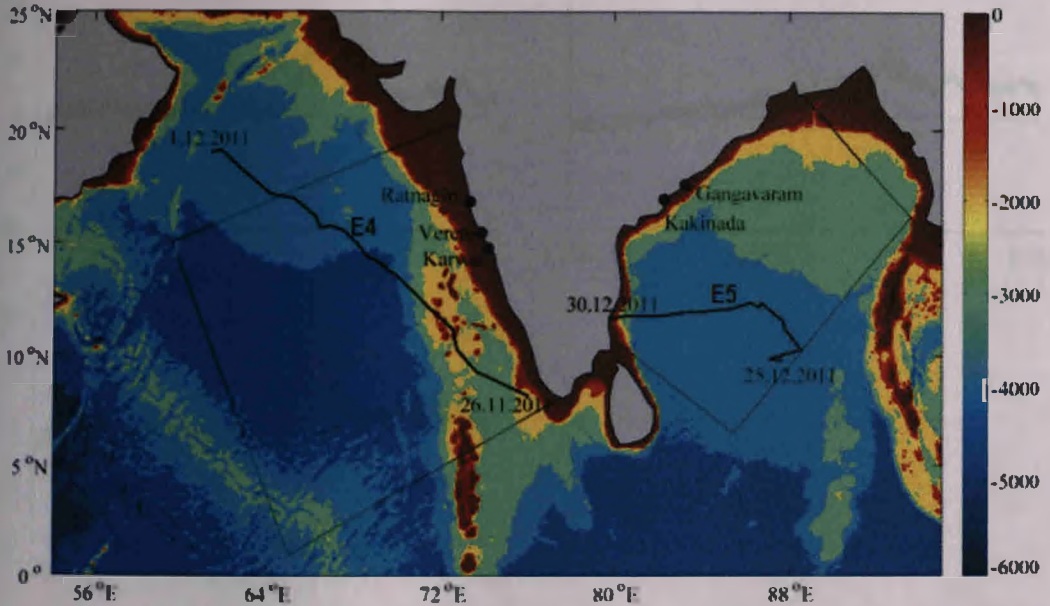


**Figure 5.6.** Setup of the storm surge model (MIKE) domain for the events E4 and E5. The colour bar shows the depth (m). Model boundary coordinates during E4 are 65.06°E, 0.9°N; 59.62°E, 20.31°N; 77.46°E, 8.10°N; 72.7°E, 20.31°N. Model boundary coordinates during E5 are 85.43°E, 6.5°N; 79.94°E, 10.8°N; 88.43°E, 21.68°N; 93.60°E, 16.21°N.

**Table 5.3.** Estimated storm surge peaks using hydrodynamic model during E4 and E5. % difference is obtained as (measured-estimated)x100 / measured.

Location	Measured surge (cm)	Estimated surge (cm)	% Difference
Ratnagiri	47	18	61
Verem	39	19	51
Karwar	42	17	59
Kakinada	33	25	24
Gangavaram	-	4	-



## Sea-level response to meteorological forcing

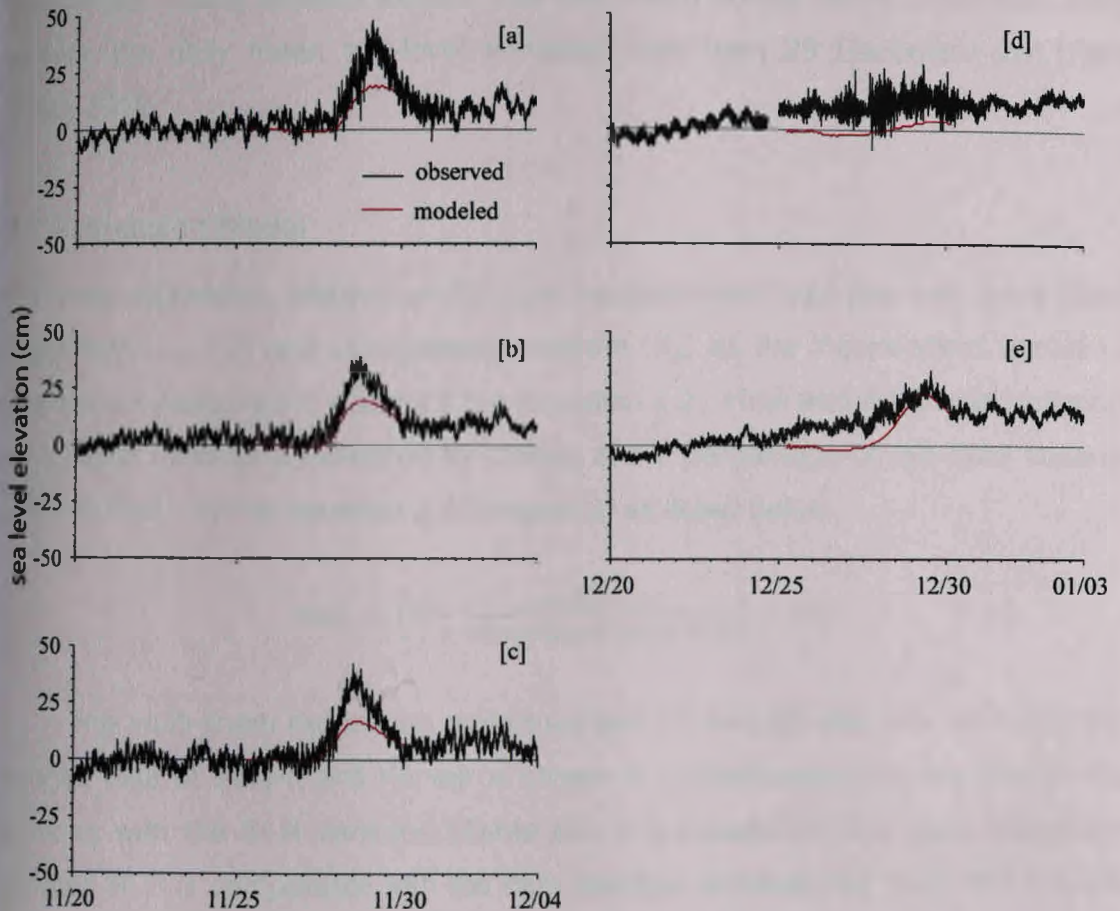


**Figure 5.7.** Measured sea-level residual (black) and SLR estimated by storm surge model (red) at [a] Ratnagiri, [b] Verem, [c] Karwar, [d] Gangavaram and [e] Kakinada.

Tropical cyclone-generated storm surge is a complex air-sea interaction problem where the meteorological and oceanographic factors influence the height, extent and duration of storm surge flooding. Various parameters involved in storm surge prediction are landfall point, intensity of cyclone, maximum sustained cyclone wind speed at landfall and offshore, size, forward speed, the angle of approach to the coastline, bathymetry of coastal waters, coastline shape and the presence of barriers or obstructions to surge waters on land. Despite advances in computational power, remote sensing and cyclone track prediction, there still exist uncertainties in storm parameters leading to inaccurate prediction of storm surges. The other limitation of surge model is that cyclone parameters are not available once it hits the coast, whereas the coastal sea-level variation is expected to persist for a few more days.

For example, Thane cyclone existed over the ocean during 25-31 December 2011. However, the daily mean sea-level remained high from 23 December 2011 to 9 January 2012.

### 5.4.2 Regression Model

Multi-linear regression analysis of SLR as the dependent variable with wind stress components ( $T_U, T_V$ ) and atmospheric pressure ( $A_p$ ) as the independent variable is performed as explained in section 2.5.4 (equation 2.2). How well the model describes the sea level residual is assessed by looking at the percentage of sea level variance explained ( $Var_e$ ) by the equation 2.3 (chapter 2) as listed below.

$$Var_e = \left( 1 - \frac{\text{variance}(\varepsilon)}{\text{variance}(\text{measured SLR})} \right) \times 100$$

The multi-linear regression performed with 10 min, 60 min, 6 h, 12 h and 24 h averaged data of Verem and Karwar is shown in supplementary figures (Fig.S1-Fig.S5) along with the SLR variance (Table S1) in annexure-III. The daily average of estimated SLR is comparable with the daily average of measured SLR, and it is able to account for the low frequency variations in the SLR during the study period of 5 months (September 2011 to January 2012). Therefore, in this section daily-averaged data series of SLR and AWS were used to perform multi-linear regression. To begin with, multi-linear regression is performed with cross-shore ( $T_U$ ), along-shore ( $T_V$ ) components of wind stress and atmospheric pressure ( $A_p$ ) individually as independent variable to regress the SLR. This would enable one to know the contribution to the SLR variability by the various surface meteorological variables individually. Then all the three independent variables [ $T_U, T_V, A_p$ ] together were used to regress the daily-mean SLR. Results are listed in Table. 5.4 and plotted in Figs. 5.8 and 5.9. The cross- and along-shore components were estimated using the local shoreline angles with respect to North from Google Earth. In AS, the local shoreline angle estimated at Ratnagiri, Verem and Karwar with respect to North is  $\sim -12^\circ$ ,  $-27^\circ$  and  $-19^\circ$ , respectively. Similarly, in BOB the local shoreline angle with respect to North is  $\sim 52^\circ$ ,  $45^\circ$  and  $50^\circ$  at Gopalpur, Gangavaram and Kakinada, respectively. The variations in  $T_U, T_V$ , and  $A_p$  results in the SLR variability. The cross-shore wind ( $U$ ) towards land (sea) will give rise to increase (decrease) in SLR due to wind stress.

Since the study region being in the northern hemisphere, the along-shore winds towards north with the coast at its right will increase the sea-level due to Coriolis force. Therefore, in AS the positive (negative) U&V will increase (decrease) the SLR (Fig. 5.8) and in BOB the positive (negative) U&V will decrease (increase) the SLR (Fig. 5.9). The relation between atmospheric pressure and sea-level is  $\sim -1 \text{ cm mb}^{-1}$ , inverse barometric effect.

### 5.4.2.1 Surge estimation in Arabian Sea

At all the three study locations in AS,  $T_U$ ,  $T_V$ , and  $A_p$  individually could explain an average 45% SLR variability; when  $T_U$ ,  $T_V$  and  $A_p$  together were used to regress the daily-mean SLR, the total  $\text{Var}_e$  was  $\sim 69\%$  (Table 5.4). The monthly  $\text{Var}_e$  is  $\sim 50\%$  during October and December 2011 (Table 5.4 and Fig. 5.10a). However, in November 2011 when E4 occurred,  $T_U$ ,  $T_V$  and  $A_p$  together were able to explain the SLR variability up to  $\sim 68\%$ . In January 2012, the  $\text{Var}_e$  is less than 20% at all the sites in AS and BOB (Fig. 5.10a & Table 5.4). At Verem (Table 5.4), the total  $\text{Var}_e$  is the highest among all the locations in AS, when  $T_U$ ,  $T_V$  and  $A_p$  together were used to estimate the daily-mean SLR variability. Daily-mean  $U(T_U)$ ,  $V(T_V)$ , measured and estimated SLR obtained from independent variables [ $T_U$ ,  $T_V$ ,  $A_p$ ] are shown in Fig. 5.8. It is observed that during E4 at Ratnagiri both U and V components are positive (Fig. 5.8a.1), favouring the sea-level rise at the coast. The estimated daily-mean SLR during E4 was able to peak up to 96.3% of the measured daily-mean SLR (Fig. 5.8a.2 & Table 5.5). The -U (V) will tend to decrease (increase) the sea-level at Verem (Fig. 5.8b.1). The estimated daily-mean SLR at Verem is comparable to the measured daily-mean SLR, with a minor overshoot by  $\sim 6.5\%$  (Table 5.5). However at Karwar, the U (-V) will tend to increase (decrease) the sea level during E4 (Fig. 5.8c.1), the estimated SLR is able to peak only upto half of the measured daily-mean SLR in this case (Fig. 5.8c.2 and Table 5.5).



## Sea-level response to meteorological forcing

**Table 5.4.** The daily-mean sea-level variability explained ( $Var_e$ ) by linear ( $T_U, T_V, A_p$  individually) and multi-linear ( $[T_U, T_V, A_p]$  together) regression during different months from September 2011 to January 2012.

Station	Variable	Total Var <sub>e</sub> (%)	Monthly Var <sub>e</sub> (%)				
			Sept	Oct	Nov	Dec	Jan
<b>Arabian Sea</b>							
Ratnagiri	$T_U, T_V, A_p$	43.9, 45.0, 59.3					
	$[T_U, T_V, A_p]$	68.4		52.6	67.8	46.7	3.4
Verem	$T_U, T_V, A_p$	48.9, 39.8, 58.2					
	$[T_U, T_V, A_p]$	73.9	85.3	72.9	54.5	42.6	7.0
Karwar	$T_U, T_V, A_p$	37.3, 29.5, 45.2					
	$[T_U, T_V, A_p]$	64.8	64.0	75.7	56.7	38.8	8.3
<b>Bay of Bengal</b>							
Gopalpur	$T_U, T_V, A_p$	43.2, 40.1, 31.2					
	$[T_U, T_V, A_p]$	53.4	58.8	8.3	44.1	74.7	10.2
Gangavaram	$T_U, T_V, A_p$	42.0, 47.6, 44.2					
	$[T_U, T_V, A_p]$	56.6	64.4	14.2	37.1	64.3	11.6
Kakinada	$T_U, T_V, A_p$	49.4, 55.6, 44.4					
	$[T_U, T_V, A_p]$	62.1	77.8	15.4	58.0	68.1	17.7

**Table 5.5.** The peak response of the daily-mean sea level residual (SLR) along with the estimated daily-mean SLR during E4 & E5.

Station	Event	Measured daily-mean peak SLR (cm)	Estimated daily-mean SLR peak (cm)	Difference (%)
Ratnagiri	E4	29.6	28.5	3.7
Verem	E4	25.8	27.4	-6.5
Karwar	E4	27.7	13.6	50.9
Gopalpur	E5	29.7	32.4	-8.9
Gangavaram	E5	13.8	18.5	-34.1
Kakinada	E5	22.3	27.1	-21.5



### 5.4.2.2 Surge estimation in Bay of Bengal

In BOB,  $T_U$ ,  $T_V$ , and  $A_p$  individually could explain an average of 44% SLR variability; however, when  $T_U$ ,  $T_V$  and  $A_p$  were used together to regress the daily-mean SLR, the total  $\text{Var}_e$  has increased to  $\sim 57\%$  (Table 5.4). The monthly  $\text{Var}_e$  is  $< 20\%$  in October and January for all the three stations as shown in Fig. 5.10b. The daily-mean of  $U(T_U)$  and  $V(T_V)$  and estimated SLR are plotted for Gopalpur, Gangavaram and Kakinada, and shown in Fig. 5.9. As stated earlier, along the east coast of India the positive (negative) U&V will decrease (increase) the sea level. Fig. 5.9a.1 shows that U (-V) at Gopalpur, which is seaward (southward) during E5 favours sea-level fall (rise) due to surface stress. However, by 1 January 2012 both the cross- and along-shore component of wind turned landward (northward) i.e -U (V), and imposed a sea-level rise (fall). Sea-level appears to be influenced more by alongshore wind, where the estimated SLR followed the forcing ( $T_V$ ) of V. Fig. 5.9a.2 presents the estimated and measured daily-mean SLR at Gopalpur which is comparable and  $\sim 9\%$  more than the measured daily-mean SLR (Table 5.5). It is also observed that the measured SLR remained high ( $\sim 15$  cm) till 5 January 2012, whereas the estimated SLR fell to zero by 31 December 2011. The U ( $T_U$ ) and V ( $T_V$ ) winds (wind-stresses) at Gangavaram are plotted in Fig. 5.9b.1, where the daily-mean along-shore (V) winds are observed to be dominated over a range of  $\sim \pm 10 \text{ ms}^{-1}$ . During E5, the measured (estimated) daily-mean SLR peaked up to 13.8 (18.5) cm; the estimate overshoot by  $\sim 34\%$  (Table 5.5). At Gangavaram, the rise in SLR residual is predominantly due to relatively strong along-shore wind (-V), as explained by  $\text{Var}_e$  for December 2011 which is 64%. Also, the measured daily-mean SLR remained high from 22 December 2011 to 9 January 2012, whereas the estimated SLR remained high from 25 December 2011 to 2 January 2012 (Fig. 5.9b.2). Similarly, at Kakinada also V winds (Fig. 5.9c.1) have dominated with peaks up to  $\sim -10 \text{ ms}^{-1}$ . During E5, the measured (estimated) daily-mean SLR peaked up to 22.3 (27.1) cm; the estimate overshoot by 21% (Table 5.5). At Kakinada, the rise in sea level residual is predominantly due to strong southward wind (V). The measured SLR started rising above zero on 23 December, reached the highest level on 29 December and descended by 9 January 2012, whereas the estimated SLR started ascending on 25 December, reached the highest level on 29 December 2011 and then dropped to zero level by 4 January 2012 (Fig. 5.9c.2).



## Sea-level response to meteorological forcing

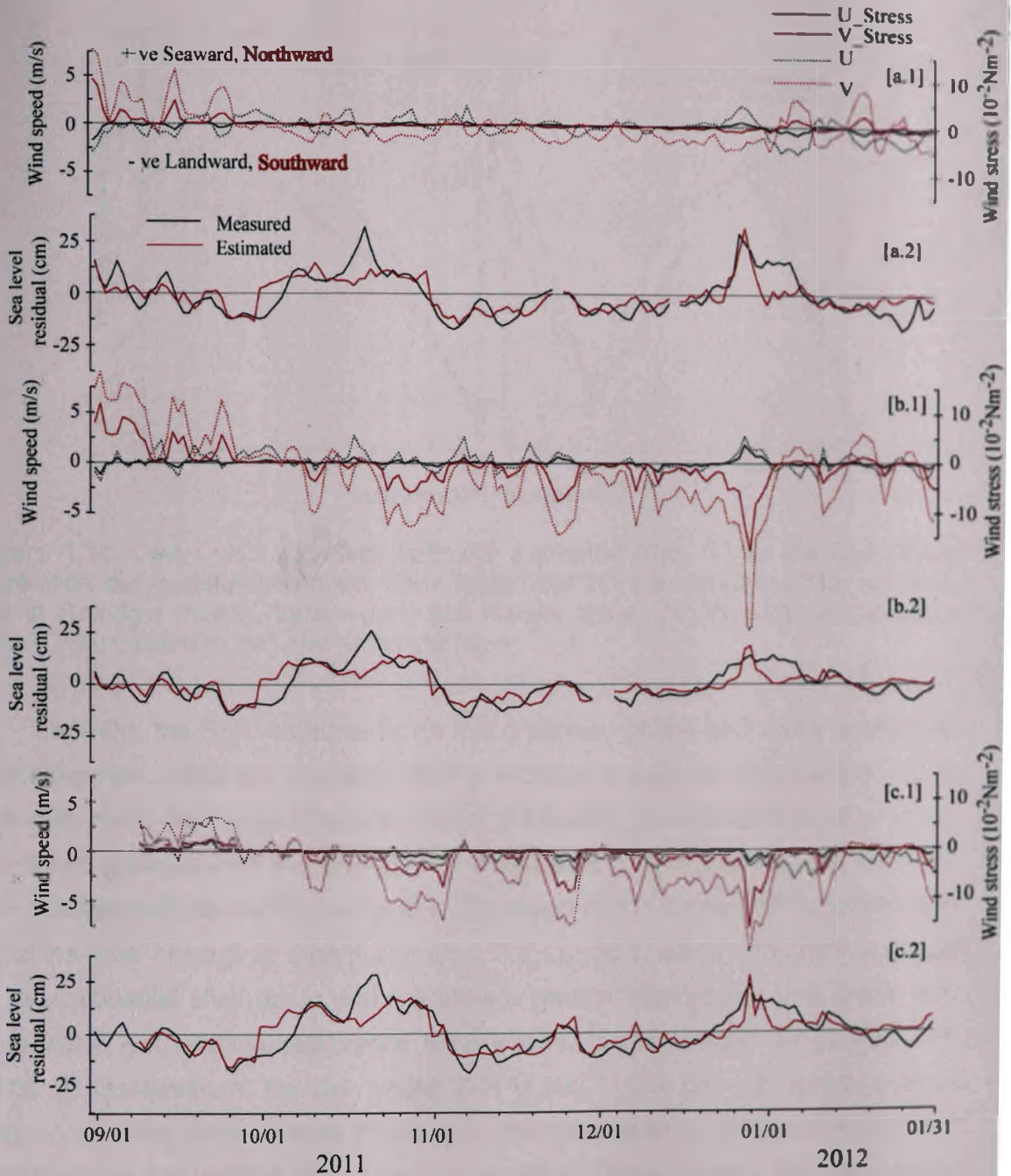


**Figure 5.9.** Daily-mean wind, wind-stress, measured sea-level residual and estimated sea level residual from September 2011 to January 2012 at [a] Gopalpur, [a.1] daily averaged cross-shore (black) and along-shore (red) winds-stress along with respective winds (dotted black or red), [a.2] daily-mean measured sea level residual (black) and estimated residual (red); [b] Gangavaram, [b.1] and [b.2] same as in [a]; [c] Kakinada, [c.1] and [c.2] same as in [a]; Daily-mean estimated SLR is obtained using the multi-linear regression method using daily-mean cross-shore ( $T_U$ ), along-shore ( $T_V$ ) components of winds-stress and atmospheric pressure ( $A_p$ ) as independent variables.

## Sea-level response to meteorological forcing

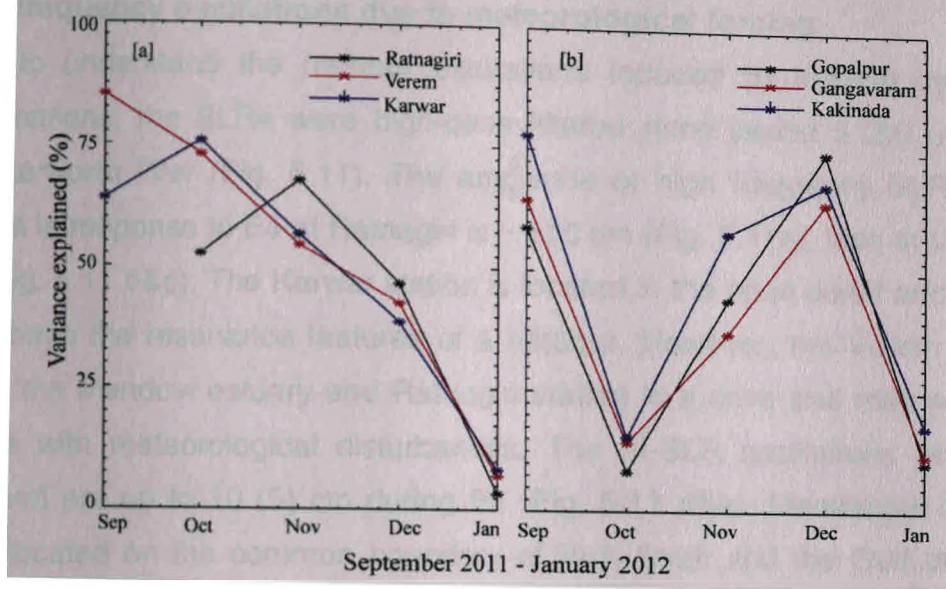


**Figure 5.10.** Daily-mean sea-level variability explained ( $Var_e$  %) by the multi-linear regression during different months from September 2011 to January 2012. [a]  $Var_e$  (%) at Ratnagiri (black), Verem (red) and Karwar (blue). [b]  $Var_e$  (%) at Gopalpur (black), Gangavaram (red) and Kakinada (blue).

In BOB, the SLR response to E5 has a plateau shape with rising peaks and prolonged falls, which the estimated SLR is not able to capture. This persistence of high daily-mean SLR state may be attributed to intensity, direction and duration of the event and distance from the source. The distance of Thane (E5) track is ~570 km from Gangavaram as shown in Fig. 5.1. The slope of the continental shelf will also affect the level of surge in a particular area. For example, areas with shallow slopes of the continental shelf (as in AS) will allow a greater storm surge and areas with deep water just offshore experience large waves, but little storm surge (SLOSH, 2003). At Gangavaram, the daily mean SLR is low (~13.8 cm) compared to other sites on the east coast of India (Table 5.5), and this could be attributed to harbour oscillations at this location (Fig. 5.5b.1). Also, when Thane crossed the Tamil Nadu coast just south of Cuddalore between 0100 and 0200 UTC of 30 December 2011, no distinct surge was observed at Mandapam and Tuticorin, even though Mandapam (Tuticorin) is in close proximity [~237 (360) km] to Thane track. The highest surge usually occurs to the right of the storm track (travelling with the storm) at approximately the radius of maximum wind, however, in this case, Mandapam and Tuticorin were to the left of the track.

### **5.5. High frequency oscillations due to meteorological forcing**

In order to understand the harbour oscillations induced by tropical cyclones at various locations, the SLRs were high-pass filtered (time period  $\leq 2$ h) using a 5<sup>th</sup> order Butterworth filter (Fig. 5.11). The amplitude of high frequency SLR (hf-SLR) oscillations in response to E4 at Ratnagiri is  $\sim \pm 10$  cm (Fig. 5.11a), less at Verem and Karwar (Fig. 5.11 b&c). The Karwar station is located in the open coast and therefore does not have the resonance features of a harbour. However, the Verem station is located in the Mandovi estuary and Ratnagiri station in a cove and may experience resonance with meteorological disturbances. The hf-SLR oscillations at Tuticorin (Mandapam) are up to 10 (5) cm during E4 (Fig. 5.11 d&e). Mandapam sea-level gauge is located on the common boundary of Palk Strait and the Gulf of Mannar, whereas the Tuticorin sea-level gauge is located in the Gulf of Mannar (Fig. 1.6). The hf-SLR oscillations at other stations located in BOB are also shown in Fig. 5.11. The hf-SLR amplitude due to E5 at Tuticorin, Mandapam is not observable and at Gopalpur a brief amplitude of 10 cm is observed (Fig. 11 d,e&f). At Gangavaram (Kakinada) the hf-SLR variations are  $\sim \pm 10$  (5) cm as both the gauges are located in the harbour (Fig. 11 g&h), and  $\sim \pm 4$  cm at Port Blair.

#### **5.5.1. SLR spectrum**

Event and background SLR spectra estimated at Karwar, Verem and Ratnagiri are presented in Fig. 5.10. The spectrum of SLR data is obtained using 'pwelch' function from Matlab with Hamming window of 256 data points and 50% overlap. The method as described in section-2.5.3 is used to understand the resonant influence of local topography and spectral characteristics of SLR during an event at a particular location. The data duration for estimating the spectrum of the SLR during E4 (background) is from 26 November - 1 December (1 September - 20 November) 2011. Similarly, the data duration during the event E5 (background) is 25-31 December (1 September - 10 December) 2011, respectively.



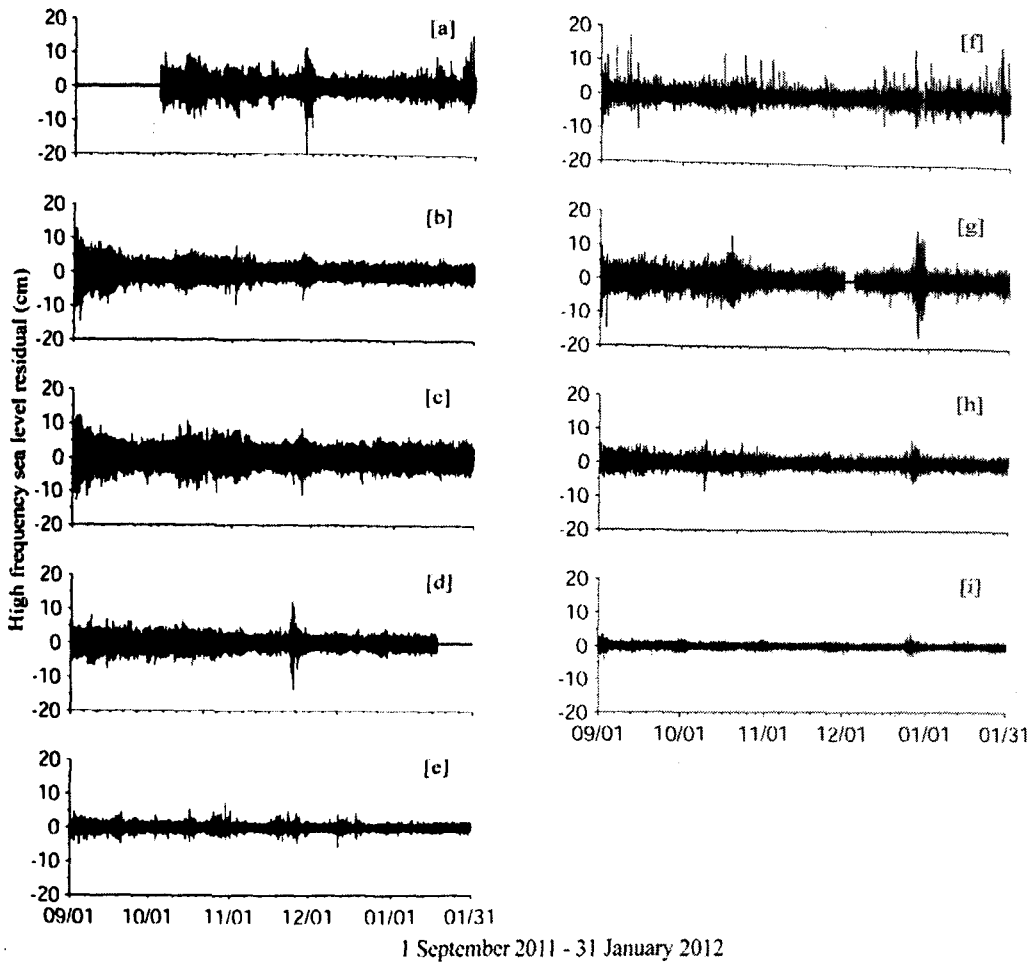


**Figure 5.11.** High-pass filtered sea-level residual (hf-SLR) using a 5th order Butterworth filter (time period  $\leq 2$ h) at [a] Ratnagiri, [b] Verem, [c] Karwar, [d] Tuticorin, [e] Mandapam, [f] Gopalpur, [g] Gangavaram, [h] Kakinada and [i] Port Blair.

### 5.5.1.1 SLR Spectrum in the AS

The background spectra of different sites have significant differences at high frequencies as seen in Fig. 5.12, indicating the influence of local topography. The event spectrum at Ratnagiri is high in energy, well lifted above that of background with major peaks at 127, 80, 47, 30, 26 and 14 min during E4 as shown in Fig. 5.12a. At Verem the event spectra is intertwined with background spectra with peaks at 182, 91, 40 and 20 min as shown in Fig. 5.12b. However, the event spectrum at Verem was energetic during the cyclone Yemyin (2007), September Sumatra Tsunami (2007), and the cyclone Phyan (2009), where a distinct peak was observed at  $\sim 43$

min (Chapter-4). Similarly, the event spectrum during E4 (Fig. 5.12c) at Karwar is similar to the background with some detectable peaks at 106, 67, 44 and 21 min and further higher frequencies are merged with the background spectra, indicating open-ocean behaviour (lack of harbour resonance). The influence of E4 is also visible at Tuticorin with dominant spectral peaks at 106, 53, 44, 24 and 18 minutes (Fig. 5.12d). However, at Mandapam (Fig. 12e) the event spectra are intertwined with background spectra with peaks at 116, 80, 42 and 26 min.

### 5.5.3 SLR Spectrum in the BOB

E5 event and background SLR spectra estimated at Gopalpur, Gangavaram, Kakinada, and Port Blair are shown in Fig. 5.13. The event spectrum during E5 (Fig. 5.13a) at Gopalpur is intertwined with the background spectra with some detectable peaks at 106, 80, 60, 45, 36, 21 and 12 min. The spectral peak at 45 and 21 min are also present in the background signal. The event spectral energy at Gangavaram (Fig. 5.13b) is higher compared to the background SLR spectra with peaks at 213, 98, 67, 41, 25 and 18 min, however the background spectra shows peaks at ~128, 98 and 17 min. At Gangavaram station the phenomena of harbour resonance is clearly visible (Fig. 5.5b.1), where it is not the surge but high frequency oscillations triggered by the long waves arriving from the open ocean. At Kakinada (Fig. 5.13c) the spectra for lower frequencies (time period > 41 min) are similar, but the energy is enhanced for higher-frequencies (shorter time-period) oscillations with time-period 41, 37, 25 and 12 min, suggesting resonance occurring in the harbour.

At Port Blair, the SLR spectra of both the event and background show similar variability with event peaks at 160, 85, 47, 41, 26 and 17 min (Fig. 5.11d). The background SLR spectrum has noticeable peaks at 41 and 26 min. Event spectra at shorter time periods are marginally above the background spectra indicating the absence of harbour resonance at Port Blair station. The high frequency water level oscillations observed at Gangavaram during the events are found to be due to the result of harbour resonance. Each location has a typical event spectrum related to the local topography. For example, Rabinovich [1997] observed two prominent peaks in Dimitrova Bay. First peak with period 50 min related to the amplification of incoming waves over the shelf of the south Kuril Islands (i.e to the shelf resonance).



# Sea-level response to meteorological forcing

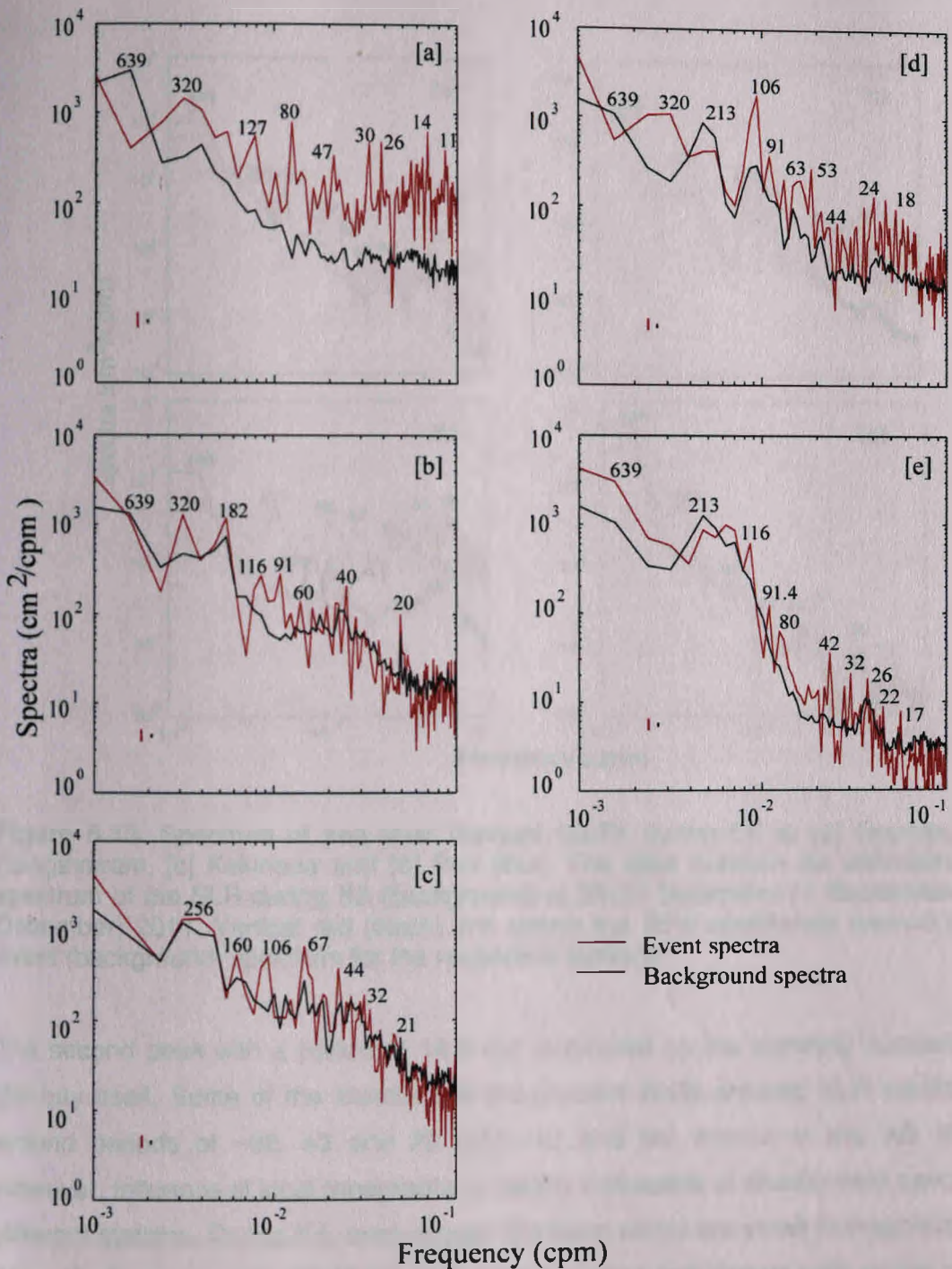


**Figure 5.12.** Spectrum of sea-level residual (SLR) during E4 at [a] Ratnagiri, [b] Verem, [c] Karwar, [d] Tuticorin and [e] Mandapam. The data duration for estimating the spectrum of the SLR during E4 (background) is from 26 November - 1 December (1 September - 20 November) 2011. Vertical red (black) line shows the 95% confidence interval of the event (background) spectrum for the respective stations.

## Sea-level response to meteorological forcing

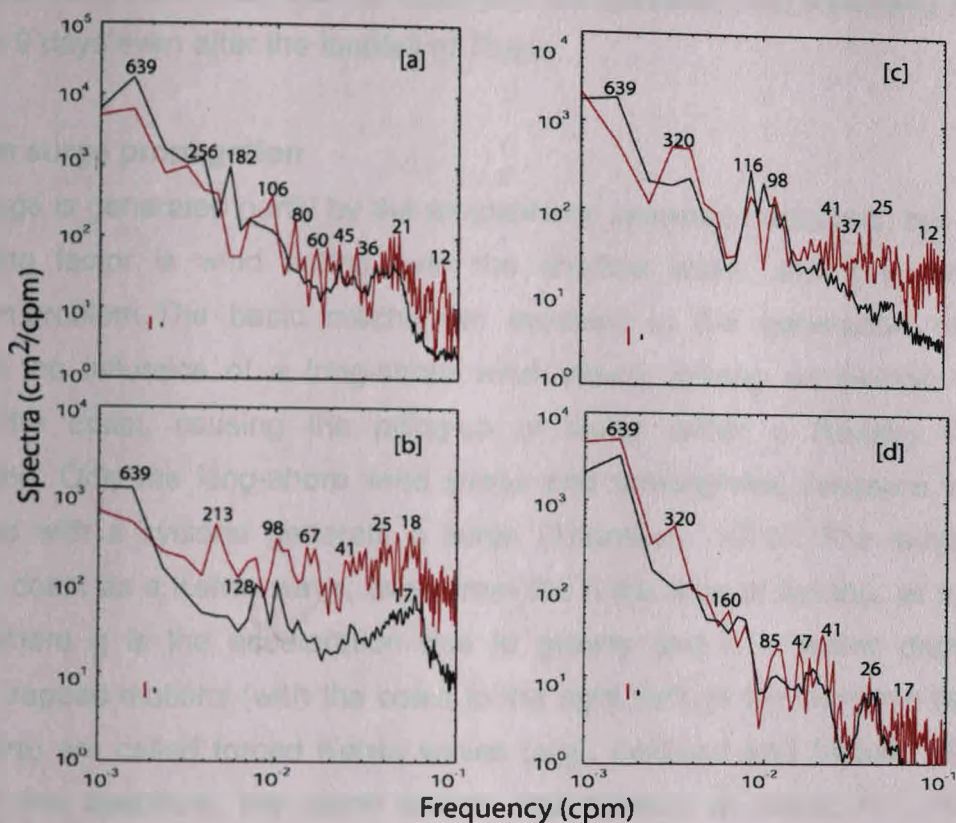


**Figure 5.13.** Spectrum of sea level residual (SLR) during E5 at [a] Gopalpur, [b] Gangavaram, [c] Kakinada and [d] Port Blair. The data duration for estimating the spectrum of the SLR during E5 (background) is 25-31 December (1 September - 10 December) 2011. Vertical red (black) line shows the 95% confidence interval of the event (background) spectrum for the respective stations.

The second peak with a period of 18.5 min is caused by the standing oscillation of the bay itself. Some of the locations in the present study showed SLR oscillations around periods of ~92, 43 and 23 (100, 42 and 24) minute in the AS (BOB). However, influence of local topography is clearly noticeable at shorter time periods at different stations. During E4, even though the local winds are small in magnitude ( $4-10 \text{ ms}^{-1}$ ), the surges are 39-47 cm at Ratnagiri, Verem and Karwar with similar peaks in SLR. In this case, the cyclone track is parallel or at an oblique angle to the coastline and hence the surge occurs on longer stretches of the shoreline. During E5 (**Thane**) the cyclone makes a perpendicular approach to the coast at landfall, and **therefore** the surges are low at Mandapam and Tuticorin, as these stations are on the **left** side of the Thane track, as compared to the stations on the right side (Gopalpur,



Gangavaram and Kakinada). SLR at Gopalpur, Gangavaram and Kakinada remained high for ~ 9 days even after the landfall of Thane.

### 5.6 Storm surge propagation

Storm surge is generated partly by the atmospheric pressure variations, but the main contributing factor is wind acting over the shallow water and it is an air-sea interaction problem. The basic mechanism involved in the generation of coastal surges is the influence of a long-shore wind stress, driving an Ekman transport towards the coast, causing the piling-up of water within a Rossby radius of deformation. Only the long-shore wind stress and atmospheric pressure variations associated with a cyclone generate a surge (Thomson, 1970). The surge travels along the coast as a Kelvin wave, away from the finite area of forcing, at a speed  $c = \sqrt{gh}$ , where  $g$  is the acceleration due to gravity and  $h$  is water depth. Such coastally trapped motions (with the coast to the right (left) in the northern (southern) hemisphere) are called forced Kelvin waves (e.g., LeBlond and Mysak, 1978; Gill, 1982). In the spectrum, the storm surges are centred at about  $10^{-4}$  Hz, which corresponds to a period of about 3h (Platzman, 1971). The estimates of a few parameters of E4 and E5 are listed in Table 5.6. To estimate the surge propagation speed, we have also added a few more locations, where hourly sea-level data is available from [www.gloss-sealevel.org](http://www.gloss-sealevel.org) (marked as red star in Fig. 5.1). Fig 5.14 shows the sea-level response from Colombo, Sri Lanka to Jask, Iran in the Indian Ocean. Some relevant parameters of the storm surge are listed in Table 5.7. The average surge propagation speed is estimated to be  $\sim 6.5 \text{ ms}^{-1}$ . The E4 moved northward with an average along-shore speed of  $\sim 6.2 \text{ ms}^{-1}$ , with the track almost parallel to the west coast of India. The match of the surge propagation speed with that of E4 alongshore speed is evidence of a forced wave. The residual surge lagged the storm by 3, 4, 6.5 and 8.5 h (Fig. 5.11 and Table 5.7) to its nearest proximity at Colombo, Kochi, Karwar and Verem respectively with a constant peak amplitude of  $\sim 34.6$  cm (Fig. 5.14). However, at Kochi, the development of secondary peak is clearly visible with time difference of  $\sim 14$  h between the two peaks of  $\sim 13.5$  cm. At Ratnagiri and Karachi, the surge peak is leading the storm by  $\sim 1$  h with the constant peak amplitude of  $\sim 33.5$  cm.

Similar response as above was observed by Fandry et al. (1984), when cyclone 'Glynis' moved slowly and almost parallel to the western coast of Australia in

February 1970. In this event, a strong coastal peak travelled down the coast well ahead of the cyclone. In this example  $\mu > \frac{U_m f}{c}$  and  $V_m < c$  (where,  $f$  is Coriolis parameter,  $U_m$  ( $V_m$ ) is eastward (northward) velocity of cyclone and  $\mu$  is decay rate, and theory predicts a coastal peak of constant amplitude moving ahead of the cyclone. In their study, they characterised the sea level response to tropical cyclone as:

- a)  $\mu < \frac{U_m f}{c}$  : Coastal peak of increasing magnitude propagating along the coast with speed  $V_m$ . The maximum peak occurs at the edge  $y=V_m t$  which is the leading (trailing) edge if  $V_m > c$  ( $V_m < c$ ), where  $y$  is alongshore axis and positive towards north,  $t$  is time.
- b)  $\mu > \frac{U_m f}{c}$  : Coastal peak of constant magnitude moving behind (ahead of) the cyclone if  $V_m > c$  ( $V_m < c$ ).

In the present study, observations indicate that surge peak lagged E4 upto Verem. From Ratnagiri to Karachi the surge peak is leading the E4 with amplitude almost constant (Table 5.7). Also it is observed that surge amplitude is almost constant (~34 cm) at all the four locations from Karwar to Karachi. The impact of E4 in the BOB at Port Blair (Fig. 5.3i) and in the northern parts of east coast of India at Kakinada, Gopalpur and Gangavaram (Fig. 5.3 f-h) is not observable. The response of sea-level due to E4 at Masirah (Fig. 5.14k) is also not observable as the location is on the right hand side of the event track. Similarly, the sea-level variations at the island locations of Minicoy and Hanimaadhoo are negligible due to E4 (Fig. 5.15), even though the track of E4 is only ~170 and 280 km, respectively away from the locations. However, the absence of closed boundary at these island locations and their locations on the left side of E4 track imply that no surges could be generated. The impact of E4 is observed only in the AS at the coastal boundary located on the right side of the event track.

**Table 5.6.** Parameter estimates of the events E4 and E5.

Name	Duration	Average eastward velocity ( $U_m$ ) (m/s)	Average northward velocity ( $V_m$ ) (m/s)	Minimum central pressure ( $P_c$ ) (mb)	Maximum wind speed ( $V$ ) (m/s)	Maximum stress ( $T_m$ ) ( $N/m^2$ )
DD (E4)	26 Nov-1 Dec 2011	1.1	6.2	998	17	0.9
Thane (E5)	25-31 Dec 2011	-1.1	0.3	969	40.8	5.2

Note:  $V = 3.44(1000 - P_c)^{0.644}$  and  $\tau_m = 0.000314V^2$  (refer Fandry et al., 1984).  $P_c$  is minimum central pressure.

**Table 5.7.** Surge propagation parameters during E4 along the coast of Arabian Sea.

Location	Peak (cm)	Time of peak (IST)	Path between two locations (km)	Propagation speed (m/s)
Colombo	31.6	26-Nov-2011 11:30		
Mandapam	24.3	26-Nov-2011 22:00	300	7.9
Tuticorin	21.4	27-Nov-2011 15:00	110	1.8
Kochi (Peak 2)	12.9	27-11-2011 23:30	400	13.1
Kochi (Peak 1)	14.14	27-11-2011 09:30		
Karwar	36.9	28-Nov-2011 12:00	577	7.6
Verem	35.5	28-Nov-2011 17:00	90	5.0
Ratnagiri	37.0	29-Nov-2011 03:00	172	4.8
Karachi	31.8	01-Dec-2011 07:30	1094	5.8
Chabahar	18.4	03-12-2011 19:30	670	3.1
Jask	13.7	04-Dec-2011 03:30	270	6.7

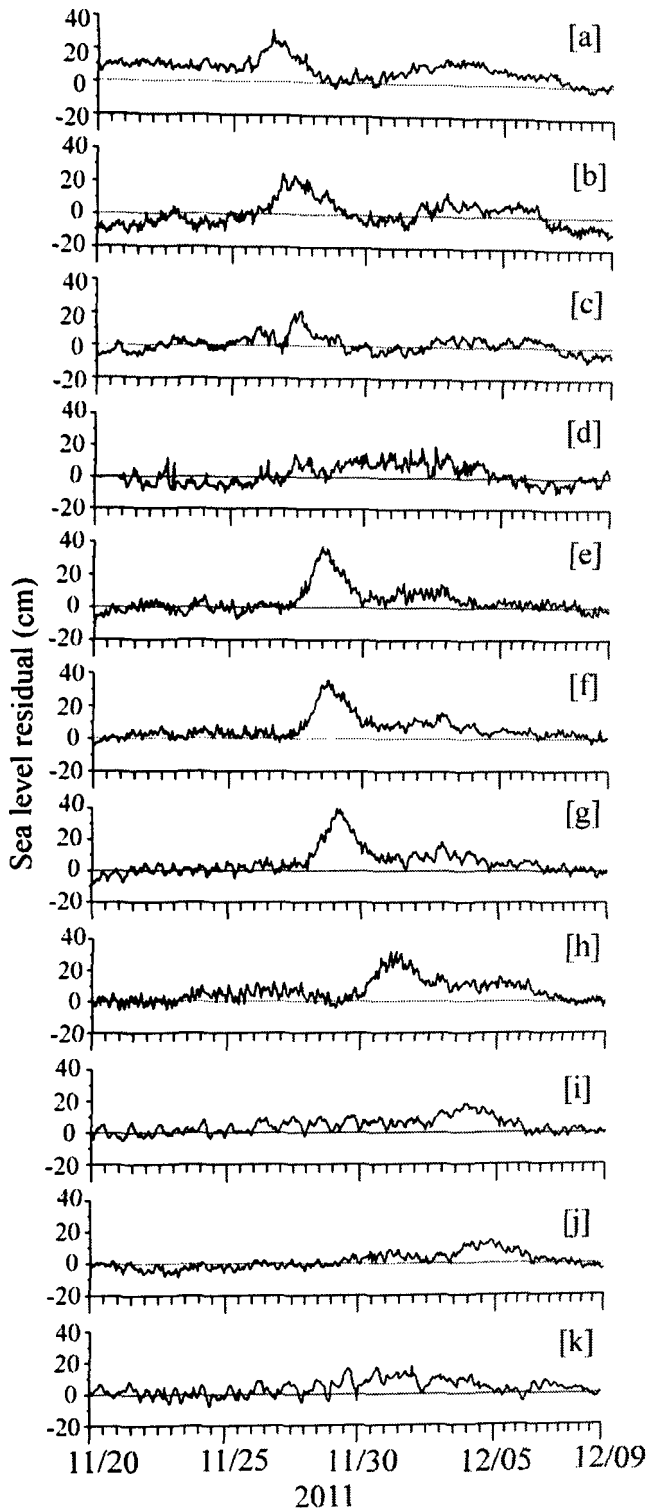


**Figure 5.14.** Hourly sea-level residual at [a] Colombo, [b] Mandapam, [c] Tuticorin, [d] Kochi, [e] Karwar, [f] Verem, [g] Ratnagiri, [h] Karachi, [i] Chabahar, [j] Jask and [k] Masirah.

**Note:** 1 Sea-level residual data at Mandapam, Tuticorin, Karwar, Verem and Ratnagiri are hourly averaged.

2 Sea level data at Colombo, Kochi, Karachi, Chabahar, Jask and Masirah are at hourly interval and downloaded from [www.gloss-sealevel.org](http://www.gloss-sealevel.org).

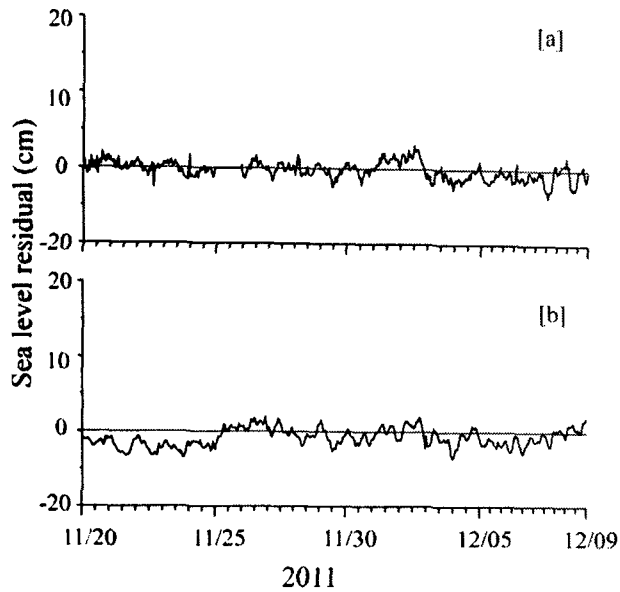


**Figure 5.15.** Sea-level residual at [a] Minicoy and [b] Hanimaadhoo.

**Note:** 1 Sea-level data at [a] Minicoy and [b] Hanimaadhoo are at hourly interval and downloaded from [www.gloss-sealevel.org](http://www.gloss-sealevel.org).

## 5.7 Conclusions

The study examined the observed storm-generated sea-level variation due to deep depression (Event-E4) in the Arabian Sea from 26 November to 1 December 2011 and a cyclonic storm "THANE" (Event-E5) over the Bay of Bengal during 25-31 December 2011. The response of the sea-level to the two events in the north Indian Ocean is summarised as:

- The sea-level and surface meteorological measurements collected during these extreme events exhibit strong synoptic disturbances leading to storm surges upto 43 cm on the west coast and 29 cm on the east coast of India due to E4 and E5.
- Events-E4 generated sea-level oscillations at the measuring stations on the west coast (Ratnagiri, Verem and Karwar) and east coast (Mandapam and Tuticorin) of India with significant energy bands centred at periods of 92, 43 and 23 minutes. The storm surge is a well defined peak with a half-amplitude width of 20, 28 and 26 h at Ratnagiri, Verem and Karwar respectively. However, on the east coast, the sea level oscillations during Thane were similar to those during calm period except

for more energy in bands centred at periods of ~100, 42 and 24 minutes at Gopalpur, Gangavaram and Kakinada respectively.

- The SLR rise (fall) in AS due to E4 reflects the winds as is also seen in the estimated SLR. The estimated SLR peak value at Ratnagiri and Verem is comparable to the measured SLR during E4 but at Karwar it is short by ~50%. The  $\text{Var}_e$  accounted by local surface meteorological parameters is ~69%.  $\text{Var}_e$  is small in January at all the locations of the present study. A significant part of the variability observed in sea-level remains unaccounted for and could be attributed to remote forcing.
- The residual sea-levels from tide gauge stations along the west coast of India and coast of Pakistan showed surge peak of constant amplitude propagating northward with a speed of  $\sim 6.5 \text{ ms}^{-1}$  during E4. The propagating surges along the western coast have been identified as forced Kelvin waves with almost constant amplitude.
- Multi-linear regression analysis shows that the local surface meteorological data (daily-mean wind and atmospheric pressure) could be able to account for ~57% and ~69% of daily-mean sea level variability along the east and west coasts of India. The remaining part of the variability observed in the sea level may be attributed to local coastal currents and remote forcing.



## Chapter 6

### Summary and conclusions

#### 6.1. Summary

There have been several studies conducted in north Indian ocean with a view to understand the seasonal, annual and sea-level rise trends using monthly-mean sea-level anomalies. Probably, this may be the first attempt to study the high-frequency sea-level oscillations with periods ranging from several minutes to a day in coastal regions of India. The specific objectives are given below:

- to understand sea-level variability at time scales from minutes to annual at different coastal and Island locations in the Indian Ocean.
- to study the influence of local surface meteorological forcings on sea-level variability.
- to study the sea-level variability during extreme atmospheric events.
- to model the sea-level variability using the dominant forces such as winds and atmospheric pressure during meteorological events.

Sea-level and surface meteorological data were collected using the indigenously developed sea-level gauges (SLG) and autonomous weather stations (AWS) installed at select coastal and island locations of India as a part of integrated coastal observation system (ICON). Apart from sea-level data under ICON, hourly sea-level data from a few more locations (Minicoy, Hanimaadhoo, Colombo, Kochi, Karachi, Chabahar, Jask and Masirah) were used ([www.gloss-sealevel.org](http://www.gloss-sealevel.org)) for the Indian Ocean. The tropical cyclone track data from the India Meteorological Department (IMD, [www.imd.gov.in](http://www.imd.gov.in)), Joint Typhoon Warning Center (JTWC, [www.usno.navy.mil/JTWC/](http://www.usno.navy.mil/JTWC/)) and UNISYS-Unisys Weather ([http:// weather.unisys.com/hurricane/](http://weather.unisys.com/hurricane/)) have been used to study the coastal sea level response during the tropical cyclones.

The Specific investigations carried out in the present study are:

- comparison of sea-level measurements between radar and pressured based sea-level gauges. The effect of atmospheric pressure on the sea-level measurements from pressure gauges.
- investigated the variation in sea-level residuals along the coastal and island locations of India with time periods ranging from a few minutes to one year.
- Identification of potential resonant frequencies for a particular location along the coast of India with varying local topographies.
- analysis of response and spectral characteristics of sea-level residuals along the Indian coast during normal weather and extreme events such as tropical cyclones and tsunami.
- investigation of seiches at a few ports and coastal estuaries.
- setting up of numerical and statistical models for the Indian Ocean, and validation of model results with measurements during tropical cyclones and remote sensing data
- characteristics of "Kelvin waves" – generation and propagation, and their influence along the west coast of India

### **6.2. Conclusions**

- Sea-level data were collected using indigenously developed microwave radar and an absolute pressure gauge at Verem, Goa (January 2009 to May 2010) and Tuticorin, and Mandapam, Tamil Nadu (June 2010 to March 2011), and the results were compared. The root-mean-square difference between the estimated sea level from radar and pressure gauge (incorporating atmospheric pressure correction) is ~2.69, 2.73, and 1.46 cm at Verem, Tuticorin, and Mandapam, respectively. Harmonic analysis of the two time-series of sea-level data at Verem produces similar residuals and tidal constituents.

- tidal amplitude increases linearly from south towards north till the central west coast of India. However, along the east coast of India, the tidal amplitude at Yanam to Gopalpur appears to be constant
- tides measured in the AS locations could be classified as mixed, mainly semi-diurnal tides with Form number varying within the range of 0.25-1.5. However, in BOB, the Form number is less than 0.25 from Port Blair to Gopalpur indicating semi-diurnal tides. At Mandapam and Tuticorin, the tides are mixed, mainly semi-diurnal type.
- sea-level residual variability exists at all the locations throughout the measurement period (or throughout the year). The SLR varies within  $\pm 25$  cm at most of the locations, except at the southern tip of India (Colachel), where the variations are up to  $\pm 50$  cm due to focussing of waves because of local topography.
- low frequency spectra of the sea-level residuals have time periods around 2.5, 3.8, 5.3, 7.6, 19.5, 36 and 64 days along the west coast of India. However, the spectra of the daily-mean SLR along east coast of India show oscillations with time periods around 2.4, 3.9, 5.1, 7.4, 9.7, 12.3, 18.9, 36.0 and 64.0 days.
- high frequency oscillations of the sea-level residual along the west coast of India have major peaks at 360, 160, 85, 75, 49 and 21 min. However, the spectral energy peaks observed at time periods of  $\sim 118$ , 90, 75, 43, 32, 20 and 14 min at locations along the east coast of India are lower compared to that at the measurement locations along the west coast of India.
- sea-level and surface meteorological data collected during storms exhibit strong synoptic disturbances leading to coherent oscillations in the Mandovi estuary with significant energy bands centered at periods of 24, 45 and 80 minutes.

- Kavaratti Island lagoon showed no prominent spectral peaks to indicate seiches (i.e. natural oscillations). The non-resonant character of Kavaratti Island lagoon remained despite intense wind forcing. The surge at this lagoon was insignificantly weak due to the combined effect of the absence of resonant amplification and lack of river water discharge into the lagoon.
- The pre-earthquake enhanced seawater temperature oscillations observed at Mandovi (tropical) estuary indicates that routine monitoring of seawater temperature with fine temporal resolution may provide early information about impending coastal earthquakes.
- Occurrence of deep depression (E4: 26 November to 1 December 2011) in the Arabian Sea generated sea-level oscillations at the measuring stations on the west coast (Ratnagiri, Verem and Karwar) and east coast (Mandapam and Tuticorin) of India with significant energy bands centred at periods of 92, 43 and 23 minutes. The storm surge has a well defined peak with a half-amplitude width of 20, 28 and 26 h at Ratnagiri, Verem and Karwar respectively. However, on the east coast, the sea level oscillations during Thane were similar to those during calm period except for high energy in bands centred at periods of ~100, 42 and 24 minutes at Gopalpur, Gangavaram and Kakinada, respectively.
- The estimated sea-level residual (SLR) peak value at Ratnagiri and Verem is comparable to the measured SLR during E4, but at Karwar it is short by ~50%. The variability ( $Var_e$ ) accounted by local surface meteorological parameters is ~69%.  $Var_e$  is small in January at all the locations of the present study. A significant part of the variability observed in sea-level remains unaccounted for and could be attributed to remote forcing.
- The residual sea levels from tide gauge stations along the west coast of India and coast of Pakistan showed a surge peak of constant amplitude propagating northward with a speed of  $\sim 6.5 \text{ ms}^{-1}$  during E4. The propagating surges along

the western coast have been identified as forced Kelvin waves with almost constant amplitude.

- Multi-linear regression analysis showed that the local surface meteorological data (daily-mean wind and atmospheric pressure) could be able to account for ~57% and ~69% of daily-mean sea level variability along the east and west coasts of India. The remaining part of the variability observed in the sea level may be attributed to local coastal currents and remote forcing.

### 6.3. Future perspective

The present work can be extended further to study the following aspects:

- ✓ Role of distant long waves in modulating sea-level variations along the coast of India, where the impact of local topography is dominant, is yet to be understood – a detailed investigation is required.
- ✓ Influence of surface meteorological force along the coast of India has to be analysed in detail utilising fine resolution atmospheric models.
- ✓ Hydrodynamic models need to be established for harbours, estuaries to estimate the Eigen frequencies and then validate them with measured data. These studies will be relevant to various ports which may exhibit harbour oscillations to avoid any damages to the ships.

## References

- Andersen, O. B. (1995): Global ocean tides from ERS1 and TOPEX/POSEIDON altimetry. *Journal of Geophysical Research*, 100, (C12), 25249-25259, 1995.
- Banse, K. (1968): Hydrography of the Arabian Sea Shelf of India and Pakistan and effects on demersal fishes. *Deep-Sea Res*, 15:45–79.
- Bell, C., Vassie, J.M. and Woodworth, P.L. (2000): Tidal Analysis Software Kit 2000 (TASK-2000). POL/PSMSL Permanent Service for Mean Sea Level, Proudman Oceanographic Laboratory, UK.
- Bernstein, L., Peter Bosch, Osvaldo Canziani, Zhenlin Chen, et al. (2007): Synthesis report-Climate change 2007. An Assessment of the Intergovernmental Panel on Climate Change, adopted section by section at IPCC Plenary XXVII (Valencia, Spain, 12-17 November 2007).
- Brown, J.M., Bolaños, R., Howarth, M.J. and Souza, A.J. (2012): Extracting sea level residual in tidally dominated estuarine environments, *Ocean Dynamics* (2012) 62:969–982, DOI 10.1007/s10236-012-0543-7.
- Candela, J., Mazzola, S., Sammari, C., Limeburner, R., Lozano, C. J. and Patti, B. (1999): The “Mad Sea” Phenomenon in the Strait of Sicily, *Journal of Physical Oceanography*, 29, 2210-2231.
- Cazenave, A. and Nerem, R.S. (2004): Present-day sea level change: observations and causes. *Reviews of Geophysics*, 42, RG3001, 1–20.
- Charls, A. and Unnikrishnan, A.S. (2013): Observed characteristics of tide-surge interaction along the east coast of India and the head of Bay of Bengal. *Estuarine, Coastal and Shelf Science* 131 (2013) 6e11
- Chambers, D.P., Merrifield, M.A., and Nerem, R.S.(2012): Is there a 60-year oscillation in global mean sea level? *GRL*, Vol. 39, L18607, doi:10.1029/2012GL052885, 2012.
- Chaturvedi, N and Narain, A. (2003): Chlorophyll distribution pattern in the Arabian Sea: seasonal and regional variability, as observed from SeaWiFS data. *International Journal of Remote Sensing*, 24, 511-518.
- Chang-Kou, T. and Carl, W. (2011): Sampling errors of the global mean sea level derived from TOPEX/Poseidon altimetry. *Acta Oceanol. Sin.*, 2011, Vol. 30, No. 6, P. 12-18.
- Chittibabu, P., Dube, S. K., Rao, A. D., Sinha, P. C., and Murty, T. S. (200): Numerical Simulation of extreme sea levels using location specific high resolution model for Gujarat coast of India. *Marine Geodesy*, 23, 133–142, 2000.

## References

---

- Chittibabu, P., Dube, S. K., Rao, A. D., Sinha, P. C., and Murty, T. S. (2002): Numerical simulation of extreme sea levels for the Tamilnadu (India) and Sri Lanka coasts. *Mar. Geod.*, 25, 235–244, doi:10.1080/01490410290051554, 2002.
- Church, J. A., Gregory, J. M., Huybrechts, Kuhn, M., Lambeck, K., Nhuan, M. T., Qin, D. and Woodworth, P. L. (2001): Changes in sealevel. In *Climate Change 2001: The Scientific Basis. Contribution of Working Group I to the Third Assessment Report of the Intergovernmental Panel on Climate Change*, Cambridge University Press, Cambridge, UK, 2001, pp. 639–693.
- Church, J. A. et al. (2013): Sea level change. In *Climate Change 2013. The Physical Science Basis, Contributions of Working Group I to the Fifth Assessment Report of the Intergovernmental Panel on Climate Change* (eds Stocker, T. F. et al.), Cambridge University Press, Cambridge, UK, 2013, pp. 1137–1216.
- Clarke, A.J. and Battisti, D.S. (1981): The effect of continental shelves on tides. *Deep-Sea Research*, Vol. 28A, No. 7, pp. 665 to 682, 1981.
- Clarke, A.J. and Liu. X. (1994): Interannual sea level in the northern and eastern Indian Ocean. *Journal of Physical Oceanography*, 24(6): pp1224–1235.
- Das, P.K. and Radhakrishna, M. (1991): An analysis of Indian tide-gauge records. *Proceedings of Indian academy of Sciences (Earth Planetary Science)* 100, 177-194.
- Das, P.K. (1994): On the Prediction of storm surges. *Sadhana*, 19, 583–595, doi:10.1007/BF02835641, 1994.
- Defant, A. (1961): *Physical Oceanography*, Vol. 2, pp. 606, Pergamon, Oxford, UK.
- DHI. (2011). Available:  
<http://www.mikebydhi.com/Products/CoastAndSea/MIKE21/Hydrodynamics.aspx>
- Dube, S.K., Rao, A.D., Sinha, P.C., Murty, T.S. and Bahulayan, N. (1997): Storm surge in the Bay of Bengal and Arabian Sea: The problem and its prediction. *Mausam*, 48, 283-304.
- Dube, S. K., Jain, I., and Rao, A. D. (2006): Numerical storm surge prediction model for the North Indian Ocean and the South China Sea. *Disaster Dev.*, 1, 47–63, 2006.
- Dube, S. K., Jain, I., Rao, A. D., and Murty, T. S. (2009): Storm surge modelling for the Bay of Bengal and Arabian Sea, *Nat. Hazards*, 51, 2–27, doi:10.1007/s11069-009-9397-9, 2009.
- Emery, K.O. and Aubrey, D.G. (1989): Tide gauges of India. *Journal of Coastal Research*, 5(3):489–501, Summer 1989.
- Fandry, C.B., Leslie, L.M., Steedman, R.K. (1984): Kelvin-type coastal surges generated by tropical cyclones. *Journal of Physical Oceanography*, Vol. 14, 582-593, 1984.

- Feng, M., Li, Y. and Meyers, G. (2004): Multidecadal variations of Fremantle sea level: Footprint of climate variability in the tropical Pacific. *Geophys. Res. Lett.*, 31, L16302, doi:10.1029/2004GL019947.
- Fritz, H.M., Blount, C.D., Albusaidi, F.B., and Al-Harthy, A.H.M. (2010): Cyclone Gonu storm surge in Oman, *Estuarine, Coastal and Shelf Science*, 86,102–106, 2010.
- Fujita, T. (1955): Results of detailed synoptic studies of squall lines. *Tellus*, 7, 405–436.
- Ghildyal, H.S. and Kumar, A. (1984): Global mean sea level investigations: Discrepancy between the local mean sea level of the Bay of Bengal and the local mean sea level of the Arabian Sea, Technical Paper, Survey of India, 1984.
- Gill, A.E. and Niiler, P.P. (1973): The theory of the seasonal variability in the ocean. *Deep Sea Res* 20:141–177.
- Gill, A.E. (1982): Atmosphere-ocean dynamics. Academic Press, New York, 1982, xv+ 662.
- Griffies, S.M. and Greatbatch, R.J. (2012): Physical processes that impact the evolution of global mean sea level in ocean climate models. *Ocean Modelling*, 51, 37-72.
- Hibiya, T. and Kajiura, K. (1982): Origin of the Abiki phenomenon (a kind of seiche) in Nagasaki Bay. *Journal of the Oceanographical Society of Japan*, 38, 172–182.
- Hirata, K., Aoyagi, M., Mikada, H., Kawaguchi, K., Kaiho, Y., Iwase, R., Morita, S., Fujisawa, I., Sugioka, H., Mitsuzawa, K., Suyehiro, K., Kinoshita, H., and Fujiwara, N. (2002): Real-time geophysical measurements on the deep seafloor using submarine cable in the southern Kurile subduction zone, *IEEE J. Oceanic Eng.*, 27(2), 170-181.
- Hilmi, K., EL Sabh, M.I., Chanut, J.P. and Tad Murty (2000): Stochastic Modeling of Short Term Variations of Sea Level in Eastern Canada. *Marine Geodesy*, 23:197–18.
- Hilmi, K., Tad Murty, EL Sabh, M.I. and Chanut, J.P. (2002), Long-Term and Short-Term Variations of Sea Level in Eastern Canada. A Review, *Marine Geodesy*, 25:61–78.
- Hastenrath, S. and Lamb, P.J. (1979): Climate Atlas of the Indian Ocean. Part I: surface climate and atmospheric circulation. Wisconsin University Press, Madison, 19 pp, 97 charts.
- IOC (2006): Manual on Sea Level Measurement and Interpretation. Volume 4: An Update to 2006, JCOMM Technical report No.31, WMO/TD.1339, Chapt.-3.
- Jain, I., Chittibabu, P., Agnihotri, N., Dube, S.K., Sinha, P.C., and Rao, A.D. (2007): Numerical storm surge model for India and Pakistan, *Nat. Hazards*, 42, 67–73, doi:10.1007/s11069-006-9060-7, 2007.



- Johannessen, O.M., Subharaju, G. and Bliondhiem, J. (1981): Seasonal variation of the oceanographic conditions off the southwest coast of India during 1971–75. *FiskDir Skr Ser HavUnders* 18:247–261.
- Joseph, A., Vijaykumar, Desa, E., Ehrlich, D., and Peshwe, V. (2002), Over-estimation of sea level measurements from water density anomalies within tide-wells – A case study at Zuari estuary Goa. *Journal of Coastal Research*, 18,2, pp-362-371.
- Joseph, A., Desai, R.G.P., VijayKumar, K., Mehra, P. and Nagvekar, S. (2005): Meteorologically induced modulation in sea level off Tikkavanipalem Coast - Central east coast of India. *J. Coast. Res.:* 21(5): 2005: 880-886.
- Joseph, A., and Prabhudesai, R.G. (2005), Need of a disaster alert system for-India through a network of real time monitoring of sea level and other meteorological events. *Curr. Sci.*, 2005, 89 (5), 864-869.
- Joseph A., Odametey, J.T., Emmanuel K. Nkebi, Desa, E., Pereira, A., . Prabhudesai, R.G., Mehra, P., Rabinovich, A.B, Vijaykumar, Prabhudesai, S., and Woodworth, P. (2006): Detection of the 26 December 2004 “Sumatra Tsunami” at the Eastern Atlantic Coast, *African Journal of Marine Science (AJMS)*, 2006 28 (3&4), pp.705-712.
- Joseph, A., Prabhudesai, R.G., Mehra, P., Sanil Kumar, V., Radhakrishnan, K.V., Vijay Kumar, Ashok Kumar, K., Agarvadekar, Y., Bhat, U.G., Luis, R., Rivankar, P. and Viegas, B. (2010), Response of west Indian coastal regions and Kavaratti lagoon to the November-2009 tropical cyclone Phyan. *Natural Hazard*, DOI 10.1007/s11069-010-9613-7, Sept., 2010.
- Joseph, A. (2011): *Tsunamis: Detection, Monitoring, and Early-Warning Technologies*. Elsevier Science & Technology book, 446 p, [ISBN: 978-0-12-385053-9].
- Kranz, S., Zenz, T. and Barjenbruch, U. ( 2001): Radar: is it a new technology applicable to water level gauging? *Physics and Chemistry of the Earth (C)*, 26(10–12), 751–754.
- Kulikov, E.A., Rabinovich, A.B., Spirin, A.I., Poole, S.L., and Soloviev, S.L. (1983): Measurement of tsunamis in the open ocean, *Mar. Geodesy*,6,311-329.
- LeBlond, P. H. and Mysak, L. A. (1978): *Waves in the Ocean*, Elsevier, Amsterdam, 602 pp., 1978.
- Levin, B. V., Likhacheva, O. N., and Uraevskii, E.P. (2006): Variability in the thermal structure of ocean waters in periods of strong seismic activity. *Atmospheric and Oceanic Physics*, 42(5), 653-657.
- Lighthill, M.J., (1969): Dynamic response of the Indian Ocean to the onset of the southwest monsoon. *Philos Trans R Soc Lond Ser A* 265:45–92

- Martin, M.B., Perez Gomez, B., and Fanjul, A.E. (2005): The ESEAS-RI sea level test station: reliability and accuracy of different tide gauges. *International Hydrographic Review*, 6(1), 44–53.
- Martin, M.B., Le Roy, R., and Woppelmann, G. (2008): The use of radar tide gauges to measure variations in sea level along the French coast. *Journal of Coastal Research*, 24(4C), 61–68. West Palm Beach (Florida), ISSN0749-0208.
- Mehra P., Prabhudesai, R. G., Joseph, A., Vijaykumar, Dabholkar, N., Prabhudesai, S., Nagvekar, S. and Agarvadekar Y. (2005): Endurance and stability of some surface meteorological sensors under land- and ship-based operating environments, *Proceedings of the National Symposium on Ocean Electronics, SYMPOL*, 15-16 December, 2005, pp. 257-264.
- Mehra, P., Joseph, A., Prabhudesai, R.G., Vijaykumar, Sundar, D. and Tengali, S. (2008): On the usability of “compensated temperature” output of Honeywell PPTR sensor for coastal oceanographic and limnological studies, *Proceedings of the International Conference: Oceans’08 MTS/IEEE-Kobe-Techno-Ocean’08 (OTO’08)* from 8-11 April 2008.
- Mehra, P., Desai, R.G.P., Joseph, A., VijayKumar, K., Agarvadekar, Y., Luis, R., Sundar, D. and Viegas, B. (2009): A one year comparison of radar and pressure tide gauge at Goa, west coast of India. *Proceedings of the International Symposium on Ocean Electronics (SYMPOL-2009)*, 18-20 November 2009, 173-183.
- Mehra, P., Tsimplis, M.N., Prabhudesai, R.G., Joseph, A., Andrew, G.P. Shaw, Somayajulu, Y.K. and Cipollini, P. (2010): Sea level changes induced by local winds on the west coast of India. *Ocean Dynamics* (2010) 60:819–833 DOI 10.1007/s10236-010-0289-z.
- Minster, J.F., Boussier, C., Rogel, P. (1995), Variation of mean sea level from TOPEX/POSEIDON data, *J Geophys Res*, 100: 25153–25161.
- Minster, J.F., Cazenave, A., Serafini, Y.V., Mercier, F., Gennero, M.C., P. Rogel, P. (1999): Annual cycle in mean sea level from Topex-Poseidon and ERS-I: Inference on the global hydrological cycle, *Global and Planetary Change*, 20, 57-66.
- Monserrat, S., and Thorpe, A.J. (1992): Gravity wave observations using an array of microbarographs in the Balearic Islands. *Quart. J. Roy. Meteor. Soc.*, 118, 259–282.
- Monserrat, S., Rabinovich, A.B. and Casa, B. (1998): On the reconstruction of the function for atmospherically generated seiches, *GRL*, Vol. 25, No.12, 2197-2200.
- Monserrat, S., Vilibic, I. and Rabinovich, A.B. (2006): Meteotsunamis: atmospherically induced destructive ocean waves in the tsunami frequency band. *Nat. Hazards Earth Syst. Sci.*, 6, 1035-1051.
- Murty, T.S. and Henry, R.F. (1983): Tides in the Bay of Bengal, *J. Geophys. Res.*, Vo.88, July 1983.

- Murty, T.S., Flather, R. A. and Henry, R.F. (1986): The storm surge problem in the Bay of Bengal. *Prog. Oceanog.* Vol. 16, pp. 195-233.
- Murty, T.S. (1999): Storm surges in the marginal seas of the north Indian Ocean, *Proceedings of the WMO/UNESCO Sub-Forum on Science and Technology in support of natural disaster reduction*, Geneva, 6-8 July 1999, pp 130-139.
- Nayak, R.K., and Shetye, S.R. (2003): Tides in the Gulf of Khambhat, west coast of India. *Estuarine, Coastal and Shelf Science* 57:249–254.
- Nerem, R.S., Haines, B.J., Hendricks J, Minster, F.J., Mitchum, G.T., White, W.B. (1997): Improved determination of global mean sea level variations using TOPEX/POSEIDON altimeter data, *Geophys Res Letters*, 24: 1331–1334
- Nerem, R.S., Chambers, D.P, Leuliette, E.W., Mitchum, G.T., Giese, B.S. (1999): Variations in global mean sea level associated with the 1997–98 ENSO event: Implications for measuring long term sea level change. *Geophys Res Letters*, 26: 3005–3008.
- Nosov, M.A. (1998): Effect of underwater earthquakes on the stratified ocean. *Vestn. Mosk. Univ., Ser. 3, Fiz., Astron*, 4, 23-27.
- Nosov, M.A., and Kolesov, S.V. (2007): Elastic oscillations of water column in the 2003 Tokachi-oki tsunami source: in-situ measurements and 3-D numerical modelling, *Nat. Hazards Earth Syst. Sci.*, 7, 243-249.
- Orlić, M. (1980): About the possible occurrence of the Proudman resonance in the Adriatic, *Thalassia Jugoslavica* 16(1), 79-88.
- Ostrovskii, L . A, and Papilova, I.A. (1974): On a nonlinear acoustic wind, *Akust. Zh.*, 20, 79-86.
- Palanisamy, H., Cazenave, A., Meyssignac, B., Soudarin, L., Wöppelmann, G. and Becker, M. (2014): Regional sea level variability, total relative sea level rise and its impacts on islands and coastal zones of Indian Ocean over the last sixty years. *Global Planet. Change*, 2014: doi:10.1016/j.gloplacha.2014.02.001.
- Panigrahi, J.K., Umesh, P.A., Padhy, C.P. and Swain, J. (2012): Nearshore propagation of cyclonic waves. *Nat Hazards* (2012) 60:605–622, DOI 10.1007/s11069-011-0030-3.
- Pasquet, S., Vilibic, I. and Sepic, J. (2013): A survey of strong high-frequency sea level oscillations along the US East Coast between 2006 and 2011, *Nat. Hazards Earth Syst. Sci.*, 13, 473–482, [www.nat-hazards-earth-syst-sci.net/13/473/2013/doi:10.5194/nhess-13-473-2013](http://www.nat-hazards-earth-syst-sci.net/13/473/2013/doi:10.5194/nhess-13-473-2013)
- Pattiaratchi, B.C. and Wijeratne Sarath, E.M. (2009): Tide Gauge Observations of 2004-2007 Indian Ocean Tsunami from Sri Lanka and Western Australia, *Pure appl. Geophys.* Vol. 166, 233-258.

- Patullo, J., Munk, W., Revelle, R., and Strong, E. (1955): The seasonal oscillation in sea level. *Journal of Marine Research*, 14(1):88–113, January 1955.
- Perigaud, C. and Delecluse, P. (1993): Interannual Sea Level Variations in the Tropical Indian Ocean from Gesat and Shallow Water Simulations. *Journal of Physical Oceanography*, Vol. 23, pp 1916-1934.
- Platzman, G.W. (1971): Ocean tides and related waves. Lectures for the American Mathematical Society, 1970, Summer seminars on mathematical problems in the geophysical sciences, held at Rensselaer Polytechnic Institute, Troy, NY, 94 pp (Also In: Reid WH (ed) *Mathematical problems in the geophysical sciences*, vol 14, Part 2, pp 239–291), 1971.
- Prabhudesai, R.G., Joseph, A., Agarvadekar, Y., Dabholkar, N., Mehra, P., Gouveia, A., Tengali, S., Vijay, K. and Parab, A. (2006): Development and implementation of cellular-based real-time reporting and Internet accessible coastal sea level gauge—a vital tool for monitoring storm surge and tsunami. *Curr Sci* 90(10):1413–1418.
- Prabhudesai, R.G., Joseph, A., Mehra, P., Agarvadekar, Y., Tengali, S. and Vijaykumar (2008): Cellular-based and Internet-enabled real-time reporting of the tsunami at Goa and Kavaratti Island due to Mw 8.4 earthquake in Sumatra on 12 September 2007. *Current Science*: 94,10 May 2008: 1151-1157.
- Prabhudesai, R.G., Joseph, A., Agarvadekar, Y., Mehra, P., VijayKumar, K. and Luis, R. (2010): Integrated Coastal Observation Network (ICON) for real-time monitoring of sea-level, sea-state, and surface-meteorological data. *Proc. Oceans'10 MTS/IEEE*: Seattle, Washington: USA: 20-23 September 2010, 9 pp.
- Prasad, K.V.S.R., and Reddy, B.S.R.(1985): Sea level variations off Madras, east coast of India. *Indian Journal of Marine Sciences*, 14:206–209, December 1985.
- Proudman, J. (1953): *Dynamical Oceanography*, London, Methuen and Co, 556 pp.
- Pugh, D.T. and Vassie, J.M. (1976): Tide and surge propagation off-shore in the Dowsing region of the North Sea, *Deutsche Hydrographische Zeitschrift*, Jahrgang 29, pp 163-213, 1976, Heft 5.
- Pugh, D.T. (1987): *Tides, Surges and Mean Sea-Level*, 472 pp., John Wiley & Sons, Chichester.
- Rabinovich, A.B. and Moserrat, S. (1996): Meteorological Tsunamis near Balearic and Kuril Island: Descriptive and statistical Analysis, *Natural Hazards*, 13: pp 55-90.
- Rabinovich, A.B. (1997): Spectral analysis of tsunami waves' Separation of source and topography effects, *JGR*, Vol. 102, No. C6, pp 12,663-12,676.
- Rabinovich, A.B., Monserrat, S. (1998), Generation of meteorological tsunamis (large amplitude seiches) near the Balearic and Kuril Islands, *Natural Hazards*, 18, 27–55.

- Rabinovich, A.B. and Stephenson, F.E. (2004): Longwave Measurements for the Coast of British Columbia and Improvements to the Tsunami Warning Capability, *Natural Hazards*, 32: pp 313-343.
- Rabinovich, A.B. (2009): Seiches and harbor oscillations, Chapter 9, *Handbook of Coastal and Ocean Engineering* (edited by Y.C. Kim), World Scientific Publ., Singapore, 2009.
- Richard, D.R., and Byrne, D.A. (2010): Bottom pressure tides along a line in the southeast Atlantic Ocean and comparisons with satellite altimetry. *Ocean Dynamics* (2010) 60:1167–1176.
- Rao, A.D., Jain, I., Murthy, M.V.R., Murty, T.S. and Dube, S.K. (2008): Impact of cyclonic wind field on interaction of surge wave computations using Finite- element and Finite-difference models, *Nat Hazards*, doi:10.1007/s11069-008-9284-9.
- Rao, A.D., Murty, P.L.N., Jain, I., Kankara, R.S., Dube, S.K., and Murty, T.S. (2013): Simulation of water levels and extent of coastal inundation due to a cyclonic storm along the east coast of India. *Nat Hazards* (2013) 66:1431–1441, DOI 10.1007/s11069-012-0193-6
- Sakova, I.V., Meyers, G., Coleman, R. (2006): Interannual variability in the Indian Ocean using altimeter and IX1-expendable bathy-thermograph (XBT) data: Does the 18-month signal exist? *Geophysical Research Letters* 33. doi:10.1029/2006GL027117 (L20603).
- Sanil Kumar, V. and Ashok Kumar, K. (2010): Waves and Currents in Tide-Dominated Location Off Dahej, Gulf of Khambhat, India. *Marine Geodesy*, 33:218–231.
- Shaji, C., Kar, S.K. and Vishal, T. (2014): Storm surge studies in the North Indian Ocean: A review. *Indian Journal of Geo-Marine Sciences*, Vol 43 (2), pp. 125-147.
- Shankar, D. and Shetye, S.R. (1997): On the dynamics of the Lakshadweep high and low in the southeastern Arabian Sea. *J Geophys Res*, 102:12551–12562
- Shankar, D. and Shetye, S.R. (1999): Are interdecadal sea level changes along the Indian Coast influenced by variability of monsoon rain fall?, *JGR*, 104, C11, 26031-26042.
- Shankar, D., (2000): Seasonal cycle of sea level and currents along the coast of India, *Curr Sci* 78:279–288.
- Shankar, D. and Shetye, S.R. (2001): Why is the mean sea level along the Indian coast higher in the Bay of Bengal than in the Arabian Sea? *Geophys Res Lett*, 28:563–565.
- Shankar, D., Vinayachandran. P.N. and Unnikrishnan, A.S. (2002): The monsoon currents in the north Indian. *OceanProgress in Oceanography*, 52 (2002) 63–120.

Shetye, S.R., Gouveia, A.D., Shenoi, S.S.C., Michael, G.S., Sundar, D., Almeida, A.M. and Santanam, K. (1991): The coastal current off western India during the northeast monsoon. *Deep-Sea Res* 38(12):1517–1529.

Shetye, S.R. (1998): West India coastal current and Lakshadweep high/low. *Sadhana*, Vol.23, Parts 5&6, 637-651.

Shetye, S.R., DileepKumar, M., Shankar, D. (2007): The Mandovi and Zuari estuaries, National Institute of Oceanography: Dona Paula, Goa: India: 2007: xiii+145 pp.

Shetye, S.R., Suresh, I., Shankar, D., Jayakumar, S., Mehra, P., Prabhudesai, R.G. and Pednekar, P.S. (2008): Observational evidence for remote forcing of the West India coastal current. *J Geophys Res*, Vol 113, 10 pp. doi:10.1029/2008JC004874.

Singh, O.P., Khan, T.M.A. and Rahman, M.S. (2001): Has the frequency of intense tropical cyclones increased in the North Indian Ocean? *Current Science*, 80(4): 575-580.

Singh, R.P., Dey, S., Bhoi, S., Sun, D., Cervone, G. and Kafatos, M. (2006): Anomalous increase of chlorophyll concentrations associated with earthquakes, *Advances in Space Research*, 37, 671-680.

Shum, C.K., Woodworth, P.L., Andersen, O.B., Egbert, G.D., Francis, O., King, C., Klosko, S.M., Provost, C.L., Li, X., Molines, J.M., Parke, M.E., Ray, R.D., Schlax, M.G., Stammer, D., Tierney, C.C., Vincent, P. and Wunsch, C.I. (1997): Accuracy assessment of recent ocean tide models. *Journal of Geophysical Research*, 102 (C11), 25173-25194, 1997.

SLOSH (2003): Sea, Lake, and Overland Surge from Hurricanes, a computerized model developed by the National Weather Service (NWS), US, to estimate storm surge heights and winds resulting from historical, hypothetical, or predicted hurricanes. SLOSH Display Training.

Srinivas, K. (2002): Coherence between interannual variability of sea level with some surface -met ocean parameters at Cochin, southwest coast of India. *Indian Journal of Marine Sciences*, 32, 285-293.

Srinivas, K. and Dineshkumar, P.K. (2002): Tide and non-tidal sea level variations at two adjacent ports on the southwest coast of India. *Indian J Mar Sci.*, Vol. 31(4), 212–224.

Srinivas, K., Kesavadas, V. and Dineshkumar, P.K. (2005a): Statistical modelling of monthly mean sea level at coastal tide gauge stations along the Indian subcontinent, *Indian J Mar Sci.*, 34:212–224.

Srinivas, K., and Dinesh Kumar, P.K. (2006): Atmospheric forcing on the variability of sea level at Cochin, southwest coast of India. *Continental Shelf Res.*, 26, 1113-1133.

- Suresh, I., Vialard, J., Lengaigne, M., Han, W., McCreary, J., Durand, F. and Muraleedharan, P.M. (2013): Origins of wind-driven intraseasonal sea level variations in the North Indian Ocean coastal waveguide, *Geophys. Res. Lett.*, VOL. 40, 5740–5744, doi:10.1002/2013GL058312, 2013.
- Sundar, D. and Shetye, S.R., (2005): Tides in the Mandovi and Zuari estuaries, Goa, west coast of India. *J. Earth Syst. Sci.* 114, No. 5, October 2005, pp. 493–503.
- Sundar, D., Shankar, D. and Shetye, S.R. (1999): Sea level during storm surges as seen in tide-gauge records along the east coast of India, *Current Science*, Vol. 77, No. 10, 25.
- Thompson, R.E. (1970): On the generation of Kelvin-type waves by atmospheric disturbances, *J. Fluid Mech.*, 42, 657-670.
- Thompson, B., Gnanaseelan, C., Anant Parekh, A., and Salvekar, P.S. (2008): North Indian Ocean warming and sea level rise in an OGCM. *J. Earth Syst. Sci.* 117, No. 2, April 2008, pp. 169–178
- Titov, V., Rabinovich, A.B., Mofjeld, H.O., Thomson, R.E., and Gonzalez, F.I. (2005): The global reach of the 26 December 2004 Sumatra tsunami, *Science*, 2005, 309,2045-2048.
- Tsimplis, M.N. and Woodworth, P.L. (1994): The global distribution of the seasonal sea level cycle calculated from coastal tide gauge data. *Journal of Geophysical research*, 99(C8):16,031–16,039, August 1994.
- Tsimplis, M.N. (1995): The response of sea level to atmospheric forcing in the Mediterranean. *JCR*, 11(4), 1309-1321. Fort Lauderdale (Florida), ISSN 0749-0208.
- Varadarajulu, R., Harikrishna, M. and Hanumantha Rao, K. (1982): Sea level changes at Paradip, East Coast of India. *Indian J. Mar. Sci.*, 11: 32-34.
- Vethamony, P and Babu, M.T. (2010): Physical processes in the Gulf of Kachchh: A review. *Indian Journal of Geo-Marine Sciences* Vol. 39(4), pp. 497-503
- VijayKumar, K. Joseph, A., Prabhudesai, R.G., Prabhudesai, S., Nagvekar, S. and Damodaran, V. (2005): Performance evaluation of Honeywell silicon piezoresistive pressure transducers for oceanographic and limnological measurements, *J. Atmos. Ocean. Technol.*, 22(12): 2005: 1933-1939.
- Vilibić, I., Domijan, N., Orlić, M., Leder, N., Pasaric, M., (2004): Resonant coupling of a traveling air-pressure disturbance with the east Adriatic coastal waters. *Journal of Geophysical Research*, 109, C10001, 10.1029/2004JC002279.
- Vinogradov, S.V. and Ponte, R.M. (2011): Low frequency variability in coastal sea level from tide gauges and altimetry. *J. Geophys. Res.*, 2011, 116, C07006: doi:10.1029/2011JC007034.

Unnikrishnan, A. S., Shetye, S.R. and Micheal, G.S. (1999): Tide propagation in the Gulf of Khambhat, Bombay High and surrounding areas. *Proceedings of the Indian Academy of Sciences (Earth and Planetary Sciences)* 108:155–177.

Unnikrishnan, A.S., Rupa Kumar, K., Sharon E.F., Michael, G.S. and Patwardhan, S.K. (2006): Sea level changes along the Indian coast: Observations and projections. *Current Science*, Vol. 90, NO. 3, pp 362-368.

Unnikrishnan, A.S., A. G. Nidheesh, A.G., and Lengaigne, M. (2015): Sea-level-rise trends off the Indian coasts during the last two decades, *Current Science*, VOL. 108, NO. 5, 10 March 2015, pp 966-971.

Willmott, C.J. (1981): On the validation of models. *Phys. Geogr.*, 2, 184-194, 1981.

Willmott, C.J. (1982): Some comments on the evaluation of model performance. *Bull. of Am. Meteorol. Soc.*, 63, 1309-1313, 1982.

Willmot, C.J, Ackleson, S.G., Davis, R.E., Feddema, J.J., Klink, K.M., David, R.L., O'Donnell, J., and Rowe, C.M. (1985): Statistics for the Evaluation and Comparison of Models. *JGR*, Vol. 90, No. C5, pp 8995-9005, September, 20,1985.

Woodworth, P.L. and Smith, D.E. (2003): A one year comparison of radar and bubbler tide gauges at Liverpool. *International Hydrographic Review*, 4(3), 2–9.

Woodworth, P.L., White, N.J., Jevrejeva, S., Holgate, S.J., Church, J.A. and Gehrels, W.R. (2009): Evidence for the accelerations of sea level on multi-decade and century timescales. *Int. J. Climatol.* 29: 777–789, DOI: 10.1002/joc.1771.

WMO/TD. No 1339, (2006): *Manual on Sea-level Measurements and Interpretation, Volume IV : An update to 2006*. Paris, Intergovernmental Oceanographic Commission of UNESCO. 78 pp. (IOC Manuals and Guides No.14, vol. IV : JCOMM Technical Report No.31: WMO/TD. No. 1339) (English).

WMO-No. 1076, (2011): *Guide to storm surge forecasting*, WMO-No. 1076, World Meteorological Organization, 2011, ISBN 978-92-63-11076-3.

Wyrski, K., (1973): Physical oceanography of Indian Ocean. In: Zeitzschel B, Gerlach SA (eds) *The biology of the Indian Ocean*, Chapman and Hall, London, pp 18–36.

Zaichenko, M. Yu., Levin, B.V., Pavlov, V.P and Yakubenko, V.G. (2002): Cooling effect of the Black Sea active layer recorded after the earthquake, *Izvestiya, Atmospheric and Oceanic Physics*, 38, 695-699.



## Annexure I

### Papers published from the thesis work

**Mehra, P., Desai, R.G.P., Joseph, A., Vijaykumar, K., Agarvadekar, Y., Luis, R. and Viegas, B. (2012);** A study of meteorologically and seismically induced water level and water temperature oscillations in an estuary located on the west coast of India (Arabian Sea). *Nat. Hazards Earth Syst. Sci.* 12; 2012; 1607-1620.

**Mehra, P., Desai, R.G.P., Joseph, A., VijayKumar, K., Agarvadekar, Y., Luis, R., and Nadaf,L. (2013);** Comparison of sea-level measurements between microwave radar and subsurface pressure gauge deployed at select locations along the coast of India. *J. Appl. Remote Sens.* 7(1); 2013; 16pp., doi: 10.1117/1.JRS.7.073569.

**Bos, M.S., Fernandes, R.M.S., Vethamony, P., and Mehra P. (2014);** Estimating absolute sea level variations by combining GNSS and Tide gauge data. *Indian Journal of Marine Science*, Vol. 43 (7). July 2014.

**Mehra, P., Soumya, M., Vethamony, P., Vijaykumar, K., Nair, T.M.B., Agarvadekar, Y., Jyoti, K., Sudheesh, K., Luis, R., Lobo, S.; Halmalkar, B. (2015);** Coastal sea level response to the tropical cyclonic forcing in the northern Indian Ocean. *Ocean Sci.:* 11(1); 2015; 159-173.

**Mehra, P., Vijaykumar, K., Soumya M., Vethamony, P., R. M. Gairola,R.M. Agarvadekar, Y., Luis, R.** Sea level variability at different coastal and Island locations in the north Indian Ocean- (under review in *Journal of Operational Oceanography*).

## Annexure II

### Conference proceedings:

**Mehra, P.; Agarwadekar, Y.; Luis, R.; Nadaf, L. (2012)** Comparison of sea-level measurements using microwave radar and subsurface pressure gauge deployed in Mandovi estuary in Goa, Central West Coast of India. Ocean Sensing and Monitoring. Eds. by: Hou, W.W.; Amone, R.(Proc. SPIE). SPIE: 8372; 2012; 837216; 7pp, Baltimore, USA.

**Mehra, P., Prabhudesai, R.G., Joseph, A., Agarwadekar, Y., Vijaykumar, K. and Luis, R. (2013);** Comparison of sea-level measurement from radar gauge with satellite altimeter in central west coast of India. IAHS-IAPSO-IASPEI, Joint Assembly Gothenburg, Sweden, 22-26 July, 2013.

**Soumya, M., Mehra, P., Vethamony, P., Vijaykumar, K., Agarwadekar, Y., Luis, R., Harmalkar, B., Devika, G. (2015);** High frequency sea level oscillations observed in the Mandovi estuary, central west coast of India. World Ocean Science Congress, 5-8 February 2015, Cochin.

**Mehra, P., Vijaykumar, K., Agarwadekar, Y., Soumya, M., Luis, R. (2014)** Comparison of satellite altimeter and sea-level gauge measurements in north Indian Ocean, GLOSS-GE-XIV Indian Ocean Sea Level Science Workshop and Fourteenth session of the Group of Experts for the Global Sea Level Observing System, 19 - 23 October 2015, Dona Paula, India.

**Mehra, P., Vijaykumar, K., Agarwadekar, Y., Soumya, M., Vethamony, P. and Luis, R. (2015),** Sea level and surface meteorological measurements during episodic events in the north Indian Ocean- experience in the last 10 years. Dynamics of the Indian Ocean: Perspective and Retrospective, International Symposium on the Indian Ocean (IO50), November 30 - December 4, 2015, Goa, India.

## Annexure III

### Supplementary figures and table

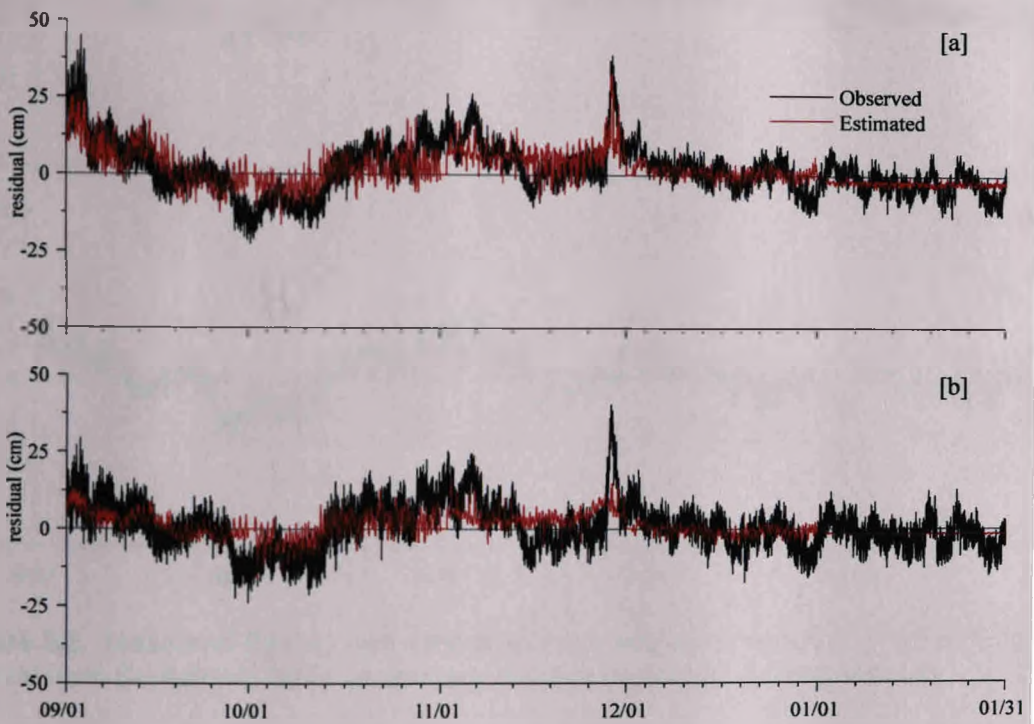


**Figure S1.** Measured (black) and estimated (red) sea-level residual at 10 minute interval from September 2011 to January 2012 at [a] Verem and [b] Karwar.

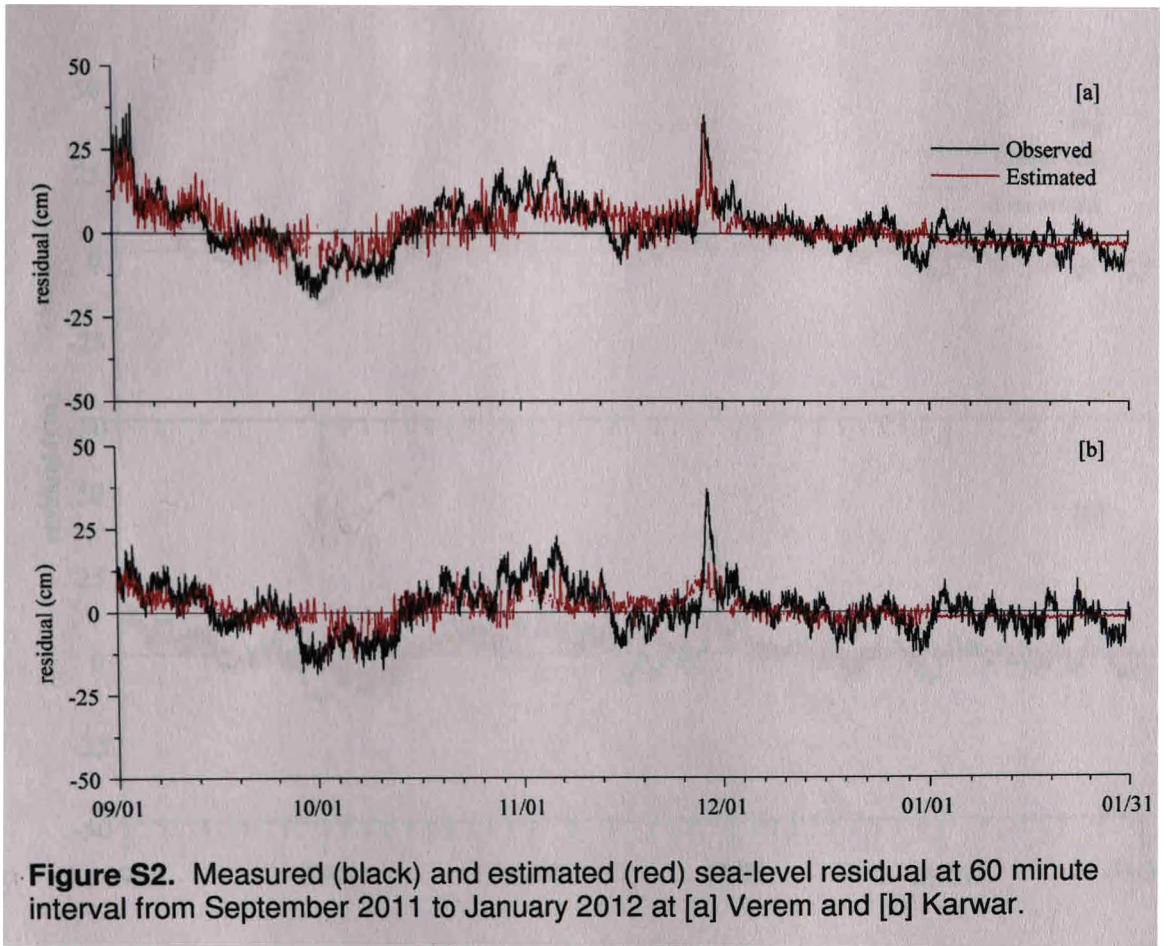


**Figure S2.** Measured (black) and estimated (red) sea-level residual at 60 minute interval from September 2011 to January 2012 at [a] Verem and [b] Karwar.

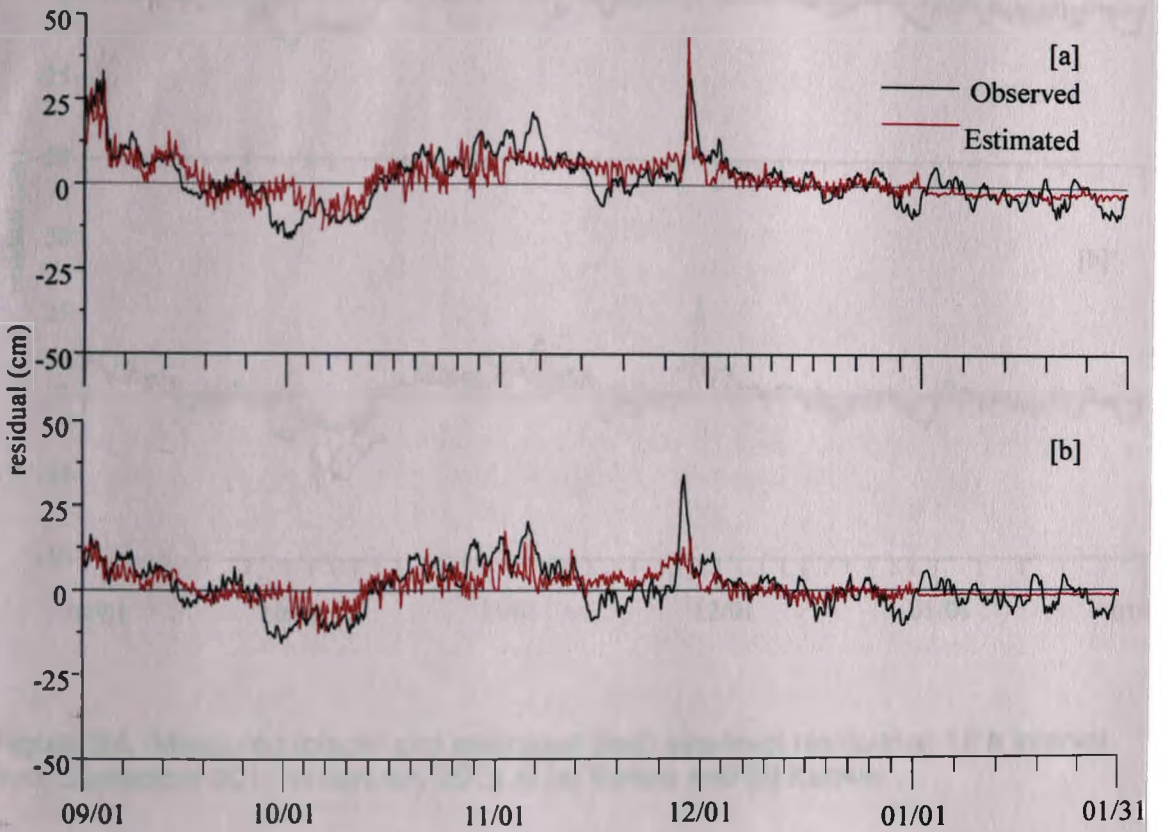


**Figure S3.** Measured (black) and estimated (red) sea-level residual at 6 h interval from September 2011 to January 2012 at [a] Verem and [b] Karwar.



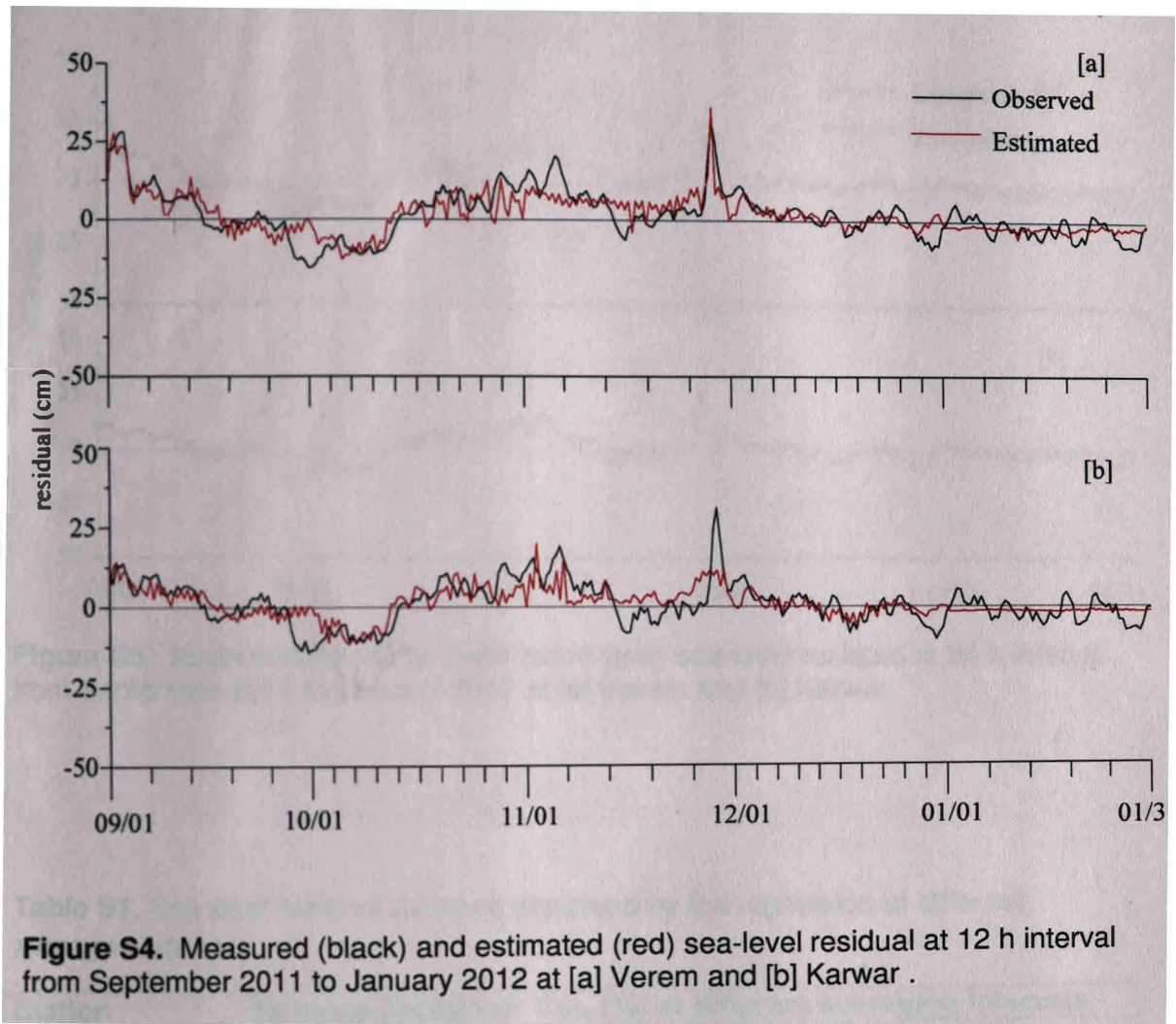


**Figure S4.** Measured (black) and estimated (red) sea-level residual at 12 h interval from September 2011 to January 2012 at [a] Verem and [b] Karwar .

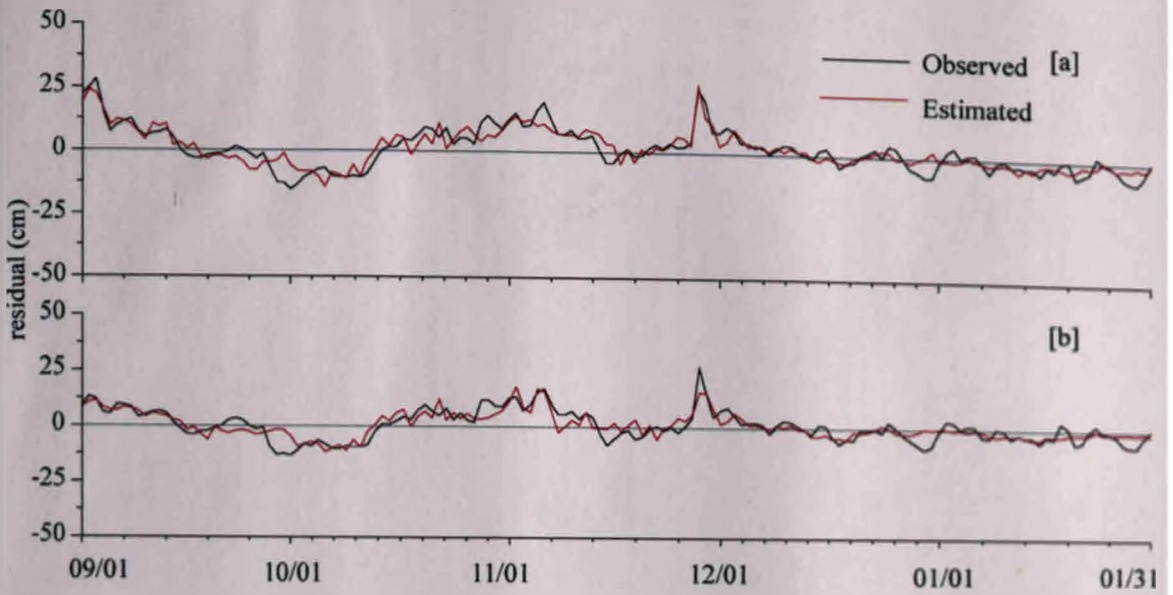


**Figure S5.** Measured (black) and estimated (red) sea-level residual at 24 h interval from September 2011 to January 2012 at [a] Verem and [b] Karwar

**Table S1.** Sea level residual variance explained by the regression at different averaged intervals

Station	Variance explained $Var_e$ (%) at different averaging intervals				
	10 m	60 m	6 h	12 h	24 h
Verem	45.8	50.5	55.3	65.3	75.8
Karwar	26.9	30.6	37.7	47.7	66.3